Mitochondrial DNA Depletion and Insulin Secretion

Donna Louise Hine
BSc (Hons)

Thesis submitted in partial fulfilment of the requirements for the degree of Doctor of Philosophy at Newcastle University

Faculty of Medical Sciences
Institute for Cell and Molecular Biosciences

September 2012

Abstract

Introduction: Type 2 diabetes is an age-related condition and is characterised by a progressive decline in insulin secretion. Mitochondria play a key role in energy generation for insulin secretion. We previously reported an age-related decline in mitochondrial DNA (mtDNA) copy number in isolated human islets. TFAM, mtDNA Transcription Factor A, regulates mtDNA transcription and mtDNA copy number.

Aims: We aimed to replicate the percentage decrease in mtDNA copy number that we observed with ageing in human islets, and to explore whether this affected mitochondrial function and insulin secretion.

Methods: Two independent models of mtDNA depletion were created. The first model knocked down *TFAM* gene expression using siRNA technology. The second model subjected cells to didanosine, a nucleoside analogue of adenosine with a high affinity to POLG, a mtDNA polymerase.

Results: Both models produced comparable levels of mtDNA depletion. Upon investigating the effects of partial mtDNA depletion on mitochondrial function, we found that both mtDNA depletion models displayed reduced mtDNA gene transcription and translation. However, neither model of mtDNA depletion affected ATP content or mitochondrial membrane potential. Glucose-stimulated insulin secretion was decreased following mtDNA depletion in the TFAM knock down cells which was rescued following treatment with the insulin secretagogue glibenclamide. Conversely, didanosine-induced mtDNA depleted cells showed increased insulin secretion.

Conclusions: Both models generated a similar degree of mtDNA depletion, which was comparable to the percentage decrease seen in human islets with ageing. Both models were seen to impair mitochondrial function, but with opposing effects on insulin secretion. The TFAM model findings are in line with previous studies of severe mtDNA depletion, suggesting that the increase in insulin secretion seen with didanosine is due to drug off target effects. Strategies to slow islet mtDNA depletion in man could help to preserve insulin secretion and delay the development of Type 2 diabetes.

I would like to dedicate this thesis to my parents,

Joe and Karen Hine,

and my fiancé Chris Nile

"Science is a wonderful thing if one does not have to earn one's living at it."

Albert Einstein

Acknowledgements

I would first like to thank my supervisor, Professor Mark Walker, for giving me the opportunity to complete my PhD in his research group, and for allowing me to indulge my passion for science. Thank you for your help and guidance over the past 4 years and for putting up with my 'purist' ways!

Secondly, I would like to thank fellow members of lab M4.094 for making it such a pleasure to come into work each day. Thank you all for you banter, wit and encouragement, and for putting up with me singing to the radio! I'd especially like to thank Audrey Brown, who I still maintain is the oracle of the lab; Michael White, for keeping me sane and for the many cups of coffee you made me; Helen Marshall, Catherine Arden and Susan Campbell for your much needed wisdom and experience along the way.

I would also like to thank my industrial supervisors, Unilever, for sponsoring the project and for allowing me to experience academic research in an industrial setting. I'd especially like to thank my industrial supervisors Dave Gunn and Louise Brown for their help and expertise along this 4 year journey; as well Alan Heath for looking after me during my time down at Colworth, and Katrina MacAulay for your continued interest in the project. Thank you also to all members of Unilever Discover for welcoming me so warmly and for making my time down at Colworth so enjoyable.

Finally, I would like to give my biggest and heartfelt thanks to my mum Karen, dad Joe, and fiancé Chris Nile. Thank you to my parents for making me who I am today, and for encouraging me to follow my dreams. Thank you Chris for your constant reassurance, love and support when things got tough. Now that I've written my thesis, I look forward to planning our wedding!

Thanks again to you all, I could not have achieved this without you.

Table of Contents

List of Tables

List of Figures

Abbreviations

3’	Three Prime
3TC	Lamivudine (2',3'-dideoxy-3'-thiacytidine)
5’	Five Prime
ABC	Abacavir ({(1*S*,4*R*)-4-[2-amino-6-(cyclopropylamino)-9*H*-purin-9-yl] cyclopent-2-en-1-yl}methanol)
AMV	Avian Myeloblastosis Virus
ADP	Adenosine Diphosphate
APS	Ammonium Persulphate
ATP	Adenosine Triphosphate
AZT	Azidothymidine (1-[(2R,4S,5S)-4-azido-5-(hydroxymethyl)oxolan 2-yl] -5-methylpyrimidine-2,4-dione[1])
B2M	β2 Microglobulin
bp	Base Pairs
BSA	Bovine Serum Albumin
$CaCl_2$	Calcium Chloride
CAPS	Cyclohexyl-3-aminopropanesulfonic Acid
CDKN2A/2B	Cyclin-Dependent Kinase Inhibitor 2A/2B
cDNA	Complementary DNA
CO_2	Carbon Dioxide
COX	Cytochrome c Oxidase (Complex IV)
COX1	Cytochrome c Oxidase Subunit 1 (mtDNA subunit of Complex IV)
Complex I	NADH Dehydrogenase
Complex II	Succinate Dehydrogenase
Complex III	Ubiquinol-Cytochrome c Reductase
Complex IV	Cytochrome c Oxidase
Complex V	ATP Synthase
CREB	Cyclic AMP Response Element (CRE) Binding Protein,
Ct	Crossing Threshold
$CuSO_4.5H_2O$	Copper Sulphate Pentahydrate
CVD	Cardiovascular Disease

d4T	Stavudine (2'-3'-didehydro-2'-3'-dideoxythymidine)
DAPI	4',6-diamidino-2-phenylindole
dATP	Deoxyadenosine Triphosphate
ddATP	Dideoxyadenosine Triphosphate
ddI	Didanosine (2',3'-dideoxyinosine)
dH_2O	Distilled Water
DMEM	Dulbecco's Modified Eagle's Medium
DMSO	Dimethyl Sulphoxide
DNA	Deoxyribose Nucleic Acid
dNTP	Deoxynucleotide Triphosphate
DTT	Dichlorodiphenyltrichloroethane
dsDNA	Double Stranded DNA
dTTP	Deoxythymidine Triphosphate
dUTP	Deoxyuracil Triphosphate
ECL	Enhanced chemiluminescence
EDTA	Ethylenediaminetetraacetic Acid
EGTA	Ethylene Glycol Tetraacetic Acid
ELISA	Enzyme-Linked Immunosorbent Assay
ETC	Electron Transport Chain
FBS	Foetal Bovine Serum
FDA	Food and Drugs Administration
FFA	Free Fatty Acid
FCS	Foetal Calf Serum
FTO	Fat Mass and Obesity-Associated
GAPDH	Glyceraldehyde-3-phosphate dehydrogenase
GSIS	Glucose Stimulated Insulin Secretion
GWA	Genome Wide Association Studies
H_2O	Water
H_2O_2	Hydrogen Peroxide
HAART	Highly Active Antiretroviral Therapy
HCl	Hydrochloric Acid

Hepes	4-(2-hydroxyethyl)-1-piperazineethanesulfonic acid
HHEX	Hematopoietically-Expressed Homeobox
HIV	Human Immunodeficiency Virus
HIV-RT	Human Immunodeficiency Virus Reverse Transcriptase
HRP	Horse Radish Peroxidase
Ins1	Insulin 1
IRS1	Insulin Receptor Substrate 1
JC-1	5,5'',6,6''-tetrachloro-1,1'',3,3''-tetraethylbenzimidazolylcarbocyanine iodide
K_2CO_3	Potassium Carbonate
kb	Kilo Base Pairs
KCl	Potassium Chloride
KCNJ11	Potassium Inwardly Rectifying Channel, Subfamily J, Member 11
Kf	Potassium Fluoride
KH_2PO_4	Potassium Phosphate Monobasic
LDH	Lactate Dehydrogenase
LHON	Leber Hereditary Optic Neuropathy
MELAS	Mitochondrial Myopathy, Encephalopathy Lactic Acidosis, Stroke-Like Episode
MERRF	Myoclonic Epilepsy and Ragged-Red Fibres
$MgCl_2$	Magnesium Chloride
MIDD	Maternally-Inherited Diabetes and Deafness
MILS	Maternally-Inherited Leigh Syndrome
MIN6	Mouse Insulinoma Cells
mRNA	Messenger RNA
mtDNA	Mitochondrial DNA
mtSSB	Mitochondrial Single Stranded Binding Protein
NaOH	Sodium Hydroxide
Na_2CO_3	Sodium Carbonate
$NaHCO_3$	Sodium Bicarbonate
nDNA	Nuclear DNA

NRF-1/-2	Nuclear Respiratory Factor -1/-2
NRTI	Nucleoside Reverse Transcriptase Inhibitor
nDNA	Nuclear DNA
ND5	NADH Dehydrogenase 5
nt	Nucleotide
NTC	No Template Control
OD	Optical Density
OH	Hydroxyl Group
oxo^{8}dG	8-oxo-2'-deoxyguanosine
PBS	Phosphate Buffered Saline
PCA	Perchloric Acid
PCR	Polymerase Chain Reaction
PDX1	Pancreatic and Duodenal Homeobox 1
PGC-1α	Peroxisome Proliferator-Activator Receptor-γ Coactivator-1α
pH	Hydrogen Ion Concentration
POLG	Polymerase-γ
PPARγ	Peroxisome Proliferator-Activator Receptor-γ
PPRE	Peroxisome Proliferator Response Element
RNA	Ribonucleic Acid
ROS	Reactive Oxygen Species
rpm	Revolutions Per Minute
rRNA	Ribosomal RNA
RXR	Retinoid X Receptor
SD	Standard Deviation
SEM	Standard Error of the Mean
SDH	Succinate Dehydrogenase
SDH70	Succinate Dehydrogenase 70 kDa subunit
SDS	Sodium Dodecyl Sulphate
SDS-PAGE	Sodium Dodecyl Sulphate Polyacrylamide Gel Electrophoresis
siRNA	Small Interfering RNA
SNP	Small Nucleotide Polymorphism

SOD	Superoxide Dismuatase
T1DM	Type 1 Diabetes Mellitus
T2DM	Type 2 Diabetes Mellitus
TBE Buffer	Tris/Borate/EDTA Buffer
TBS-T	Tris Buffered Saline with Tween
TCA cycle	Tricarboxylic Acid Cycle
TCF7L2	Transcription Factor 7-Like 2
TE Buffer	Tris/EDTA Buffer
TEMED	Tetramethylethylenediamine
TFAM	Mitochondrial Transcription Factor A
TFB1M	Mitochondrial Transcription Factor B1
TFB2M	Mitochondrial Transcription Factor B2
TMB	3,3′,5,5′-Tetramethylbenzidine (TMB) Substrate
tRNA	Transfer RNA
TZD	Thiazolidinedione
UCP2	Uncoupling Protein 2
WAT	White Adipose Tissue
WST-1	Water Soluble Tetrazolium Salt-1

Chapter 1

Introduction

1 Introduction

1.1 Diabetes Mellitus

Diabetes mellitus is one of the most common non-communicable diseases. The condition is characterised by abnormally high blood plasma glucose levels over a sustained period of time (chronic hyperglycaemia). The clinical diagnosis of diabetes is prompted by the presence of other classical symptoms including the passage of increased volumes of water (polyuria) as the renal glucose threshold is breached, which ultimately causes an increase in thirst (polydipsia). The increased blood glucose levels are also the ideal environment for yeast and bacteria, and so other symptoms of diabetes include slow wound healing and thrush. The reduced ability of the body to metabolise glucose can culminate in weight loss and in extreme cases, drowsiness and coma (WHO, 1999). These diabetic symptoms can often culminate in more serious complications such as retinopathy, neuropathy and nephropathy; resulting in blindness, nerve damage and kidney problems respectively.

Diabetes is diagnosed when fasting plasma glucose is too high, typically ≥7.0 mM (≥126 mg/dl). Chronic exposure to such high glucose could culminate in microvascular damage (WHO, 2006). Normogylcaemia, the normal blood glucose level, is defined between the range of 4 mM (72 mg/dl) and 7 mM (126 mg/dl) prior to a meal (NICE, 2008). Deviations from this normoglycaemic range are termed hypoglycaemia (low blood glucose, <4 mM or <72 mg/dl) and hyperglycaemia (high blood glucose, >10 mM or >180 mg/dl) (Diabetes UK, 2006).

In 1670 Thomas Willis was the first to differentiate between diabetes mellitus and diabetes insipidus simply by the taste of the patients' urine: whether it tasted sweet (indicating diabetes mellitus) or had no taste (indicating diabetes insipidus) (Willis, 1674-1675). The two main types of diabetes mellitus were first fully characterised in 1951 by Lister and Nash based on their different aetiologies (Lister & Nash, 1951):

Type 1 Diabetes Mellitus (T1DM) is characterised by the loss of pancreatic beta cells (β-cells), thought to be due to the body's auto-immune attack on pancreatic islets (Atkinson & Maclaren, 1994). Consequently, patients produce

little or no insulin and so, need to take exogenous insulin by injection; hence the reason why T1DM is often referred to as insulin-dependent diabetes. The age of onset is relatively early, usually before 40 years.

Type 2 Diabetes Mellitus (T2DM), also known as non-insulin-dependent diabetes, tends to have a more delayed age of onset of 40-60 years compared to T1DM. T2DM is characterised by a decreased sensitivity to insulin, also referred to as insulin resistance, together with decreased insulin secretion from pancreatic β-cells. However, we are now seeing an increase in childhood T2DM, due to the increase in childhood obesity.

1.1.1 Glucose Homeostasis

Blood glucose levels are kept in equilibrium by homeostasis and the hormones insulin and glucagon (Figure 1). When blood glucose levels increase, this causes pancreatic β-cells to secrete the hormone insulin. Insulin lowers blood glucose levels by promoting the uptake of glucose, via glucose transporters, by the liver. Once in the liver, the glucose is converted to glycogen in a process called glycogenesis. Insulin also promotes the uptake of glucose by other tissue cells such as muscle and fat. The uptake of glucose by liver, fat or muscle cells causes a decrease in blood glucose concentration.

If, however, the blood glucose level falls below the normoglycaemic range, this prompts pancreatic α-cells to secrete the hormone glucagon. Glucagon promotes the breakdown of stored glycogen in the liver to glucose, in a process called glycogenolysis. Glucose is then released into the bloodstream subsequently increasing the blood glucose concentration.

Pancreatic α- and β-cells are found in the islet of Langerhans and constitute the endocrine section of the pancreas, a glandular organ located in the abdominal cavity, beneath the stomach and attached to the duodenum of the small intestine.

Chronic inability to maintain blood glucose homeostasis culminates in the onset of diabetes mellitus.

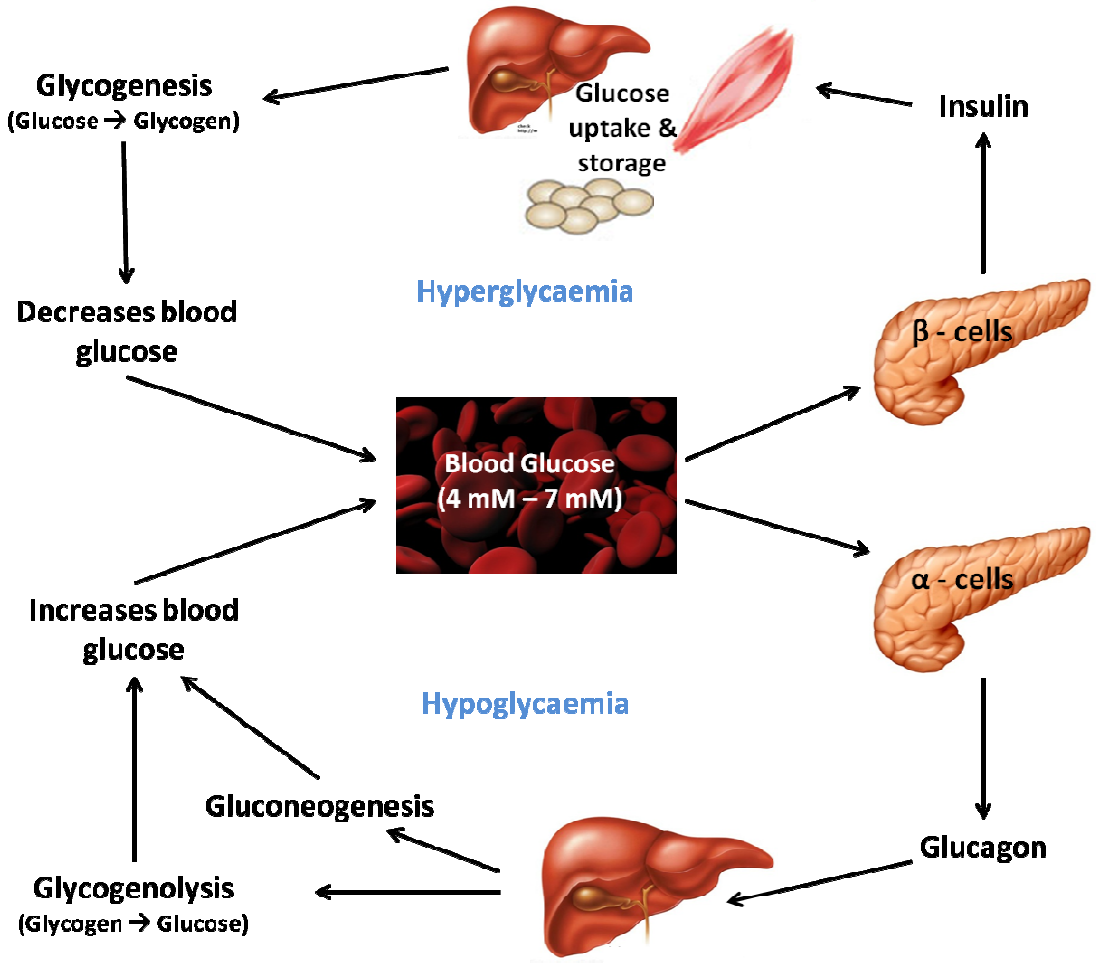

Figure 1 Glucose homeostasis

Blood glucose levels are maintained between 4 mM and 7 mM by homeostasis. When glucose levels are too high, pancreatic β-cells are prompted to secrete the hormone insulin, which promotes the uptake of glucose by liver, muscle and fat cells. In the liver, glucose is converted to glycogen by glycogenesis. Uptake of glucose from the blood causes a decrease in blood glucose concentration. When blood glucose levels are too high, the hormone glucagon is secreted from pancreatic α-cells. Glucagon targets the liver where it promotes the hydrolysis of stored glycogen to glucose, via glycogenolysis. It also promotes the synthesis of new glucose molecules from non-carbohydrate carbon substrates via gluconeogenesis. Glucose is released from the liver cell causing a rise in blood glucose concentration.

1.1.2 Type 2 Diabetes Mellitus (T2DM)

The development of T2DM has been linked to a decrease in insulin action, referred to as insulin resistance, as target cells are no longer sensitive to the effects of insulin. This insulin resistance is coupled with a decrease in insulin secretion from the pancreatic β-cells. Impaired glucose tolerance (IGT) is thought to be an intermediary step in the pathogenesis of T2DM, and is associated with impaired insulin secretion (IDF, 2011). IGT is determined following an oral glucose tolerance test (OGTT) whereby the patient is administered a maximum of 75 g oral glucose after an 8-12 hour fast and the whole blood glucose level measured after 2 hours. IGT is diagnosed if the whole blood glucose level is ≥ 6.7 mmol/l (venous) or ≥ 7.8 mmol/l (capillary) following the 2 hour post glucose load (WHO, 2006). IGT is not a clinical entity on its own, but predisposes the patient to developing diabetes if the IGT is not addressed (WHO, 2006). It has been suggested that insulin resistance in muscle as well as defective insulin secretion contribute to IGT (WHO, 2006).

T2DM is thought to account for 90% of all diabetes cases worldwide (WHO, 2008a). The prevalence of diabetes was predicted to be around 366 million people in 2011; this is expected to rise to 552 million by 2030 (IDF, 2011). In the UK alone, the prevalence of diabetes was estimated to be 1,765,000 in 2000, predicted to rise to 2,668,000 by 2030 (WHO, 2008b). It is believed that around half of the people with diabetes are undiagnosed, with diabetes causing 4.6 million deaths in 2011 (IDF, 2011). There has also been an alarming increase in the number of children developing T2DM, the main underlying cause of this is thought to be linked to sedentary lifestyle and obesity.

These facts and figures simply highlight the scale of the problem and prompt the need for further research into the disease.

1.1.3 T2DM Risk Factors

Over recent years, especially in developed countries, there has been a general increase in the average human life expectancy. This has contributed, along with other factors such as improved hygiene, healthcare, and the development of treatments for many infectious diseases, to an overall increase in the prevalence of age-related, non-communicable diseases such as T2DM, cardiovascular disease (CVD) and some cancers (Hitman, 1999).

1.1.3.1 Environmental Risk Factors

Several environmental factors have been linked to the onset of T2DM, the main one being obesity. This can be attributed to people leading a more sedentary lifestyle and so, exercising less. In children especially, since the advancements in technology and the development of computers, games consoles and mobile phones for example, children are more likely to stay indoors rather than go outside and exercise. Poor diet and our current fast-food and junk food culture can also be held accountable for increases in obesity and ultimately, T2DM. Exercise intervention (Trenell *et al.*, 2008; Praet & Van Loon, 2009) and severe calorie restriction (R. Taylor, 2011) have both proven effective means of preventing T2DM disease progression, or even reversing T2DM.

1.1.3.2 Genetic Risk Factors

The majority of T2DM risk is environmental, but there is a growing body of evidence detailing genetic predisposition. Previous family history of T2DM, especially first degree relatives, has been seen to increase risk of developing T2DM (Annis *et al.*, 2005). The presence of any genetic markers or 'thrifty gene(s)' has also been implicated as a genetic risk factor for T2DM (Hitman, 1999). The Thrifty Gene Hypothesis was first proposed in 1962 by James Neel and proposes that so-called 'thrifty' genes, genes that are now thought to predispose to T2DM, were once beneficial and hence, favoured in the process of natural selection. In time however, these genes have been rendered detrimental (Neel, 1962).

Candidate gene studies (listed in Table 1) have identified many T2DM susceptibility genes including: *PPARG* (encodes the peroxisome proliferator-activator receptor-γ protein) (Altshuler *et al.*, 2000; Florez *et al.*, 2007) and *KCNJ11* (encodes the Kir6.2 subunit of the β-cell ATP sensitive K^+ channel) (Hani *et al.*, 1998). Both protein products of these genes are targets of the anti-diabetes treatment drugs thiazolidinediones and sulphonylureas respectively. Risk alleles in the *TCF7L2* gene, encoding a key transcription factor component of the Wnt signalling pathway, have also been associated with increased risk of developing T2DM (Grant *et al.*, 2006; Cauchi *et al.*, 2007).

The increasing use of genome wide association (GWA) studies to identify single nucleotide polymorphisms (SNPs) has identified new T2DM susceptibility genes (listed in Table 1). Genes identified as containing T2DM susceptibility SNPs by

GWA studies include *HHEX* (encodes a protein thought to be essential for β-cell development) (Pascoe *et al.*, 2007; Sladek *et al.*, 2007), *IRS1* (encodes insulin receptor substrate 1, which is involved in insulin signalling) (Rung *et al.*, 2009) and *FTO* (fat mass and obesity associated gene) (Frayling *et al.*, 2007). Important regulators of the cell cycle have also been identified as T2DM susceptibility genes, including *CDKN2A/2B*, *CDC123* and *CDKAL1*, thus opening up the possibility of additional therapeutic approaches for the treatment of T2DM (Pascoe *et al.*, 2007; Sladek *et al.*, 2007; Steinthorsdottir *et al.*, 2007; Zeggini *et al.*, 2008).

There are now approximately 40 DNA variants of T2DM susceptibility genes that have been identified (Imamura & Maeda, 2011), but these are thought to only account for 10% of the known T2DM heritability (Bonnefond *et al.*, 2010).

1.1.3.3 Demographic Risk Factors

Demographic risk factors including age, ethnicity and sex have also been implicated in the development of T2DM. The increased prevalence of T2DM has been linked with ageing, due to a decrease in insulin secretion and decreased β-cell function (discussed in Section 1.1.4). T2DM is seen more commonly in South-Asian or African-Caribbean ethnic groups in the UK (Diabetes UK, 2009). Females who are overweight and have polycystic ovary syndrome, or have previously had gestational diabetes are also more prone to developing T2DM (Diabetes UK, 2009).

Gene (suggested)	Locus	Protein	Assumed effect of risk allele
Biological candidate gene studies			
PPARG	3p25	Peroxisome proliferator-activated receptor-*γ*	Decreased insulin sensitivity, decreased insulin clearance
KCNJ11	11p15.1	K inwardly-rectifying channel, subfamily J, member 11	Decreased β-cell function, decreased glucose-stimulated insulin secretion (GSIS), decreased insulin sensitivity
HNF1B	17cenq-21.3	Hepatocyte nuclear factor 1-beta	Decreased β-cell function
WFS1	4p16	Wolfram syndrome 1 (wolfamin)	Decreased β-cell function, decreased insulin secretion
GCK	7p15.3-p15.1	Glucokinase (Hexokinase 4)	Decreased β-cell function, decreased GSIS, increased fasting glucose, increased glycated haemoglobin
Exploration of linkage peaks			
TCF7L2	10q25.3	Transcription factor 7-like 2 (T-cell specific, HMG-box)	Decreased β-cell function, decreased incretin-stimulated insulin secretion, decreased GSIS, decreased proinsulin conversion, decreased insulin sensitivity, decreased disposition index, increased fasting glucose, increased 2h-glucose
GWAS for T2D			
CDKN2A/2B	9p21	Cyclin-dependent kinase inhibitor 2A/2B	Decreased β-cell function, decreased GSIS, decreased disposition index
CDKAL1	6p22.3	CDK5 regulatory subunit associated protein 1-like 1	Decreased β-cell function, decreased GSIS, decreased proinsulin conversion, decreased disposition index
SLC30AB	8q24.11	Solute carrier family 30 (zinc transporter) member 8	Decreased β-cell function, decreased GSIS, decreased proinsulin conversion, decreased disposition index, increased fasting glucose, increased 2h-glucose, increased glycated haemoglobin
IGF2BP2	3q27.2	Insulin-like growth factor 2 mRNA binding protein 2	Decreased β-cell function, decreased GSIS, decreased disposition index
THADA	2p21	Thyroid adenoma associated	Decreased β-cell function, decreased insulin sensitivity, decreased second-phase insulin secretion, decreased disposition index, decreased GLP-1 and arginine-stimulated insulin response
NOTCH2	1p13-p11	Neurogenic locus notch homolog protein 2 (*Drosophila*)	NA
CDC123	10p13	Cell division cycle 123 homolog (*Saccharomyces cerevisiae*)	Decreased β-cell function, decreased insulin secretion
CAMK1D		Calcium/calmodulin-dependent protein kinase type 1D	
HHEX	10q23	Haematopoietically expressed homeobox	Decreased β-cell function, decreased GSIS, decreased insulin sensitivity, decreased proinsulin conversion, decreased disposition index
IDE		Insulin-degrading enzyme	
TSPAN8	12q14.1-q21.1	Tetraspanin 8	Decreased β-cell function, decreased insulin secretion, decreased insulin sensitivity
LGR5	12q22-q23	Leucine-rich repeat-containing G protein-coupled receptor 5	
ADAMTS9	3p14.3-p14.2	ADAM metallopeptidase with thrombospondin type 1 motif. 9	Decreased insulin sensitivity
JAZF1	7p15.2-p15.1	Juxtaposed with another zinc finger protein 1	Decreased β-cell function, increased insulin secretion, increased fasting insulin
IRS1	2q36	Insulin receptor substrate 1	Increased insulin resistance, decreased insulin sensitivity, increased fasting insulin, increased 2h-insulin
KCNQ1	11p15.5	K voltage-gated channel, KQT-like subfamily, member 1	Decreased β-cell function, decreased insulin secretion, decreased incretin secretion
FTO	16q12.2	Fat mass and obesity-associated protein	Increased risk of obesity, increased body mass index, increased fat mass, increased triglycerides and cholesterol
GWAS for T2D-related traits			
GCKR	2p23	Glucokinase (Hexokinase 4) regulator	Increased insulin resistance, increased fasting insulin, increased fasting glucose, increased 2h-glucose
MTNR1B	11q21-q22	Melatonin receptor 1B	Decreased β-cell function, decreased GSIS, decreased disposition index, increased fasting glucose, increased glycated haemoglobin
ADCY5	3q13.2-q21	Adenylated cyclase 5	Decreased β-cell function, increased fasting glucose, increased 2h-glucose
PROX1	1q32.2-q32.3	Prospero homeobox 1	Decreased β-cell function, increased fasting glucose
DGKB	7p21.2	Diacylglycerol kinase, beta 90 kDa	Decreased β-cell function, increased fasting glucose
TMEM195		Transmembrane protein 195	

Table 1 The most reported T2DM susceptibility genes and associated small nucleotide polymorphism (SNP) loci

This table is taken from (Bonnefond *et al.*, 2010) and records the most popularly reported susceptibility genes associated with increased T2DM risk along with associated SNP loci and suspected disease phenotype.

1.1.4 T2DM and Ageing

The increased prevalence of T2DM can be attributed to many underlying factors, the predominantly documented risk factor being obesity. But there is clear evidence that the increase in T2DM prevalence is also linked to the effects of ageing. In an American population of 20-74 year olds, the prevalence of total diabetes was found to increase from 2.0% in individuals under 44 years old, to 17.7% at age 65-74 years (Harris *et al.*, 1987). The National Health and Nutrition Examination Survey (NHANES) found that the prevalence of diabetes increased with advancing age with approximately one third of the American elderly population being diagnosed with T2DM (Cowie *et al.*, 2009).

T2DM prevalence in the over 65 population has increased from 17.7% in the 1976-1980 NHANES survey (Harris *et al.*, 1987), to 21.6% in the 1999-2002 NHANES survey (Cowie *et al.*, 2006) and 31.6% in the 2005-2006 NHANES survey (Cowie *et al.*, 2009). This increase in T2DM prevalence in the over 65s may be due to the elderly living longer, but it does not explain why the prevalence of T2DM consistently increases with advancing age (Harris *et al.*, 1987; Cowie *et al.*, 2006; Cowie *et al.*, 2009; Centre for Disease Control and Prevention, 2011). It has also been shown that the prevalence of undiagnosed diabetes and isolated post-challenge hyperglycaemia increased with advancing age (Resnick *et al.*, 2000).

So why does the prevalence of T2DM increase with advancing age? There is evidence to suggest an age-related deterioration in glucose tolerance linked to a progressive decrease in pancreatic β-cell function may be to blame. Basu and colleagues demonstrated that tolerance to glucose deteriorates with age. They investigated 67 elderly and 21 young healthy participants after ingestion of a mixed meal followed by an intravenous injection of glucose 14 hours later. The group were able to show that the elderly participants had increased fasting glucose and exhibited decreased insulin secretion, suggesting impairment of β-cell function (Basu *et al.*, 2003).

Animal models of T2DM have been presented including the Goto-Kakizaki (GK) rat. The GK rat is a non-obese substrain of the Wistar rat produced by selective breeding, with glucose intolerance as selection criterion, which develops T2DM early in life. The GK rat was originally developed by Goto and Kakizaki back in

1975 (Goto *et al.*, 1976) and since then, has been used as a putative model of T2DM in the study of many pathways and processes including prediabetes (Movassat *et al.*, 2008), glucagon-like peptide-1 (GLP-1) (Tourrel 2002 Diabetes), superoxide generation in vascular tissue (Gupte *et al.*, 2010) as well as ageing (Gao *et al.*, 2011; Nie *et al.*, 2011). Investigations using GK rats have shown that impaired glucose-stimulated insulin secretion, increased insulin resistance, decreased β-cell mass and increased hyperglycaemia all correlate with advancing age (Goodman *et al.*, 1983; Berthelier *et al.*, 1997; O'Rourke *et al.*, 1997; Suzuki *et al.*, 1997; Movassat *et al.*, 2008; Gao *et al.*, 2011).

It is now widely recognised that progressive impairment of pancreatic β-cell function seems to be a key perpetrator in the pathogenesis of T2DM (Porte, 2001; Poitout & Robertson, 2002; Prentki *et al.*, 2002; Leahy, 2005). Rudenski *et al.* developed a mathematical linear regression model to predict islet β-cell function and insulin sensitivity, and concluded that in 131 T2DM patients, β-cell function declines at a rate of 1.5% per year, but with no significant change in insulin sensitivity (Rudenski *et al.*, 1988). This study shows that there is a reduced β-cell function in patients with T2DM, which is age-dependent. Furthermore, there is evidence that insulin secretion (Chang & Halter, 2003) and β-cell function (Basu *et al.*, 2003) decline with age in the general, non-diabetic population.

As well as the growing body of evidence suggesting the progressive decline in β-cell function, coupled with deterioration in glucose tolerance being implicated in the increased prevalence of T2DM in the ageing population, other factors associated with ageing have also been suggested. These include increased adiposity, medication, less physical activity and other coexisting illnesses (Chang & Halter, 2003). As we are continually making advancements in medical science, people are living a lot longer and so, the age-related onset of T2DM will only increase further.

1.1.5 Glucose Metabolism in the Pancreatic β-cell

The release of insulin from pancreatic β-cells begins with cellular stimulation by glucose. Glucose enters the β-cell by a glucose transporter (GLUT) protein on the cell surface. There are many glucose transporters, each specific for individual cell types, GLUT2 transporters are predominantly found in pancreatic β-cells as well as liver hepatocytes. GLUT4 proteins however, are restricted to cells where glucose transport is insulin sensitive, such as muscle cells and adipose tissue. Other glucose transporters include GLUT1 (ubiquitously found in most tissues, but abundant in red blood cells), GLUT 3 (preferentially expressed in brain neurones), GLUT5 (fructose transporter found in human enterocyte luminal membrane, adipocytes and skeletal muscle), GLUT6 (pseudogene with no protein product) and GLUT7 (intracellular glucose transporter found in liver) (Klip *et al.*, 1994).

Once inside the cell, glucose is then metabolised by glycolysis in the cytosol, followed by the tricarboxylic acid cycle and the electron transport chain in the mitochondria.

1.1.5.1 Glycolysis

Glycolysis, derived from the Greek words 'glyk' meaning sweet and 'lysis' meaning dissolution, is the first step in glucose metabolism. It occurs in the cell cytosol and is a sequence of reactions resulting in the breakdown of glucose into pyruvate. Carbohydrates such as glucose are the principal fuel source for β-cells, but other substrates include amino acids and fatty acids. Once glucose enters the β-cell, it is rapidly phosphorylated to form glucose-6-phosphate by glucokinase, also known as hexokinase IV or D (Matschinsky *et al.*, 2006). Glucokinase is thought to play a dual role by initiating the storage of glucose to glycogen in the liver, as well as being a glucose sensor in pancreatic β-cells and subsequently the rate limiting step in glycolysis (Matschinsky & Ellerman, 1968). This second role of glucokinase was first proposed by Matchinsky and Ellerman in 1968, but it was initially received with a mixed reception. It was only accepted many years later when evidence was published in the 1990's on the role glucokinase mutations played in hypo- and hyperglycaemia, coupled with the discovery and development of glucokinase activator drugs (Matschinsky *et al.*, 2006).

Following formation of glucose-6-phosphate via glucose phosphorylation by glucokinase, glucose-6-phosphate is metabolised further by a series of reactions to eventually form pyruvate. Pyruvate is then converted to acetyl-CoA in the mitochondrial matrix, which is the main substrate for the tricarboxylic acid cycle. Glycolysis is a low energy yielding process compared to the electron transport chain, but following the breakdown of one molecule of glucose to form two molecules of pyruvate, there is a net yield of two molecules of ATP (Stryer, 1995).

1.1.5.2 Tricarboxylic Acid Cycle

After pyruvate, the end product of glycolysis, has been converted to acetyl-CoA in the mitochondrial matrix, acetyl-CoA enters the tricarboxylic acid cycle for further metabolism. The tricarboxylic acid (TCA) cycle is so called because citric acid, a form of tricarboxylic acid, is both an entry product and end product in this series of reactions thus, completing the cycle. Also commonly referred to as the Krebs cycle, after Sir Hans Adolf Krebs's discovery in the 1930's, the TCA cycle consumes acetate and water to generate CO_2 and the electron carriers NADH and $FADH_2$. Acetyl-CoA (two carbon) condenses with oxaloacetate (four carbon) to generate cycle intermediate citrate (six carbon). After a series of oxidation reactions, two carbon atoms leave the cycle in the form of two CO_2 molecules, and the four carbon oxaloacetate is regenerated. The TCA cycle is often described as an anaplerotic pathway in that pyruvate can be converted to acetyl-CoA (via pyruvate dehydrogenase) or to oxaloacetate (via pyruvate carboxylase) and so, ensures restoration of the TCA cycle intermediates (see Figure 3). The cycle can then continue and the overall products of the reaction, NADH and $FADH_2$, used to shuttle electrons across the electron transport chain.

1.1.5.3 Electron Transport Chain

The electron transport chain (ETC), also known as oxidative phosphorylation, utilises the electron carriers generated from the TCA cycle to shuttle electrons across the respiratory chain complexes, to maintain a H^+ concentration gradient across the inner mitochondrial membrane. Protons then flow back down the concentration gradient via ATP Synthase, thus generating ATP by oxidative phosphorylation in the process. The respiratory chain, situated on the inner

mitochondrial membrane, consists of five complexes, Complex I – V. Complexes I, III and IV are H^+ pumps, Complexes II and V however are not.

Electrons are first transported to Complex I (NADH Dehydrogenase) by NADH, where they are transferred onto coenzyme-Q (CoQ, also known as ubiquinone). CoQ then shuttles the electrons to Complex III (Ubiquinol-Cytochrome c Reductase). Both Complexes I and III are H^+ pumps and so, as the electrons are transferred onto the electron carriers, they are used to pump H^+ ions across the mitochondrial inner membrane, into the intermembrane space. This maintains a H^+ concentration gradient across the inner mitochondrial membrane. Complex II (Succinate Dehydrogenase) does not act as a H^+ pump, but functions as part of the TCA cycle, catalysing the conversion of succinate to fumarate, generating $FADH_2$ in the process. Electrons are then transferred from Complex II to Complex III by CoQ, the same electron carrier used to shuttle electrons from Complex I. Once at Complex III, electrons are transferred onto a different electron carrier, cytochrome c, and are subsequently shuttled across to Complex IV. Complex IV (Cytochrome c Oxidase) is the final H^+ pump in the ETC and catalyses the transfer of electrons from cytochrome c to molecular oxygen, the terminal acceptor. The electrochemical H^+ gradient generated by Complexes I, III and IV is used to generate ATP. As H^+ ions flow back down the protein gradient into the mitochondrial matrix, ADP is converted to ATP by oxidative phosphorylation, catalysed by Complex V (ATP Synthase). It is estimated that for every molecule of glucose metabolised, 38 molecules of ATP are generated in total: 32 molecules of ATP are produced by the electron transport chain, 2 molecules are produced by the Krebs cycle, and 4 molecules are produced by glycolysis. However, 2 molecules of ATP are used in glycolysis and so, the net gain of ATP molecules per molecule of glucose metabolised is 36 (Stryer, 1995).

All complexes of the respiratory chain, except Complex II, consist of many subunits that are both nuclear DNA (nDNA) and mitochondrial DNA (mtDNA) encoded. Complex II is the only complex that is entirely nDNA encoded. ATP generated by the ETC cannot diffuse from the mitochondrial matrix into the cell cytosol, but is instead exported by adenosine nucleotide translocator, ANT (Maechler & Wollheim, 2001) (refer to Figure 3).

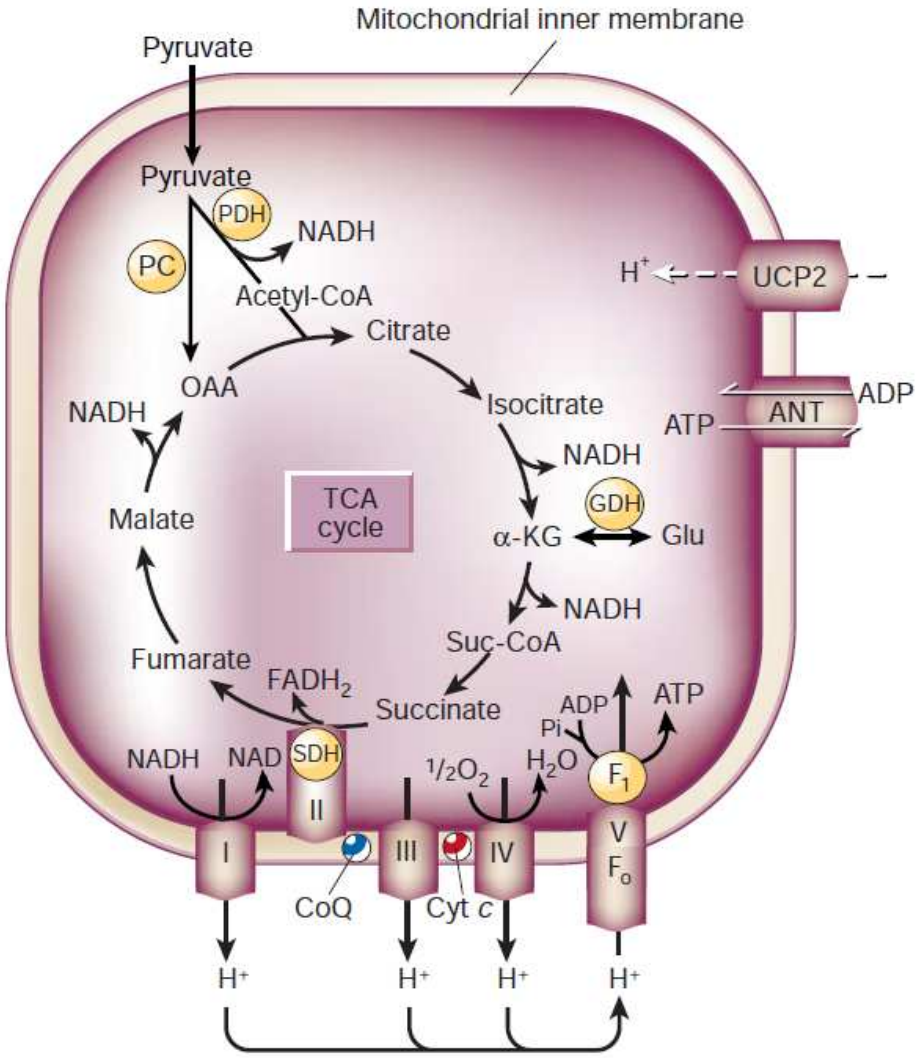

Figure 2 The tricarboxylic acid (TCA) cycle and the electron transport chain (ETC)

Pyruvate, generated from glycolysis in the cell cytosol, enters the mitochondrial matrix where it becomes converted to acetyl-CoA. Acetyl-CoA enters the TCA cycle, where a series of oxidation reactions generate the electron carriers NADH and $FADH_2$, which shuttle electrons across the ETC. The ETC is situated along the inner mitochondrial membrane and consists of five complexes, Complex I – V. Protons are pumped into the mitochondrial intermembrane space by Complexes I, III and IV. The H^+ ions then flow back down the proton gradient via Complex V, generating ATP by oxidative phosphorylation in the process. Complex II converts succinate to fumarate, both intermediate metabolites in the TCA cycle.

Figure taken from (Maechler & Wollheim, 2001).

1.1.6 Glucose-Stimulated Insulin Secretion

In pancreatic β-cells, glucose metabolism is closely associated with insulin secretion (Wollheim, 2000). There are two phases of insulin secretion. The first phase (acute or early insulin secretion) is instantaneous using intracellular vesicle stores of insulin, reaching a maximum level of secretion within 3 – 5 minutes and lasting for approximately 10 minutes (Porte, 2001). The second phase (late secretion) happens after first phase insulin secretion and relies on *de novo* insulin synthesis as well as intracellular insulin stores. It is gradual, in contrast to the short sharp first phase insulin release, and continues for as long as there is a glucose stimulus (Porte, 2001).

Metabolism of glucose by glycolysis, the TCA cycle and the ETC subsequently causes an increase in the ATP/ADP ratio in the cell cytosol, as ATP is released from the mitochondria. This rise in ATP promotes the closure of ATP-sensitive K^+ channels (K_{ATP}) on the β-cell plasma membrane. These K_{ATP} channels pump K^+ ions out of the cells giving the inside of the plasma membrane a more negative charge compare to the outside of the plasma membrane. Therefore, closure of the K_{ATP} channels causes plasma membrane depolarisation and subsequent opening of voltage-gated Ca^{2+} channels (Ashcroft *et al.*, 1994). This is a key step in glucose-stimulated insulin secretion. The increase in cytosolic Ca^{2+} as a result of Ca^{2+} channels opening induces the migration of intracellular insulin granules to the cell surface (Ashcroft *et al.*, 1994). Fusion of intracellular insulin vesicles with the plasma membrane promotes exocytosis and secretion of insulin from the β-cell. Several other additive signals are proposed to assist in this metabolism-secretion coupling, as indicated in Figure 3 (Maechler & Wollheim, 2001).

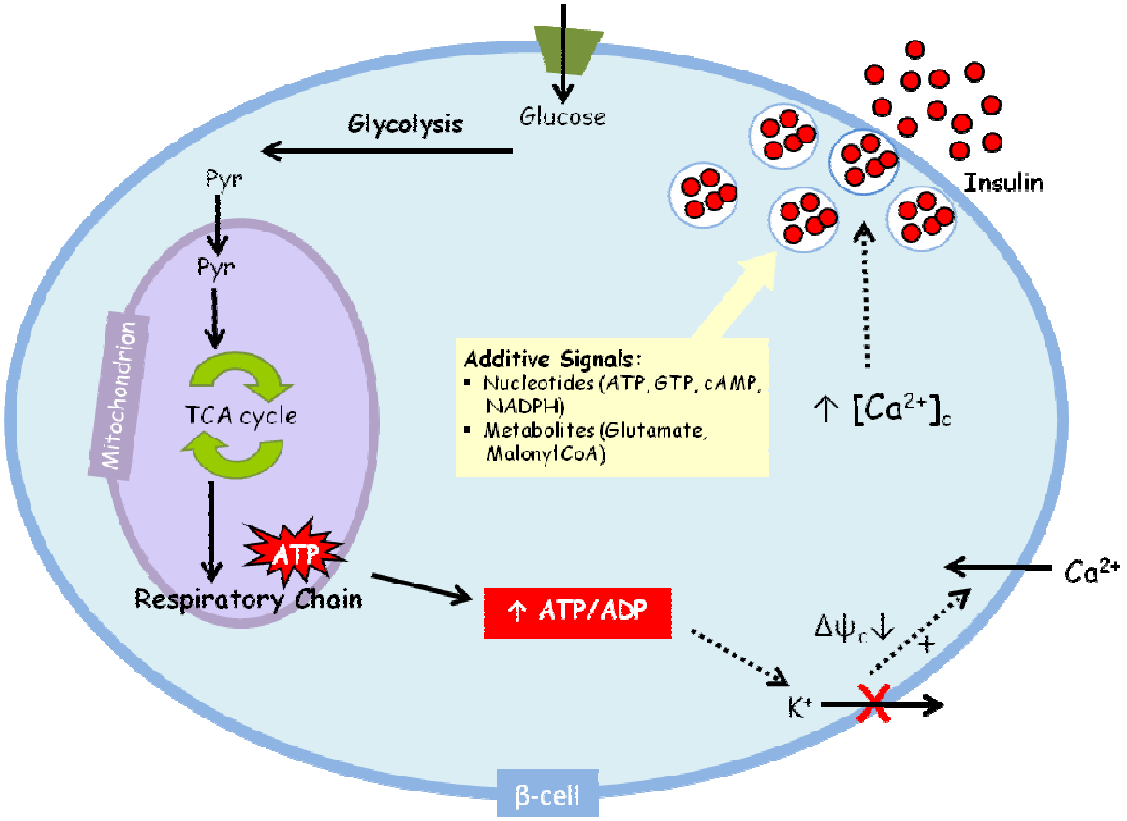

Figure 3 Model for glucose-stimulated insulin section (GSIS) in pancreatic β-cells

Glucose is taken up by the cell where it is then converted to pyruvate (Pyr) by glycolysis. Pyr then enters the mitochondria where it is converted to acetyl-CoA which is then able to enter the TCA cycle. The electron carriers generated in the TCA cycle (NADH and $FADH_2$) are then used to shuttle electrons along the respiratory chain located on the inner mitochondrial membrane, where ATP is generated by oxidative phosphorylation. ATP enters the cell cytosol, resulting in an increase in the ATP/ADP ratio and ultimately, depolarisation of the cell membrane via the closure of the ATP-sensitive K^+ channels. This causes an influx of Ca^{2+} ions, which subsequently promotes insulin exocytosis following vesicular fusion with the plasma membrane.

Figure adapted from (Maechler & Wollheim, 2001).

1.2 Mitochondria

1.2.1 Mitochondrial Structure and Function

The term mitochondria was derived from the Greek ‘mitos’, meaning thread, and ‘chondros’, meaning granule. The expression was originally coined by Carlos Benda back in 1898 whilst investigating spermatogenesis (Benda, 1898). Mitochondria are double membrane bound organelles often described as the ‘power packs’ of the cell, as they are the major source of cellular energy in the form of adenosine triphosphate (ATP). Mitochondria are divided into four main structural units: two membranes (inner and outer mitochondrial membrane) that enclose two aqueous spaces (intermembrane space and mitochondrial matrix respectively). The inner mitochondrial membrane is highly convoluted producing structures called cristae. The cristae give a large surface area in which oxidative phosphorylation can occur, as the components of the respiratory chain are embedded in the inner mitochondrial membrane. The outer mitochondrial membrane encloses the inner mitochondrial membrane, and produces the intermembrane space, the region between the two membranes. The second aqueous compartment, the mitochondrial matrix, is encompassed by the inner mitochondrial membrane and contains enzymes and metabolite intermediates required for the TCA cycle, as well as mtDNA (Stryer, 1995).

1.2.2 Mitochondrial DNA

Mitochondrial DNA (mtDNA) is a circular, double stranded DNA molecule of 16.6 kb in length in humans (Attardi & Schatz, 1988). It encodes only 37 genes, including 13 polypeptides essential for the respiratory chain, as well as RNA molecules required for the translation of these polypeptides within the mitochondria, including 22 transfer RNAs (tRNAs) and 2 ribosomal RNAs (rRNAs) (Maechler & Wollheim, 2001; Taylor & Turnbull, 2005) (Figure 4). The remaining protein components required to complete the respiratory chain complexes are nuclear encoded, as are the cellular machinery involved in mtDNA replication and maintenance. Human mtDNA is not inherited by traditional Mendelian genetics, but is instead maternally inherited. Also, unlike chromosomal nuclear DNA, there is more than one copy of the mitochondrial genome present within each cell (Taylor & Turnbull, 2005).

Like nuclear DNA, mtDNA is packaged into structures called nucleoids in order to maintain genetic stability. These nucleoid structures are thought to consist of several copies of mtDNA as well as a group of proteins believed to be involved in mtDNA replication including: mitochondrial transcription factor A (TFAM), mitochondrial single stranded binding protein (mtSSB) and the helicase Twinkle (Wang & Bogenhagen, 2006). The nucleoid structure of mtDNA has striking similarities to that of the nucleoid structure bacterial DNA. These similarities include both nucleoid structures being of approximately 70 nm in diameter, containing 5-7 genome copies per nucleoid as well as both nucleoid structures being anchored to the membrane (Clay Montier *et al.*, 2009). These similarities can be seen to support the endosymbiont hypothesis that strives to explain the origin of mtDNA.

1.2.3 The Endosymbiont Hypothesis

Mitochondria are believed to have evolved from an endosymbiotic relationship between a prokaryotic bacterium and a eukaryotic cell containing nDNA (Margulis, 1981; Gray, 1989). The endosymbiont hypothesis proposes that mitochondria and chloroplasts were originally descendants of the archaic eubacteria, more specifically from the cyanobacteria and α-purple bacteria phyla respectively (Gray, 1988). These bacteria then formed a close endosymbiotic relationship with an as yet unidentified nDNA-containing eukaryotic cell, and through a series of evolutionary process(es), have ultimately formed internal cellular organelles with their own distinct genome. This distinct genome is thus believed to be a remnant of the original archaic relationship. Mitochondria are semi-independent in that they are capable of mtDNA replication independent of the cell cycle but conversely, they are incapable of functioning autonomously (Gray, 1989).

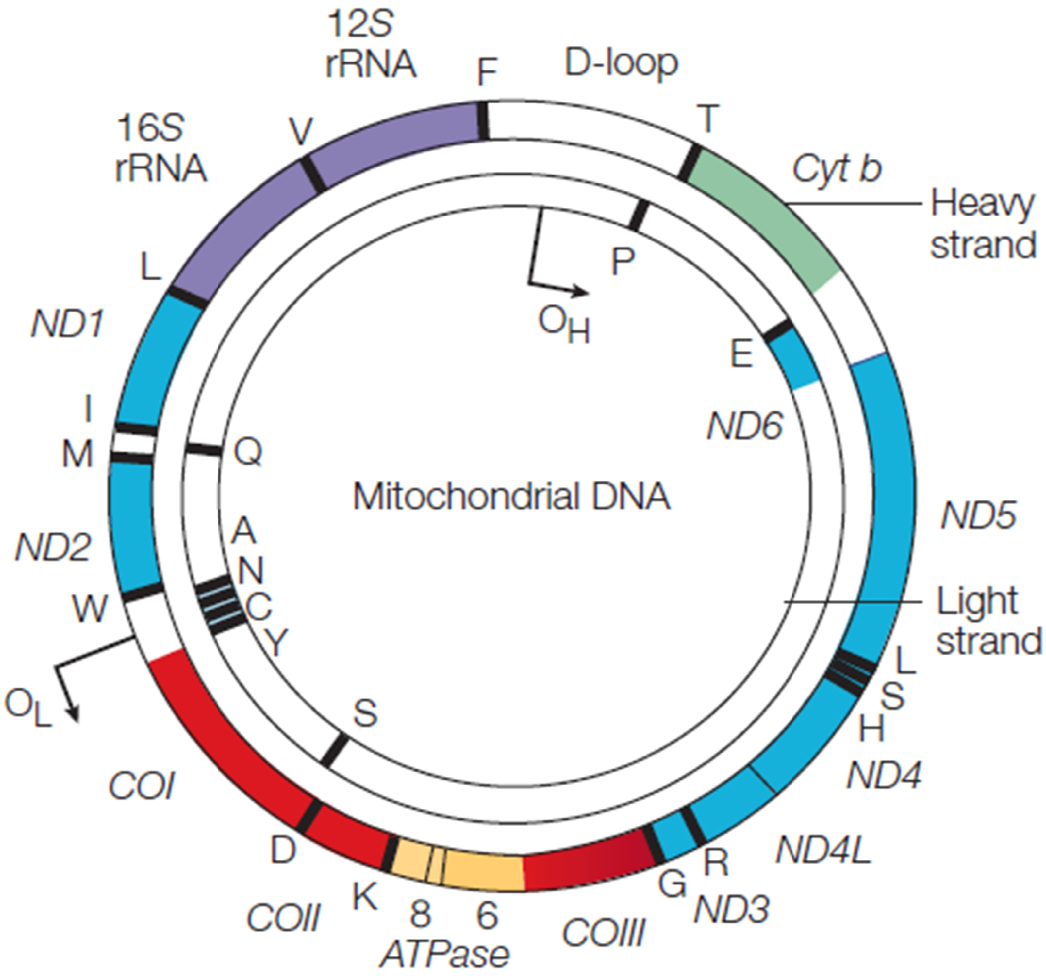

Key:

Components of Complex I (NADH Dehydrogenase)

Components of Complex III (Ubiquinol-Cytochrome c Reductase)

Components of Complex IV (Cytochrome c Oxidase)

Components of Complex V (ATP Synthase)

Ribosomal RNAs

Black lines and letters denote transfer RNAs

Figure 4 Human mitochondrial DNA (mtDNA) genetic map

Human mtDNA is a 16.6 kb circular, double stranded molecule located in the mitochondrial matrix. It encodes 13 polypeptides that are essential for oxidative phosphorylation. The other components of the respiratory chain are nuclear encoded, as are the components essential for the replication and maintenance of mtDNA. The displacement loop (D-loop) contains the heavy strand origin of replication (O_H), which is where mtDNA replication and transcription are thought to initiate. O_L; light strand origin of replication.

Taken from (Taylor & Turnbull, 2005).

1.2.4 mtDNA Replication and Transcription

Although it is widely accepted that the replication of mtDNA occurs independently of the cell cycle and hence, nuclear DNA replication (Bogenhagen & Clayton, 1977), the precise mechanism of mammalian mtDNA replication is still hotly debated. Two possible mechanisms elucidating the process of mtDNA replication have been proposed. The strand-displacement model was initially presented in 1982 (Clayton, 1982) and suggests that mtDNA replication is asynchronous and unidirectional. The model implies that replication of the leading, heavy (H) strand occurs first at an origin referred to as O_H, situated in the displacement (D)-loop region of mtDNA (Figure 4). This is then followed by replication of the lagging, light (L) strand, which begins when H-strand synthesis is about two-thirds complete, thus exposing the origin O_L and allowing L-strand synthesis to begin. The synthesis of H- and L-strands occur in opposing directions.

In 2000, however, Holt *et al.* suggested a mechanism of mtDNA replication that involves a coupling of both leading- and lagging-strand synthesis. This suggestion is supported by the groups' results, which were based on two-dimensional agarose gel electrophoresis (Holt *et al.*, 2000). These findings have been substantiated by additional investigations (Yang *et al.*, 2002; Bowmaker *et al.*, 2003).

The replication of mtDNA is tightly coupled to the mtDNA transcription and so, many of the key components involved in mtDNA transcription are utilised in mtDNA replication also. mtDNA transcription factor A (TFAM) is a mtDNA transcription factor thought to be involved in regulating mtDNA copy number as well as a key player in mtDNA transcription (Alam *et al.*, 2003; Ekstrand *et al.*, 2004). TFAM, together with RNA polymerase, binds mtDNA in order to synthesise an RNA primer. This primer is then processed by a mitochondrial RNA processing (MRP) complex and the processed primer is then used to help initiate mtDNA replication. The daughter mtDNA molecule is synthesised via DNA polymerase γ (POLG), a heterodimeric polymerase with proof-reading ability due to the catalytic subunit PolγA, and processivity capabilities due to the subunit PolγB (Carrodeguas *et al.*, 2001). mtDNA single-stranded binding (mtSSB) proteins bind single stranded mtDNA to prevent the mtDNA reverting

back to its natural double stranded form and promote mtDNA stabilisation. The helicase Twinkle has also been implicated in mtDNA replication, destabilising the mtDNA double helical structure prior to replication by utilising its 5'-3' helicase activity (Spelbrink *et al.*, 2001). These are the key components of mtDNA replication and transcription, and are also part of mtDNA nucleoids. All of these accessory proteins required for mtDNA transcription and replication are nuclearly encoded, perhaps suggesting an overall nuclear control of mtDNA.

1.2.5 Homoplasmy and Heteroplasmy

Mitochondrial DNA differs greatly from nuclear DNA in that it exhibits polyploidy: there is more than one complete copy of the mtDNA genome per cell. The mtDNA copy number can vary, but it is thought that there can be up to several thousand copies of the mtDNA genome per cell (Taylor & Turnbull, 2005). These mtDNA copies can be exact replicas of one another, homoplasmic, or they can exhibit slight variations between copies culminating in more than one mtDNA genotype, heteroplasmic.

The terms homoplasmy and heteroplasmy are generally used to describe various mutations of mtDNA and whether these mutations affect all copies of mtDNA within the cell (homoplasmic mutation) or only some copies (heteroplasmic mutation). Cells are still capable of functioning correctly up to a certain level of mtDNA mutation, or mutational threshold. Once the heteroplasmic mutational level exceeds this threshold, then the result is normally manifestation of disease symptoms due to possible disruption in biochemical and/or cellular processes (Taylor & Turnbull, 2005).

1.3 mtDNA Copy Number

1.3.1 mtDNA Threshold Effect

As mentioned previously, mtDNA is polyploid, and the multiple copies of mtDNA present per cell can be heteroplasmic or homoplasmic (Section 1.2.5). Heteroplasmic cells harbouring both mutant and wild type mtDNA can function normally, as long as the ratio of mutant to wild type mtDNA does not exceed a certain threshold. Once this threshold is surpassed, then the mutant mtDNA load may be visible as a phenotypic or biochemical defect (Rossignol *et al.*, 2003). This so called 'phenotypic threshold effect' has been shown in multiple patients and cell models (Moraes *et al.*, 1992; Sciacco *et al.*, 1994; Bai *et al.*, 2000).

Sciacco and colleagues took muscle biopsies from four patients with mitochondrial myopathy and using PCR, found the levels of deleted (Δ) mtDNA, exhibiting a common deletion of around 755 bp, varied amongst microdissected muscle fibres. In normal muscle fibres the levels of Δ-mtDNA were predicted to be around 31% ± 26. This was found to increase in diseased muscle fibres, with the levels of Δ-mtDNA reaching 95% ± 2. The group concluded that a mutant mtDNA load of >85% was needed to impair respiratory function (Sciacco *et al.*, 1994). Similarly, whilst investigating the A3243G point mutation in MELAS patients, Moraes *et al.* found that a mutant load greater than 90% caused mitochondrial proliferation in muscle fibres, culminating in the ragged red fibre phenotype associated with MELAS patients (Moraes *et al.*, 1992). Finally, Bai and colleagues showed that a nonsense mutation in ND5, a mtDNA encoded subunit of Complex I of the respiratory chain, resulted in decreased glutamate/malate dependent mitochondrial respiration when mutant mtDNA exceeded 40% of the overall mtDNA population (Bai *et al.*, 2000). Taken together, these studies indicate that mitochondrial dysfunction ensues only when the heteroplasmic ratio of mutant to wild type mtDNA exceeds a certain threshold.

1.3.2 Regulation of mtDNA Copy Number

In recent years, much insight has been gained with regards to mitochondrial function, genetics and biology; however, there are still gaps in our knowledge as

to the precise mechanism by which mtDNA copy number is regulated. There are several key proteins that have been implicated with the maintenance of mtDNA copy number, the main ones including mitochondrial transcription factor A, B1 and B2 (TFAM, TFB1M and TFB2M), nuclear respiratory factor 1 and 2 (NRF-1/-2), peroxisome proliferator-activator receptor-γ coactivator-1α (PGC-1α), and polymerase-γ (POLG).

1.3.3 Peroxisome Proliferator-Activator Receptor-γ Coactivator-1α (PGC-1α)

PGC-1α is a coactivator of peroxisome proliferator-activator receptor-γ (PPARγ), a ligand-activated transcription factor involved in adipogenesis (Tontonoz *et al.*, 1994), and is thought to mediate mitochondrial biogenesis. PCG-1α transcription is activated through many signalling pathways including cAMP, MAPK and nitric oxide (Figure 5) (Puigserver & Spiegelman, 2003). PGC-1α is known to confer transcriptional specificity by only interacting with, and activating, specific genes and transcription factors in certain cell types (Handschin & Spiegelman, 2006).

The regulation of PGC-1α transcription involves many external stimuli and differs from cell type to cell type. In brown adipose tissue (BAT), thermogenesis induces PGC-1α expression whereas in muscle, low ATP levels and exercise cause PGC-1α transcription. PGC-1α, once expressed, is capable of auto-regulating its own transcription and additionally, factors that bind PGC-1α further downstream, for example PPARγ, Foxo1 and MEF2, are also involved in the regulation of PGC-1α (Handschin & Spiegelman, 2006). Cyclic AMP response element (CRE) binding protein, CREB, is the main transcription factor involved in PGC-1α expression. It has been suggested that the proteasomal degradation pathways, as well as PGC-1α proteolysis by calpain proteins in response to increased Ca^{2+} levels, are responsible for the regulation of PGC-1α turn over (Rasbach *et al.*, 2008).

1.3.4 Nuclear Respiratory Factor 1 and 2 (NRF-1 & NRF-2)

NRF-1 and NRF-2 are nuclear encoded transcription factors thought to be activated by PGC-1α. Initially, NRF-1 was found to activate cytochrome c gene expression (Evans & Scarpulla, 1989) but in 1994, Virbasius and Scarpulla

reported that both NRF-1 and NRF-2 are responsible for activation of TFAM (Virbasius & Scarpulla, 1994). Virbasius and Scarpulla demonstrated that the TFAM proximal promoter requires interaction with the NRF-1 and NRF-2 recognition sites at guanine nucleotide contacts prior to activation. When these guanine nucleotide contacts were mutated, NRF-1 and NRF-2 binding was inhibited and promoter activity in the COS-1 transfected cells was dramatically reduced (Virbasius & Scarpulla, 1994). Both NRFs have also been implicated in the regulation of the mitochondrial transcription specificity factors, TFB1M and TFB2M (Gleyzer *et al.*, 2005).

1.3.5 Mitochondrial Transcription Factor B1 and B2 (TFB1M & TFB2M)

The essential mitochondrial transcription machinery required in order to initiate mtDNA transcription include: mitochondrial RNA polymerase (POLRMT), mitochondrial transcription factor B2 (TFB2M) and mitochondrial transcription factor A (TFAM) (Falkenberg *et al.*, 2002; Metodiev *et al.*, 2009). TFB2M and POLRMT first interact to form a heterodimer, before co-localising with TFAM on the mtDNA promoter (Falkenberg *et al.*, 2002). Mitochondrial transcription factor B1 is a paralogue of TFB2M, but is technically not a transcription factor *per se* (Metodiev *et al.*, 2009; Litonin *et al.*, 2010). Instead, TFB1M functions as a 12S rRNA methyltransferase, required for the integrity of the small mtDNA encoded ribosomal subunit (Metodiev *et al.*, 2009).

1.3.6 Mitochondrial Transcription Factor A (TFAM)

Mitochondrial transcription factor A, more commonly known as TFAM but previously known as mtTFA, is a transcription factor involved in the transcription and replication of mtDNA, as well as the regulation of mtDNA copy number. But the precise role of TFAM is still unknown. TFAM is nuclear encoded and upon activation, translocates from the nucleus to the mitochondria where it initiates mtDNA transcription and replication (Shadel & Clayton, 1993). There are three promoter regions in mtDNA: light strand promoter (LSP), heavy strand promoter 1 (HSP1) and heavy strand promoter 2 (HSP2); TFAM is thought to bind to the LSP and HSP1 promoters to initiate mtDNA gene transcription (Campbell *et al.*, 2012).

The mature human TFAM protein shares 78% homology with the murine TFAM protein (Kaufman *et al.*, 2007). TFAM is a 25 kDa high mobility group (HMG) protein, and contains two conserved HMG box domains of ~80 amino acids, which are found in many eukaryotic transcription factors and chromosomal proteins (Parisi & Clayton, 1991). The HMG domains, HMG box 1 and HMG box 2, facilitate TFAM binding to the minor grooves of mtDNA, enabling the transcription factor to bend mtDNA, thus allowing easier access for other proteins. Situated between the two HMG domains is the linker domain, responsible for strengthening TFAM/DNA binding by making additional contacts to the phosphodiester backbone of DNA (Campbell *et al.*, 2012). Downstream of the second HMG domain is the carboxyl (C)-terminal tail, believed to be important during initiation of mtDNA transcription (Ohgaki *et al.*, 2007). Overlapping the HMG box 2 domain and the C-terminal tail is the coiled-coil domain, implicated in TFAM homodimerisation (Kaufman *et al.*, 2007; Campbell *et al.*, 2012).

As well as having roles in mtDNA transcription, TFAM also has an important role in packaging mtDNA into nucleoids (Larsson, 2010). The TFAM protein is often described as exhibiting positive cooperativity, that is, when one TFAM protein binds to DNA, it encourages the binding of other TFAM proteins, possibly due to the DNA already having a kinked structure (Kaufman *et al.*, 2007). It has been suggested that TFAM binds to DNA as a homodimer at a stoichiometry of one TFAM homodimer per 37.2 bp and so, approximately 900 TFAM molecules per mtDNA genome (Campbell *et al.*, 2012). This high TFAM abundance is supported by other independent studies (Ghivizzani *et al.*, 1994; Dairaghi *et al.*, 1995; Kaufman *et al.*, 2007). Other groups have suggested that TFAM coats the entire length of mtDNA, much like a single stranded binding protein (Takamatsu *et al.*, 2002; Alam *et al.*, 2003; Ohgaki *et al.*, 2007). Conversely, low TFAM abundance has also been documented. In HeLa cells, it was predicted that there were only 50 TFAM proteins per mtDNA genome (Cotney *et al.*, 2007), and in HEK293 cells, a mere 35 TFAM proteins per mtDNA genome (Maniura-Weber *et al.*, 2004). Whether the abundance of TFAM molecules per mtDNA genome is specific to cell type remains to be elucidated.

In vivo studies looking at TFAM knockdown models have highlighted the importance of this protein. Larson *et al.* produced heterozygous and homozygous knockdowns of the *TFAM* gene in mice. They documented that the heterozygous mice had ~35-40% depletion in mtDNA, in comparison to the wild-type, as well as respiratory chain deficiency in the heart. The homozygous mice, however, failed to reach the end of gestation due to a severe depletion in mtDNA and serious respiratory chain deficiencies such as abolished oxidative phosphorylation (Larsson *et al.*, 1998). This was the first time TFAM was found to have a direct role in mitochondrial biogenesis *in vivo*. Since then, the same group have successfully knocked down TFAM expression in mice in various cell types including pancreatic β-cells (Silva *et al.*, 2000), cardiomyocytes (J. Wang *et al.*, 1999; Li *et al.*, 2000), skeletal muscle cells (Wredenberg *et al.*, 2002) and pyramidal neurones (Sorensen *et al.*, 2001).

In 2004, Erkstrand *et al.* linked TFAM function with direct regulation of mtDNA copy number in mammals. The group developed transgenic mice containing large genomic fragments harbouring the human *TFAM* gene. The resultant mice were found to ubiquitously overexpress the human TFAM protein, which resulted in a general increase in mtDNA copy number. Southern blotting was conducted to quantify the level of mtDNA relative to 18S nuclear DNA, and the result was an increase in mtDNA in heart, kidney and muscle cells of the transgenic mice overexpressing human TFAM when compared to wild-type mice (Ekstrand *et al.*, 2004).

The mechanism by which TFAM is able to regulate mtDNA copy number *in vivo* is still hotly debated. Two possible mechanisms have been proposed. The first involves transcription-mediated copy number control in which an increase in *TFAM* gene expression causes an increase in mtDNA transcription as the imported TFAM proteins target the LSP and promote priming for DNA synthesis (Campbell *et al.*, 2012). The second implies that the non-specific genome wide binding of TFAM to mtDNA is involved in regulating copy number as it stabilises mtDNA steady-state levels, possibly reducing mtDNA turnover (Campbell *et al.*, 2012).

1.3.7 Polymerase γ (POLG)

Polymerase γ (POLG) is the main DNA polymerase involved in mtDNA replication. The enzyme contains a polymerase domain and an exonuclease domain, thus enabling high-fidelity replication of mtDNA, with an estimated 1 error per 500,000 bp (Longley *et al.*, 2001; Lee & Johnson, 2006). There are over 80 pathogenic mutations in POLG in humans, which are often linked to the onset of progressive external ophthalmoplegia (PEO), Alpers syndrome and ataxia (Kujoth *et al.*, 2007). Most POLG mutations are recessive, but a few display dominant inheritance (Kujoth *et al.*, 2007). Mutations in POLG result in reduced polymerase fidelity as incorrect nucleotides are incorporated, or in large scale mtDNA deletions due to the polymerase stalling (Kujoth *et al.*, 2007).

Mouse models have been developed in which the exonuclease domain of POLG was rendered inactive following a point mutation, producing *Polg*^{D257A} knock-in mice with limited mtDNA proofreading ability (Trifunovic *et al.*, 2004; Kujoth *et al.*, 2005). Both groups were able to demonstrate that mtDNA replication error rates increased at least 3- to 5-fold (Trifunovic *et al.*, 2004), culminating in the accumulation of age-related mtDNA mutations. Not only that, but the mice also showed signs of premature ageing such as greying hair and hair loss, early loss of fertility, weight loss, as well as reduced bone density and muscle mass (Trifunovic *et al.*, 2004; Kujoth *et al.*, 2005). Kujoth *et al.* concluded that the accumulation of mtDNA mutations that promote apoptosis was to blame for the accelerated ageing seen in these mice (Kujoth *et al.*, 2005).

In summary, it is clear that PGC-1α, NRF-1/-2, TFB1M, TFB2M, TFAM and POLG all play important roles during the process of mitochondrial biogenesis, and these roles are all integrated. Figure 5 graphically summarises the process of mitochondrial biogenesis under the control of PGC-1α.

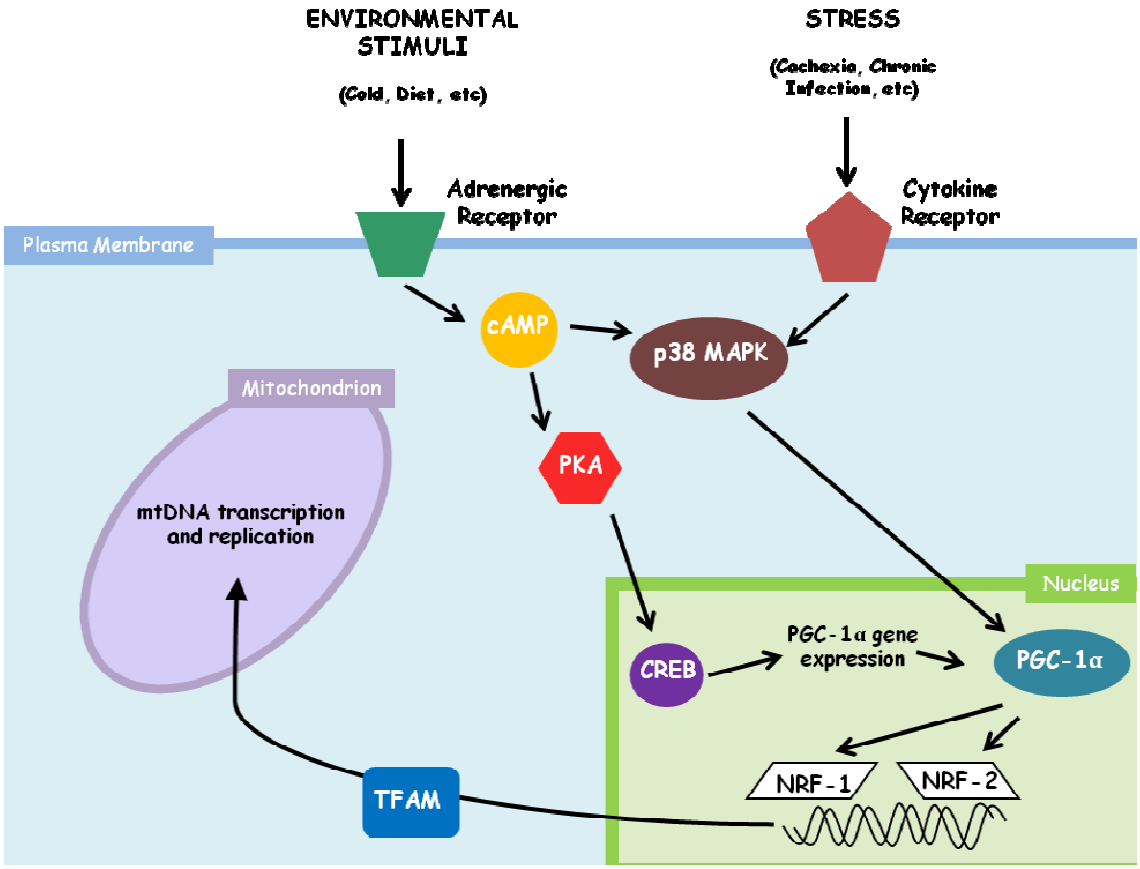

Figure 5 Potential model for mitochondrial biogenesis and gene expression

(1) Adrenergic or cytokine receptor activation triggers the PKA and p38 MAPK cell signalling cascades (2) Activated PKA phosphorylates the transcription factor, CREB, and the *PCG-1α* gene is transcribed (3) Activated p38 MAPK directly phosphorylates the PGC-1α protein, thus activating it (4) PGC-1α activates the NRFs resulting in TFAM transcription and activation (5) TFAM translocates to the nucleus culminating in transcription and replication of mtDNA. cAMP, cyclic adenosine monophosphate; PKA, protein kinase A; MAPK, mitogen-activated protein kinase; CREB, cAMP response element (CRE) binding protein; PGC-1α, peroxisome proliferator-activator receptor-γ coactivator-1α; NRF-1 and -2, nuclear response factors -1 and -2; TFAM, mitochondrial transcription factor A.

Figure adapted from (Puigserver & Spiegelman, 2003).

1.4 mtDNA Abnormalities and Diabetes

1.4.1 mtDNA Depletion and Pancreatic β-cell Function

There is an age-dependent progressive decline in β-cell function seen in the normal non-diabetic population (Basu *et al.*, 2003; Chang & Halter, 2003). The cause of this reduced β-cell function has been attributed in part to the effects of mtDNA depletion (Soejima *et al.*, 1996; E. D. Kennedy *et al.*, 1998; Silva *et al.*, 2000; Cree *et al.*, 2008). Severe mtDNA depletion has been produced in rodent pancreatic β-cells with the use of ethidium bromide (EtBr), an inhibitor of mtDNA replication (Soejima *et al.*, 1996; E. D. Kennedy *et al.*, 1998; Tsuruzoe *et al.*, 1998). EtBr-induced mtDNA depleted cells exhibited decreased glucose-stimulated insulin secretion, which was accredited to severe mitochondrial dysfunction, shown by reduced cytochrome c oxidase enzyme activity (Soejima *et al.*, 1996; E. D. Kennedy *et al.*, 1998; Tsuruzoe *et al.*, 1998). Similarly, Silva *et al.* (Silva *et al.*, 2000) produced tissue specific disruption of the *TFAM* gene in mouse pancreatic β-cells, which resulted in substantial mtDNA depletion compared to littermate control mice. Akin to the EtBr-induced mtDNA depletion studies, Silva *et al.* also showed that insulin secretion was reduced in mutant islets, which was accompanied by deficient cytochrome c oxidase activity; in addition to reduced mitochondrial membrane hyperpolarisation and impaired Ca^{2+} signalling.

A paper published during my studentship described how transcriptional silencing of the pancreatic duodenal homeobox 1 (*Pdx1*) gene *in vivo* in rat models resulted in partial mtDNA depletion (Gauthier *et al.*, 2009). PDX1 is a β-cell specific transcription factor believed to play a regulatory role in embryonic development and differentiated function (Servitja & Ferrer, 2004; Oliver-Krasinski & Stoffers, 2008). It was shown that PDX1 deficiency causes mitochondrial dysfunction as well as defective insulin secretion, which was postulated to occur through TFAM suppression. These findings were further confirmed following adenoviral overexpression of TFAM, which was found to increase mtDNA copy number, mitochondrial function and insulin secretion (Gauthier *et al.*, 2009). However, in view of the critical role of PDX1 in global β-cell function, it remains to be determined whether targeted TFAM knockdown and partial mtDNA depletion affects insulin secretion.

The impaired stimulus-secretion coupling reported in these studies is due to a defective electron transport chain and loss of mitochondrial ATP production, as a result of the loss of mtDNA encoded subunits following mtDNA depletion (Soejima *et al.*, 1996; E. D. Kennedy *et al.*, 1998; Tsuruzoe *et al.*, 1998). Glucose-stimulated insulin secretion was restored following treatment with agents that increased intracellular Ca^{2+} concentration such as the depolarising agent KCl (E. D. Kennedy *et al.*, 1998) or the insulin secretagogue glibenclamide (T. Hayakawa *et al.*, 1998; Tsuruzoe *et al.*, 1998), thus demonstrating that the cause of impaired stimulus-secretion coupling was mitochondrial in origin.

Taken together, these studies indicate that mtDNA depletion, whether partial or severe, drastically affects pancreatic β-cell function by causing reduced insulin secretion as well as mitochondrial dysfunction.

1.4.2 mtDNA Mutations and Diabetes

Mitochondrial DNA mutations are thought to account for approximately 1% of all diabetes cases (Maassen *et al.*, 2001) and there is evidence to show an increased prevalence of diabetes in patients with inherited mtDNA abnormalities (Maassen *et al.*, 2004). The most common mtDNA mutation associated with diabetes is the A3243G mutation in the $tRNA^{Lys(UUR)}$ gene. This A→G transition at nucleotide 3243 is thought to prevent transcription termination, as this is the recognition site for a protein involved in terminating transcription of rRNA genes (Christianson & Clayton, 1986; Kruse *et al.*, 1989). The A3243G mutation was first discovered in patients with mitochondrial myopathy, encephalopathy lactic acidosis, stroke-like episode (MELAS), a progressive neurodegenerative disorder with diabetes often seen as an accompanying symptom (Goto *et al.*, 1990). But the mutation has also been implicated in the onset of maternally inherited diabetes and deafness (MIDD) (van den Ouweland *et al.*, 1992). The exact biochemical consequences of the A3243G mutation are unknown, but the diabetogenic nature of the A3243G mutation has been hypothesised by a reduction in the cytosolic ATP/ADP ratio, culminating in impaired insulin secretion (Maassen *et al.*, 2004). Indeed, impaired insulin secretion is a key characteristic of diabetic patients with mtDNA abnormalities (Lynn *et al.*, 2003). Maassen *et al.* showed carriers of the A3243G mutation to exhibit an impaired first and second phase insulin response to a 10 mmol/l hyperglycaemic clamp,

when compared to non-carriers of the mutation (Maassen *et al.*, 2004). A key finding from the study by Lynn *et al.* was that there was a low percentage ratio of A3243G mutated to wild type mtDNA in β-cells (<25%) compared to other tissues examined such as muscle (60%) and brain (66-78%). These findings suggest that there is an increased susceptibility in β-cells to mitochondrial dysfunction (Lynn *et al.*, 2003).

1.4.3 Mitochondrial Dysfunction and T2DM

T2DM has been associated with β-cell specific knockdown of the mitochondrial transcription factor TFAM, in which diabetes presented in the TFAM knockout mice from 5 weeks of age (Silva *et al.*, 2000). Interestingly, Silva *et al.* also demonstrated that the phenotype of the TFAM knockout mice changed with time. The group observed that young mutant mice (7 weeks of age) were diabetic with normal β-cell mass, whereas older mutant mice (>14 weeks of age) remained diabetic, but were seen to have reduced β-cell mass, suggesting that impaired insulin secretion occurs at younger ages. The group were able to conclude that during the progression of mitochondrial diabetes, there is first an impaired stimulus-secretion coupling in mutant cells, which is followed by β-cell loss (Silva *et al.*, 2000).

T2DM has also been associated with a common gene variant in mitochondrial transcription factor B1 (TFB1M), a mtDNA methyltransferase (Koeck *et al.*, 2011). The rs950994 risk allele correlated with reduced insulin secretion, elevated postprandial glucose levels and increased risk of developing T2DM (Koeck *et al.*, 2011). In addition, it has been postulated that an age-dependent deterioration of β-cell function is to blame for the onset of diabetes in carriers of the A3243G mutation, rather than a cellular resistance to insulin (Maassen *et al.*, 2004).

1.5 Mitochondrial Dysfunction and Ageing

1.5.1 Free Radical Theory of Ageing and Reactive Oxygen Species (ROS)

In 1956, Denham Harman proposed the free radical theory of ageing from his observations on radiation and reactive oxygen species (ROS). Harman was the first to advocate that ageing, and age-related degenerative diseases, may be

the result of cellular oxidative damage from endogenously generated ROS (Harman, 1956). It was not until McCord and Fridovich's discovery of the superoxide scavenger enzyme superoxide dismutase in 1969, that Harman's free radical theory of ageing was considered seriously (J. M. McCord & Fridovich, 1969; Balaban *et al.*, 2005). Further investigations have corroborated Harman's original theory, and current understanding is that metabolic rate and resultant generation of ROS are the cause of ageing in man, due to the accumulation of cell oxidative damage with age (Balaban *et al.*, 2005).

Reactive oxygen species (ROS) are very small, highly reactive molecules. They are predominantly generated by the mitochondria (estimated around 90%) however, other sources of ROS generation include peroxisomal lipid metabolism, cyclooxygenase enzymatic activity as well as plasma membrane bound NADPH oxidase activity (Balaban *et al.*, 2005). In the mitochondria, the main sites of ROS generation are thought to be at Complex I and Complex III on the respiratory chain, when electrons react with free molecular oxygen, producing free radicals (Balaban *et al.*, 2005).

Natural defences against ROS include the enzyme superoxide dismutase (SOD) as well as antioxidants such as vitamin E, uric acid and vitamin C. The scavenging enzyme SOD functions by converting superoxide molecules into oxygen and hydrogen peroxide, H_2O_2 (J. M. McCord & Fridovich, 1969; J.M. McCord & Fridovich, 1988). H_2O_2 is then broken down further by the catalase enzyme to form oxygen and hydrogen, which have a much less damaging effect on cells.

1.5.2 Role of mtDNA mutations and oxidative damage in ageing

mtDNA mutations can culminate in a variety of clinical disorders, mainly because mitochondria are ubiquitously expressed in most cell types. Some of the main disorders associated with mtDNA mutations are categorised in Table 2. Holt *et al.* were the pioneering group to link deletions in mtDNA with the onset of human disease in 1988 (Holt *et al.*, 1988). Patients with mutations in nuclear encoded genes involved in oxidative phosphorylation or mtDNA maintenance are thought to develop symptoms similar to patients with mitochondrial disorders (Shoubridge, 2001; Zhu *et al.*, 2009), indicating the importance of mtDNA maintenance in disease progression also. The majority of

mtDNA deletions occur in the major arc of the mtDNA genome, which is between O_H, nucleotides 110-441, and O_L, nucleotides 5721-5798 (He *et al.*, 2002) (see Figure 4).

The formation of 8-oxo-2'-deoxyguanosine (oxo^{8}dG), a known product of radiation damage, has commonly been used as a biomarker of DNA oxidative damage, where increased levels of DNA damage and hence oxo^{8}dG formation, are found to correlate with increasing age (Balaban *et al.*, 2005). An age-dependent accumulation of oxo^{8}dG has been reported in human skeletal muscle (Zhang *et al.*, 1998) and human diaphragm muscle (M. Hayakawa *et al.*, 1991). The levels of oxo^{8}dG were found to be significantly higher in mtDNA compared to nDNA of rat liver tissue (Richter *et al.*, 1988). The general consensus is that this is because mtDNA are more prone to oxidative damage, which could result in mutations, because of their close proximity to the major source of ROS generation, the electron transport chain. This is not helped by the fact that there is a distinct lack of mtDNA repair mechanisms and so, when mutations do occur, they are not always corrected (Clayton *et al.*, 1974; Richter, 1988).

It is widely accepted that mtDNA base-substitution mutations also accumulate with advancing age in multiple tissues and species, including rodents, rhesus monkeys and humans (Kujoth *et al.*, 2007; Larsson, 2010). The age-dependent accumulation of these point mutations has been attributed to ROS-induced oxidative damage or replication errors caused by POLG (Michikawa *et al.*, 1999).

However, there is emerging evidence that argues that mutations in mtDNA are not solely the result of oxidative damage, but could be the consequence of errors in replication, thus implicating POLG (Madsen *et al.*, 1993; Zheng *et al.*, 2006; Larsson, 2010).

mtDNA Disorder	Clinical Phenotype	Mutation	Gene	Hetero- or Homoplasmic	Mode of Inheritance
Kearns-Sayre syndrome	Progressive myopathy, opthalmoplegia, cardiomyopathy	Single large-scale deletion	Several deleted genes	Heteroplasmic	Usually sporadic
Pearson syndrome	Pancytopoenia, lactic acidosis	Single large-scale deletion	Several deleted genes	Heteroplasmic	Usually sporadic
MELAS	Myopathy, encephalopathy lactic acidosis, stroke-like episode	3243A>G 3271T>C	*TRNL1*	Heteroplasmic	Maternal
		Individual mutations	*ND1* & *ND5*	Heteroplasmic	Maternal
MIDD	Diabetes, deafness	3243A>G	*TRNL1*	Heteroplasmic	Maternal
LHON	Optic neuropathy	3460G>A	*ND1*	Hetero/Homoplasmic	Maternal
		11778G>A	*ND4*	Hetero/Homoplasmic	Maternal
		14484T>C	*ND6*	Hetero/Homoplasmic	Maternal
Myopathy and diabetes	Myopathy, weakness, diabetes	14709T>C	TRNE	Hetero/Homoplasmic	Maternal
MILS	Progressive brain stem disorder	8993T>C	*ATP6*	Heteroplasmic	Maternal
MERRF	Myoclonic epilepsy, myopathy	8344A>G 8356T>C	*TRNK*	Heteroplasmic	Maternal

Table 2 Conditions that have been linked to mutations in mtDNA

This table has been adapted from (Taylor & Turnbull, 2005) and details some of the diseases that can manifest as a result of mtDNA mutation. MELAS: Mitochondrial myopathy, encephalopathy lactic acidosis, stroke-like episode; MIDD: maternally-inherited diabetes and deafness; LHON: Leber hereditary optic neuropathy; MILS: maternally-inherited Leigh syndrome; MERRF: myoclonic epilepsy and ragged-red fibres.

1.5.3 Mitochondrial Dysfunction Increases with Age

It is widely documented that mitochondrial dysfunction increases with advancing age (Shigenaga *et al.*, 1994; Balaban *et al.*, 2005). This may be owing to the age-dependent accumulation of mutations caused by oxidative damage to mtDNA. For example, in COX1 deficient cells, cells devoid of the mtDNA encoded cytochrome c oxidase subunit 1 (COX1) of Complex IV, there are high levels of mutant mtDNA (Sciacco *et al.*, 1994; Moslemi *et al.*, 1996). The high level of mutant mtDNA in COX1 deficient cells is possibly due to clonal expansion of individual deletions/point mutations (He *et al.*, 2002). These COX1 deficient cells have been shown to have severe respiratory chain dysfunction (Sciacco *et al.*, 1994; Moslemi *et al.*, 1996). It has also been shown that accumulation of COX1 deficient cells correlates with advancing age (Muller-Hocker, 1990; Cottrell, Blakely, Johnson, Ince, Borthwick*, et al.*, 2001).

There is thought to be a mosaic respiratory chain deficiency in ageing (Larsson, 2010). Mitochondrial DNA replication occurs independently of the cell cycle (Bogenhagen & Clayton, 1977) and so, one molecule of mtDNA can be replicated multiple times, or not at all. This clonal expansion of mtDNA explains how some daughter cells exhibit respiratory function and some do not: because they contain different levels of mutated mtDNA. As discussed in Section 1.3.1, the levels of mtDNA mutation need to exceed the mtDNA threshold before we see their phenotypic effects on the respiratory chain. This theory is supported by studies that show mosaicism of respiratory chain deficiency in various ageing human tissues including heart (Muller-Hocker, 1989), skeletal muscle (Fayet *et al.*, 2002), neurones (Cottrell, Blakely, Johnson, Ince, & Turnbull, 2001; Bender *et al.*, 2006), and colon (Taylor *et al.*, 2003).

1.5.4 mtDNA Copy Number Depletion and Ageing

In addition to mutations or deletions in mtDNA being associated with advancing age, there is also a body of evidence linking decreased mtDNA abundance with ageing (Laderman *et al.*, 1996; Barazzoni *et al.*, 2000; Short *et al.*, 2005; Kaaman *et al.*, 2007; Cree *et al.*, 2008; Hartmann *et al.*, 2011). An age-related decline in mtDNA copy number has been reported in various human tissues including skeletal muscle (Welle *et al.*, 2003; Short *et al.*, 2005; Menshikova *et al.*, 2006; Lanza *et al.*, 2008), pancreatic islets (Cree *et al.*, 2008), fibroblasts (Laderman *et al.*, 1996) and adipocytes (Kaaman *et al.*, 2007). In human pancreatic islets for example, mtDNA copy number was significantly reduced in non-diabetic islet donors aged ≥50 years compared to donors aged ≤50 years. The mean mtDNA copy number was found to decrease by 50% in individuals aged between 17 and 75 years of age (see Figure 6).

These findings have been replicated in rodent (Barazzoni *et al.*, 2000) and fish (Hartmann *et al.*, 2011) animal models, investigating the mtDNA abundance in various extracted tissues. But it seems the mtDNA loss seen with age may be tissue specific, as Barazzoni *et al*. reported a significant age-dependent reduction in mtDNA copy number in rat skeletal muscle and liver, but mtDNA levels remained the same in aged heart (Barazzoni *et al.*, 2000). Similarly, Hartman *et al.* reported that mtDNA copy number was significantly reduced in fish muscle, liver, brain, skin and dorsal fin tissues, but remained unchanged with advancing age in kidney, gill, eye or spleen (Hartmann *et al.*, 2011).

It is known that various conditions can affect mtDNA copy number, which may explain the tissue specific effect of age-dependent changes in mtDNA copy number. For example, cardiac hypertrophy, a condition in which there is an increase in cardiac muscle mass, is commonly associated with ageing in humans and rodents (Lakatta, 1993). Artificially-induced cardiac hypertrophy was found to increase the mtDNA content in chickens (J. M. Kennedy *et al.*, 1991) and rats (Meerson & Pomoinitsky, 1972; Rajamanickam *et al.*, 1979). It has also been shown that endurance exercise can increase both mitochondrial density (Holloszy & Coyle, 1984) and mtDNA content (Menshikova *et al.*, 2006; Lanza *et al.*, 2008) in human skeletal muscle. Therefore, these are considerations that need to be taken into account when analysing the mtDNA abundance of specific tissues.

Conversely, there are also reports that mtDNA copy number does not change in ageing human heart or skeletal muscle (Miller *et al.*, 2003), or increases with age in fibroblast cell culture (Shmookler Reis & Goldstein, 1983) and human neurones (Barrientos *et al.*, 1997). Although Schmookler Reis and Goldstein reported an increase in mtDNA abundance in late passage fibroblast cells compared to early passage fibroblasts, it was also reported that late passage cells were generally of a greater mass than younger passage cells and so, when mtDNA was normalised to volume of cytoplasm or protein mass, passage-dependent increases in mtDNA abundance were eradicated (Shmookler Reis & Goldstein, 1983). Similarly, Barrientos *et al.* also showed that mtDNA copy number increases with age, but the group also demonstrated that mtDNA transcript levels decreased with advancing age, so could the increase in mtDNA copy number compensate for the loss of mtDNA transcription? And is this a cell specific trait? (Barrientos *et al.*, 1997).

In summary, a reduction in mtDNA abundance has been reported to correlate with advancing age (Laderman *et al.*, 1996; Barazzoni *et al.*, 2000; Short *et al.*, 2005; Kaaman *et al.*, 2007; Cree *et al.*, 2008; Hartmann *et al.*, 2011). However, there are also contradictory reports whereby mtDNA copy number does not change (Barazzoni *et al.*, 2000; Miller *et al.*, 2003; Hartmann *et al.*, 2011), or increases with advancing age (Shmookler Reis & Goldstein, 1983; Barrientos *et al.*, 1997). These conflicting reports may be due to tissue specific responses to ageing. But it has been reported that there is an age-dependent reduction in mtDNA copy number in human islets (Cree *et al.*, 2008).

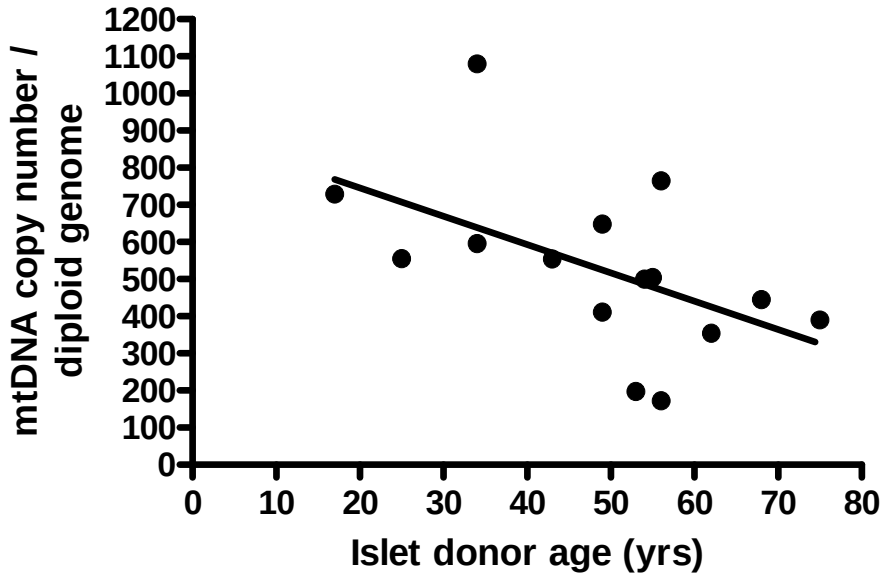

Figure 6 Relationship between mtDNA copy number and islet donor age

These data are taken from (Cree *et al.*, 2008). The group investigated the relationship between mtDNA copy number and age in isolated clinical grade human islet preparations from 15 non-diabetic donors. The group were able to demonstrate that the mean mtDNA copy number declined by around 50% in non diabetic islet donors aged between 17 and 75 years of age (r^2 = -0.53, p=0.04).

1.5.5 Artificial mtDNA Depletion

Loss of mtDNA copy number in cell lines has previously been achieved following chemical intervention using inhibitors of mtDNA replication, most commonly ethidium bromide (Chandel & Schumacker, 1999; Singh, 2006; Magda *et al.*, 2008). Cells were chemically treated for prolonged periods of time to produce p^0 cells that are completely devoid of mtDNA, also known as rho^0 cells. As mtDNA encodes key components of the respiratory chain, these p^0 cells are typically incapable of aerobic respiration, becoming dependent on pyruvate and uridine for growth (King & Attardi, 1989). Previous studies in pancreatic β-cells found that mitochondrial transcription, translation and insulin secretion were greatly impaired in p^0 cells compared to untreated control cells (Soejima *et al.*, 1996).

1.5.6 Nucleoside Reverse Transcriptase Inhibitors (NRTIs)

Ethidium bromide is capable of intercalating with any double stranded DNA, including nDNA. Therefore, more specific chemical treatments are being deployed to reduce mtDNA copy number, including nucleoside reverse transcriptase inhibitors (NRTIs). NRTIs are nucleoside analogues of the naturally occurring nucleotides used in the replication of viral DNA: adenosine, thymidine, guanosine, cytidine and uridine. They are a family of chemicals used to treat patients suffering from the human immunodeficiency virus (HIV). NRTI triphosphates were originally synthesised in the 1960s (Mitsuya *et al.*, 1990), but it was in 1987 that the Food and Drug Administration (FDA) first approved clinical use of the first NRTI, zidovudine (AZT), to treat HIV patients (FDA, 2009). There are now seven NRTIs approved by the FDA for the treatment of HIV: zidovudine (AZT), didanosine (ddI), zalcitabine (ddC), stavudine (d4T), lamivudine (3TC), abacavir (ABC) and emtricitabine (FTC) (Höschele, 2006).

By targeting the HIV reverse transcriptase (HIV-RT) enzyme, NRTIs prevent viral DNA replication and halt disease progression. NRTIs preferentially target HIV-RT, but they are also known to have high affinity for POLG (Kakunda, 2000; Lewis *et al.*, 2003). There seems to be a hierarchy of NRTI affinity for certain polymerases: HIV-RT >> POLG > DNA pol-β > DNA pol-α = DNA pol-ε (Kakunda, 2000; Lewis *et al.*, 2003). There also seems to be a hierarchy of

NRTI influence on POLG inhibition: zalcitabine (ddC) ≥ didanosine (ddI) ≥ stavudine (d4T) > lamivudine (3TC) > zidovudine (AZT) > abacavir (ABC) (Kakunda, 2000).

Several mechanisms of POLG inhibition have been proposed. These include NRTI competition with naturally occurring dNTPs; mtDNA daughter strand termination following NRTI incorporation; the incorporated NRTI molecule being resistant to exonucleolytic removal by POLG; and the cellular accumulation of monophosphorylated forms of the NRTI drug, thus inhibiting the exonucleolytic activity of POLG (Lewis, 2003). Inhibition of this polymerase ultimately culminates in mtDNA synthesis impairment, which is believed to be the perpetrator in NRTI-induced mitochondrial toxicity, a symptom seen in HIV patients undergoing highly active antiretroviral therapy (HAART) (Hoschele, 2006; Lee, 2003).

Indeed, one of the major issues with long term NRTI treatment is mitochondrial toxicity. In a mouse study, it was shown that long term treatment with AZT resulted in oxidative damage in liver mtDNA (de la Asuncion *et al.*, 1999). NRTI-induced mitochondrial oxidative damage has also been shown in rats (Szabados *et al.*, 1999) and cell lines (Yamaguchi *et al.*, 2002). It has even been reported that some HIV strains have started to develop a resistance to AZT treatment (Mitsuya *et al.*, 1990). Long term NRTI use has also been implicated with insulin resistance in HIV-infected women (Tien *et al.*, 2008). Tien *et al.* investigated insulin resistance in a cohort of 2870 women from a variety of ethnic backgrounds, between 2000 and 2007. Insulin resistance was calculated using the homeostatic model assessment (HOMA) model, in which fasting glucose and insulin levels were inputted into a mathematical equation. The group concluded that there was a positive correlation between the number of years of stavudine use and insulin resistance in HIV-infected women, with insulin resistance increasing at a rate of 6% per additional year of stavudine treatment. It is interesting to note that 284 patients were actually excluded from this study after developing T2DM (Tien *et al.*, 2008). This study is supported by other reports demonstrating a relationship between insulin resistance and duration of NRTI use, and like the Tien *et al.* study, a proportion of the HIV-infected patients studied were already diagnosed with T2DM (Hadigan *et al.*, 2001; Brown *et al.*, 2005; Lo *et al.*, 2005). Hadigan *et al.* demonstrated that

hyperinsulinaemia was greater in HIV-infected patients receiving HAART compared to non-HIV-infected control individuals (Hadigan *et al.*, 2001). Lo *et al.* illustrated that HIV patients receiving NRTI therapy had high lactate levels (hyperlactataemia), possibly due to the increase in lactate production as glucose is metabolised via glycolysis as a result of NRTI-induced mitochondrial toxicity (Lo *et al.*, 2005).

These studies show that long term usage of NRTI triphospahtes prevents the pathogenesis of HIV, but at the cost of mitochondrial toxicity with long term NRTI exposure.

1.5.6.1 Didanosine (ddI)

Didanosine (ddI), one of the seven FDA approved NRTIs for the treatment of HIV, is a nucleoside analogue of adenosine. When ddI enters the cell, it is converted to its active form dideoxyadenosine triphosphate (ddATP) through a series of phosphorylations. This active form of ddI then competes with the active form of adenosine, deoxyadenosine triphosphate (dATP) for incorporation into the newly synthesised DNA strand (Mitsuya *et al.*, 1990; Lewis *et al.*, 2003). Newly incorporated nucleosides are attached to the growing DNA daughter strand by phosphodiester linkages, which occur between the 5' phosphate group of one nucleoside and the 3'-OH group of the adjacent nucleoside. As ddI lacks the 3'-OH group required for phosphodiester linkage, strand termination ensues following ddI incorporation (Mitsuya *et al.*, 1990) (Figure 7).

Didanosine is one of the more potent inhibitors of POLG (Kakunda, 2000), but it is also one of the less cytotoxic (Lake-Bakaar *et al.*, 2001). Whilst investigating the effect of various NRTIs on human pancreatic Capan-1 cells, Lake-Bakaar *et al.* concluded that ddI, and its intracellular metabolite ddA (dideoxyadenosine), caused least cytoxicity compared to the other three NRTIs investigated. All NRTIs studied had an effect on mtDNA elongation as expected, but of all the parameters measured, including cell proliferation, ATP content, lactate release into culture medium, and oxygen consumption, ddI seemed to exhibit less cytotoxic effects in the Capan-1 cells (Lake-Bakaar *et al.*, 2001).

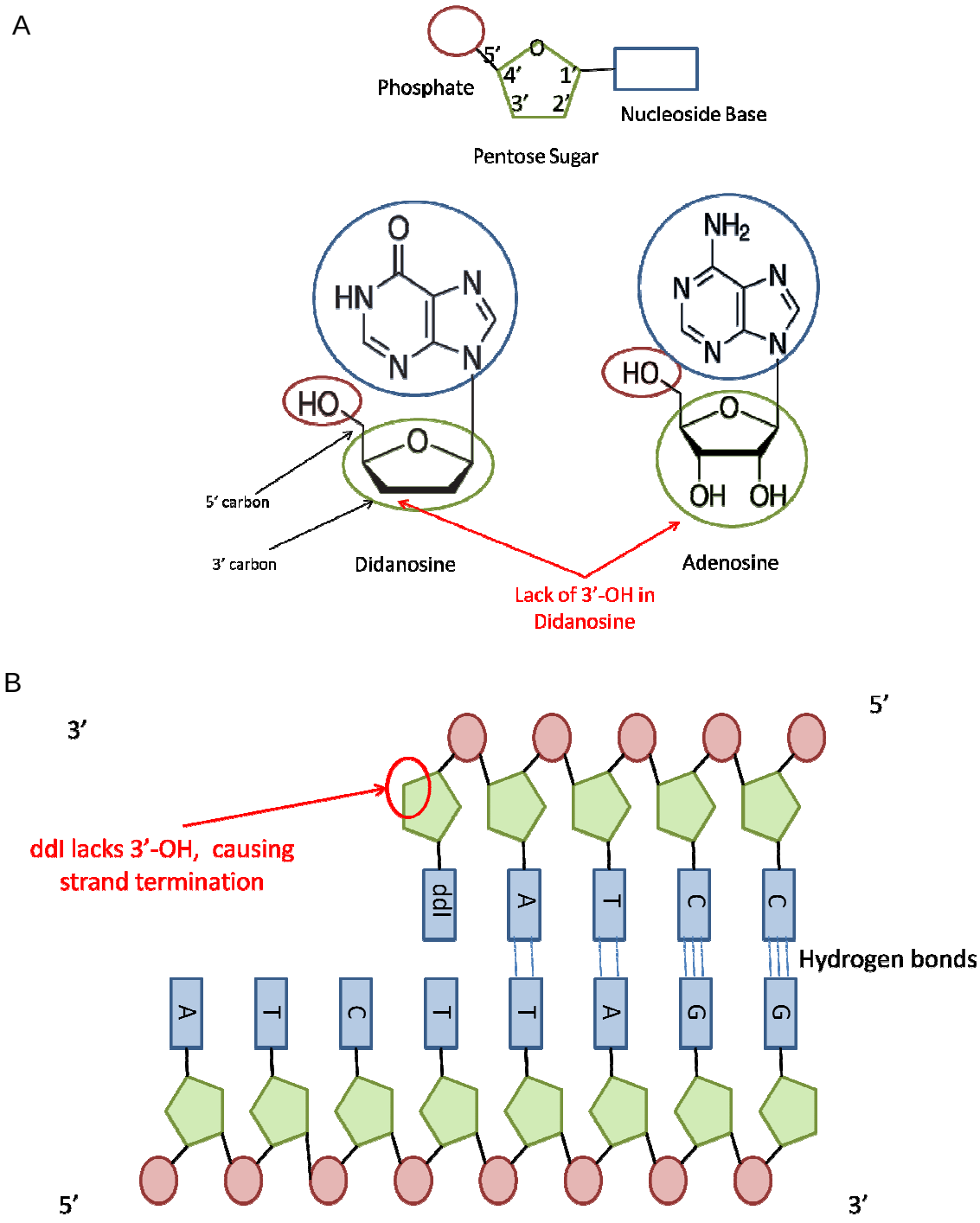

Figure 7 Didanosine structure and mechanistic action

(A) Didanosine (ddI) is a nucleoside reverse transcriptase inhibitor (NRTI) and an analogue of the nucleoside adenosine. (B) Once in the cell, ddI is metabolised to its active moiety, dideoxyadenosine triphosphate (ddATP), which competes with native deoxyadenosine (dATP) during DNA replication. As ddI lacks the hydroxyl (OH) group on the 3' carbon of the pentose sugar, this prevents the formation of the phosphodiester linkage needed to join adjacent nucleosides together on the newly synthesised DNA strand, resulting in strand termination. As well as the HIV-reverse transcriptase enzyme, ddI also has high affinity for polymerase-γ (POLG), the polymerase responsible for the replication of mtDNA.

1.6 Aims

The principal aim of this work was to investigate the hypothesis that an age-related decline in mtDNA copy number in pancreatic β-cells contributes to the decrease in insulin secretion seen with advancing age.

To explore this hypothesis, we aimed to satisfy the following objectives:

- To develop models of mtDNA depletion using the mouse pancreatic β-cell line, MIN6.
- To use these models to explore the effect(s) of mtDNA depletion upon indices of β-cell function, including insulin synthesis and secretion, mitochondrial function and cell proliferation.
- To investigate whether insulin secretagogues such as Glibenclamide could rescue the loss of insulin secretion seen with partial mtDNA depletion.

Chapter 2

Methods

2 Methods

2.1 MIN6 cell culture

Mouse insulinoma, or MIN6 cells, are a mouse pancreatic β-cell line derived from transgenic mice expressing the simian virus 40 large T antigen under the control of the rat proinsulin promoter (Miyazaki *et al.*, 1990). They are particularly useful in that they respond well to external changes in glucose concentration and secrete insulin accordingly. MIN6 cells were kindly donated by Dr Susan Campbell and Dr Catherine Arden and all experiments conducted when the cells were between passages 23 and 31. Unless otherwise stated, all cell culture reagents used were manufactured by Gibco, and supplied by Life Technologies (Paisley, UK).

2.1.1 Media preparation

MIN6 cells were grown in Dulbecco's Modified Eagle Medium (DMEM) supplemented with 4500 mg/L D-glucose, L-glutamine, sodium pyruvate and sodium bicarbonate. The DMEM was then further supplemented in house with 15% (v/v) filter sterilised foetal bovine serum (FBS), 100 U/ml penicillin, 100 mg/ml streptomycin, and 0.0005% (v/v) β-mercaptoethanol (Sigma, Dorset, UK).

2.1.2 Thawing cells

Cells were rapidly thawed in a water bath before adding to 9 ml pre-warmed complete growth medium. The cell suspension was then centrifuged at 1750 rpm for 3 mins to pellet the cells. The supernatant was removed and cells were resuspended in 10 ml complete growth medium before transferring to a 75 cm^2 flask. Cells were then incubated at 37 °C 5% CO_2 in a humidified incubator.

2.1.3 Passaging cells

Cells were passaged when approximately 80-90% confluent, which tended to be between 5-7 days after initially seeding them. Complete growth medium was aspirated from the flask and residual traces of serum were removed by washing the cells with Dulbecco's Phosphate Buffered Saline (PBS). Cells were detached from the flask by adding 2 ml 1X trypsin-EDTA solution and incubating

for 3-5 mins at 37 °C until the majority of cells had detached. To aid detachment of remaining cells, the flask was gently tapped on the palm of the hand. Eight ml complete medium was then added to the flask to deactivate the trypsin, before centrifuging the cell suspension at 1750 rpm for 3 mins. The supernatant was removed and pelleted cells resuspended in an appropriate volume of complete growth medium. Typically, a confluent flask was split 1:5. Growth medium was changed every 2-3 days.

2.1.4 Freezing cells

Cells were washed and trypsinised as previously described in Section 2.1.3. The cell pellet was resuspended in 1 ml MIN6 freeze juice, which consisted of FBS with 10% (v/v) DMSO, and was immediately transferred into a cryo preservation tube. Cells were then frozen down in a Nalgene 5100 1°C 'Mr Frosty' containing isopropanol alcohol and stored overnight at -80°C. The 'Mr Frosty' freezes down the cells at 1°C per minute, thus preventing the formation of ice crystals inside the cells. This prevents the cells becoming full of water and bursting when they are later thawed.

2.2 Culturing cells with didanosine (ddI) to deplete mtDNA

2.2.1 Preparation of ddI stocks

Didanosine (Sigma, Dorset, UK) was reconstituted with Dulbecco's PBS to make a stock concentration of 10 mM. The 10 mM stocks were further diluted in PBS to produce 1 mM working stocks. One mM working stocks were then used to treat the MIN6 cells, and diluted in complete MIN6 growth medium to the desired concentration.

2.2.2 Haemocytometer cell count

A confluent 75 cm^2 flask was trypsinised and put into suspension as previously described in Section 2.1.3. Once the cell pellet was resuspended in 10 ml growth medium, a haemocytometer was used to estimate the number of cells per ml. Ten µl of the cell suspension was mixed with 10 µl trypan blue 0.4% (Sigma, Dorset, UK). Trypan blue is a diazo dye that permeates cells with a compromised plasma cell membrane, and can be used to exclude dead cells during a cell count. Ten µl of the 1:2 dilution of cells/trypan blue was then

added to the haemocytometer counting chamber and counted under a light microscope.

2.2.3 Treatment of MIN6 cells with ddI to deplete mtDNA

Cells were seeded at 200,000 cells per well and left overnight to settle. Cells were then treated for 5 days with 50 µM ddI or PBS. One hundred µl 1 mM ddI was diluted in 1900 µl complete growth medium and the 2 ml volume added to each well of a 6 well plate. PBS was used as the drug vehicle control. Cells were then incubated at 37 °C 5% CO_2 in a humidified incubator, with treatment medium replaced every 2-3 days. Because the cells were seeded at such a sparse density, they were able to grow in the same culture vessel for the duration of the 5 day treatment.

2.3 Neon transfections of MIN6 cells to knock down TFAM mRNA expression

Optimal transfection conditions for the MIN6 cells were found to be by electroporation, using the Neon transfection system (Life Technologies, Paisley, UK).

2.3.1 MIN6 transfection medium

MIN6 transfection medium differs from normal MIN6 growth medium in that it does not contain penicillin or streptomycin (see Section 2.1.1). The antibiotics could enter the transfected cell through the compromised cell plasma membrane and cause cell death, which is why they are excluded.

2.3.2 Preparing adherent cells

When cells reached ~80% confluency, they were trypsinised, pelleted and washed with PBS prior to cell counting using trypan blue exclusion, as previously described in Section 2.2.2. The required number of cells were pelleted and resuspended in Resuspension Buffer R, from the 10 µl Neon transfection kit (Life Technologies, Paisley, UK). It was important that the cells were resuspended in a suitable volume, so that each 10 µl volume contained 200,000 cells, this was the number of cells transfected and added per well. The TFAM-429 or the TFAM-193 siRNA probe was then added to the 200,000 cells

at a final concentration of 100 nM per well. A Scrambled medium GC content siRNA probe (Life Technologies, Paisley, UK) was used as a transfection control. The Scrambled siRNA is not complementary to any mammalian mRNA sequence and so would not produce gene knock down, but the cells would still be exposed to foreign siRNA.

2.3.3 Electroporation

The Neon transfection system is unique in that it uses the electroporation chamber created in the 10 µl tip in order to deliver a high voltage electric field to the biological sample. Once the Neon tip was attached to the Neon pipette, 10 µl of the cell suspension / siRNA probe mixture was taken up, and the pipette locked into the Neon pipette docking station. Two pulses, each of 1200 V and 20 ms apart, were delivered to the cells. The Neon pipette was detached from the docking station and cells pipette into a 24 well plate, each well containing 0.5 ml of pre-warmed transfection medium. It was imperative that no air bubbles were in the pipette tip prior to electroporation as this would result in arcing of the electrical pulse, visible as a spark at the tip electrode, and a possible reduction in transfection efficiency. After transfection was complete, cells were mixed by gently rotating the plate and incubated for 72 hours in a humidified incubator (37 ˚C, 5% CO_2).

2.4 Real-time PCR

Real-time PCR uses fluorescent dyes / probes and the heat-stable *Thermus aquaticus* (Taq) polymerase in the amplification of a target gene. The amount of fluorescence is proportional to the amount of amplified PCR product and can be measured in ‘real-time’, with fluorescence emitted from the well being measured per PCR cycle using a thermal cycler detector. There are different probes, dyes and fluorophores that can be utilised during real-time PCR. The two that were used in this thesis were the TaqMan hydrolysis probes and the SYBR-Green fluorescent dye.

2.4.1 SYBR Green

Real-time PCR using the SYBR Green dye was utilised when quantifying mtDNA levels relative to a nuclear encoded reference gene. DNA was

extracted from the MIN6 cells and quantified prior to real-time PCR. SYBR-Green is a cyanine fluorescent dye capable of binding to the minor groove of double stranded DNA (dsDNA). When bound to DNA, SYBR-Green fluoresces and the degree of fluorescence is directly proportional to the amount of dsDNA present.

2.4.1.1 DNA extraction

DNA was extracted from the MIN6 cells using the DNeasy Blood & Tissue DNA extraction kit (Qiagen, Crawley, UK) according to the manufacturer's instructions. Briefly, cells were washed with PBS, trypsinised and pelleted. The cell pellets were then snap frozen in liquid nitrogen and stored at -80 ˚C until DNA extraction. To extract the DNA, cell pellets were first rapidly thawed and resuspended in PBS. Cells were lysed and proteins, especially nucleases, were degraded following addition of Buffer AL and proteinase K respectively. Cell lysis was aided by a 10 minute incubation at 56 ˚C after which, 100% ethanol was added to precipitate the DNA. Samples were thoroughly homogenised by vortexing before transferring into a DNeasy Mini spin column. DNA was bound to the column membrane following centrifugation at 6000 g. The bound DNA was then washed with Buffer AW1 and Buffer AW2. The column was centrifuged for 3 min at 16,000 g to dry the membrane and ensure all ethanol was removed. Finally, after transferring the column into a new collection tube, DNA was eluted from the column using Buffer AE, incubating at room temperature for 1 min and then centrifuging at 6000 g for 1 min.

2.4.1.2 DNA quantification

The NanoDrop ND-1000 Spectrophotometer was used to determine the concentration of DNA. One µl of DNA was placed onto the lower loading pad. The top pad was then closed thus creating a column of fluid through which a light beam could be passed through. An absorbance curve was generated, ideally peaking at 260 nm for nucleic acids. The amount of DNA, given in ng/µl, was then used to standardise all DNA samples to the same concentration prior to real-time PCR. DNA was diluted in 100 ng/ml tRNA as the tRNA prevents the DNA adhering to the plastic tubes/plates, this is particularly important at lower DNA concentrations.

2.4.1.3 SYBR Green real-time PCR

Following DNA extraction and standardisation, real-time PCR was used to assess the relative expression of mtDNA encoded target gene ND5 to the nDNA encoded reference gene GAPDH, using the SYBR Green fluorescent dye. All reactions were performed in triplicate in a LightCycler 480 Multiwell Plate 96 (Roche, Welwyn Garden City, UK) and sealed with LightCycler 480 Sealing Foil (Roche, Welwyn Garden City, UK).

Primer sequences for ND5, 87 bp amplicon:

Forward Primer: 5' – CTGGCAGACGAACAAGAC – 3'

Reverse Primer: 5' – GAGGCTTCCGATTACTAGG – 3'

Reaction components for ND5 reaction:

Reaction components	Supplier	Volume per 20 µl reaction	Final concentration
LightCycler 480 SYBR Green I Master, 2x conc.	Roche	10 µl	1x
Forward primer, 5 µM	Sigma	1.2 µl	300 nM
Reverse primer, 5 µM	Sigma	1.2 µl	300 nM
PCR Water	Roche	5.6 µl	N/A
DNA, 25 ng/µl	N/A	2 µl	50 ng

Primer sequences for GAPDH, 208 bp amplicon:

Forward Primer: 5' – CAATGTGTCCGTCGTGGATCT – 3'

Reverse Primer: 5' – GTCCTCAGTGTAGCCCAAGAT – 3'

Reaction components for GAPDH reaction:

Reaction components	Supplier	Volume per 20 µl reaction	Final concentration
LightCycler 480 SYBR Green I Master, 2x conc.	Roche	10 µl	1x
Forward primer, 5 µM	Sigma	2 µl	500 nM
Reverse primer, 5 µM	Sigma	2 µl	500 nM
PCR Water	Roche	4 µl	N/A
DNA, 25 ng/µl	N/A	2 µl	50 ng

Primer oligonucleotide sequences for both genes were synthesised by Sigma and supplied lyophilised. Primers were reconstituted in TE buffer (Sigma, Dorset, UK) to a stock concentration of 100 µM as per manufacturer's instructions. Primers were then further diluted in TE buffer to working stocks of 5 µM.

PCR was conducted using the Roche LightCycler 480 thermo cycler and the following parameters:

Pre-incubation:	Enzyme activation	95 ˚C	5 min	
Amplification:	Denaturation	95 ˚C	10 sec	50 cycles
	Annealing/Extension	60 ˚C	20 sec	
Melt Curve:	Denaturation	95 ˚C	5 min	
	Annealing	65 ˚C	1 min	
	Increase temp to 97 ˚C at rate of 0.11 ˚C / sec			
	5 acquisitions per ˚C			
Hold:		40 ˚C	∞	

2.4.2 TaqMan

Real-time PCR using the TaqMan hydrolysis probes was employed when investigating mRNA gene expression. In this instance, RNA was extracted from the MIN6 cells and quantified prior to real-time PCR. Unlike SYBR-Green which is capable of binding to any dsDNA, TaqMan hydrolysis probes are specific to the region of interest. The probe has a 5' reporter and a 3' quencher. Upon incorporation into the amplified region of interest, the Taq polymerase cleaves the quencher, which has an inhibitory effect of the reporter dye. This means the reporter is no longer inhibited by the quencher, and so it fluoresces. As with SYBR-Green, fluorescence is proportional to the amount of amplified DNA.

2.4.2.1 RNA extraction

RNA was extracted from cells using the GenElute Mammalian Total RNA Miniprep kit (Sigma, Dorset, UK). Cell lysis solution (10 µl β-mercaptoethanol in 1 ml lysis buffer) was added directly to the wells after adherent cells had been washed with PBS. Lysates could be snap frozen with liquid nitrogen and stored at -80 ˚C for later RNA isolation if required. RNA lysates were then spun through a filtration column to aid DNA shearing and remove cellular debris. Filtrate was retained and 70% ethanol added to precipitate the RNA. RNA filtrates were then spun through a second RNA binding column. Bound RNA was washed and an on-column DNase digest (Qiagen, Crawley, UK) performed, ensuring any contaminating genomic DNA was degraded. Bound RNA was washed again to remove the DNase enzyme and eluted in elution buffer.

2.4.2.2 RNA quantification and integrity

RNA was quantified using the Agilent 2100 BioAnalyzer, a unique machine capable of the accurate analysis and quantification of RNA. Samples are loaded onto an RNA chip containing interconnecting microchannels used for the electrophoretic separation of RNA fragments based on size. The Agilent RNA 6000 Nano Kit (Agilent Technologies, Stockport, UK) was used to analyse RNA. Briefly, the RNA chip was pressurised using the chip priming station and filtered matrix gel. Five µl marker was pipetted into all 12 sample wells as well as the marker well on the chip, followed by 1 µl RNA or 1 µl molecular weight ladder. The chip was then run on the Agilent BioAnalyzer machine. RNA samples were

only reverse transcribed if the RNA integrity number (RIN) was ≥8 and there were only two bands present on the electropherogram, indicating the 18S and 28S ribosomal subunits.

2.4.2.3 cDNA synthesis

RNA concentrations obtained from the Agilent BioAnalyzer were used to standardise all RNA samples to 150 ng RNA. RNA was reverse transcribed following manufacturer's instructions in the First Strand cDNA Synthesis Kit (Invitrogen, Life Sciences Ltd, Paisley, UK). Reactions were set up as follows:

Reaction components	Stock concentration	Volume per 20 µl reaction	Final concentration
Random Hexamer Primer	50 ng/µl	1 µl	2.5 ng/µl
RNA	X ng/µl	X µl	150 ng
DEPC-Treated Water	N/A	X µl	N/A
dNTP Mix	10 mM	2 µl	1 mM
cDNA Synthesis Buffer	5x	4 µl	1x
DTT	0.1 M	1 µl	5 mM
RNase OUT	40 U/µl	1 µl	2 U/µl
Cloned AMV RT	15 U/µl	1 µl	0.75 U/µl

RNA was denatured by heating at 70 ˚C for 2 mins to remove secondary structures before preparing cDNA synthesis reactions. Complementary DNA was reverse transcribed following 10 min incubation at room temperature, allowing the primers to anneal, and then incubating at 50 ˚C for 45 mins to allow cDNA synthesis to occur. The reaction was terminated by incubating 85 ˚C for 5 mins, consequently inactivating the AMV RT enzyme.

2.4.2.4 TaqMan real-time PCR

TaqMan hydrolysis probes were obtained from Applied Biosystems (Life Sciences Ltd, Paisley, UK) and are detailed below.

TaqMan probe	Species	Gene accession number	Assay ID	Amplicon length	Exon boundary
TFAM	Mouse	NM_009360.4	Mm00447485_m1	81	2-3
COX1	Mouse	NC_005089.1	Mm04225243_g1	78	1-1
Ins1	Mouse	NM_008386	Mm_01259683_g1	77	1-2
B2M	Mouse	NM_009735.3	Mm_00437762.m1	77	1-2

Reaction components for TaqMan real-time PCR reaction:

Reaction components	Supplier	Volume per 20 µl reaction	Final concentration
LightCycler 480 Master I, 2x conc.	Roche	10 µl	1x
TaqMan primer/probe, 20X	ABI	1 µl	1x
PCR Water	Roche	7 µl	N/A
cDNA, 150 ng/µl	N/A	2 µl	300 ng

PCR was conducted using the Roche LightCycler 480, adhering to the parameters below.

Pre-incubation:	Enzyme activation	95 ˚C	10 min	
Amplification:	Denaturation	95 ˚C	15 sec	50 cycles
	Annealing/Extension	60 ˚C	1 min	
Hold:		40 ˚C	∞	

2.4.3 Qiagen AllPrep Kit for simultaneous DNA/RNA extraction

For samples where DNA and RNA were required from the same sample, DNA and RNA was extracted using the AllPrep DNA/RNA Mini Kit (Qiagen, Crawley, UK). Briefly, cells were washed with ice cold PBS before adding 350 µl Buffer RLT/β-mercaptoethanol (10 µl β-mercaptoethanol per 1 ml Buffer RLT) directly

to each well to lyse the cells. Cell lysates were scraped into a screw cap Eppendorf using a cell scraper/pipette, and could be snap frozen and stored at -80 ˚C for later extraction if required. Homogenised lysates were then transferred to an AllPrep DNA spin column and centrifuged for 30 sec at >8000 g. This allowed the DNA to bind to the column, and RNA to pass through into the flow-through. The DNA-bound columns were transferred into a new collection tube and kept at 4 ˚C until RNA extraction was complete. Two hundred and fifty µl of 100% ethanol was added to the RNA flow-through and mixed thoroughly to precipitate RNA. RNA precipitate was transferred to an RNeasy spin column and spun for 15 sec at >8000 g to allow RNA to bind to the column. Flow-through was discarded and bound RNA was washed following addition of 350 µl Buffer RW1 and spinning >8000 g for 30 sec. At this stage, we carried out the optional on-column DNase digest to ensure limited DNA contamination using the Qiagen DNase kit (Qiagen, Crawley, UK). After the 15 min incubation with DNase, bound RNA was washed again with 350 µl Buffer RW1. This was followed by washing twice with 500 µl Buffer RPE, discarding eluate between each wash and centrifuging >8000 g for 30 sec. After the final wash, the columns were spun for 2 mins at >8000 g to remove excess ethanol. Finally, RNA was eluted following addition of 35 µl RNase-free water and centrifuging >8000 g. Eluted RNA was stored at -80 ˚C, quantified (Section 2.4.2.2), and reverse transcribed (Section 2.4.2.3) prior to real-time PCR (Section 2.4.2.4).

DNA columns were retrieved from 4 ˚C temporary storage. Columns were washed by adding 500 µl Buffer AW1 and centrifuging >8000 g for 30 sec. Flow-through was discarded and columns were washed again with 500 µl Buffer AW2. Columns were centrifuged for 2 mins at full speed to ensure complete removal of ethanol, and flow-through was discarded. Finally, DNA was eluted from the column by adding 50 µl Buffer EB (preheated to 70 ˚C). Columns were incubated for 2 min at room temperature before centrifuging for 1 min at >8000 g. Purified DNA was stored at -20 ˚C and quantified (Section 2.4.1.2) prior to real-time PCR using SYBR-Green (Section 2.4.1.3).

2.4.4 Gel electrophoresis

To ensure that only the gene of interest was amplified, real-time PCR products were separate on a 1% agarose gel, which was prepared using 1X TBE buffer (89 mM Tris-base, 89 mM Boric acid, 2 mM EDTA pH 8.0). Two µl of 10 mg/ml ethidium bromide (Sigma, Dorset, UK) was added per 100 ml molten gel to allow visualisation of the separated DNA fragments. PCR products were prepared for gel electrophoresis by adding an appropriate volume of 6X DNA loading dye (10 ml dH_2O, 15% (w/v) Ficoll 900, 0.25% (w/v) Bromophenol Blue) to the 20 µl PCR reaction. The gel was run with a potential difference of 70-90V across the gel using 1X TBE buffer. Bands were visualised using AlphaImager 2200 UV transilluminator system and captured images were printed using a Mitsubishi P91D printer doc.

2.4.5 Delta Ct quantification

Quantification of gene expression following the TaqMan assays was performed using the Delta-Delta Ct (ΔΔCt) method (Schmittgen & Livak, 2008). Briefly, the ΔCt for the treated samples ($\Delta Ct_{treated}$) was calculated by finding the Ct difference between the target and reference genes for the treated sample $(Ct_{target} - Ct_{reference})_{treated}$. The ΔCt for the control/calibrator/untreated samples ($\Delta Ct_{untreated}$) was then calculated by finding the Ct difference between the target and reference genes for the untreated sample $(Ct_{target} - Ct_{reference})_{untreated}$. The ΔΔCt was then calculated by $\Delta Ct_{treated} - \Delta Ct_{untreated}$. Fold change was finally calculated by raising 2 to the power of –ΔΔCt, to take into account the reaction efficiency.

$$Target/Reference\ Gene\ Ratio\ (Gene\ Expression) = 2^{-\Delta\Delta Ct}$$

For the mtDNA copy number assay, the same calculation was performed however; we multiplied the ΔΔCt ratio by 2 to compensate for GAPDH being diploid.

$$Target/Reference\ Gene\ Ratio\ (mtDNA\ Copy\ Number) = 2\ (2^{-\Delta\Delta Ct})$$

Standard deviations were calculated using the sum of squares formula below, where *s1* is the target gene standard deviation and *s2* is the reference gene standard deviation.

$$Standard\ Deviation\ (\sigma) = \sqrt{[\ (s1^2)\ +\ (s2^2)\ ]}$$

Graphs were then plotted using the target/reference gene ratio and sum of squares calculated standard deviation. When data was compiled from multiple experiments, the standard error of the mean (SEM) was used to represent variability, which was calculated as follows. Where *n* represents the number of repeated experiments.

$$SEM = \frac{\sigma}{\sqrt{n}}$$

2.5 Glucose-stimulated insulin secretion (GSIS)

Method detailed below has been adapted from (Ishihara *et al.*, 1994).

2.5.1 Krebs-Hepes buffer

Krebs-Hepes buffer (119 mM NaCl, 4.74 mM KCl, 2.54 mM $CaCl_2$, 1.19 mM $MgCl_2$, 1.19 mM KH_2PO_4, 25 mM $NaHCO_3$, 10 mM Hepes, 0.5% BSA) was made fresh upon each use. Buffer was made up in dH_2O and the pH was brought down to 7.4 using 1M HCl before addition of the BSA. The buffer was then filter sterilised using 0.22 micron filters, and preheated to 37 ˚C before use.

2.5.2 GSIS

Cells were washed twice with Krebs-Hepes buffer to remove traces of growth medium, before pre-incubating cells with Krebs-Hepes buffer at 37 ˚C for 30 mins. After the 30 min pre-incubation, cells were washed again with Krebs-Hepes buffer before stimulating them with either 3 mM or 25 mM glucose. An appropriate volume of 10% glucose solution (Sigma, Dorset, UK) was added to Krebs-Hepes buffer and cells were incubated at 37 ˚C for 1 hour. During the glibenclamide experiments (Chapter 6), cells were also incubated with 0.1 μM glibenclamide (Sigma, Dorset, UK) in addition to 3 mM or 25 mM glucose during the 1 hour incubation period. The medium containing the secreted insulin was collected in ice cold tubes and centrifuged at 1000 g at 4 ˚C for 5 min to remove cell debris. Supernatant was retained and stored at -20 ˚C for later determination of insulin secretion. Cells were washed with PBS and harvested in protein extraction buffer as described in Section 2.9.1.

2.5.3 Insulin ELISA

Insulin secretion was determined using the high range rat insulin ELISA kit (Mercodia AB, Upsala, Sweden) following the manufacturer's protocol. The kit utilises the sandwich ELISA (enzyme-linked immunosorbant assay) technique, which uses two different monoclonal antibodies, the capture and detector antibody, to detect and quantify the antigen of interest, insulin. In brief, the samples were diluted in Krebs-Hepes buffer at a dilution that allowed them to fall in the middle of the linear range of the standard curve. This would have been determined in an initial ELISA that ran a few samples in a variety of dilutions. The diluted samples were added to the ELISA well, already pre-coated with the capture antibody, along with the enzyme conjugate solution, which contained the detector antibody. The plate was incubated for 2 hours at room temperature on a plate shaker. This incubation allowed any insulin present in the samples to be captured by the capture antibody coating the bottom of the well. The detector antibody present in the enzyme conjugate solution would then be able to bind to the bound insulin. After the 2 hour incubation period, unbound insulin and detector antibody was removed by a series of 6 washes. Substrate TMB was then added to the wells and plates were incubated for 15 min at room temperature. The detector antibody is an enzyme-linked antibody and so following addition of the substrate, the enzyme is cleaved and a chromogenic signal generated. The intensity of the chromogenic signal therefore, is proportional to the amount of insulin present. The substrate reaction was stopped following addition of the acid stop solution and absorbance was recorded at 450 nm. Insulin concentration of unknown samples was calculated using a standard curve of known insulin concentrations.

2.5.4 Protein normalisation

Insulin concentrations generated from the ELISA were normalised to protein concentration, thus ensuring that differences in insulin secretion were due to glucose stimulus and not differences in cell number. Proteins were extracted from cells as detailed in Section 2.9.1 and quantified using the Bradford assay, as detailed in Section 2.9.2.

2.6 Insulin content

To determine the insulin content of cells following GSIS, cells were first washed with ice cold PBS. PBS was again added to the wells and cells were scraped from the bottom of the well using a rubber policeman or a pipette tip. Cell lysates were transferred to a screw cap tube and snap frozen using liquid nitrogen. To ensure insulin was liberated from intracellular insulin-containing vesicles, cell lysates were repeatedly freeze-thawed. This entailed rapidly thawing cell lysates in a water bath before freezing them again in liquid nitrogen, and was repeated a total of three times. Insulin-containing lysates were kept on ice at all times and insulin content was determined using the Mercodia Insulin ELISA kit (as described in Section 2.4.3). Protein quantification was performed as described in Section 2.4.4 in order to normalise insulin content data to whole cell protein content. It was ensured that the insulin ELISA and protein quantification were performed on the same day as insulin was liberated from the cells via liquid nitrogen freeze-thaw, in order to try and prevent degradation of the samples.

2.7 ATP assay

2.7.1 ATP extraction

ATP was extracted from cells using 10% perchloric acid (PCA; Sigma, Dorset, UK). Ten % PCA was prepared by diluting 70% PCA stock solution and adding 2% (v/v) universal indicator solution (Sigma, Dorset, UK). After addition of 10% PCA to the well, cell lysates were scraped into screw cap tubes and samples briefly sonicated to aid ATP liberation. Samples were centrifuged 13,000 g for 12 min at 4 ˚C to pellet cell debris, which was retained for later protein extraction and quantification (see Sections 2.6.2 and 2.6.4). The supernatant was transferred to a separate tube and could be snap frozen for later ATP quantification if required.

2.7.2 Protein extraction

Protein was extracted from the cell pellet obtained after centrifuging the 10% PCA cell lysates. This was to allow normalisation of ATP content to whole cell protein content. After removing as much of the PCA supernatant as possible,

the cell pellet was resuspended in a suitable volume of 0.15 M NaOH in order to extract protein. A control well was always used in each experiment in which cells were extracted in 0.15 M NaOH only, to compare against the protein extraction of the PCA cell pellets. It was always found that protein content was reduced by approximately 50% following PCA extraction. This loss in protein was then corrected using the protein obtained from the control well. Samples could be snap frozen and stored at -80 ˚C for later protein quantification if required.

2.7.3 ATP quantification

2.7.3.1 Sample neutralisation

Samples were extracted in acidic PCA which needed to be neutralised before ATP could be quantified. As the universal indicator solution had already been added to the 10% PCA prior to addition to the cells, pH changes could be witnessed via a colour change, where acidic solution would be red, neutral pH was green, and alkaline solutions would be dark blue / purple. Samples were neutralised by slowly adding 3 M K_2CO_3 until samples changed colour from red to green. Following addition of K_2CO_3, PCA came out of solution and formed a white precipitate at the bottom of the tube. Samples were incubated on ice for 10 min before centrifuging at 13,000 g for 6 min at 4 ˚C to pellet the white PCA precipitate. Neutralised samples were then kept on ice ready for quantification using the ATP assay.

2.7.3.2 ATP standard preparation

ATP stocks were diluted to 10 mM and stored at -80 ˚C. Working stocks of 1 mM were prepared fresh for each assay, and ATP standards were prepared in neutralised 10% PCA. ATP is not stable at low concentrations so 1 mM ATP stocks were discarded after use.

2.7.3.3 ATP assay

ATP was quantified using the ATP Bioluminescent Assay Kit (Sigma, Dorset, UK) as per manufacturer's instructions. The kit consists of an ATP Assay Mix which contains the luciferin and luciferase needed for the conversion of ATP to adenyl-luciferin, and an ATP Assay Mix Dilution Buffer used to dilute the ATP Assay Mix. The assay exploits the following two reactions:

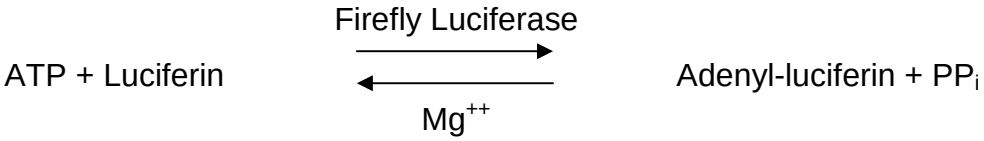

When ATP is the limiting factor in the reaction, the amount of light emitted is proportional to the ATP present and so, can be used to quantify the amount of ATP present.

After loading 10 µl sample/standard to a white 96-well microtitre plate, 100 µl main reagent was added per well and luminescence read immediately using the Spectramax M5E luminometer. The main reagent was prepared immediately prior to use by adding 70 µl ATP Assay Mix to 7 ml ATP Assay Mix Dilution Buffer. ATP concentrations of unknown samples were calculated using the ATP standard curve of known ATP concentrations.

2.7.4 Protein quantification

Protein extracted in 0.15 M NaOH from the PCA cell pellet was quantified using the Lowry assay (Lowry *et al.*, 1951) as opposed to the Bradford assay (Bradford, 1976), the reason for this being that the Coomassie Blue reagent was not compatible with 0.15 M NaOH. The Lowry assay was first described by Lowry *et al.* (1951) and relies on the reduction of the Folin-phenol reagent by proteins, resulting in a yellow to blue colour change. The reaction occurs in two stages: firstly, proteins react with the copper in an alkaline copper tartrate solution; secondly, the copper-treated proteins then react with the Folin-phenol reagent. A colour change is visible as the oxidised amino acids in the protein reduce the Folin-phenol reagent.

The alkaline copper tartrate solution was made up to begin with, and consisted of 10% (w/v) NA_2CO_3 in 0.5 M NaOH, dH_2O, 2% (w/v) Na^+ / K^+ tartrate, 1% (w/v) $CuSO_4.5H_2O$, always made up in the ratio 10:40:1:1 respectively. One hundred µl of the alkaline copper tartrate solution was then added to 10 µl protein sample per well of a clear 96-well microtitre plate. The samples were then incubated at room temperature for 15 min to allow the proteins to react with the copper. After which, 150 µl Folin-Ciocalteu's reagent (Sigma, Dorset,

UK; diluted 1:20 in dH_2O) was added per well. Plates were then incubated at room temperature for 30 min to allow the copper-treated proteins to reduce the Folin-phenol reagent. Absorbance was measured at 750 nm using a plate reader and protein concentration estimated using a BSA standard curve of known concentrations.

Estimated protein concentrations were then used to normalise data generated from the ATP assay.

2.8 Lactate Dehydrogenase (LDH) assay

The LDH assay was performed using the PromoKine LDH Cytotoxicity II Kit (PromoKine, Heidelberg, Germany) in order to ascertain percentage cell cytotoxicity. The assay quantifies LDH release from cells in the cell culture medium. LDH converts the end product of glycolysis, pyruvate, into lactate during anaerobic respiration in a reversible reaction. It would only be released from cells if the cell plasma membrane was compromised, indicating cell damage or cell death due to possible toxicity. LDH release is detected with the help of the WST-1 reagent in the kit. LDH oxidises lactate producing NADH in the process, which reacts with WST-1 forming a water soluble yellow-orange formazan dye. The intensity of this colour change reaction is directly proportional to the amount of LDH present. LDH cytotoxicity of the samples is then expressed as a percentage of the LDH positive control used in the assay.

The cell medium supernatant was retained from cells to be assessed for the effects of cellular cytotoxicity. An aliquot of normal MIN6 cell culture medium was taken at the same time for use as a negative control. All samples were kept at -20 ˚C.

All kit reagents were reconstituted as per manufacturer's instructions. An LDH assay reaction mix was made up by diluting WST 1: 50 in the LDH assay buffer. Ten µl of sample to be analysed was added to a clear flat bottomed 96-well plate, with each sample assayed in triplicate. One µl of the LDH positive control was added to the positive control wells. Normal cell culture medium was used as a negative control and 10 µl was added to the negative control wells. Finally, 100 µl of the LDH reaction mix was added to all wells and the plate was

incubated at 37 ˚C for 30 mins. After the 30 min incubation, absorbance was read at 450 nm using a plate reader.

The average OD readings for the negative control wells was subtracted from the OD readings of all other wells, including sample wells and LDH positive wells. This is because LDH can be detected from the serum and phenol red present in most cell culture mediums. Therefore, to prevent false positive results, we deduct this background LDH from all OD readings.

The cytotoxicity for the samples was then calculated as a percentage relative to the average OD reading for the LDH positive wells, which exhibited 100% cytoxicity.

2.9 Western blotting

2.9.1 Protein extraction

Cells were washed with ice cold PBS and extracted in ice cold protein extraction buffer (100 mM Tris-HCl, pH 7.4, 100 mM KCl, 1 mM EDTA, 25 mM KF, 0.1% Triton X-100, 0.5 mM sodium orthovanadate, 1X protease inhibitor cocktail). Protein lysates were scraped from the bottom of the cell culture plate using a rubber policeman / pipette tip before being transferred into a screw cap eppendorf tube. Samples were sonicated at 5-10 µm amps for 10 sec to aid cell lysis and liberate proteins. Protein samples were then snap frozen using liquid nitrogen, and stored at -80 ˚C until protein quantification.

2.9.2 Protein quantification

Extracted proteins were quantified using the colorimetric Bradford assay (Bradford, 1976) and the Coomassie Blue reagent (Pierce, Thermo Fisher Scientific, Cramlington, UK). Under acidic conditions, the Coomassie-dye reagent binds to certain protein residues, and in doing so, causes a shift in absorbance which is measured at 595 nm using a plate reader. This shift in absorbance can be seen as a colour change from brown to blue and the degree of blue colour change is proportional to the amount of protein present.

Two hundred and fifty µl Coomassie Blue reagent was added to 5 µl of the protein sample in a clear microtitre 96-well plate. After 10 min incubation at

room temperature, absorbance was measured using a plate reader at 595 nm. Protein concentrations were estimated against a BSA standard curve of known concentrations.

2.9.3 Protein sample preparation

Using the protein concentrations estimated from the Bradford assay, samples were prepared in 4X SDS loading buffer (0.25 M Tris-HCl, pH 6.8, 8% SDS, 40% Glycerol, 0.008% Bromophenol blue, 20% β-mercaptoethanol, dH_2O) and protein extraction buffer so that all samples contained 25 µg protein. Samples were then denatured by incubating for 10 min at 37 ˚C and cell debris removed by centrifuging 13,000 rpm for 3 min. By denaturing the samples, secondary / tertiary protein structures were removed, thus ensuring that proteins were separated according to polypeptide chain length and not protein structure. The supernatant was retained and used when loading samples during SDS-PAGE.

2.9.4 SDS-PAGE

SDS-PAGE (sodium dodecyl sulphate polyacrylamide gel electrophoresis) was implemented to separate proteins on the basis of polypeptide length only. The detergent SDS (sodium dodecyl sulphate) binds to the polypeptide backbone and aids protein denaturation. In the process, the negatively charged SDS molecule results in the proteins having an overall negative charge. This allows the proteins to migrate through the polyacrylamide gel when an electrical current is applied.

SDS-PAGE gels are formed when the acrylamide is polymerised by TEMED and APS (ammonium persulphate). The pores formed during acrylamide polymerisation enable the migration of the polypeptides. The higher the percentage of acrylamide used, the smaller the gel pores formed and so, allows easier separation of smaller polypeptides. Vice versa, the lower the percentage acrylamide used, the larger the pores formed, and so, allows easier separation of larger polypeptides.

Twelve % SDS-PAGE gels were prepared using the Mighty Small SE200 Series multiple gel casters (Hoefer Scientific Instruments, San Francisco, USA). A 12% resolving gel (dH_2O, 12% acrylamide, 375 mM Tris pH 8.8, 0.1% SDS, 0.1%

APS, 0.05% TEMED) was prepared and poured into the gel caster. When the resolving gel had set, a 4% stacking gel (dH_2O, 4% acrylamide, 125 mM Tris pH 6.8, 0.1% SDS, 0.1% APS, 0.05% TEMED) was prepared and poured into the gel caster on top of the resolving gel. When the stacking gel had set, SDS-PAGE gels were released from the gel caster and the Mighty Small II SE250 (Hoefer Scientific Instruments, San Francisco, USA) gel electrophoresis apparatus set up. The tank was filled with 1X electrode running buffer (2.5 mM Tris, 19.2 mM Glycine, 0.1% SDS) and 25 µg protein was loaded per lane. A full range rainbow molecular weight marker (Amersham Biosciences, GE Healthcare, Chalfont St. Giles, UK) was also loaded to estimate protein size. A current of 30-50 mA was applied per gel. The gels were allowed to run until the bromophenol blue indicator dye had reached the bottom of the gel, which typically took 1.5 – 2 hrs.

2.9.5 Western blot

After SDS-PAGE, the separated proteins were transferred onto a Hybond-ECL nitrocellulose membrane (Amersham Biosciences, GE Healthcare, Chalfont St. Giles, UK) using the Hoefer TE Series Transfer Electrophoresis Unit (Hoefer Scientific Instruments, San Francisco, USA). The transfer tank was filled with transfer buffer (dH_2O, 10% CAPS buffer (0.1 M CAPS, pH 11.1), 10% methanol). All sponges, blotting paper and nitrocellulose membranes were pre-soaked in transfer buffer before setting up the transfer cassette. The transfer cassette was then loaded into the transfer tank, and a 250 mA current passed through the system for a period of 2 hrs, allowing the transfer of proteins from the SDS-PAGE gel, to the nitrocellulose membrane. Correct transfer of proteins to the nitrocellulose membrane was checked using Ponceau S (Sigma, Dorset, UK). Membranes were stained with Ponceau S for a few minutes and if transfer was successful, the proteins would show up as distinct red bands. Ponceau S staining is reversible and so, proteins were de-stained following a series of washes with TBS-T wash buffer (65 mM Tris pH 7.4, 150 mM NaCl, 0.1% Tween-20).

Antibody	Supplier	Catalogue number	Raised in	Expected protein size	Reacts with	Dilution	Polyclonal/ Monoclonal
Anti-COX1	MitoSciences (AbCam)	MS404-SP	Mouse	40 kDa	Anti-mouse, human, rat, bovine	1:10,000	Monoclonal
Anti-SDH70	MitoSciences (AbCam)	MS204-SP	Mouse	70 kDa	Anti-mouse, human, rat, bovine	1:10,000	Monoclonal
Anti-β-Actin	Sigma	A5441-2ML	Mouse	42 kDa	Anti-mouse, canine, guinea pig, feline, pig, chicken, sheep, rabbit, rat, human, bovine	1:10,000	Monoclonal
Anti-TFAM	Sigma	SAB1401383-100UG	Rabbit	27 kDa	Anti-mouse, human	1:1000	Polyclonal
Anti-Mouse IgG (γ-chain specific)-Peroxidase antibody	Sigma	A3673-1ML	Goat	N/A	Anti-mouse	1:2000	Polyclonal
Anti-Rabbit IgG (whole molecule) Peroxidase Antibody	Sigma	A0545-1ML	Goat	N/A	Anti-rabbit	1:1000	Polyclonal

Table 3 Western blotting antibody details

2.9.6 Immunodetection

Immunodetection began by first blocking non-specific binding sites using a 5% Marvel solution (5% Marvel milk powder in TBS-T). Membranes were blocked by incubating at room temperature for 1 hr with agitation, after which, membranes were washed for 5 mins, three times with TBS-T. Membranes were probed with the primary antibody for 16 hrs overnight at 4 ˚C with agitation. Primary antibodies used are listed in Table 3, and were made up in TBS-T with 1% Marvel.

The following day, blots were washed thoroughly with 3 x 5 min washes, before addition of the secondary detection antibody, which was conjugated to the horseradish peroxidase (HRP) enzyme. As with the primary antibody, the secondary antibody solutions were made up in wash buffer TBS-T with 1% Marvel (detailed in Table 3). Blots were incubated for 1 hr at room temperature with agitation after which, blots were thoroughly washed with 3 x 5 min washes. Bound antibodies were detected by addition of an enhanced chemiluminescent (ECL) solution, which contains a peroxide substrate for the secondary antibody conjugated HRP enzyme. Blots were incubated for 5 min at room temperature with agitation, with 2.5 ml SuperSignal West Pico Luminol Enhancer solution (Thermo Fisher Scientific, Cramlington, UK) and 2.5 ml SuperSignal West Pico Stable Peroxide solution (Thermo Fisher Scientific, Cramlington, UK). After the ECL incubation, blots were placed in a Saran wrap envelope and secured in a developing cassette with tape, ready for autoradiography.

2.9.7 Chemiluminescent Detection

Following addition of the ECL solution, the peroxide substrate in the ECL solution reacts with the secondary antibody conjugated HRP enzyme, resulting in light being emitted as a product of the reaction. When a photographic film is placed on top of the membrane, the light emitted from the HRP-peroxide reaction exposes the film and when developed, can be seen as dark bands depicting the protein of interest. Blue X-ray film (Thermo Fisher Scientific, Cramlington, UK) was placed on the nitrocellulose membrane in the Saran wrap envelope, inside the developing cassette. The cassette was closed and the film exposed for a certain amount of time. It was important that the film was not

over exposed, which would affect densitometric quantification of the protein bands. The film was then developed by first incubating in Kodak GBX Developer (Sigma, Dorset, UK) for 1 min, washing in dH_2O for 20 sec, incubating in Kodak GBX Fixer (Sigma, Dorest, UK) for 1 min followed by washing again in dH_2O for 20 sec. The developer and fixer were diluted 1:10 in dH_2O prior to use and all developing was carried out in a dark room.

2.9.8 Densitometry

Protein bands were quantified using the GS-800 Calibrated Densitometer (BioRad Laboratories, Bath, UK) and the Quantity One 4.2.3 BioRad software. Beta Actin was used as a loading control and so all proteins were normalised to β-Actin.

2.10 Fluorescent Microscopy

2.10.1 MitoTracker

MIN6 cell mitochondria were stained using MitoTracker Orange CMTMRos (Sigma, Dorset, UK), which passively diffuses across the cell plasma membrane, and accumulates in active mitochondria. There are many MitoTracker stains available but the Orange CMTMRos was chosen as it is retained after cells have been fixed and permeabilised.

2.10.1.1 MitoTracker Stock Preparation

Lyophilised MitoTracker was resuspended in DMSO to a stock concentration of 1 mM as per manufacturer's instructions. MitoTracker working stocks were then prepared in non-supplemented DMEM high glucose medium.

2.10.1.2 MitoTracker Staining

Cells were cultured in 75 cm^2 flasks until ~80% confluent. 24hrs prior to MitoTracker staining, cells were split into 6 well plates, with each well containing a glass coverslip. Cells were incubated with MitoTracker staining solution for 30 min at 37 ºC. Following incubation, the MitoTracker staining solution was removed and cells washed with pre-warmed PBS. Cells were then fixed by incubating in complete MIN6 growth medium containing 3% formaldehyde for 15 min at 37 ºC, and washed thrice with pre-warmed PBS. Finally, cells were permeabilised with PBS containing 0.1% Triton X-100 for 40 min at 37 ˚C. After

washing three times with pre-warmed PBS, coverslips were removed from the bottom of each well, and mounted onto glass slides using Vectashield mounting medium with DAPI (Vector Laboratories, Peterborough, UK). The coverslip was kept in place by applying a layer of clear nail polish to the edges of the coverslip. The MitoTracker (mitochondrial) and DAPI (nuclear) stains were excited at 554 nm and 360 nm respectively, emitting at 576 nmn and 460 nmn respectively. The fluorescence was viewed using the TRITC filter (MitoTracker) and the UV filter (DAPI) on a Leica SP2 UV upright confocal system. Gain and offset were kept the same during analysis of the series.

2.10.2 JC-1

Cells were stained with JC-1 to measure mitochondrial membrane potential. The JC-1 dye is unique in that when in the cell cytosol, it exists in its monomeric form and emits a green fluorescence. When the dye enters the mitochondrial matrix however, it forms J-aggregates and there is a spectral shift, resulting in the dye emitting a red fluorescence. Therefore mitochondrial membrane potential can be measured as a ratio of red / green fluorescence.

2.10.2.1JC-1 Stock Preparation

Lyophilised JC-1 dye (Invitrogen, Life Sciences Ltd, Paisley, UK) was reconstituted by resuspending in DMSO to a stock concentration of 5 mg/ml. JC-1 was then further diluted in DMSO to working stocks of 400 µg/ml. All stocks were stored protected from light at -20 ºC.

2.10.2.2JC-1 Staining

MIN6 cells were cultured in 6-well plates prior to staining. Cells were washed with pre-warmed PBS before addition of JC-1 staining medium, which consisted of normal MIN6 growth medium supplemented with JC-1 and the nuclear stain Hoechst 33342 (Sigma, Dorset, UK) to final concentrations of 2 µg/ml and 5 mM per well, respectively. Cells were incubated in JC-1 staining medium for 10 min at 37 ºC to allow both dyes to permeate the cells. Excess dye not taken up by the cells was removed by washing the cells twice in pre-warmed PBS. Normal MIN6 growth medium was then added to cells before imaging the cells immediately. Cells were placed in the live cell imaging chamber which was pre-warmed to 37 ºC, and images were taken on the Nikon Eclipse TE2000-S inverted microscope at x40 magnification using the Photometrics CoolSNAP

HQ^2 Turbo 1394 camera. JC-1 cytoplasmic monomers were imaged using a 470 nm ± 40 nm excitation filter, 520 nm ± 40 nm emission filter whereas JC-1 mitochondrial J-aggregates were imaged using a 575 nm ± 25 nm excitation filter, 632 nm ± 40 nm emission filter. Nuclei were imaged using a 402 nm ± 15 nm excitation filter, 455 nm ± 50 nm emission filter. All images were taken with 1.5 sec exposure (JC-1 monomer), 1 sec exposure (JC-1 aggregate) and 0.5 sec exposure (nuclear stain).

2.10.2.3JC-1 Image Quantification

All images were quantified using ImageJ. Fluorescence was quantified between the threshold of 45-255 for green fluorescence and 30-255 for red fluorescence. A 100 µm size bar (102.67 pixels) was used to calculate area. The ratio of red / green fluorescence, and hence mitochondrial membrane potential, was calculated for each field. The mean and standard deviation were then calculated from the six fields taken for each well.

2.11 Statistical Analysis

All statistical analyses were performed using GraphPad Prism version 5.01 (GraphPad Software, San Diego, California, USA) and presented as mean ± SEM (for multiple experiments) or SD (for singular experiments). Significance was tested with one-way ANOVA followed by a paired t test. If data were not normally distributed, then data were transformed using $y=\sqrt{y}$ prior to statistical analysis. A probability (p) value of <0.05 was considered significant.

Chapter 3

Mitochondrial DNA depletion in MIN6 cells: Didanosine treatment

3 Mitochondrial DNA depletion in MIN6 cells: Didanosine treatment

3.1 Introduction

The aim of the research reported in this chapter was to develop a model of mtDNA depletion specifically in the murine pancreatic β-cell line MIN6. A reduction in mtDNA copy number has been linked to ageing in many cell types, including fibroblasts (Laderman *et al.*, 1996), muscle cells (Short *et al.*, 2005) and pancreatic β-cells (Cree *et al.*, 2008). It is thought that mitochondrial dysfunction, possibly caused by the reduction in mtDNA copy number, plays a role in the development of many age-related diseases, including T2D (Mootha *et al.*, 2003; Petersen *et al.*, 2003). It is not known whether this reduction in mtDNA is causative of T2DM, or merely a biomarker of the disease.

mtDNA copy number has been artificially reduced in cell lines following treatment with inhibitors of mtDNA replication such as ethidium bromide (Chandel & Schumacker, 1999; Singh, 2006; Magda *et al.*, 2008). Certain anti-retroviral NRTI drugs have been more commonly used in recent years as they have greater specificity for mtDNA (Lake-Bakaar *et al.*, 2001; Höschele, 2006). Didanosine (ddI), a nucleoside analogue of adenosine, is thought to be one of the less toxic NRTIs (Lake-Bakaar *et al.*, 2001), but still has high affinity for the mitochondrial polymerase γ, POLG (Kakunda, 2000). Treatment of human pancreatic cells with ddI has shown to severely deplete mtDNA levels, but with less cellular cytoxicity than other NRTIs investigated (Lake-Bakaar *et al.*, 2001).

Many p^0 hybrids have been cultured in which mtDNA has been completely depleted and unsurprisingly, cells have shown severe respiratory chain dysfunction (King & Attardi, 1989; Soejima *et al.*, 1996). In pancreatic β-cells for example, mitochondrial function as well as insulin secretion were impaired in p^0 hybrid cells (Soejima *et al.*, 1996). These studies are particularly useful in understanding the interplay between nDNA and mtDNA but are, however, unrealistic in a clinical setting. What seems to be missing from the literature is the effect of partial mtDNA copy number depletion beyond the mtDNA threshold, but not complete removal of mtDNA.

So we know that there is believed to be a mtDNA phenotypic threshold, beyond which, the deleted or mutated mtDNA presents as a phenotypic symptom (Rossignol *et al.*, 2003). We also know that p^0 pancreatic β-cells completely devoid of mtDNA have severe impairment of mtDNA transcription, translation and glucose-stimulated insulin secretion (Soejima *et al.*, 1996). However, what remains unknown is the effect of partial mtDNA depletion of wild type mtDNA, specifically in pancreatic β-cells. What happens when mtDNA copy number is depleted beyond the mtDNA threshold to cause a phenotypic effect, but cells still had mtDNA to carry out limited respiration? How would this affect insulin secretion? Cree *et al.* demonstrated that mtDNA copy number declined by around 50% in non diabetic islet donors aged between 17 and 75 years of age (Cree *et al.*, 2008). Therefore, could we create a model of mtDNA depletion in a pancreatic β-cell line such as MIN6, whereby mtDNA levels were decreased by 50-60% following treatment with an inhibitor of mtDNA replication such as didanosine?

3.2 Aims

The main aim of this chapter was to develop a model of mtDNA depletion in MIN6 cells using the nucleoside analogue didanosine. We started by:

- Confirming the presence of mitochondria in MIN6 cells using MitoTracker dye and confocal microscopy.
- Assessing the expression of ND5 and GAPDH in MIN6 cells using real-time PCR and establishing the optimal PCR conditions for both pairs of primers.
- Investigating the dose-response effect of didanosine on the MIN6 cells and determining what drug concentration resulted in an overall 50% depletion in mtDNA.
- Examining the effect of ddI treatment removal to determine how long the mtDNA depletion was stable for, which would enable us to determine what time period we had in order to conduct further β-cell functional studies.

3.3 Methods

3.3.1 Real-time PCR using SYBR-Green

Mitochondrial DNA depletion was calculated by exploiting the technique of relative real-time PCR and the cyanine fluorescent dye SYBR-Green. A slight limitation of SYBR-Green is that it is not specific; it will bind to any dsDNA. Therefore, quality checks are needed to ensure the fluorescence generated is from the target gene amplification only, and not genomic contamination or primer dimer amplification, for example. A dissociation curve, also known as a melting curve, was performed at the end of the PCR protocol, and involved slowly increasing the temperature to 95 ˚C in order to denature the DNA. The point at which the DNA denatures is determined by the product sequence as well as product size, and is denoted as the melting temperature (T_m). When the PCR product denatures to single strands, the SYBR-Green dye can no longer bind and so, rapidly dissociates, seen as a decrease in fluorescence. Therefore, the melting curve is depicted as a steep curve, peaking at the T_m and is unique for each amplified product. Typical amplification curves, dissociation curves and melt curves can be seen in Figure 8 (GAPDH) and Figure 9 (ND5).

3.3.2 Absolute and Relative Real-time PCR

Real-time PCR can be quantified absolutely, giving the actual amount of amplified product as a concentration with the aid of a standard curve, or it can be given relative to the expression of a reference gene. In the interest of the mitochondrial DNA copy number assay, it was thought that relative quantification would be better, simply because of the vast number of samples to be processed. Although standard curves serially diluted 1:5 were amplified for both the target and reference gene to check reaction efficiencies (see Section 3.4.2).

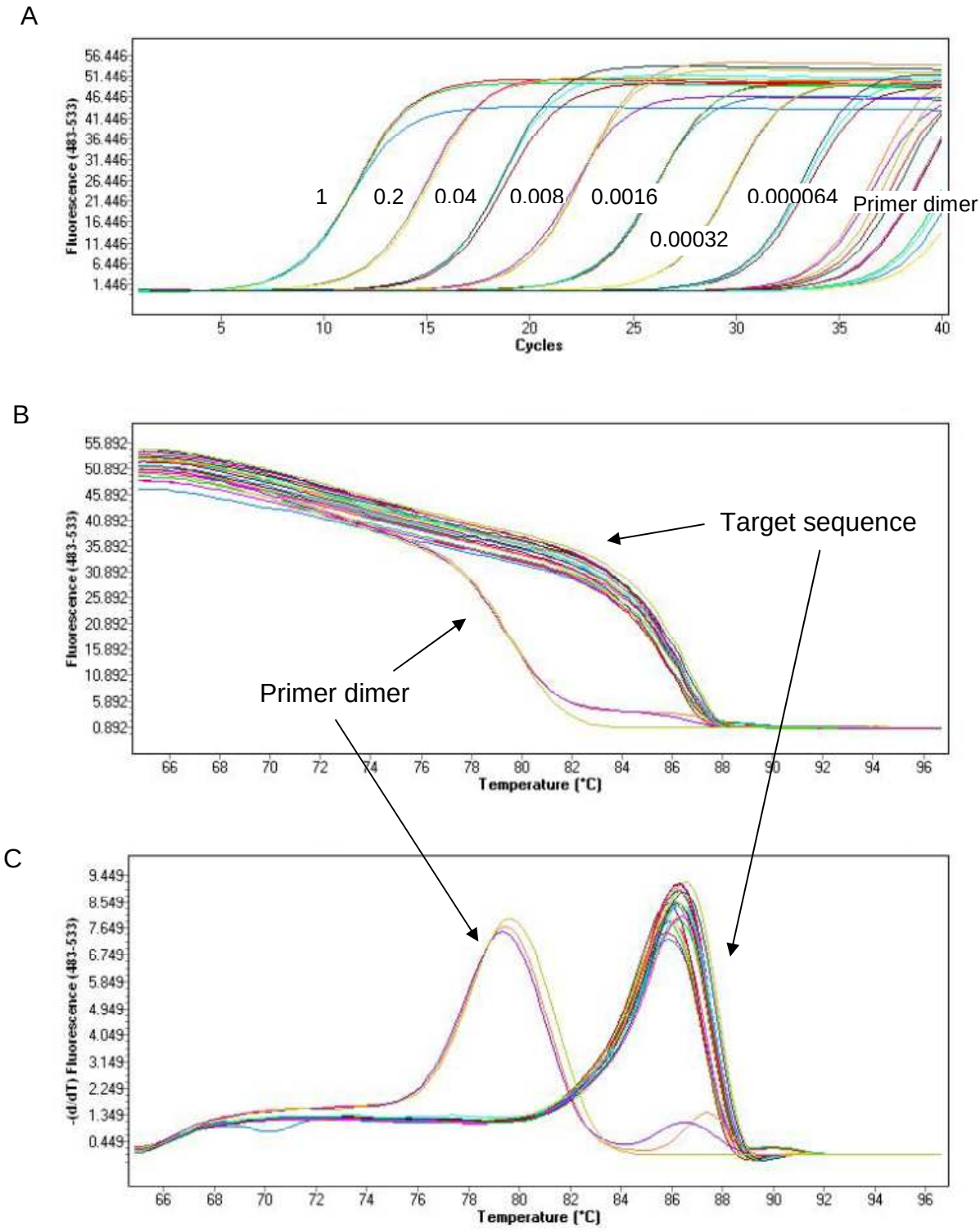

Figure 8 GAPDH amplification, dissociation and melting curves.

A typical GAPDH standard curve amplified by real-time PCR using SYBR-Green. A) The amplification curves depicting the increase in fluorescence over cycle number. The crossing threshold, Ct, value is denoted as the point at which the fluorescence exceeds a given threshold and can be seen when the amplification curve begins to increase exponentially. B) Dissociation curves were routinely performed at the end of the real-time PCR protocol to ensure PCR specificity. Primer dimers were amplified in the no template controls only, not when DNA was present in the reaction. C) Melt peaks were generated from the dissociation curves and are unique for each PCR product. These can be used to discriminate primer dimers (seen on the left) from the PCR target sequence (seen on the right).

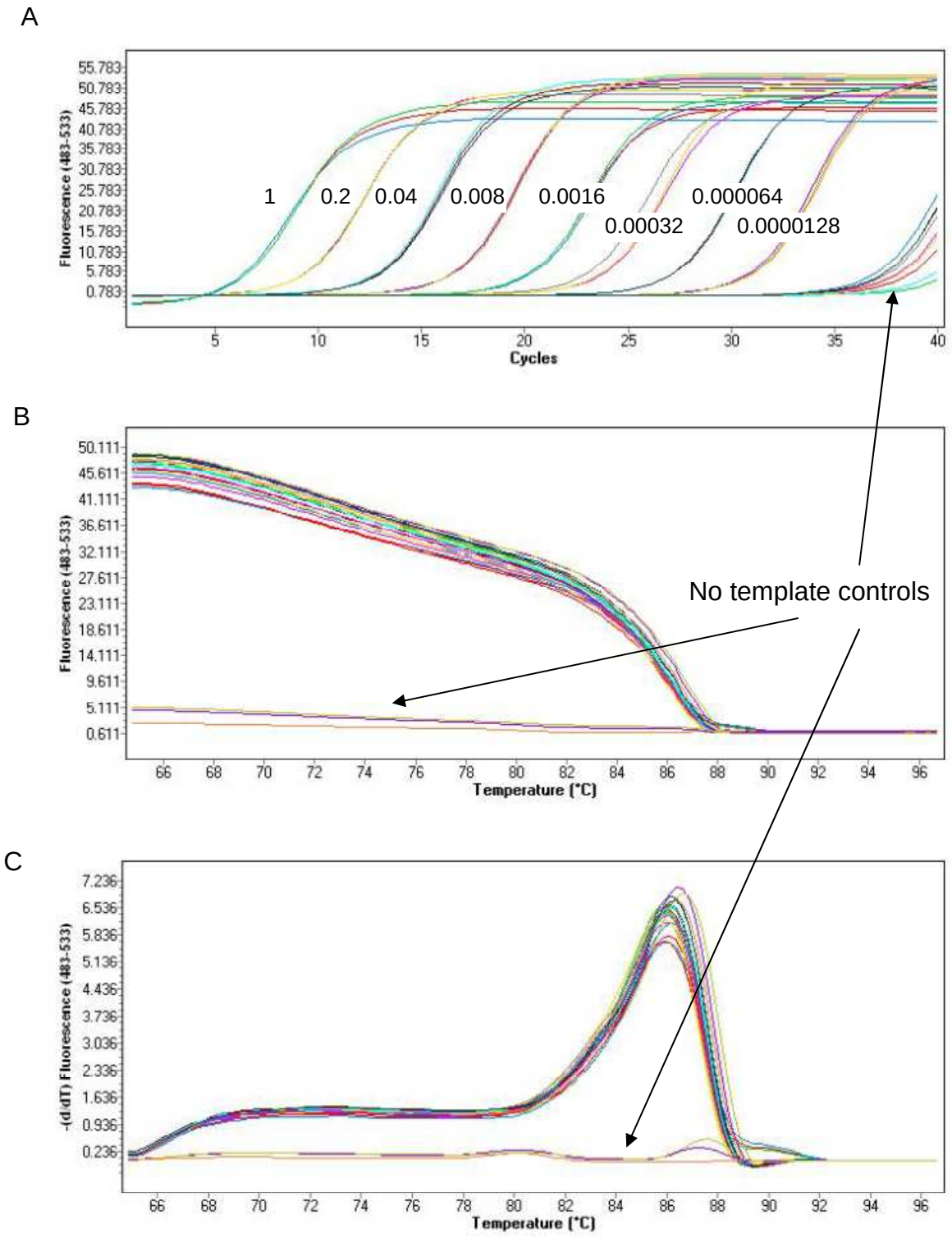

Figure 9 ND5 amplification, dissociation and melting curves.

A typical ND5 standard curve amplified by real-time PCR using SYBR-Green. A) Amplification curves from a 50 ng 1:5 serially diluted DNA standard curve B) Dissociation curves noting the lack of primers dimers, which are specific to GAPDH primers only. C) Melt peaks showing no amplification in the no template control negatives.

3.3.3 Mitochondrial DNA Copy Number Assay

Depletion in mtDNA levels was detected with the use of the mtDNA copy number assay, which was developed by Dr. Lynsey Cree formerly of the Mitochondrial Research Group, Newcastle University (unpublished data). The expression of the ND5 target gene was calculated as an arbitrary ratio relative to the GAPDH reference gene using the Delta Delta Ct method (see Section 2.4.5). ND5, NADH dehydrogenase 5, is a mtDNA encoded subunit of Complex I (NADH Dehydrogenase) of the mitochondrial electron transport chain. The ND5 gene is situated on the heavy strand of mtDNA and is approximately 1.8 kb in length (nt 11,742 – nt 13,565), producing a protein of 607 amino acids in length. The mtDNA copy number assay targets an amplicon within the ND5 gene of 87 bp (nt 12,789 – nt 12,875). Figure 10 shows part of the FASTA sequence of the *Mus musculus* mtDNA genome, specifically the ND5 gene and the regions targeted by forward and reverse primers, which are highlighted in blue.

GAPDH, glyceraldehyde 3-phosphate dehydrogenase, is a glycolytic enzyme and was used as our reference gene. In mice, the GAPDH gene is approximately 4.6 kb in length and is situated on chromosome 6. The GAPDH gene consists of 7 exons and the total transcript length is 1420 bp, producing a protein of 333 amino acids in length. Figure 11 shows the FASTA sequence of the GAPDH gene from the C57BL/6J mouse. The primers used in the mtDNA copy number assay are highlighted in blue, and can be seen to span exons 5 – 6. The amplicon produced using these primers is 208 bp in size and contains the intervening sequence (intron) between exons 5 and 6.

Methods are covered in detail in Section 2.4. Briefly, after DNA was extracted, quantified and standardised, real-time PCR was performed using a LightCycler 480 detector. Fifty ng DNA was amplified using either GAPDH or ND5 primers using the PCR parameters detailed in Section 2.4.1. Primer specificity was ensured by running a melt curve as well as separating the PCR products on a 1% agarose gel. Delta Ct quantification was performed using the real-time PCR Ct values, allowing calculation of the mtDNA / nDNA ratio.

ND5 FASTA Sequence (NC_005089.1)

5′ –

ATCAATATTTTCACAACCTCAATCTTATTAATCTTCATTCTTCTACTATCCCCAATCCTAATTTCAATAT
CAAACCTAATTAAACACATCAACTTCCCACTGTACACCACCACATCAATCAAATTCTCCTTCATTATTAG
CCTCTTACCCCTATTAATATTTTTCCACAATAATATAGAATATATAATTACAACCTGGCACTGAGTCACC
ATAAATTCAATAGAACTTAAAATAAGCTTCAAAACTGACTTTTTCTCTATCCTGTTTACATCTGTAGCCC
TTTTTGTCACATGATCAATTATACAATTCTCTTCATGATATATACACTCAGACCCAAACATCAATCGATT
CATTAAATATCTTACACTATTCCTGATTACCATGCTTATCCTCACCTCAGCCAACAACATATTTCAACTT
TTCATTGGCTGAGAAGGGGTGGGAATTATATCTTTCCTACTAATTGGATGATGGTACGGACGAACAGACG
CAAATACTGCAGCCCTACAAGCAATCCTCTATAACCGCATCGGAGACATCGGATTCATTTTAGCTATAGT
TTGATTTTCCCTAAACATAAACTCATGAGAACTTCAACAGATTATATTCTCCAACAACAACGACAATCTA
ATTCCACTTATAGGCCTATTAATCGCAGCTACAGGAAAATCAGCACAATTTGGCCTCCACCCATGACTAC
CATCAGCAATAGAAGGCCCTACACCAGTTTCAGCACTACTACACTCAAGTACAATAGTAGTTGCAGGAAT
TTTCCTACTGGTCCGATTCCACCCCCTCACGACTAATAATAACTTTATTTTAACAACTATACTTTGCCTC
GGAGCCCTAACCACATTATTTACAGCTATTTGTGCTCTCACCCAAAACGACATCAAAAAAATCATTGCCT
TCTCTACATCAAGCCAACTAGGCCTGATAATAGTGACGCTAGGAATAAACCAACCACACCTAGCATTCCT
ACACATCTGTACCCACGCATTCTTCAAAGCTATACTCTTTATATGCTCTGGCTCAATCATTCATAGC**CTG**
GCAGACGAACAAGAC**ATCCGAAAAATAGGAAACATCACAAAAATCATACCATTCACATCATCATG****CCTAG**
TAATCGGAAGCCTCGCCCTCACAGGAATACCATTCCTAACAGGGTTCTACTCAAAAGACCTAATTATTGA
AGCAATTAATACCTGCAACACCAACGCCTGAGCCCTACTAATTACACTAATCGCCACTTCTATAACAGCT
ATGTACAGCATACGAATCATTTACTTCGTAACAATAACAAAACCGCGTTTTCCCCCCCTAATCTCCATTA
ACGAAAATGACCCAGACCTCATAAACCCAATCAAACGCCTAGCATTCGGAAGCATCTTTGCAGGATTTGT
CATCTCATATAATATTCCACCAACCAGCATTCCAGTCCTCACAATACCATGATTTTTAAAAACCACAGCC
CTAATTATTTCAGTATTAGGATTCCTAATCGCACTAGAACTAAACAACCTAACCATAAAACTATCAATAA
ATAAAGCAAATCCATATTCATCCTTCTCAACTTTACTGGGGTTTTTCCCATCTATTATTCACCGCATTAC
ACCCATAAAATCTCTCAACCTAAGCCTAAAAACATCCCTAACTCTCCTAGACTTGATCTGGTTAGAAAAA
ACCATCCCAAAATCCACCTCAACTCTTCACACAAACATAACCACTTTAACAACCAACCAAAAAGGCTTAA
TTAAATTGTACTTTATATCATTCCTAATTAACATCATCTTAATTATTATCTTATACTCAATTAATCTCGA
GTAA

-3′

Figure 10 ND5 mtDNA encoded target gene.

FASTA sequence taken from the NCBI website of a section of the *Mus musculus* mtDNA genome, nt 11,742 – nt 14,144, on the positive strand. The section shown corresponds to the ND5 gene (NCBI reference sequence NC_005089.1). Highlighted in blue are the regions targeted by the ND5 forward and reverse primers used in the mtDNA copy number assay, with the 87 bp amplicon in bold text.

GAPDH FASTA Sequence (MGI: 95640; Ensembl gene ID: 14433)

5′-

AGAGACGGCCGCATCTTCTTGTGCAGTGCCAGGTGAAAATCGCGGAGTGGGCCGCAGGAGGCCGGGGACA
GTCGGAAACTGGGAAGGGGAGTGGGCACTGTACGGGTCTAGGGATGCTGGTGCGAAGTGTGCAAGCCGGA
CCCAGGCTCCGCATTGCAGGGGGGGGATGATGGAGGACGTGATGGGGCGCACGGCGGGAATGGAGGCGGG
GTGGGGGAGGGGACTGCCTGGTGTCCTTCGGGCCACGCTAATCTCATTTTCTTCTCCTGCAGCCTCGTCC
CGTAGACAAAATGGTGAAGGTCGGTGTGAACGGGTGAGTTCCAGGGCGGGGCCCTGCTCCGTTGCCTACG
CAGGTCTTGCTGACCCGGGGGCTCTGCAGTACTGTGGGGAGGTGGATGAGGTGGCCGAAGCGCCCAAGGA
GACCTCAAGGTCAGCGCTCGGACCTGGCGATGGCTCGCACTTGCGGCCCCCAGCTGCTGCACCTCTGGTA
ACTCCGCCTTTGCGGGGATGAGCGGCCCGGAGTCTTAAGTATTAGGAACAACCCCACGCGCCCGTTCAGA
CCCATCCCGTAATCCCCAGTCCGGGGCTTCTTTCTTTACTTTCGCGCCCTGAGGAGTCACGTGCCAGGAG
GGAAGCCCCTCCCCCATCTCCCCCTTCCTCGGGGTCGGTGGCATGGCGTTGTGAGGTGCATACCTTTGCG
CATCATCTCCCAGGCTTGGGCTTCCTTTAGGGTAACTGGCCGCCGCCATGTTGCAAACGGGAAGGAAATG
AATGAACCGCCGTTATGAAATCTTGCTTAGGCCTTCCTTCTTCCTAGCTTGTGACTAACCTCATTCCTCT
CGGCTGGGTGGAGTGTCCTTTATCCTGTAGGCCAGGTGATGCAAGGCTTCCGTGCTCTCGAGAGAGTTCT
ACCTCACAATCTGTCTCACCTTATTAGCCTTAAAAGCCCTTGAGCCTTATTGTCCTCGGGCATAATGCGT
ATTCTAGATTATTCTCTGAAAATCAAAGCGGACTTACAGAGGTCCGCTTGACCTCCCAACCCCAGAGGTA
GTTATGGCGTAGTGCAGAGCCGTGGGATGGGGAGCTGAGTCATGGTGGTTCTGAAAAGAAATTTTCCACC
ACAAAATGGCTCCTGTAGTAGCAGCCCCTTCCATCCCCTGCACTTCCCATCACAGCCTCGCACTGACCCA
GGCCCTATAGGCCAGGATGTAAAGGTCATTAAGAGGATTGGGTGTCCCTGCGCCTCAGAATCCTGCCCTT
CTCCCCGTTCCATCCTCCAGAAACCAGATCTCTCCACTCCGCCCTGATCTGAGGTTAAATTTAGCCGTGT
GACCTTTCTGGATCTGGGGTCTGAGCGGGCTCTCCACCCTGCTCCCCCTACACACATCTGTTGCTCCGGC
TCTCATTTTTGCCCGAGAAGAACAGGTGTTTCGCGAACGAGCCCTGGGATTAGGGTTGGAAACCCCCCAC
ATGTTTTCTCAGTCTTTCCCCTTAGTTCGAGGGACTTGGAGGACACAGGTGGGCCCGCCCTGTGCTGCTC
ACGCTGACCTTTAGCCTTGCCCTTTGAGCTTGCTGATGAATGAGTTCACAGGTCTGCCCTGTCCAGGGGG
TGTAGCCTGAAGTCCAGCCATGCTGGAACAAACTTCCCAGGGCATGAGTGATGGGGGTGATGTGCCAAGC
TTGTACCCAGACTGGGGCAAACTGCCACTTCTTAAGAGACTTAGAATGACTTGGAGGAGGTTTGCTGGGC
AAGCAATCACCTCTTGGACAGGAAAGAAACCTCCACTTTATAACCGTGCTATAAAAGCCCTGCCAGGCCT
CGGCTGCTCAAAGAATATAAAATTAGATCTCTTTGGACTTTCTAGGGTGGGAACAGTCTATATTTGGGTT
GTACATCCAAGCATTCAACTAGCTTTATTAAAGGGAATTCTGAACAAAACATGAACTTCCTGATGCATAC
ATTTCTAATGTACTGTGTCTGCATAAAGGCTTGTACCTTTGTTGTGGTACGTGCATAGCTGATGGCTGCA
GGTTCTCCACACCTATGGTGCAACAGTATTCCACTCTGAAGAACATGAGATAGCCTGGGGCTCACTACAG
ACCCATGAGGAGTTCTGATCTCAGCTCCCCTGTTTCTTGTCTTTCAGATTTGGCCGTATTGGGCGCCTGG
TCACCAGGGCTGCCATTTGCAGTGGCAAAGTGGAGATTGTTGCCATCAACGACCCCTTCATTGACCTCAA
CTACATGGTCTACATGTTCCAGTATGACTCCACTCACGGCAAATTCAACGGCACAGTCAAGGCCGAGAAT
GGGAAGCTTGTCATCAACGGGAAGCCCATCACCATCTTCCAGGAGCGAGACCCCACTAACATCAAATGGG
GTGAGGCCGGTGCTGAGTATGTCGTGGAGTCTACTGGTGTCTTCACCACCATGGAGAAGGCCGGGGTAAG
TGGCCGGAAAGCTGAAGGTGACGGGCACCCTTGATATGGTGCAACCTGAAAACCAAGAACTGAGTCTGAA
ATCAACTTCTTTCCCTTAAACAGGCCCACTTGAAGGGTGGAGCCAAAAGGGTCATCATCTCCGCCCCTTC
TGCCGATGCCCCCATGTTTGTGATGGGTGTGAACCACGAGAAATATGACAACTCACTCAAGATTGTCAGC
AATGCATCCTGCACCACCAACTGCTTAGCCCCCCTGGCCAAGGTCATCCATGACAACTTTGGCATTGTGG
AAGGGCTCATGGTATGTAGGCAGTGGGGAGACAGCTCATGCATTTCTTATCTTACCCTGCCATGAGTGGA
CCCTTCTTTGTAGGTGTCCCTTTTGGGTAGAGGGGTGCCGTGCAGGACCTCACTCATTGCCCCCGTGTTT
TCTAGACCACAGTCCATGCCATCACTGCCACCCAGAAGACTGTGGATGGCCCCTCTGGAAAGCTGTGGCG
TGATGGCCGTGGGGCTGCCCAGAACATCATCCCTGCATCCACTGGTGCTGCCAAGGCTGTGGGCAAGGTC
ATCCCAGAGCTGAACGGGAAGCTCACTGGCATGGCCTTCCGTGTTCCTACCCC**CAATGTGTCCGTCGTGG**
ATCTGACGTGCCGCCTGGAGAAACCTGTATGTATGGGGAGAGCTGGGCTTGTCTCTGGTGTGACAGTGAC
TTGGGACAAGGATAGTCATTTTGGGGTTTGTTCTTATCAGGCCAAGTATGATGACATCAAGAAGGTGGTG
AAGCAGGCATCTGAGGGCCCACTGAAGGGCATCTTGGGCTACACTGAGGACCAGGTTGTCTCCTGCGACT
TCAACAGCAACTCCCACTCTTCCACCTTCGATGCCGGGGCTGGCATTGCTCTCAATGACAACTTTGTCAA
GCTCATTTCCTGGTATGTGGGGATGGGAAACCTGACTTTTAAGAGCAACTGGGGGTTTGGTGCCCTCTGG
TGGCTAGCTCAGAAAAGAAACCCAAACTAACAGTTGTCCCAATTTGTTCTAGGTATGACAATGAATACGG
CTACAGCAACAGGGTGGTGGACCTCATGGCCTACATGGCCTCCAAGGAGTAAGAAACCCTGGACCACCCA
CCCCAGCAAGGACACTGAGCAAGAGAGGCCCTATCCCAACTCGGCCCCCAACACTGAGCATCTCCCTCAC
AATTTCCATCCCAGACCCCCATAATAACAGGAGGGGCCTAGGGAGCCCTCCCTACTCTCTTGAATACCAT
CAATAAAGTTCGCTGCACCCAC -3′

Figure 11 GAPDH nDNA encoded reference gene.

FASTA sequence, taken from NCBI (MGI: 95640; Ensembl gene ID: 14433), of the GAPDH gene. Situated on chromosome 6 of the C57BL/6J mouse, GAPDH contains 7 exons, highlighted in green. The primers used in the mtDNA copy number assay flank exons 5-6, and are highlighted in blue, with the 208 bp amplicon in bold text.

3.3.4 MitroTracker staining in MIN6 cells

MitoTracker probes passively diffuse across the cell plasma membrane and accumulate in active mitochondria and so were used to stain the mitochondria of MIN6 cells. The rosamine-based MitoTracker Orange CMTMRos was used as the orange dye is retained after the cells have been fixed and permeabilised. The reduced dye does not fluoresce until it enters a live cell, where it is then oxidised and sequestered by the mitochondria. Cells were then fixed and permeabilised prior to mounting using a Vectorshield mounting medium containing DAPI. DAPI, 4',6-diamidino-2-phenylindole, is a nuclear staining blue fluorescent dye capable of binding to A-T rich regions of the minor groove of dsDNA (Kubista *et al.*, 1987). When DAPI binds dsDNA, its fluorescence is increased, thought to be due to the displacement of water molecules from DAPI as well as the minor grooves of dsDNA (Barcellona *et al.*, 1990).

Cells were incubated in MitoTracker staining medium (see Section 2.10.1 for further details) for 30 mins at 37 ºC, after which, they were mounted onto microscope slides and imaged using confocal microscopy. When measuring fluorescence, a beam of light was used to excite the electrons in molecules of the dye, which then subsequently emanate light which is of a lower energy and therefore, a higher wavelength is used to measure the emission of light. The MitoTracker dye was excited at 554 nm and emitted light was viewed at 576 nm (orange) using the TRITC filter. The DAPI stain however, has an excitation maximum of 358 nm and an emission maximum of 461 nm (blue) and so was viewed using the UV filter. Gain and offset were kept the same during analysis of the series.

3.4 Results

3.4.1 MitoTracker staining in MIN6 cells

It is widely understood that mitochondria are dynamic organelles that vary considerably in number and morphology, especially between cell types. β-cells, like other high energy demanding cells such as muscle cells and neurones, contain many mitochondria (Lodish *et al.*, 2004). We wanted to begin our studies by first confirming that MIN6 cells do indeed contain many mitochondria, which is of course, where mtDNA resides.

MIN6 mitochondria were labelled using MitoTracker CMTMRos, which fluoresces orange when excited under a TRITC filter. In Figure 12, we see that MIN6 cells do certainly contain a plentiful supply of mitochondria, visible in the cell as an expansive and complex network. When no MitoTracker dye was added to the cells, we see no fluorescence under the TRITC filter, only the nuclei are seen under the UV filter from the DAPI dye, showing that there is no background fluorescence (Figure 12A). In some instances we can pick out an individual mitochondrion (Figure 12B), which is of expected size at 1.28 µm.

Images were taken of early passage 25 MIN6 cells and late passage 31 MIN6 cells. MIN6 cells were typically used during this passage range and so we wanted to see if passage number had an effect on mitochondrial content. Visually, it seems that both early and late passage MIN6 cells have a plentiful supply of mitochondria, as expected (Figure 12B and Figure 12C). As mitochondria accommodate mtDNA, and there are multiple copies of mtDNA per mitochondria, we should be able to detect mtDNA in MIN6 cells.

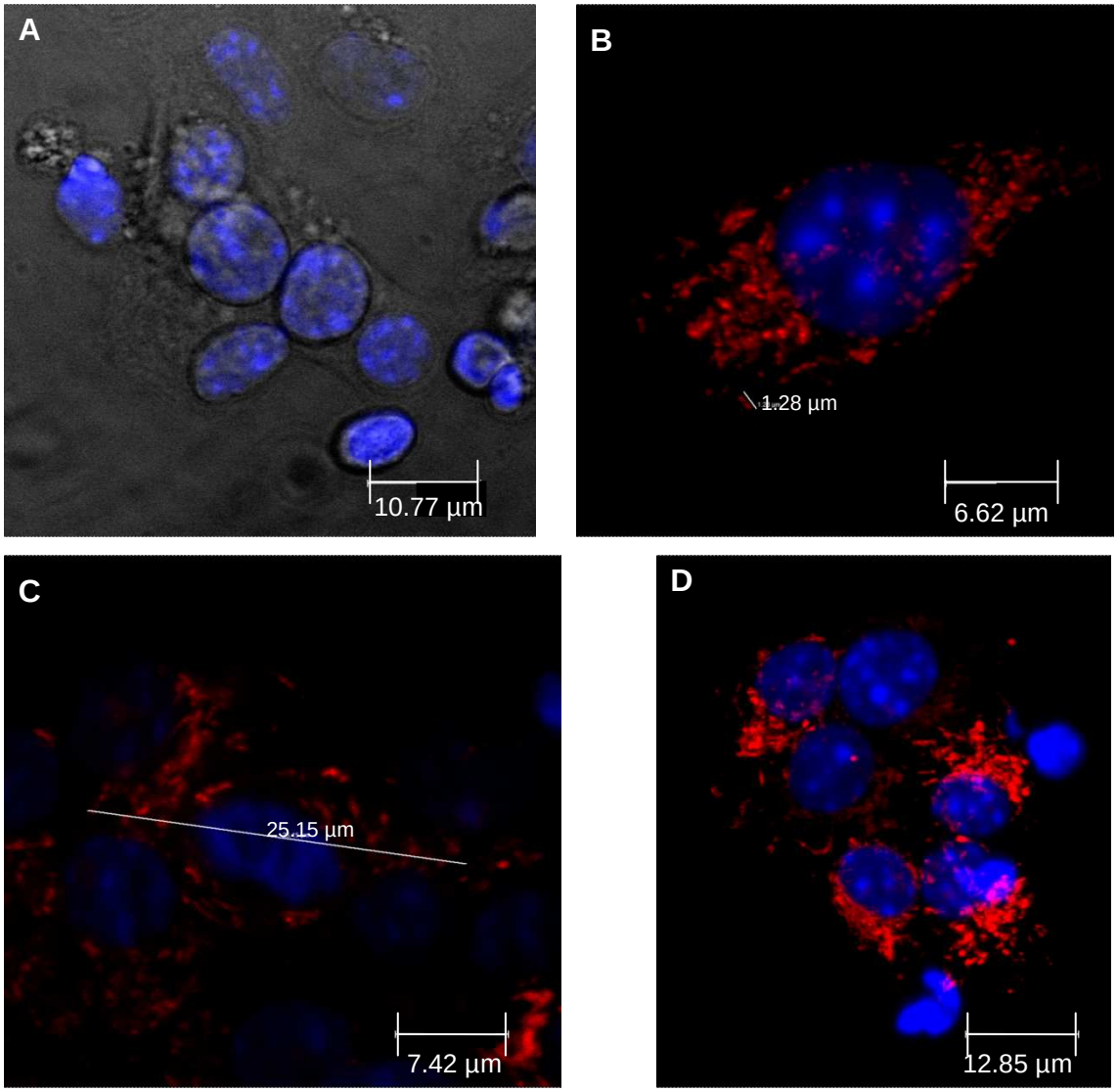

Figure 12 Confocal microscopy images of MIN6 cells following staining with MitoTracker (orange) and nuclear stain DAPI (blue).

MIN6 cells were cultured on coverslips in 6 well plates. Cells were stained with MitoTracker Orange CMTMRos for 30 mins before being permeabilised and fixed with 0.1% Triton X-100 and 3% formaldehyde respectively. Coverslips were then mounted on slides using Vectashield mounting medium with DAPI. A) Negative control where no MitoTracker was added. B) A single early passage (passage 25) MIN6 cell, single mitochondrion has been highlighted, dimension of which (1.28 µm) is of expected size. C) A single late passage (passage 31) MIN6 cell, the length of the cell is shown (25.15 µm). D) A cluster of late passage 31 MIN6 cells. MIN6 cells preferentially grow in cell clusters like this.

3.4.2 Mitochondrial DNA Copy Number Assay: Real-time PCR Primer Optimisation

Mitochondrial DNA depletion in MIN6 cells would be measured using the mtDNA copy number assay. The assay was developed by Dr. Lynsey Cree formerly of the Mitochondrial Research Group at Newcastle University. Dr. Cree kindly provided the primer sequences for the ND5 target gene and GAPDH reference gene. Using these sequences, the first stage of developing the mtDNA copy number assay in MIN6 cells was primer optimisation. We began this process by running a primer matrix consisting of combinations of forward and reverse primers at 300 nM, 500 nM and 900 nM.

Ideally, it is desirable to have the same concentration of forward and reverse primer. In the ND5 reaction, the 300 nM forward and reverse primers produced a good reaction efficiency of 86%. When higher concentrations of the ND5 primers were used, this efficiency did not improve much beyond 86%. Therefore, it was quickly decided that the optimal concentration of both of the ND5 primers would be 300 nM per 20 µl reaction.

When the ND5 PCR products were separated on an agarose gel (Figure 13B), bands could be seen slightly below the 100 bp marker. The ND5 primers are predicted to produce an amplicon of 87 bp, thus it is likely that the bands visible just under the 100 bp marker are the ND5 amplified product. Only one band is present demonstrating that the primers are specific for the target sequence only. No template control (NTC) wells were used in every PCR plate to show that amplification only occurs when DNA is present in the reaction, ruling out possible reagent contamination with genomic DNA. The NTC wells contained the same master mix as sample wells, but instead of adding template DNA, PCR water was added instead. Therefore, no amplification should take place in the NTC wells. There is no product in the NTC wells in Figure 13B, showing that there was no genomic DNA contamination of PCR reagents.

The next stage was to make sure the GAPDH reaction efficiency was as close to that of the ND5 reaction as possible. By doing this, we were ensuring that both standard curves were parallel and so, relative quantification could be accurately made across the linear range of the standard curve. Figure 14 shows a direct comparison of three GAPDH standard curves using either 300

nM, 400 nM or 500 nM forward and reverse primers, to the optimal ND5 300 nM standard curve. It appears that the ND5 standard curve and GAPDH 300 nM standard curve begin to taper at the higher DNA concentrations and so, are not parallel (Figure 14A). There is a ~4% difference in both of the reaction efficiencies also indicating that 300 nM GAPDH may not be the best primer concentration for us to use. When we increase the GAPDH primer concentration to 400 nM (Figure 14B), we see that the two standard curves do not narrow as much at the top end of the standard curve, and the reaction efficiency is slightly better at 84%, only 2% less than that of ND5. In Figure 14C when 500 nM GAPDH primers are used, we can see the curves seem to be closest to being parallel at this concentration, with a reaction efficiency of 86% for both the GAPDH and ND5 reactions. Therefore, the optimal GAPDH forward and reverse primer concentration seems to be 500 nM.

When the GAPDH products were separated on an agarose gel (Figure 13A), we can see that bands are visible just above the 200 bp marker. The GAPDH primers are predicted to produce a product of 208 bp in size and so, it is likely that the bands present are those of the amplified GAPDH amplicon. A single band is present indicating that the primers are specific for the target sequence. GAPDH PCR products are not present in the NTC wells however, very faint and fuzzy bands are present at the very bottom of the gel image, highlighted by a red circle in Figure 13A. These are classical indications of primer dimers and corroborate the results from the melt curve analysis.

Therefore, in summary, the optimal primer concentrations were found to be 300 nM for ND5 and 500 nM for GAPDH. Both primers produced a reaction efficiency of 86% and both standard curves were parallel, allowing accurate relative quantification of unknowns across the linear range of the standard curves. Both ND5 and GAPDH primers could be seen to be specific, only producing a single band of expected size, 87 bp and 208 bp respectively, when PCR products were separated on an agarose gel. When no DNA template was added to the GAPDH reactions, primer dimers formed. These were discriminated from genomic contamination by melt curve analysis and gel electrophoresis. They only occur in the NTC wells and so, were deemed non problematic.

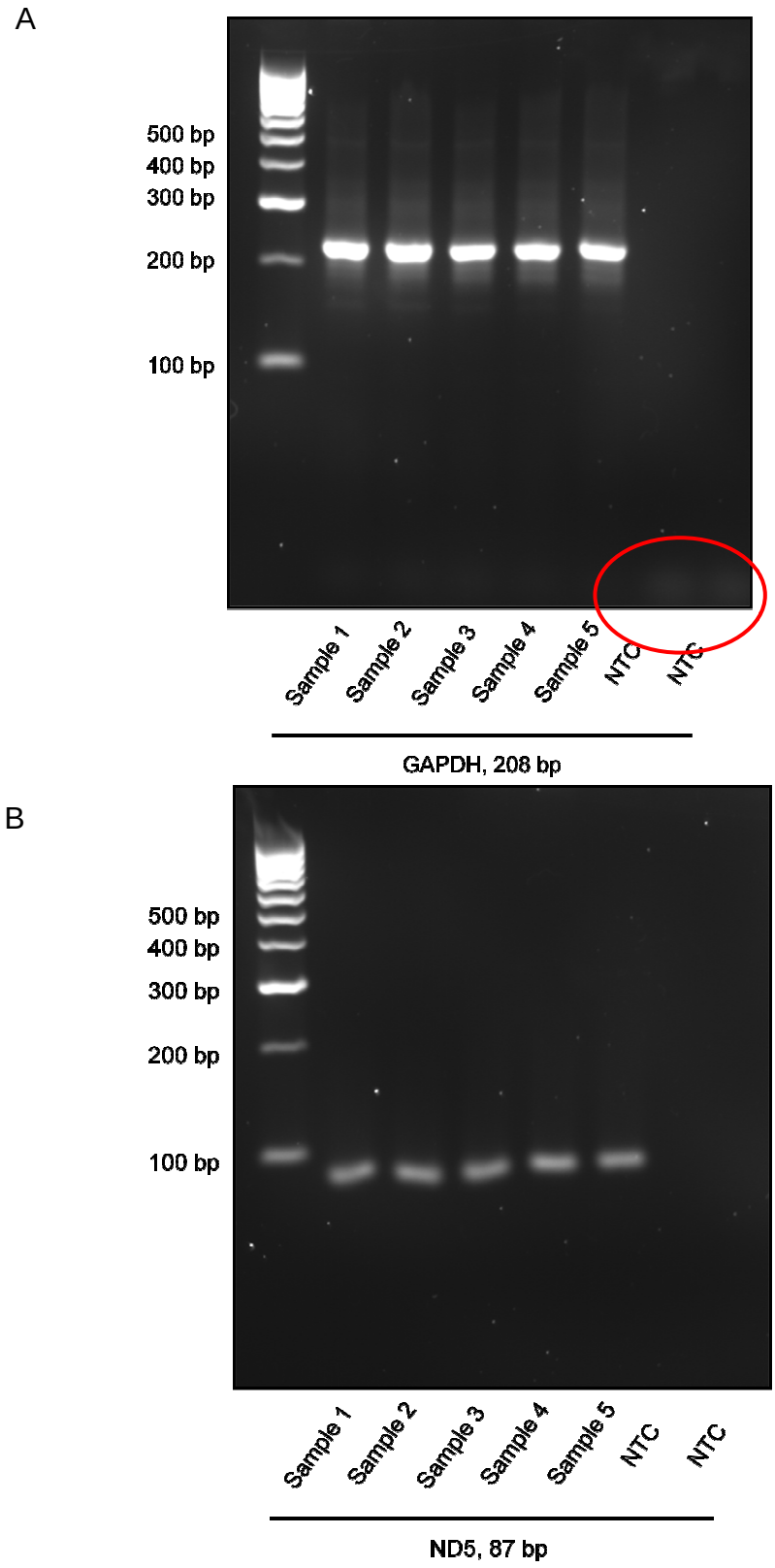

Figure 13 Agarose gel electrophoresis of real-time PCR products.

Real-time PCR was performed using 500 nM GAPDH primers (A) and 300 nM ND5 primers (B). The PCR products were then separated on a 1% agarose gel to check primer specificity. This gel shows the PCR products from 5 different samples. Two no template controls (NTC) are also shown where DNA template was replaced with PCR water, and so, no amplification should occur. GAPDH primer dimers show up as feint bands at the bottom of the gel, and can be vaguely seen in the red circle.

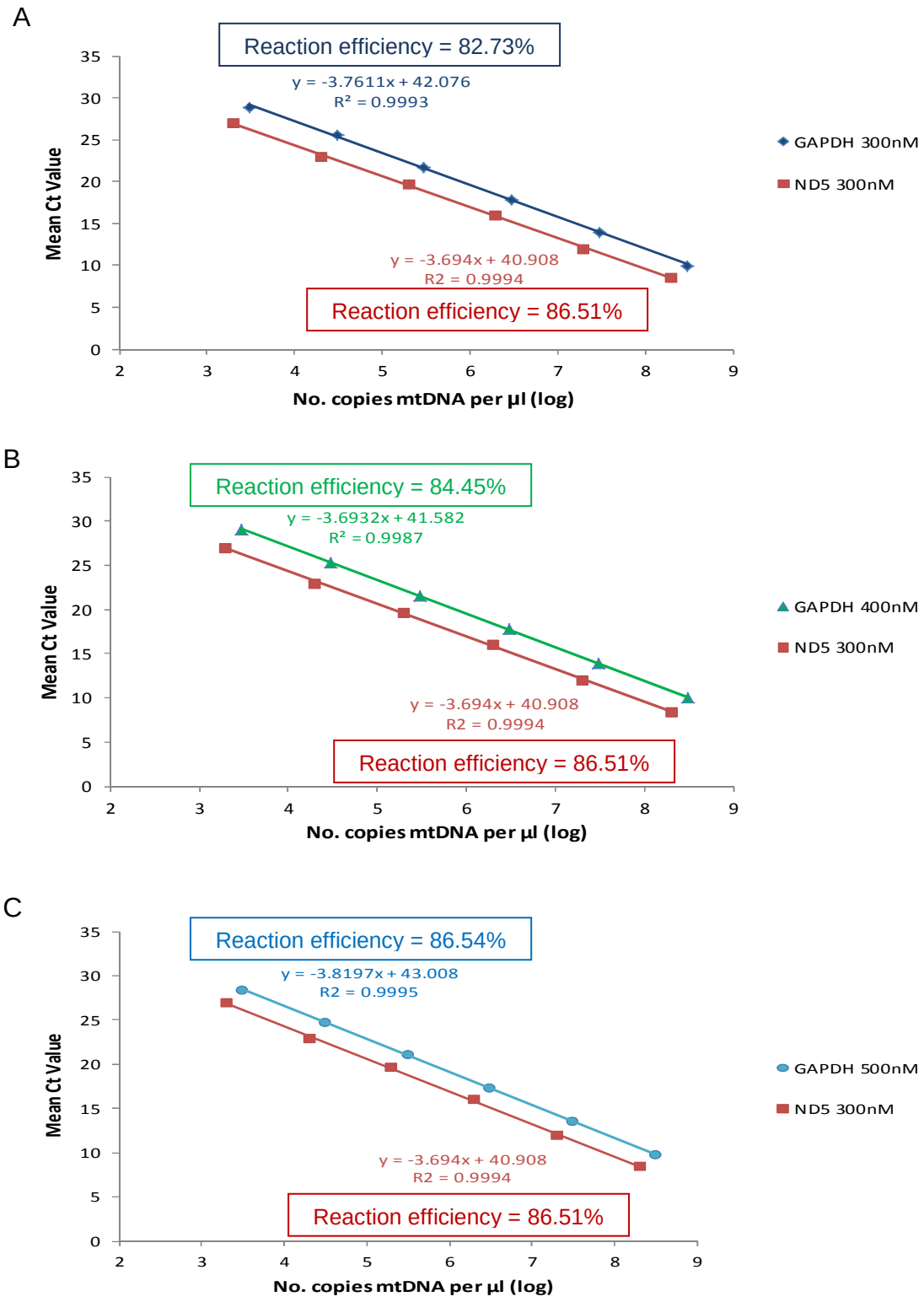

Figure 14 Mitochondrial DNA copy number assay optimisation.

Extracted DNA was quantified and serially diluted 1:5 in 100 ng/ml tRNA. Real-time PCR was then performed comparing the standard curves using 300 nM (A), 400 nM (B) or 500 nM (C) forward and reverse GAPDH primers, with the ND5 standard curve. The aim was to see which primer concentration produced the standard curve closest to that of ND5 in terms of reaction efficiency and generating parallel standard curves.

3.4.3 The effect of didanosine treatment on MIN6 cells

Following optimisation of the mtDNA copy number assay, we were able to accurately measure mtDNA levels in MIN6 cells. The next step was to see if we could then deplete mtDNA levels in MIN6 cells. We aimed to deplete mtDNA using the nucleoside reverse transcriptase inhibitor (NRTI), didanosine (ddI).

Preliminary work performed by Patrick Chinnery's Mitochondrial Research Group at Newcastle University has shown how ddI has a concentration dependent decrease on mtDNA copy number in cultured muscle cells (unpublished data). There are also many cell culture models that have been developed, exploring NRTI-induced mitochondrial toxicity and how this differs across different cell types (Höschele, 2006). In Capan-1 cells (human pancreatic cells) for example, ddI along with 3 other NRTIs were capable of depleting mtDNA, but ddI and ddA, the intracellular metabolite of ddI, resulted in less cellular cytotoxicity (Lake-Bakaar *et al.*, 2001).

Patrick Chinnery's group were able to produce a substantial 90-100% decrease in the levels of mtDNA by incubating muscle cells with 50 µM ddI for a period of 7 days. Similarly, the Capan-1 cells described above were also treated with 50 µM didanosine. Therefore, as a starting point, we decided to treat the MIN6 cells with ddI concentrations ranging from 5 µM – 50 µM for a period of 7 days, to see what effect this had on the MIN6 cells. Didanosine was reconstituted in PBS and so, PBS was added to the negative control cells as the drug vehicle control. Cells were harvested after the 7 day treatment period, DNA extracted and mtDNA copy number assay performed to assess the mtDNA:nDNA ratio.

In Figure 15A, we see that the MIN6 cells also respond to didanosine in a dose-dependent manner, with the greatest decrease in mtDNA:nDNA ratio occurring with the highest concentration of didanosine. Following 50 µM treatment, we see an approximate 75% decrease in the ratio of mtDNA:nDNA when compared to the PBS negative control. After 25 µM treatment, the decrease in mtDNA:nDNA ratio is only 60% compared to that of the PBS negative control. Whereas when cells were exposed to 10 µM and 5 µM ddI, we see only a 30% and 20% decrease in the mtDNA:nDNA ratio respectively, when compared to the PBS negative control.

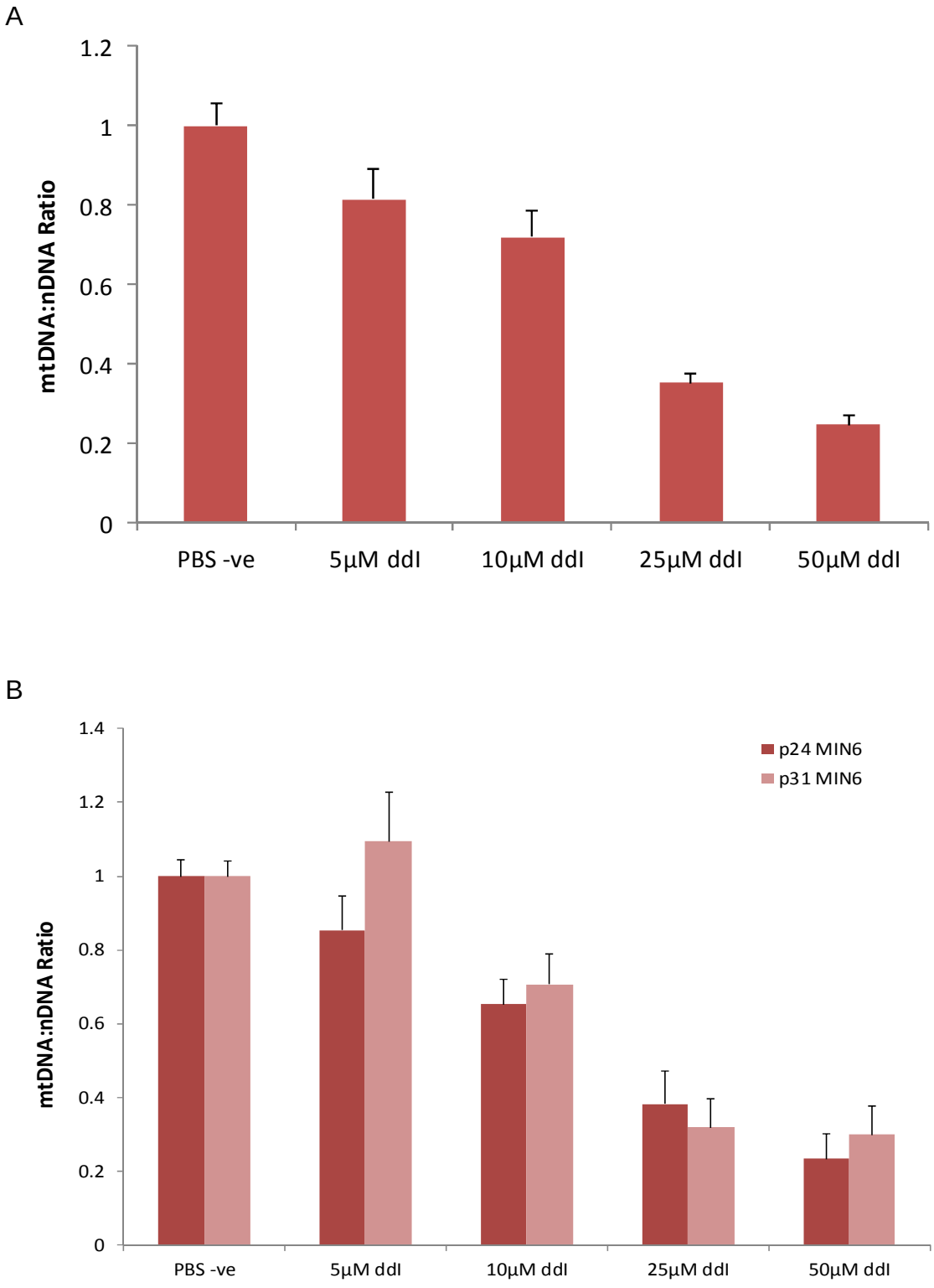

Figure 15 The effect of didanosine of MIN6 cells.

(A) Passage 27 MIN6 cells were treated for 7 days with concentrations of ddI ranging from 5 – 50 µM. Cells were then harvested, DNA extracted and quantified, and real-time PCR performed. The target (ND5) / reference (GAPDH) gene ratio was calculated using the Delta Ct method. (B) Experiment was repeated on early passage 24 and late passage 31 MIN6 cells to check the effect was uniform across passage number. Graph shows a direct comparison of passage 24 and passage 31 cells. Both experiments performed in triplicate in all passage numbers indicated. Error bars are representative of SD.

Throughout all experiments, MIN6 cells were used only between passage numbers 23 - 31. Therefore, to ascertain that the MIN6 cells would respond in a similar manner to the didanosine treatment, no matter what the passage number within this range, we directly compared the response to ddI treatment of early passage 24 MIN6 cells to that of late passage 31 MIN6 cells. The experiment was repeated in passage 24 and passage 31 cells. The results are shown in Figure 15B, and they can be seen to mirror initial data shown in Figure 15A in terms of the ddI dose-dependent effect on mtDNA depletion. We can see that in both passage 24 and passage 31 MIN6 cells, there is an approximate 70-80% reduction in the mtDNA:nDNA ratio when compared to the PBS negative control, following 50 µM ddI treatment. In both passage 24 and passage 31 cells, the degree of mtDNA depletion was reduced when lower ddI concentrations were used; with only a 60-70% decrease and a 50-60% decrease in the mtDNA:nDNA ratio compared to the PBS vehicle control cells following 25 µM and 10 µM ddI treatment respectively.

Therefore, in our MIN6 mtDNA depletion model, when using cells between the passages of 24 and 31, we can reliably deplete mtDNA levels to approximately 70-80% when using 7 day 50 µM ddI treatment, and 60-70% when using 7 day 25 µM ddI treatment. Ideally we are looking to deplete MIN6 mtDNA levels by approximately 50-60% and so, we will be looking to use 25 µM and 50 µM ddI subsequently.

3.4.4 Time course optimisation of ddI treatment on MIN6 cells

Now that we had observed how the MIN6 cells responded to didanosine treatment, we wanted to optimise the length of time of ddI exposure. Currently, cells were seeded at 200,000 cells per well and were treated with 50 µM ddI for a period of 7 days, producing a 70-80% decrease in mtDNA levels. There was a potential problem in treating for this length of time in that, after the 7 day treatment period, the MIN6 cells were extremely confluent in the 6 well plates. After treating the cells with ddI to decrease mtDNA levels, our main aim was to measure β-cell function, particularly glucose-stimulated insulin secretion (GSIS). We were concerned that if the cells were too confluent, they may become stressed, which may influence the future β-cell functional experiments we were looking to perform. Therefore, we began investigating whether or not the ddI

treatment period could possibly be reduced from the current 7 day treatment program.

We focused on 50 µM ddI treatment to begin with, as this concentration produced the greatest decrease in mtDNA depletion. MIN6 cells were again seeded at a density of 200,000 cells per well in a 6 well plate. The following day, after allowing the cells to settle overnight, cells were treated with either 50 µM ddI or PBS, the drug vehicle control, with treatment medium changed every 2-3 days. Cells were harvested 4, 5, 6 and 7 days post ddI treatment, and DNA extracted. The mtDNA copy number assay was then used to establish the mtDNA:nDNA ratio and hence, the degree of mtDNA depletion.

In Figure 16, we can see that after only 4 days of 50 µM ddI treatment, there is a 54.6% decrease in the mtDNA:nDNA ratio, when compared to the PBS cells harvested at the same time. This percentage of mtDNA depletion gradually decreases with prolonged 50 µM ddI exposure, until 7 days 50 µM ddI treatment, when there is a significant 64.9% decrease in mtDNA levels of ddI treated cells compared to PBS control cells harvested at the same time. The PBS treated cells on the other hand, can be seen to maintain a relatively consistent mtDNA:nDNA ratio that ranges between 2.4 and 2.8 arbitrary units throughout days 4 to 7 of ddI treatment. It is encouraging to find that after only 4 days 50 µM ddI treatment, we can achieve the desired 50-60% mtDNA depletion, which signifies that it would be possible to decrease the drug treatment time from 7 days. We decided that treating cells for 5 days would be optimal as we have found that upon ddI treatment removal, mtDNA levels begin to slowly increase (Figure 17) and so we did not want to remove the treatment too soon. It was decided that 5 days 50 µM ddI treatment would be enough to deplete mtDNA levels to the desired level of 50-60%, but may also allow mtDNA levels to remain at this level for enough time as to enable us to perform ensuing β-cell and mitochondrial functional assays.

For the mtDNA depletion model, it has become apparent that we are able to achieve our target of 50-60% mtDNA depletion by seeding cells at a density of 200,000 cells per well in a 6 well plate, and treating them with 50 µM ddI for 5 days. Therefore, it did not seem necessary to continue using the lower 25 µM ddI concentration as this produced a lesser degree of mtDNA depletion.

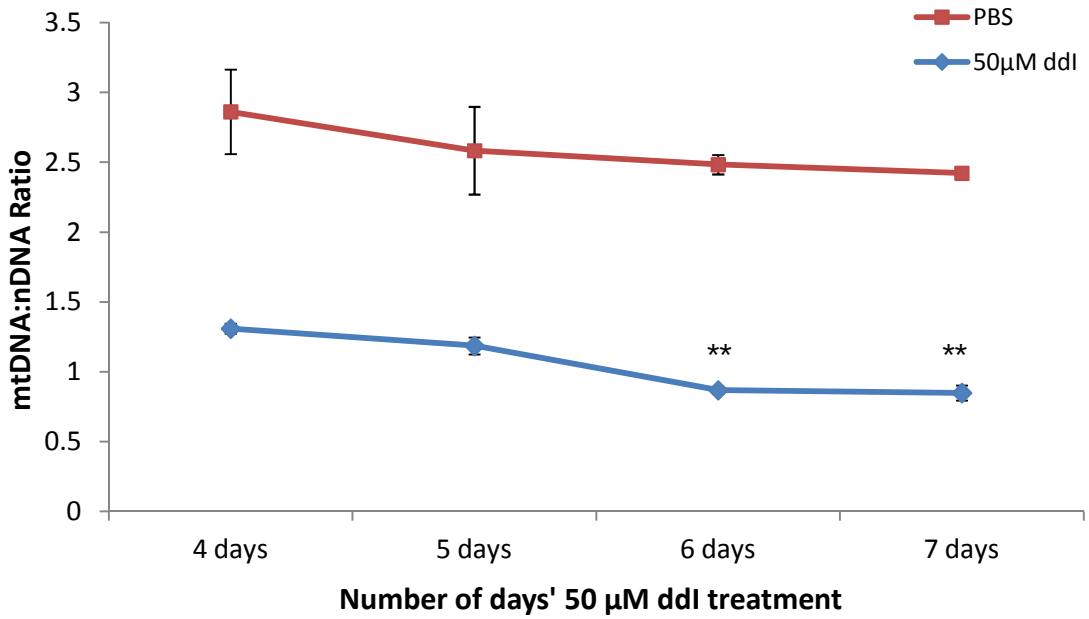

Days post ddI treatment:	4	5	6	7
PBS mtDNA:nDNA Ratio:	2.83	2.58	2.48	2.42
50 µM ddI mtDNA:nDNA Ratio:	1.31	1.18	0.87	0.85
mtDNA remaining:	45.45%	46.51%	35.08%	35.12%
mtDNA depletion:	54.55%	53.49%	64.92%	64.88%

Figure 16 Time course optimisation of ddI treatment on MIN6 cells.

Passage 31 MIN6 cells were seeded at 200,000 cells per well in 6 well plates and incubated overnight to allow cells to settle. The next day, cells were treated with 50 µM ddI or PBS (drug vehicle control). Cells were trypsinised and harvested at days 4, 5, 6 and 7 post treatment. DNA was then extracted from the cell pellet and real-time PCR carried out to ascertain the degree of mtDNA depletion. The mtDNA:nDNA ratio was then calculated using the Delta Ct method, normalising target gene ND5 expression to reference gene GAPDH expression. Experiment was performed in triplicate with error bars representative of SD. The Student's t-Test was performed on the mtDNA:nDNA ratios, with each ratio compared to the mtDNA:nDNA ratio at 4 days for each of the data series. ** $p < 0.01$

3.4.5 mtDNA recovery following ddI treatment removal

As the main aim of developing the mtDNA depletion model was to allow the measurement of β-cell and mitochondrial function following mtDNA depletion, we thought it was important to ascertain how long the mtDNA remains depleted at 50-60% before it starts to recover. To confirm this, cells were treated with 50 µM ddI for the optimal 5 day treatment period, before treatment medium was removed from cells and replaced with normal MIN6 growth medium. Cells were then harvested at various time points up to 48 hours post treatment removal, with 0 hours being the point at which the ddI treatment was removed. The mtDNA copy number assay was then used to ascertain mtDNA depletion and is shown in Figure 17.

We were interested in the time point in which the mtDNA:nDNA ratio in ddI treated cells differed significantly to the mtDNA:nDNA ratio of ddI cells harvested at time 0 hours, when ddI treatment was removed. As with the results seen in Figure 16, we see that the mtDNA:nDNA ratio of PBS treated cells remains relatively stable, ranging between 1.46 and 2.05 arbitrary units. Comparing this to the ddI treated cells, we see that upon ddI removal at time 0 hours, mtDNA levels are depleted by 63.33%. This degree of mtDNA depletion is maintained at 6 hours and 12 hours post treatment removal. At 24 hours post ddI removal however, we begin to see a slight increase in mtDNA levels, but not significantly so. By 36 and 48 hours post treatment removal, we see a marked increase in the mtDNA:nDNA ratio compared to that at 0 hours, with $p < 0.001$ and $p < 0.0001$ respectively. We can therefore conclude that for the first 24 hours post treatment removal, we have stable mtDNA depletion, whereby mtDNA remains depleted by around 60%. This gives us a window of 24 hours in which we can conduct future β-cell and mitochondrial functional experiments, in the knowledge that mtDNA levels are still depleted to around 50-60%.

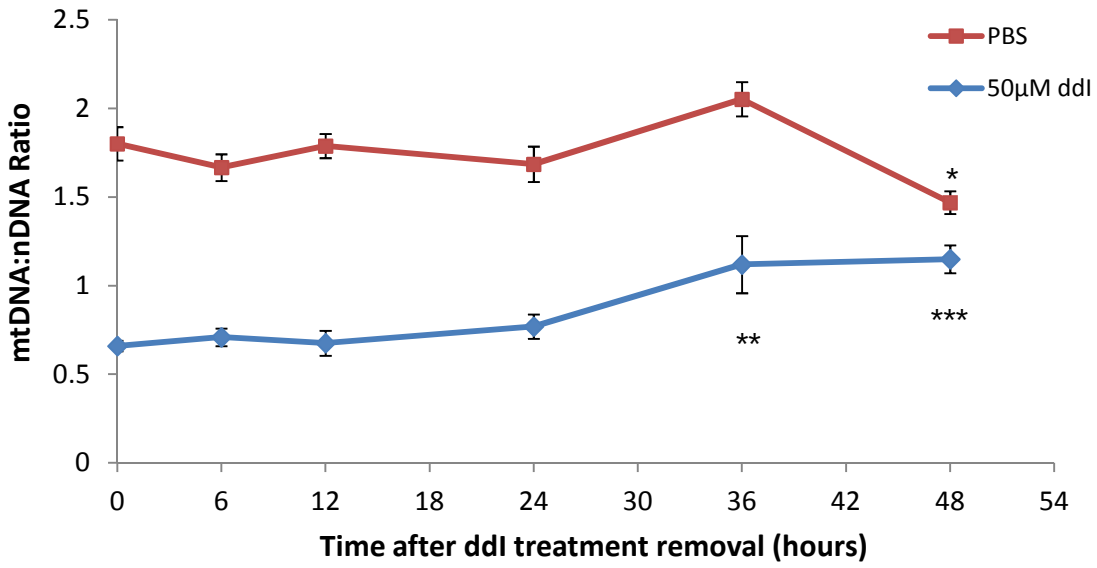

Hours after ddI treatment removal:	0	6	12	24	36	48
PBS mtDNA:nDNA Ratio:	1.80	1.67	1.79	1.69	2.05	1.46
ddI mtDNA:nDNA Ratio:	0.66	0.71	0.66	0.77	1.12	1.15
mtDNA remaining:	36.67%	42.51%	36.87%	45.56%	54.63%	78.77%
mtDNA depletion:	63.33%	57.49%	63.13%	54.44%	45.37%	21.23%

Figure 17 mtDNA recovery following ddI treatment removal.

Passage 31 MIN6 cells were seeded at 200,000 cells per well in 6 well plates and treated for 5 days with either 50 µM ddI or the PBS vehicle control. Didanosine treatment was removed after 5 days and replaced with normal MIN6 growth medium. Cells were harvested at 0, 6, 12, 24, 36 and 48 hours post treatment removal and mtDNA:nDNA ratio calculated. Experiment was performed in triplicate with error bars representative of SD. The Student's t-Test was performed on the mtDNA:nDNA ratios, with each ratio compared to the mtDNA:nDNA ratio at 0 hrs for each of the data series.
* $p = 0.01$ ** $p < 0.001$ *** $p < 0.0001$

3.4.6 The effect of ddI treatment on MIN6 cell number and cell morphology

The final stage of developing the mtDNA depletion model in MIN6 cells was to assess the effect of didanosine treatment on MIN6 cell proliferation, cell cytotoxicity and cell morphology, to explore whether the drug was having an adverse affect on the MIN6 cells. Firstly, we compared MIN6 cell proliferation rates of ddI treated cells with PBS drug vehicle control cells. Cells were seeded at a density of 200,000 cells per well in 6 well plates, before treating the following day with either 50 µM ddI or PBS. Cells were then harvested 4, 5, 6 and 7 days post ddI treatment by trypsinisation. Cell proliferation was assessed using a trypan blue exclusion haemocytometer cell count (see Section 2.2.2). At each time point, one 6 well plate was harvested consisting of 3 ddI treated wells, and 3 PBS treated wells. Four counts were made from the haemocytometer cell counting chamber for each well. The average count for each well was used to calculate the average of the 3 ddI treated or PBS treated wells at each time point and can be seen in Figure 18A.

As expected, we see a gradual increase in MIN6 cell number from days 4 to 7 for both ddI treated cells and PBS treated cells, indicating that the cells are actively proliferating. By day 6, we see a doubling in cell number from the number of cells harvested at day 4, for both ddI treated cells and PBS treated cells. There is no statistical difference between the cell numbers of ddI treated cells and PBS treated cells, at any of the time points. Therefore, it seems that the ddI drug treatment does not have an obvious adverse affect on MIN6 cell proliferation.

To measure cell cytotoxicity, we performed an LDH, lactate dehydrogenase, assay. After treating MIN6 cells for 5 days with 50 µM didanosine, the cell culture medium supernatant was retained and stored at -20 °C and later analysed using the PromoKine LDH Cytotoxicity Kit II (see Section 2.8). Cell cytotoxicity was calculated as a percentage relative to the average of the LDH positive control wells, which exhibited 100% cytotoxicity. In Figure 18B, we can see that for both ddI treated cells and PBS treated cells, there is 4% and 3% cell cytotoxicity respectively. Therefore, it seems that the didanosine treatment does not seem to be having an adverse cytotoxic effect on the MIN6 cells.

Finally, we wished to examine MIN6 cellular morphology of 50 µM ddI treated cells with PBS negative control cells, throughout duration of the 5 day treatment program. Phase contrast images of the cells were taken using the Nikon Eclipse TE2000-S microscope and Photometrics CoolSNAP HQ2 Turbo 1394 camera at x10 magnification. Cells were seeded in 6 well plates at a density of 200,000 cells per well and allowed to settle overnight. The following day, at time 0 hours, cells were incubated with either 50 µM ddI or PBS, with treatment medium being replaced every 2 – 3 days. Images were taken between 0 hours, when treatment commenced, and 120 hours, when treatment finished, at 24 hour intervals and can be seen in Figure 18C.

At 0 hours, we can see that there are still some cells that are recovering after passaging, as they take on a small, dense, balled up morphology. By 24 hours, we can see that the cells have started to spread out a bit more and have begun to grow again. At this point, there does not seem to be an obvious difference in cell morphology or cell number when comparing ddI treated cells with PBS treated cells. During hours 48 to 96, we can see the cells continuing to grow, and can witness the typical MIN6 cell morphology: the cells have a ‘spiky’ appearance, and prefer to grow in clusters with neighbouring cells. This can be seen in ddI treated cells and PBS treated cells. By 120 hours of treatment, we can start to see the cells becoming confluent, with the small dark dots on top of cell clusters indicating dying cells. Because the cells grow in clusters, they never form a perfect monolayer, therefore, these dying cells on top of the cell clusters are what we look for when determining how confluent the cells are. This also corroborates why we needed to decrease the didanosine treatment time, as culturing the cells with ddI for 7 days was far too long without splitting the cells.

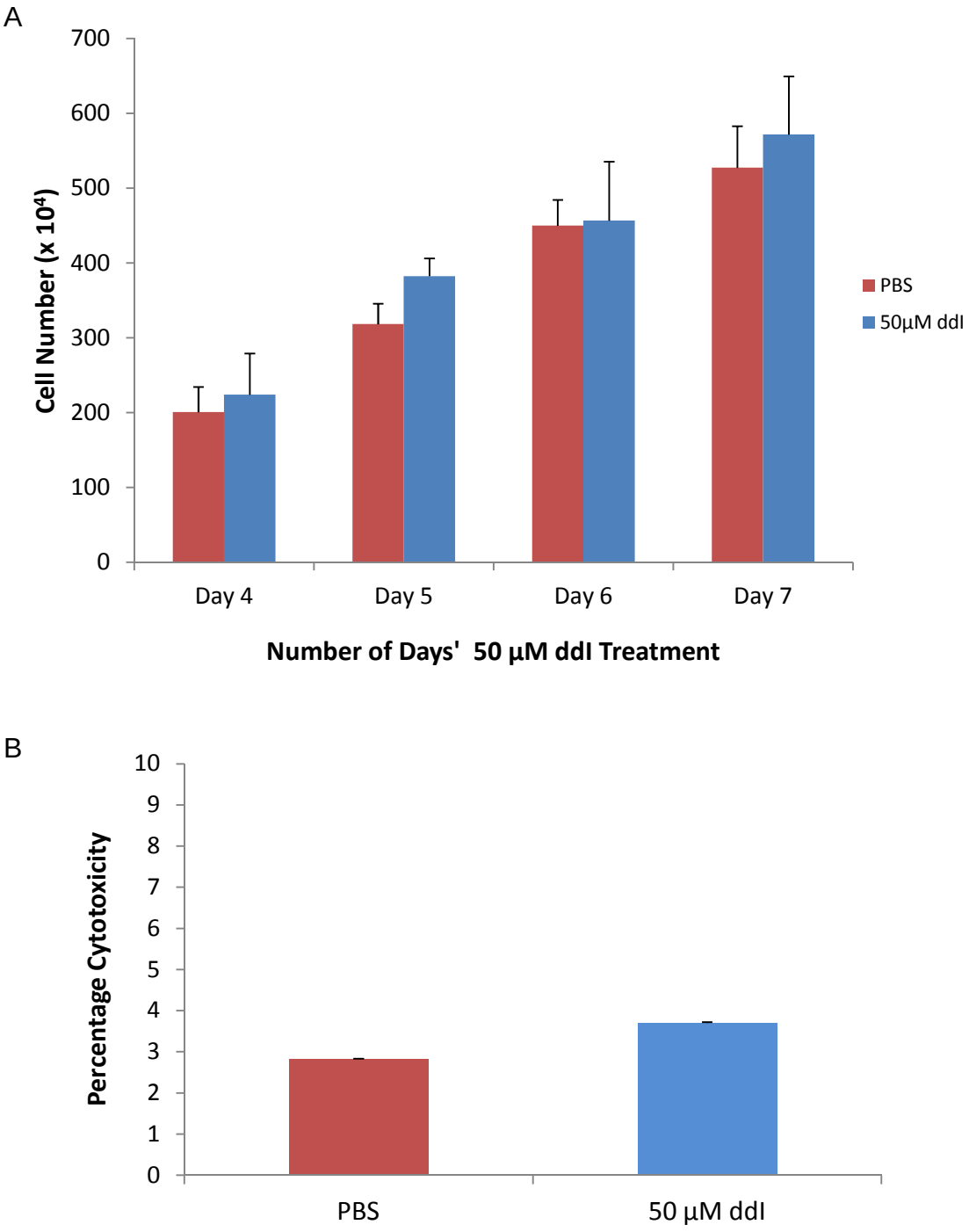

Figure 18 The effect of ddI treatment on MIN6 cell number, cell cytotoxicity and cell morphology.

MIN6 cells were treated up to 7 days with 50 µM ddI or PBS (drug vehicle control). Cells were harvested at days 4, 5, 6, and 7 post ddI treatment and cell number of ddI treated cells compared to PBS control cells (A). Cell cytotoxicity was analysed using an LDH assay after 5 days ddI treatment (B). Cells were imaged using a Nikon Eclipse TE2000-S microscope and Photometrics CoolSNAP HQ2 Turbo 1394 camera at x10 magnification between 0 hours, when treatment commenced, and 120 hours, when treatment finished, at 24 hour intervals (C).

C

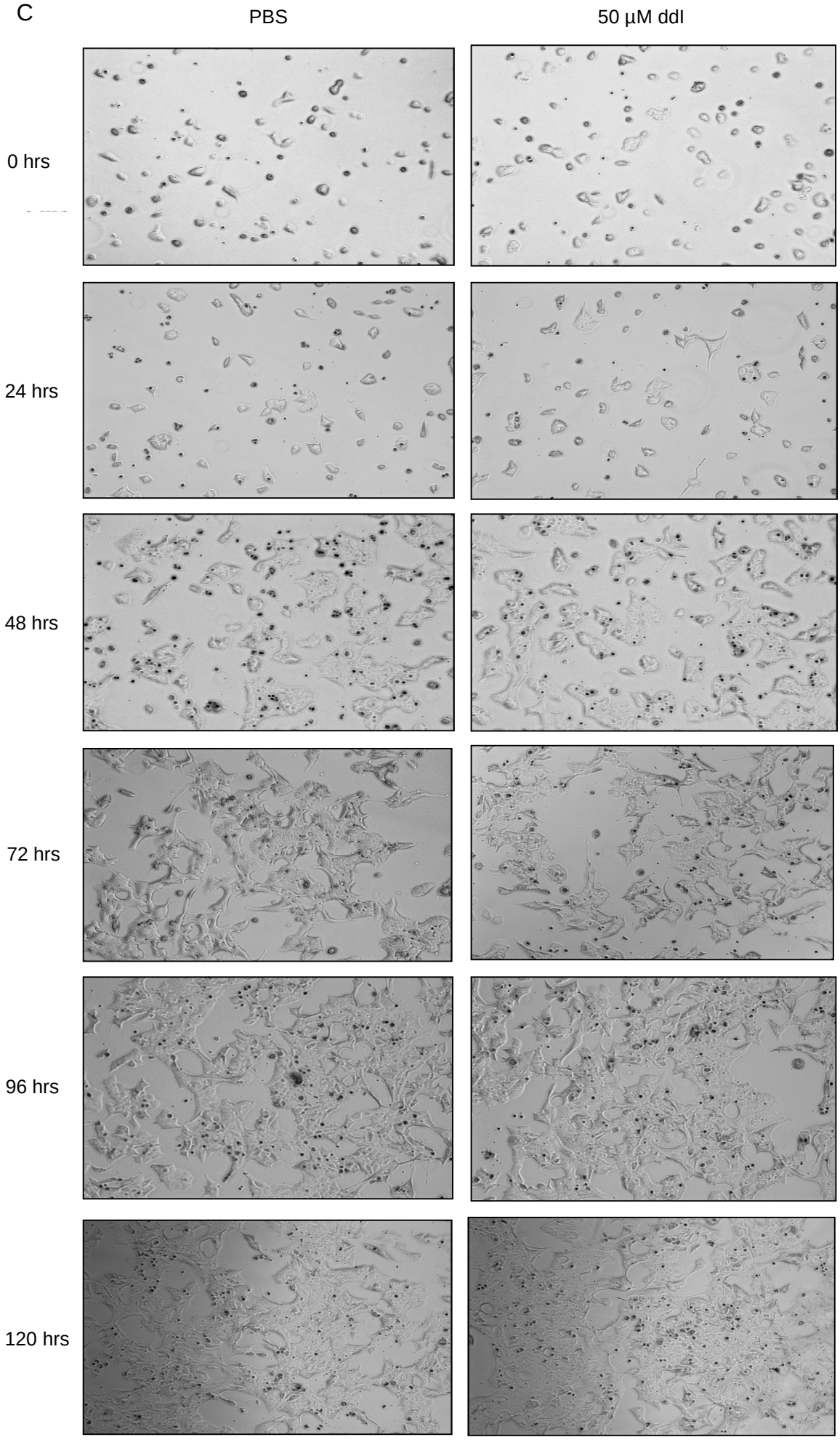

3.5 Discussion

The main aim of this chapter was to develop a model of partial mtDNA copy number depletion specifically in MIN6 cells. MIN6 were chosen as they are responsive to external changes in glucose concentration, and secrete insulin accordingly (Miyazaki *et al.*, 1990). When this work was initially started, there was no human cell line equivalent. However, this may change as last year Revassard *et al.* reported that they had established a human insulin secreting pancreatic β-cell line, EndoC-βH1 cells. As with MIN6 cells, the EndoC-βH1 cells express the SV40LT antigen under control of the insulin promoter (Ravassard *et al.*, 2011). These cells look promising but further investigations are needed to ascertain how robust the cells are as a model of human pancreatic β-cell function.

The first step in producing a model of mtDNA depletion in MIN6 cells was to show that MIN6 cells contained the many mitochondria required to fuel glucose-stimulated insulin secretion. We labelled mitochondria using MitoTracker Orange CMTMRos, an orange fluorescent dye that accumulates in active mitochondria and is retained after cells have been fixed and permeabilised. Using confocal microscopy, we could see the mitochondria assembled in vast complex networks within the cell (Figure 12). In some instances, individual mitochondria could be seen measuring approximately 1.28 µm. Mitochondria can vary in size measuring less than 1 µm, or measuring up to 10 µm (Kennady *et al.*, 2004). So the mitochondria we have managed to measure are of expected size.

The mtDNA genome resides inside the mitochondria and so, we moved on to quantifying mtDNA levels in MIN6 cells. Using real-time PCR, the gene expression of mtDNA encoded ND5 was expressed relative to the nDNA encoded reference gene GAPDH, generating the mtDNA:nDNA ratio. Optimal PCR conditions were found using 300 nM ND5 forward and reverse primers, 500 nM GAPDH forward and reverse primers. This produced a reaction efficiency of 86% for both reactions, allowing accurate relative quantification. The standard curves were not used during the quantification of unknown samples, but instilled confidence that we could accurately predict the mtDNA:nDNA ratio across the linear range of the standard curve.

Once the mtDNA copy number assay was optimised, we wanted to see if we could deplete mtDNA levels following treatment with the mtDNA replication inhibitor didanosine, ddI. Didanosine is a nucleoside analogue of adenosine, but differs in that it lacks the hydroxyl (OH) group at the 3' carbon position on the pentose sugar moiety (Figure 7). As ddI lacks the 3'-OH group required for phosphodiester linkage, strand termination ensues following ddI incorporation.

Didanosine is a member of a family of chemicals known as nucleoside reverse transcriptase inhibitors (NRTIs). Many cell culture models have been developed that explore NRTI-induced mitochondrial toxicity and how this toxicity differs in different cell types (Hoschele, 2006). Lake-Bakaar and colleagues compared the effects of ddI with 3 other NRTIs in Capan-1 cells (human pancreatic cells). The group conclude that all nucleoside analogues investigated were capable of depleting mtDNA, but ddI and ddA (dideoxyadenosine, the intracellular metabolite of ddI) resulted in less cellular cytotoxicity (Lake-Bakaar *et al.*, 2001).

Our results support the literature in that ddI seems to be a potent inhibitor of mtDNA synthesis in MIN6 cells, causing mtDNA depletion (Figure 15). The effect of ddI on MIN6 cells was dose-dependent, with the greatest mtDNA depletion occurring when cells were exposed to 50 µM ddI. Similarly to Lake-Bakaar and colleagues, we found that ddI had little toxic effects on cell proliferation, cell morphology or cell cytotoxicity (Figure 18). It took some time to find optimal conditions in which we could culture the MIN6 cells in ddI to produce the desired 50-60% mtDNA depletion. But by seeding the MIN6 cells at a density of 200,000 cells per well, and culturing for 5 days in 50 µM, we could reliably deplete mtDNA levels by 50-60%. We wanted our MIN6 cell model to have 50-60% mtDNA depletion in support of the work of Cree *et al.*, who found that the age-related decrease in mtDNA copy number averaged 50% in non-diabetic islet donors aged 17 – 75 years (Cree *et al.*, 2008).

Chemical intervention using inhibitors of mtDNA synthesis has proven a popular method to deplete mtDNA levels. Most commonly, prolonged treatment with ethidium bromide (EtBr) has been an effective means of creating p^0 cells completely devoid of mtDNA. Soejima *et al.* produced two MIN6 cell derivatives: p^0 MIN6 and mtDNA repopulated MIN6 cell cybrids. The group

found that unsurprisingly, the p^0 MIN6 cells were unable to respond to glucose during glucose-stimulated insulin secretion, and suffered severe loss of mitochondrial transcription, translation and respiratory activity. However, when the p^0 MIN6 cells were repopulated with foreign mitochondria containing wild type mtDNA (repopulated MIN6 cell cybrids), insulin secretion was effectively restored (Soejima *et al.*, 1996). Similarly, Hayakawa *et al.* showed that by treating βHC-9 pancreatic β-cells with EtBr for 6 days, mtDNA transcription was decreased to 10-20% of the control cells. Insulin secretion was also affected in these cells, which was supported by a disruption in the Ca^{2+} dynamics of the cells.

Finally, upon removal of didanosine treatment, we found that mtDNA remains significantly decreased by 50-60% for the first 24 hours post treatment removal. After 24 hours post treatment removal however, mtDNA levels begin to increase as mtDNA repopulates. This gives us a time period of 24 hours in which to perform β-cell and mitochondrial functional studies, in the knowledge that mtDNA levels still remain depleted by around 50-60%. Studies using EtBr have also found that the mtDNA depletion and the cellular defects caused by the EtBr treatment are reversed following treatment removal (Hayakawa *et al.*, 1998; Maniura-Weber *et al.*, 2004; Park & Lee, 2007). The fact that mtDNA levels repopulate following treatment removal demonstrates unequivocally that it is ddI (or EtBr) causing the mtDNA depletion.

Using the didanosine dependent mtDNA depletion model, we then wanted to see what effect partial mtDNA depletion had on β-cell function, particularly glucose-stimulated insulin secretion, and mitochondrial function.

Chapter 4

Mitochondrial DNA depletion in MIN6 cells: TFAM mRNA Knockdown

4 Mitochondrial DNA depletion in MIN6 cells: TFAM mRNA knock down

4.1 Introduction

To complement the didanosine mtDNA depletion model developed in Chapter 3, we wanted to develop a second model of mtDNA depletion in MIN6 cells. The didanosine mtDNA depletion model disrupts mitochondrial biogenesis through chemical intervention; we wanted a complementary model using genetic techniques. From the literature, it seemed that TFAM, an important mtDNA transcription factor, may be a suitable target. We would then use both mtDNA depletion models to investigate the effect of mtDNA depletion on β-cell and mitochondrial function.

It has long been established following TFAM knock out studies, that TFAM plays an integral role in mitochondrial biogenesis (Larsson, et al., 1998; Li, et al., 2000; Silva, et al., 2000; Sorensen, et al., 2001; Wang, et al., 1999; Wredenberg, et al., 2002). TFAM function was directly linked to mtDNA copy number by Erkstrand *et al.* when their transgenic mice harbouring the human *TFAM* gene were found to ubiquitously overexpress the TFAM protein, which subsequently caused an increase in mtDNA copy number (Ekstrand, et al., 2004). *In vivo* TFAM knockout mice were reported to have a 35-40% reduction in mtDNA levels (Larsson, et al., 1998). Tissue specific TFAM knockout mice were found to exhibit similar levels of mtDNA depletion in neurones (Sorensen, et al., 2001) and skeletal muscle (Wredenberg, et al., 2002).

These studies imply that mtDNA levels and TFAM expression are tightly correlated. This theory is supported by studies on TFAM / mtDNA stoichiometry that report highly abundant TFAM association with mtDNA (Campbell, et al., 2012; Dairaghi, et al., 1995; Ghivizzani, et al., 1994; Kaufman, et al., 2007) or that TFAM coats the entire mtDNA molecule (Alam, et al., 2003; Ohgaki, et al., 2007; Takamatsu, et al., 2002).

Whilst previous *in vitro* studies investigating TFAM knock down have cultured primary tissues extracted from TFAM knock out animal models (Silva, et al., 2000; Sorensen, et al., 2001; Wang, et al., 1999), we would like to target TFAM

gene expression by exploiting siRNA technology in the MIN6 cell line. By transfecting cells with TFAM siRNA probes, can we effectively silence TFAM gene expression in MIN6 cells and does this have a knock on effect on mtDNA levels, as suggested in the literature?

4.2 Aims

The main aim of this chapter was to develop a second model of mtDNA depletion to complement the didanosine mtDNA depletion model. We aimed to achieve this by tackling the following objectives:

- To repeat the TFAM transfection protocol optimised by Invitrogen to see if we could knock down TFAM mRNA expression by 70%.
- To investigate whether TFAM knock down had an effect on mtDNA levels using the mtDNA copy number assay previously optimised.
- To ensure that MIN6 cell viability was not compromised following transfection.

4.3 Methods

4.3.1 Design and Synthesis of TFAM siRNA probes

The design, synthesis and validation of the TFAM small interfering RNA (siRNA) duplexes was performed by Invitrogen (Life Technologies, California, USA). Invitrogen began by first designing five Stealth RNAi duplexes specific for the mouse TFAM gene, accession number NM_009360.4, using the BLOCK-iT RNAi Designer (Figure 19). The sense sequences of the Stealth RNAi probes were then used to create inserts for the pSCREEN-iT-GW/LacZ vector. Insert cassettes were created by flanking the sequence targeted by the RNAi duplex (highlighted in red in Figure 20B) with approximately 30 nucleotides both upstream and downstream. The five Stealth RNAi duplexes, and five pSCREEN-iT insert sequences were then synthesised, and the five pSCREEN-iT sequences were annealed to form double stranded DNA (dsDNA). The dsDNA was then cloned into the pSCREEN-iT-GW/LacZ vector, downstream of the LacZ coding region (Figure 20A).

Stealth™ Name	Sense / Antisense	Sequence
NM_009360.4 - 193	Sense	CCUCGUCUAUCAGUCUUGUCUGUAU
	Antisense	AUACAGACAAGACUGAUAGACGAGG
NM_009360.4 - 232	Sense	CCAGCAUGGGUAGCUAUCCAAAGAA
	Antisense	UUCUUUGGAUAGCUACCCAUGCUGG
NM_009360.4 - 284	Sense	CACAGAACAGCUACCCAAAUUUAAA
	Antisense	UUUAAAUUUGGGUAGCUGUUCUGUG
NM_009360.4 - 429	Sense	UACAAAGAAGCUGUGAGCAAGUAUA
	Antisense	UAUACUUGCUCACAGCUUCUUUGUA
NM_009360.4 - 695	Sense	GGCAUAUAUUCAGCUUGCUAAAGAU
	Antisense	AUCUUUAGCAAGCUGAAUAUAUGCC

Figure 19 Design of Stealth RNAi Duplexes by Invitrogen (Life Technologies, California, USA)

Using the BLOCK-iT RNAi Designer, five RNAi duplexes were designed targeting the mouse TFAM gene, accession number NM_009360.4.

A

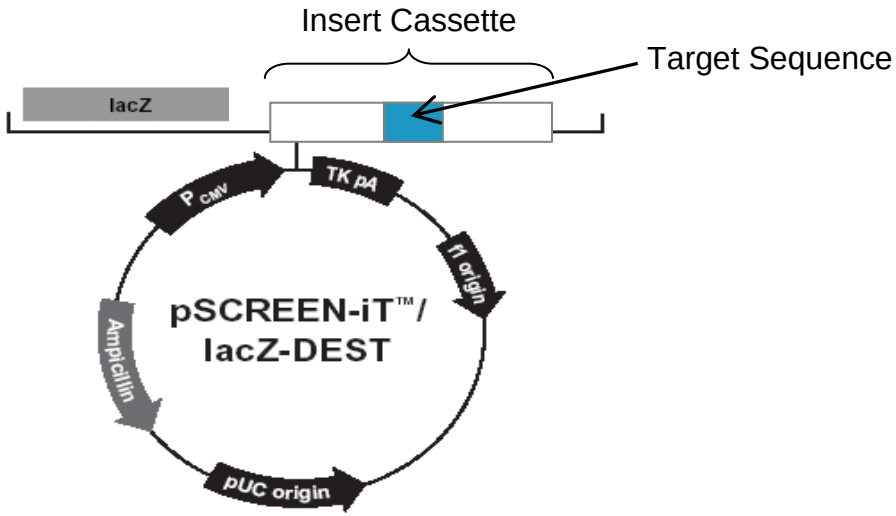

B

NM_009360.4 - 193	AGATGTGCGCGGGCTGCGGGGGTCGCATCCCCTCGTCTATCAGTCTTGTCTGTATTCCGAAGTGTTTTTCCAGCATGGGTAGCTA
NM_009360.4 - 232	TCAGTCTTGTCTGTATTCCGAAGTGTTTTTCCAGCATGGGTAGCTATCCAAAGAAACCTATGAGTTCATACCTTCGATTTTCCAC
NM_009360.4 - 284	GAAACCTATGAGTTCATACCTTCGATTTTCCACAGAACAGCTACCCAAATTTAAAGCTAAACACCCAGATGCAAAACTTTCAGAA
NM_009360.4 - 429	GAAGCTGATTTTAAAGCTGAGTGGAAAGCATACAAAGAAGCTGTGAGCAAGTATAAAGAGCAGCTAACTCCAAGTCAGCTGATGG
NM_009360.4 - 695	TTGGAAAAATCTGTCTCCTGAGGAAAAGCAGGCATATATTCAGCTTGCTAAAGATGATAGGATTCGTTACGACAATGAAATGAAG

Figure 20 pSCREEN-iT/LacZ Vectors and Insert Cassettes

Using the five sense sequences listed in Figure 19, insert cassettes were designed by adding approximately 30 nucleotides upstream and downstream of the region targeted by the siRNA duplexes (highlighted in red) (B). These insert cassettes were then annealed to form double stranded DNA, before being cloned into the pSCREEN-iT/LacZ vector, immediately downstream of the LacZ coding region (A).

A

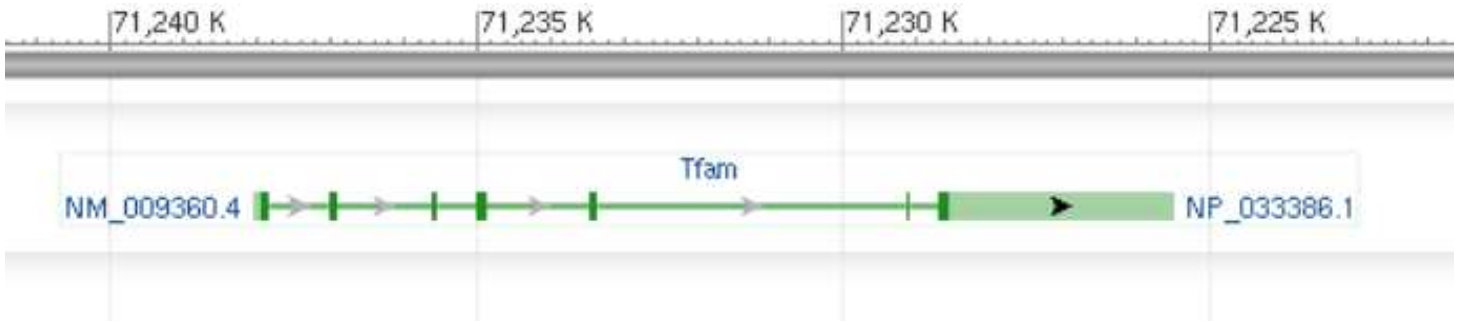

B

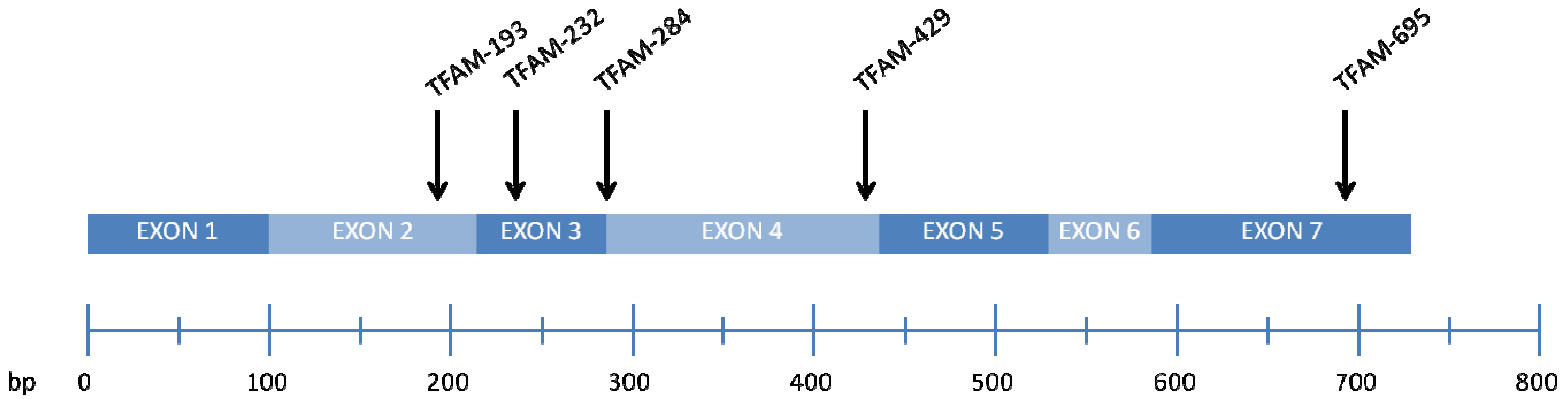

Figure 21 *Mus Musculus* TFAM gene and mRNA

The mouse TFAM gene is approximately 12.8 kb in length. It is situated on chromosome 10 and consists of 7 exons, shown in dark green (A). The gene is transcribed to produce a 4171 bp mRNA molecule with a 341 bp 5' untranslated region (UTR) and 3098 bp 3' UTR, but only the exons are shown (B). The arrows represent the areas targeted by the five TFAM siRNA duplexes. The mRNA is then translated producing the 243 aa TFAM protein which is 28 kDa in size.

Information adapted from the NCBI AceView program found at http://www.ncbi.nlm.nih.gov/IEB/Research/Acembly/av.cgi?db=mouse&q=Tfam

The cloned pSCREEN-iT-GW/LacZ vector was then propagated in *E.coli* and glycerol stocks made, which were shipped to Newcastle and stored at -80 °C. Invitrogen also supplied all five siRNA probe duplexes that had been reconstituted in water to a final concentration of 20 µM. The areas of the TFAM mRNA molecule targeted by the five TFAM siRNA duplexes can be seen in Figure 21.

4.3.2 Validation of TFAM siRNA probes

The five siRNA duplexes were then validated in GripTite293 MSR cells, human kidney HEK293 derived cells expressing the human macrophage scavenger receptor, using the pSCREEN-iT assay system. This work was also carried out by Invitrogen (Life Technologies, California, USA). Briefly, GripTite293 MSR cells were transfected in triplicate in 96 well plates with the Stealth RNAi duplexes. Each pSCREEN-iT/LacZ-target vector was co-transfected with the Scrambled Med GC negative control Stealth RNAi duplex, the Stealth RNAi LacZ positive control duplex, or the target-specific Stealth RNAi duplex. Cells were then harvested 24 hrs post transfection and β-galactosidase activity measured.

Beta-galactosidase activity was measured following addition of the CUG substrate to an aliquot of the cell lysate. If active β-galactosidase was present, then it catalysed the cleavage of the CUG substrate to form 7-hydroxycoumarin-3-carboxylic acid, which is highly fluorescent. Fluorescence was then measured using a plate reader, with excitation centred around 390 nm and emission centred around 460 nm. Cells co-transfected with the LacZ RNAi duplex were used as the positive control as the LacZ RNAi targets and downregulates *LacZ* gene expression. *LacZ* encodes the β-galactosidase protein and so, little β-galactosidase protein is produced, resulting in minimal β-galactosidase activity. The Scrambled RNAi probe however, was used as the negative control as it does not target any mammalian gene and so, produces negligible knock down. The effectiveness of each of the five TFAM siRNA duplexes was then compared against the negative and positive controls (Figure 22).

It is clear that all five TFAM siRNA probes are specific for the target sequence on the pSCREEN-iT/LacZ cloned vector and are thus effective at knocking down β-galactosidase activity. From the data in Figure 22, we subsequently chose to use the TFAM-193 and TFAM-429 siRNA duplexes in our experiments as they target different regions of the TFAM mRNA (Figure 21), and also produced the best knock down in the pSCREEN-iT assay.

4.3.3 TFAM knock down in MIN6 cells

Once Invitrogen had developed the TFAM siRNA duplexes and validated the probes in GripTite293 MSR cells, the next stage was to check we could knock down TFAM gene expression specifically in MIN6 cells. We had previously attempted to transfect MIN6 cells using lipid-based transfection systems that had been successfully used to silence gene expression in human and mouse muscle cells (data not shown), but this approach proved unsuccessful in MIN6 cells, which led us to enlist the expertise of Invitrogen through links with our industrial collaborators, Unilever Plc. Similarly, Invitrogen also found that transfecting the MIN6 cells using lipid-based transfection systems such as Lipofectamine RNAiMAX and Lipofectamine 2000 yielded poor transfection efficiencies. Therefore, Invitrogen attempted electroporation instead to see if this was more successful. The Neon Transfection System was used to develop a protocol for the MIN6 cells. The initial optimisation was performed using the BLOCK-iT Fluorescent Oligo for electroporation, and transfection efficiency was measured by GFP flow cytometry. The transfection efficiency was only estimated to be around 30%, but the group found that the p53 positive control Stealth RNAi caused significant reduction in p53 mRNA levels. Encouraged by these results, the group investigated TFAM mRNA levels and found that TFAM mRNA expression was decreased by 70% for both the TFAM-193 and TFAM-429 siRNA duplexes. The experiment was repeated twice, each time in triplicate. The optimal electroporation conditions were found to be by shocking the MIN6 cells at a voltage of 1200 V for 20 ms, for 2 pulses.

Figure 23 briefly explains MIN6 transfection using the Neon Electroporation System, more specific details are given in Section 2.3.

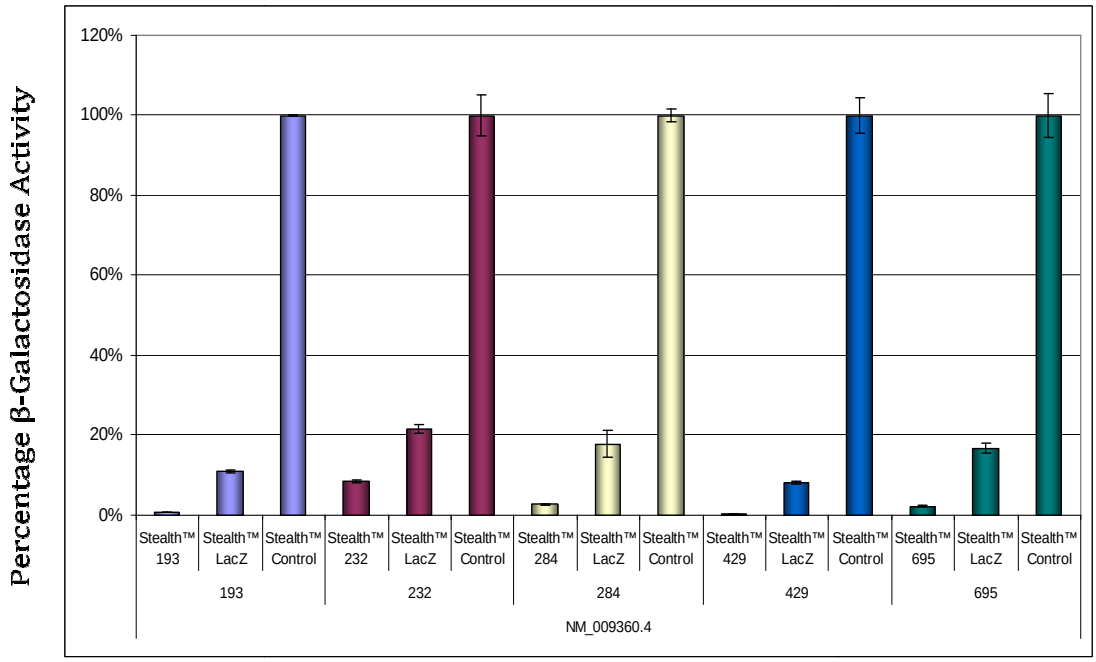

Figure 22 siRNA probe validation using the pSCREEN-iT assay system

The 5 Stealth siRNA probes were validated by transfecting GripTite293 MSR cells with Stealth RNAi duplexes. Each pSCREEN-iT/LacZ-target vector was co-transfected with the Scrambled Med GC Stealth RNAi (negative control), the LacZ Stealth RNAi (positive control) or the TFAM Stealth RNAi duplexes. Beta-galactosidase activity was measured following addition of substrate CUG to the cell lysate and measuring fluorescence. Results were performed in triplicate wells and were normalised to the Scramble Stealth RNAi negative control. Error bars are representative of standard deviation.

Validation assay performed by Invitrogen (Life Technologies, California, USA). Data taken from a Custom Services Project Report, dated 04.01.10 (prepared by Megan Palm), project number CB5052.

A

B

C

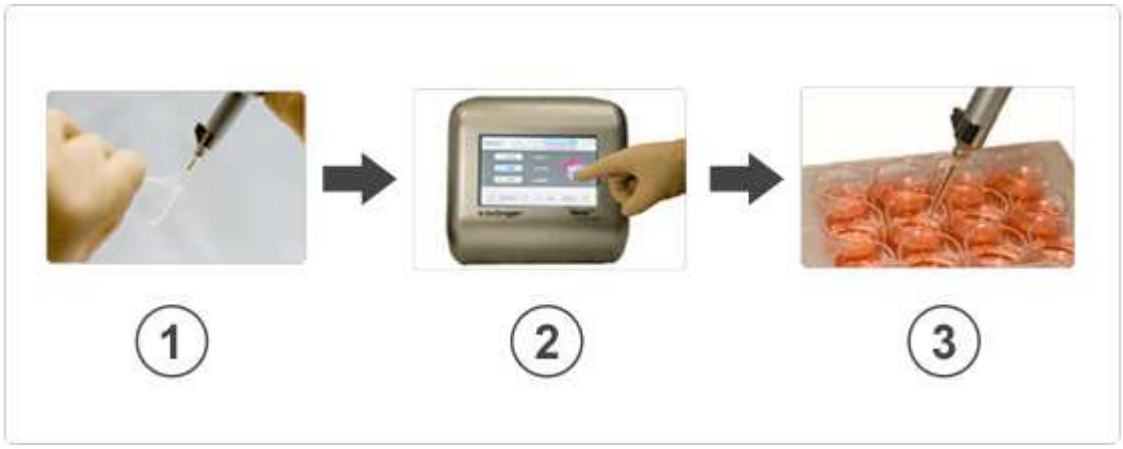

Figure 23 Neon Transfection System

The Neon Transfection System (Life Technologies, Paisley, UK) consists of a grey touch screen device, attached to which is a Neon pipette station used to dock the Neon pipette (A). The Neon pipette is adapted to fit a uniquely designed 10 µl or a 100 µl plastic tip, which contains a gold electrode piston (B). The Neon pipette is used to pipette 10 µl of a pre-mixed solution containing cells and siRNA (C1). The pipette is secured into the docking station and cells are transfected according to the selected protocol (C2). Transfected cells are then pipetted in to 24 well plate containing 0.5 ml pre-warmed transfection medium per well (C3). After transfection was complete, cells were incubated in a humidified incubator (37 ˚C, 5% CO_2).

All images taken from www.invitrogen.com.

4.4 Results

4.4.1 TFAM mRNA knock down in MIN6 cells

Now that we had a fully optimised protocol from Invitrogen, the first step was to check we could replicate the results. Using the Neon Transfection System also, we electroporated MIN6 cells in suspension with 100 nM TFAM-193 siRNA, TFAM-429 siRNA or Med GC Stealth Scrambled negative control siRNA. The Shocked cells were resuspended in Resuspension Buffer R and shocked, but no siRNA was added, thus serving as a negative control also. Cells were electroporated using the same conditions optimised by Invitrogen, 1200 V for 20 ms for 2 pulses, before seeding in a 24 well plate with 500 µl transfection medium (without antibiotics). The transfected cells were then incubated at 37 °C for 48 hrs or 72hrs before harvesting. These time periods were chosen to allow time for the TFAM knock down to impact on mtDNA replication. RNA was extracted, quantified and reverse transcribed. The degree of TFAM mRNA knock down was assessed by real-time PCR using TaqMan hydrolysis probes, relative to reference gene β2 Microglobulin (B2M) (see Section 2.4.2 and 2.4.3).

We were able to knock down TFAM mRNA expression by more than 80% ($p<0.0001$) compared to the Scrambled and Shocked controls, 48 hrs post transfection (Figure 24A). This corroborates Invitrogen's result, who reported a 70% decrease in TFAM mRNA expression 24 hrs post transfection. Seventy two hrs post transfection, we see a slight increase in TFAM expression, but mRNA is still significantly knocked down by more than 80% ($p<0.0001$) (Figure 24B). We can also see that the Scrambled siRNA seems to be having no adverse effect on TFAM gene expression, with relative expression mirroring that of the Shocked control, in which no siRNA was added.

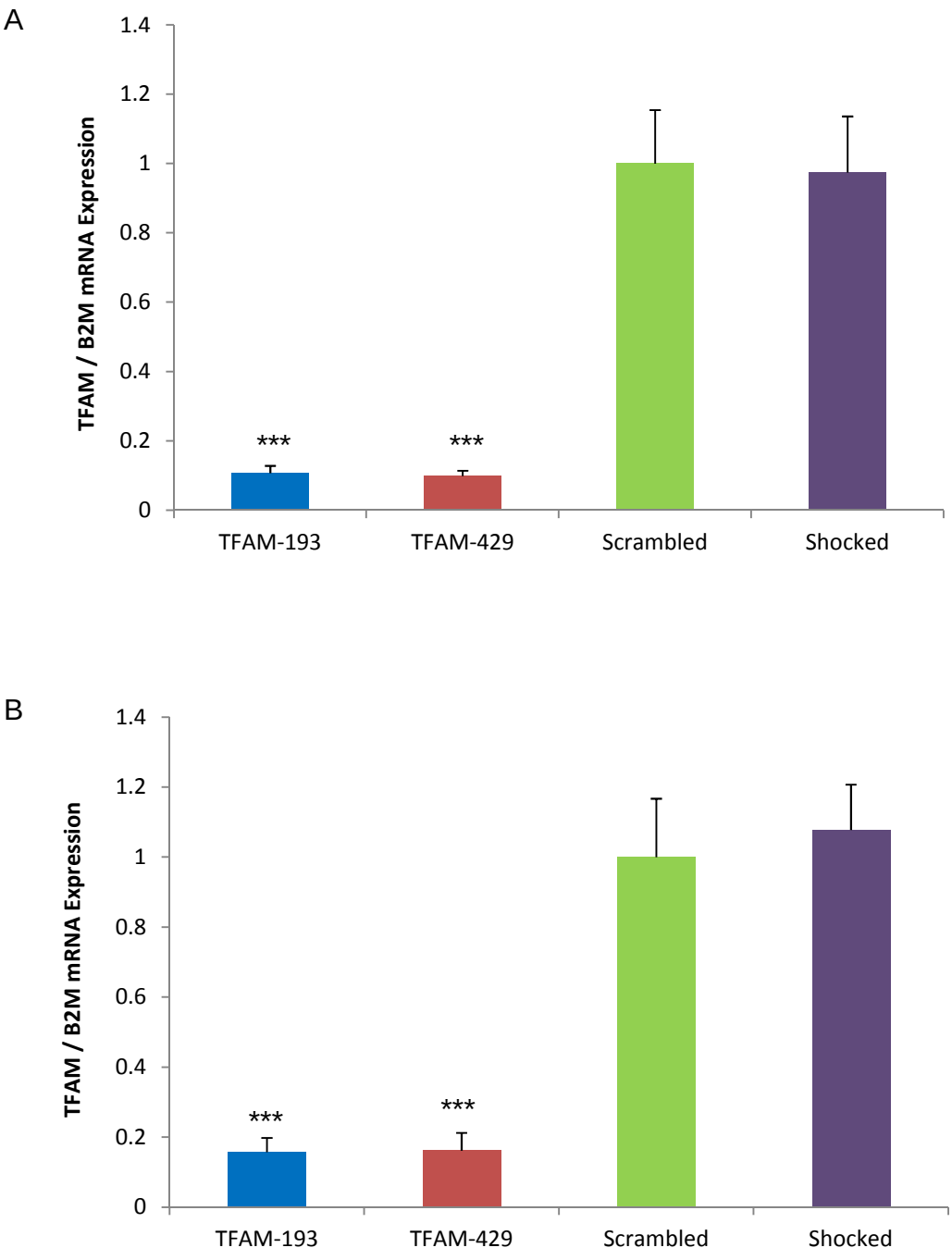

Figure 24 TFAM siRNA knock down 48 hrs and 72 hrs post transfection

MIN6 cells were transfected in suspension using the Neon Transfection System with 100 nM TFAM-193 siRNA, TFAM-429 siRNA, Scrambled negative control siRNA, or no siRNA (Shocked). Transfected cells were transferred into a 24 well plate containing transfection growth medium (without antibiotics), and were incubated at 37 ˚C. Cells were harvested 48 hrs (A) or 72 hrs (B) post transfection, and RNA extracted, quantified and reverse transcribed. TFAM mRNA expression was quantified relative to control gene B2M by real-time PCR. (A) Experiment repeated twice, each repeat performed in triplicate. (B) Experiment repeated four times, each repeat performed in triplicate. Error bars representative of SEM. Results normalised to Scrambled negative control. *** $p<0.0001$ relative to Scrambled control.

4.4.2 TFAM mRNA knock down causes mtDNA depletion

Encouraged by the success of the TFAM knock down, we repeated the electroporation and extracted DNA and RNA from the harvested cells (see Section 2.4.3 for further detail), 48 hrs and 72 hrs post transfection. We wanted to measure TFAM mRNA expression using the extracted RNA, but we also wanted to measure the mtDNA:nDNA ratio using the extracted DNA and the mtDNA copy number assay optimised in Chapter 3.

After measuring the TFAM mRNA expression relative to the B2M reference gene, we found that TFAM mRNA levels were depleted by >80% in both the TFAM-193 and TFAM-429 transfected cells compared to the Scrambled and Shocked control cells (data are one of the repeats shown in Figure 24). Again, TFAM levels were lowest 48 hrs post transfection in TFAM siRNA transfected cells, but TFAM expression was still significantly reduced by >80% 72 hrs post transfection in TFAM siRNA transfected cells compared to Scrambled and Shocked control cells.

We found that 48 hrs post transfection, there was no difference in the mtDNA:nDNA ratio of TFAM siRNA transfected cells compared to Scrambled and Shocked control cells (Figure 25A). After 72 hrs post transfection however, we see approximately 40% decrease in the mtDNA:nDNA ratio of TFAM transfected cells in comparison to the control cells (Figure 25B). It is also apparent that the TFAM-429 siRNA probe is slightly more effective by producing a slightly greater decrease in the mtDNA:nDNA ratio.

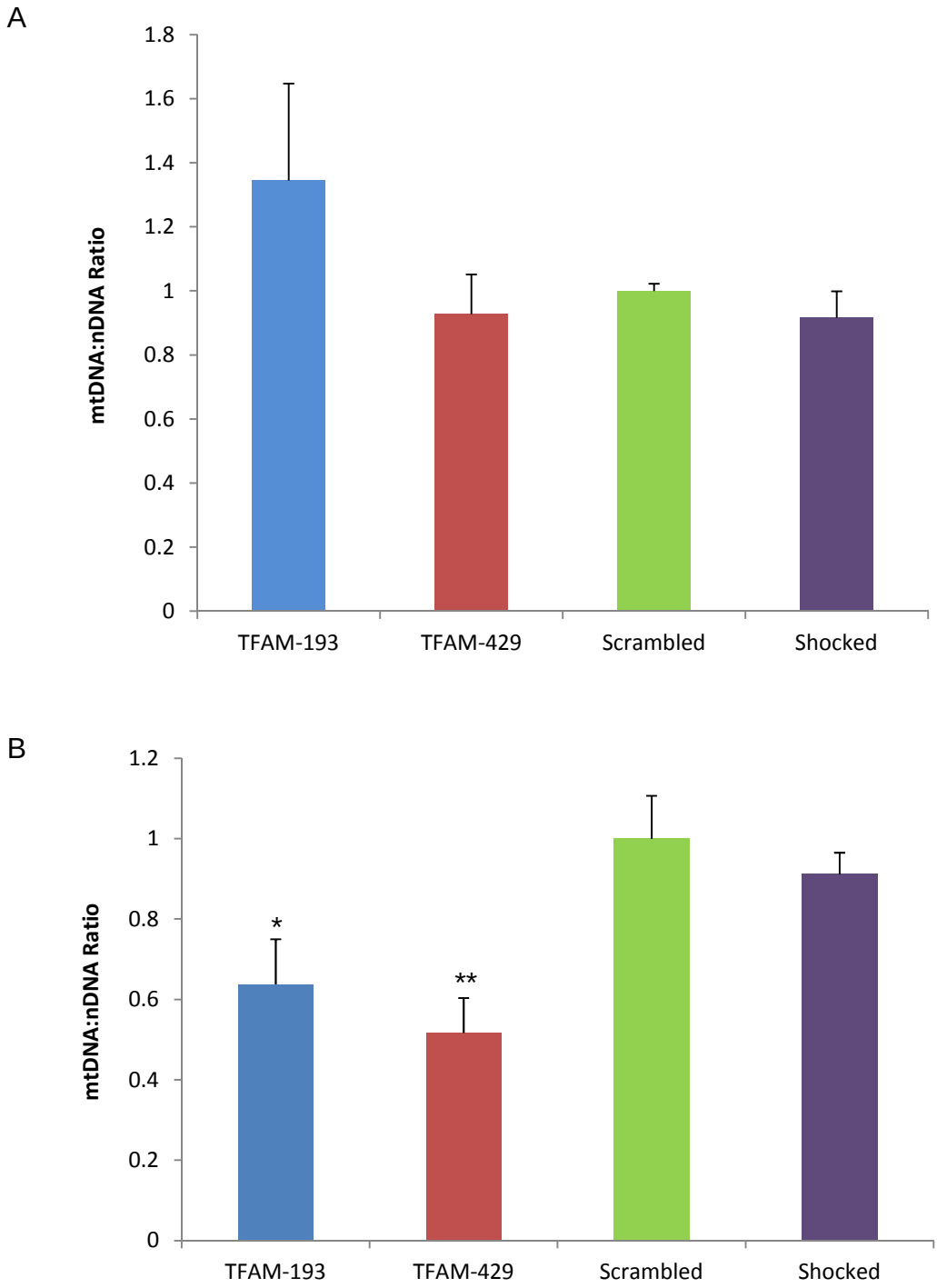

Figure 25 Effect of TFAM knock down on mtDNA levels in MIN6 cells, 48 hrs and 72 hrs post transfection

TFAM mRNA expression was silenced following transfection using the Neon Electroporation System. Cells were incubated at 37 ˚C and harvested 48 hrs (A) and 72 hrs (B) post transfection. DNA and RNA were extracted from the cells and the mtDNA copy number assay performed to ascertain the degree of mtDNA depletion, by quantifying ND5 target gene expression relative to the GAPDH reference gene. Experiment repeated once in triplicate. Error bars representative of SD. Results normalised to Scrambled negative control. * $p<0.05$, ** $p<0.01$ relative to Scrambled control.

4.4.3 Validation of mtDNA depletion following TFAM siRNA knock down

To validate our findings so far, that 72 hrs post transfection TFAM mRNA is reduced by >80%, and this seems to have the desired effect of depleting mtDNA levels by around 40%, we first repeated the transfections to ensure this was not an anomaly. MIN6 cells were again transfected and harvested 72 hrs post transfection. The DNA and RNA was extracted and used to quantify mtDNA:nDNA and TFAM mRNA expression respectively. In Figure 26A, we can see that after repeating the experiment four times, each repeat performed in triplicate, mtDNA:nDNA levels were significantly depleted by an average of 40% in cells transfected with TFAM-193 or TFAM-429 ($p<0.0001$) compared to Scrambled and Shocked control cells. The TFAM-429 siRNA probe performed consistently better than the TFAM-193 siRNA probe in terms of producing slightly greater mtDNA depletion.

Combining the results of the four transfection repeats, we were confident that TFAM siRNA knock down was having an effect on mtDNA copy number. But to confirm our findings further, we wanted to express mtDNA encoded ND5 relative to a second nDNA encoded reference gene. The gene chosen was CDKN2A, cyclin dependent kinase inhibitor 2A. Also known as p16, CDKN2A is a tumour suppressor protein implicated in cell cycle regulation, and has recently been identified as a T2DM susceptibility gene (Saxena, et al., 2007). Standard curves serially diluted 1:5 were amplified using the CDKN2A QuantiTect assay (Assay ID Mm_Cdkn2a_va.1_SG; Qiagen, Crawley, UK) and compared to GAPDH and ND5 standard curves. Once it was confirmed that reaction efficiencies for CDKN2A were comparable to those for GAPDH and ND5 (see Appendix, Figure 1), real-time PCR was performed on transfection samples and mtDNA encoded target gene ND5 was expressed relative to nDNA encoded reference gene CDKN2A. In Figure 26B, we can see that the results echo those obtained using the GAPDH nDNA encoded reference gene in that the mtDNA:nDNA ratio is significantly reduced by around 40% in both TFAM siRNA transfected cells. Again, the TFAM-429 siRNA probe seems to produce slightly greater mtDNA depletion.

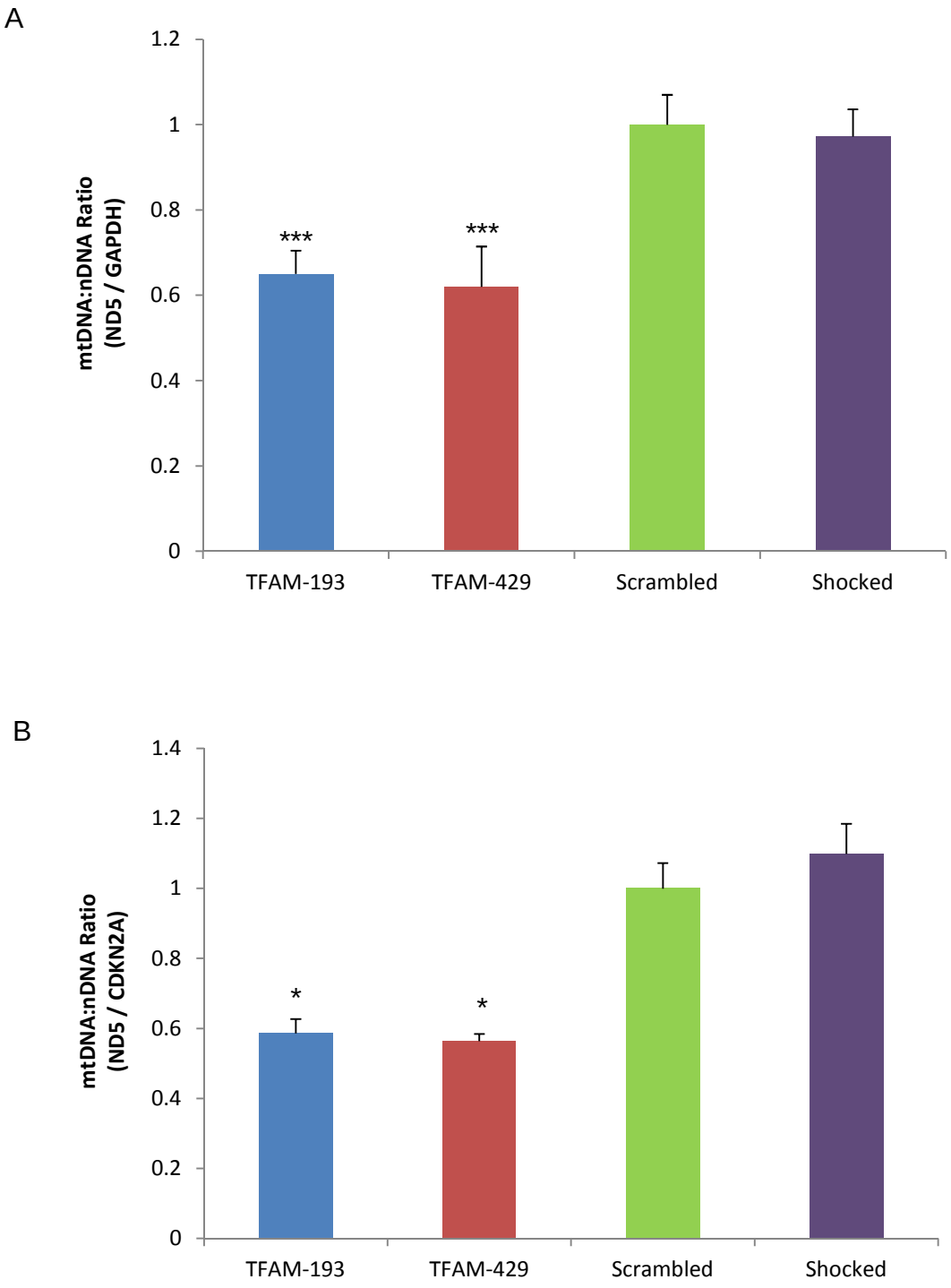

Figure 26 Validation of mtDNA depletion following TFAM knock down

The mtDNA depletion seen following TFAM gene silencing was validated by first repeating the transfection experiment and measuring mtDNA levels relative to the GAPDH nDNA encoded reference gene 72 hrs post transfection (A). Experiment repeated 4 times, each time in triplicate. Error bars representative of SEM. *** $p<0.0001$. mtDNA levels were also calculated relative to a second nDNA encoded reference gene, CDKN2A, cyclin-dependent kinase inhibitor 2A (B). Experiment repeated twice in triplicate, error bars representative of SEM. Results normalised to Scrambled negative control. * $p<0.05$ relative to Scrambled control.

4.4.4 mtDNA depletion 96 hrs and 144 hrs post transfection

By transfecting MIN6 cells with two different siRNA probes, we could reliably knock down TFAM gene expression by >80%. This then resulted in an overall 40% decrease in mtDNA levels 72 hrs post transfection, compared to control cells. As with the didanosine mtDNA depletion model, we were still looking to deplete mtDNA levels by approximately 50%. Because we only witnessed mtDNA depletion 72 hrs post transfection, and not 48 hrs post transfection, we wanted to see if leaving the cells for longer than 72 hrs after initial transfection resulted in an even greater decrease in mtDNA.

We transfected the MIN6 cells as we had done previously, and incubated them at 37 ˚C before harvesting cells 96 hrs and 144 hrs post transfection. RNA and DNA were extracted and quantified before real-time PCR was performed to ascertain the degree of mtDNA depletion. In Figure 27A, we can see that 96 hrs post transfection, mtDNA levels in cells transfected with the TFAM-429 probe have decreased by approximately 50% compared to the control cells, which is a 10% greater mtDNA depletion than TFAM-429 cells harvested 72 hrs post transfection. TFAM-193 transfected cells on the other hand, still have 40% mtDNA depletion compared to control cells 96 hrs post transfection, which is the same degree of mtDNA depletion seen 72 hrs post transfection. Similarly, 144 hrs post transfection, mtDNA levels still remain depleted by 50% in TFAM-429 transfected cells but only by 30% in TFAM-193 transfected cells, when compared to the Scrambled and Shocked control cells (Figure 27B).

When we analysed the RNA samples to determine TFAM knock down, we could see that 96 hrs after initial transfection, the transient effects of the siRNA probes had started to wear off, with TFAM mRNA expression knocked down by only 60-70% in TFAM-193 and TFAM-429 cells (Figure 28A). TFAM mRNA expression further increases 144 hrs post transfection, as TFAM knock down is only 40-60% in TFAM-193 and TFAM-429 cells compared to Scrambled and Shocked control cells (Figure 28B). If TFAM mRNA levels are beginning to increase 96 hrs and 144 hrs post transfection, this may explain why we are struggling to deplete mtDNA levels by more than 40-50% using the two TFAM siRNA probes.

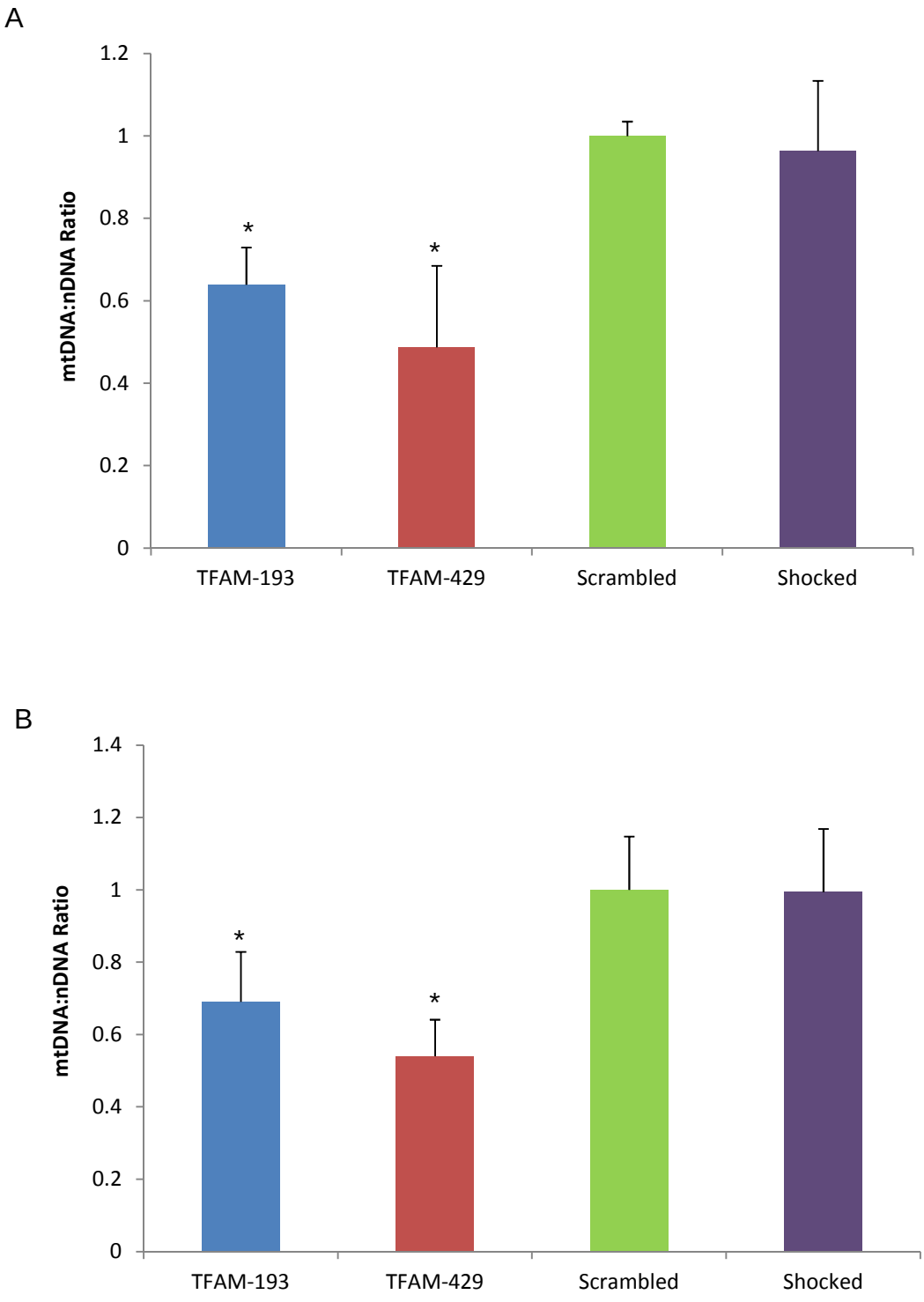

Figure 27 mtDNA depletion 96 hrs and 144 hrs post transfection

MIN6 cells were transfected and incubated at 37 ˚C before being harvested 96 hrs (A) and 144 hrs (B) post transfection. DNA and RNA were extracted from the samples and real-time PCR carried out to assess the relative expression of target gene ND5 to reference gene GAPDH, expressed as the mtDNA:nDNA ratio. Experiment was performed once in triplicate. Error bar representative of SD. Results normalised to Scrambled negative control. * $p<0.05$ relative to Scrambled control.

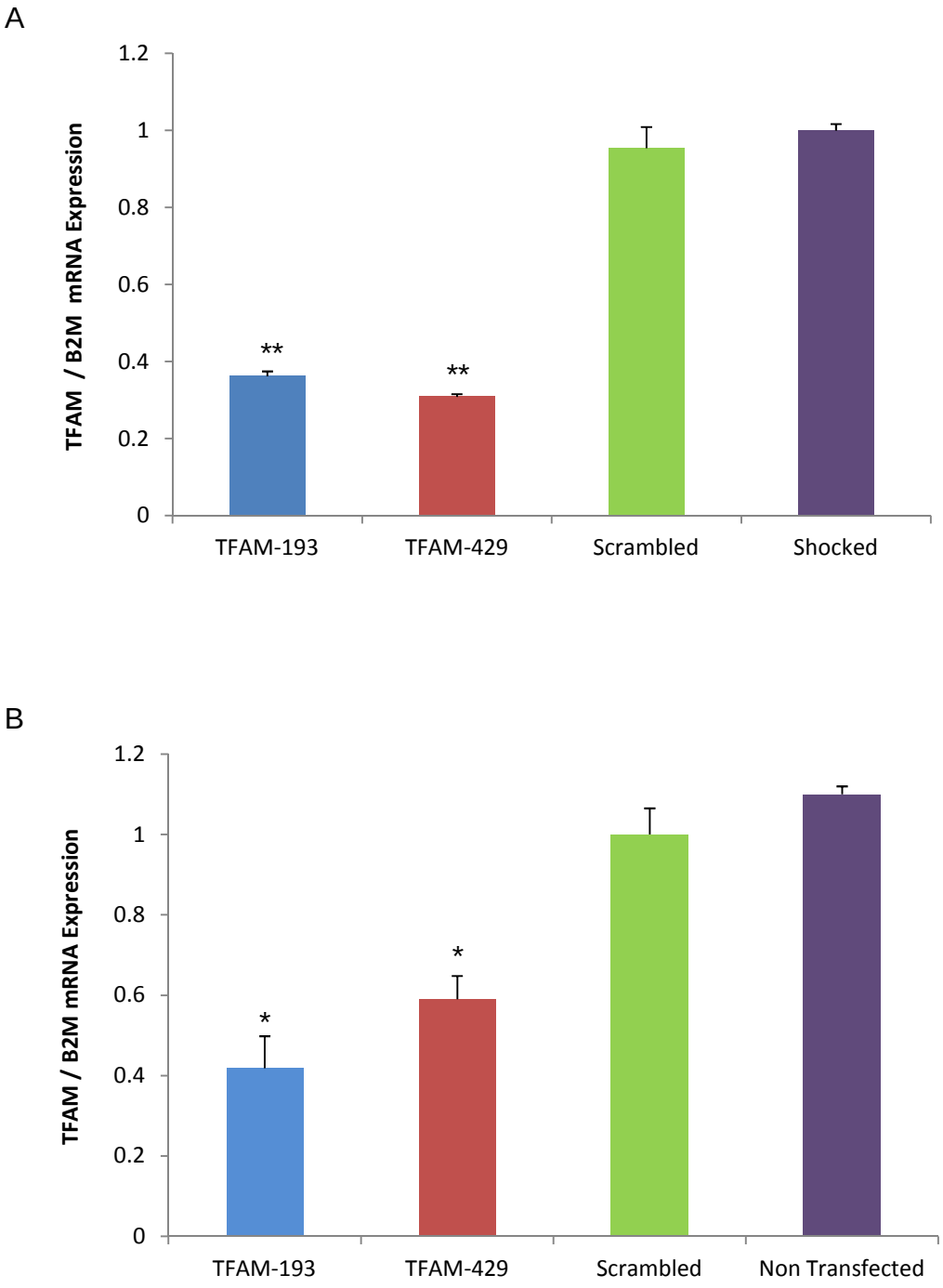

Figure 28 TFAM mRNA knock down 96 hrs and 144 hrs post transfection

MIN6 cells were transfected and incubated at 37 ˚C before being harvested 96 hrs (A) and 144 hrs (B) post transfection. DNA and RNA were extracted from the samples and real-time PCR carried out to determine TFAM mRNA expression relative to reference gene B2M. Experiment was perform once in triplicate. Error bar representative of SD. Results normalised to Scrambled negative control. * $p<0.05$, ** $p<0.01$ relative to Scrambled control.

4.4.5 The effect of siRNA probes on MIN6 cell cytotoxicity and cell morphology

To finally complete the optimisation of the TFAM mtDNA depletion model in MIN6 cells, we wanted to investigate what effects the siRNA probes were having on MIN6 cell cytotoxicity and cell morphology. As with the didanosine mtDNA depletion model, we measured cell cytotoxicity using an LDH assay. MIN6 cells were transfected and allowed to settle overnight. Twenty four hrs after initial transfection, cells were washed and the transfection medium was changed to remove dead cells that had not survived the transfection procedure. An aliquot of transfection medium supernatant was then harvested 72 hrs and 96 hrs post transfection, and LDH activity measured as a percentage of the positive control (see Section 2.8 for details). Seventy two hrs post transfection, cell cytotoxicity is <2% in cells transfected with either of the two TFAM siRNA probes or the Scrambled siRNA probe (Figure 29A). This is the same level of cytotoxicity seen in Shocked cells in which no siRNA was added and so, we can conclude that the siRNA probes used do not seem to cause cell cytotoxicity 72 hrs post transfection. An optical density (OD) reading was taken of an aliquot of MIN6 culture medium and used as a negative control to subtract from sample readings, which explains the negative percentage cytotoxicity in TFAM-193 cells in Figure 29A. This is because LDH is sometimes present in the phenol red and serum used in culture mediums and so, would give a false positive result. Cell cytotoxicity levels are still low 96 hrs post transfection, but we can see that there is a 5-fold increase in cell cytotoxicity in TFAM-193 cells and almost a doubling in TFAM-429 cells, when compared to the cytotoxicity levels 72 hrs post transfection (Figure 29B).

We looked at cell morphology by imaging cells 24 hrs, 48 hrs and 72 hrs post transfection using a Nikon Eclipse TE2000-S microscope and Photmetrics CoolSNAP HQ2 Turbo 1394 camera at x20 magnification. We can see that 24 hrs post transfection, cells appear to still be recovering from the procedure, as some cells are still small and compact. This is evident for all three siRNA probes used as well as the Shocked control cells, proving that this is due to the electroporation and not the presence of siRNA. By 48 hrs hours post transfection, we can see that the cells have started to grow again. Visually, there does not seem to be a difference in proliferation rate across the transfection conditions used. Also, all cells grow in clusters and can be seen to take on the typical MIN6 cell morphology, and thus, seem to be growing normally. The same can be said about the images taken 72 hrs post transfection. All cells seem to be growing normally, with no obvious difference in proliferation rate or cell morphology.

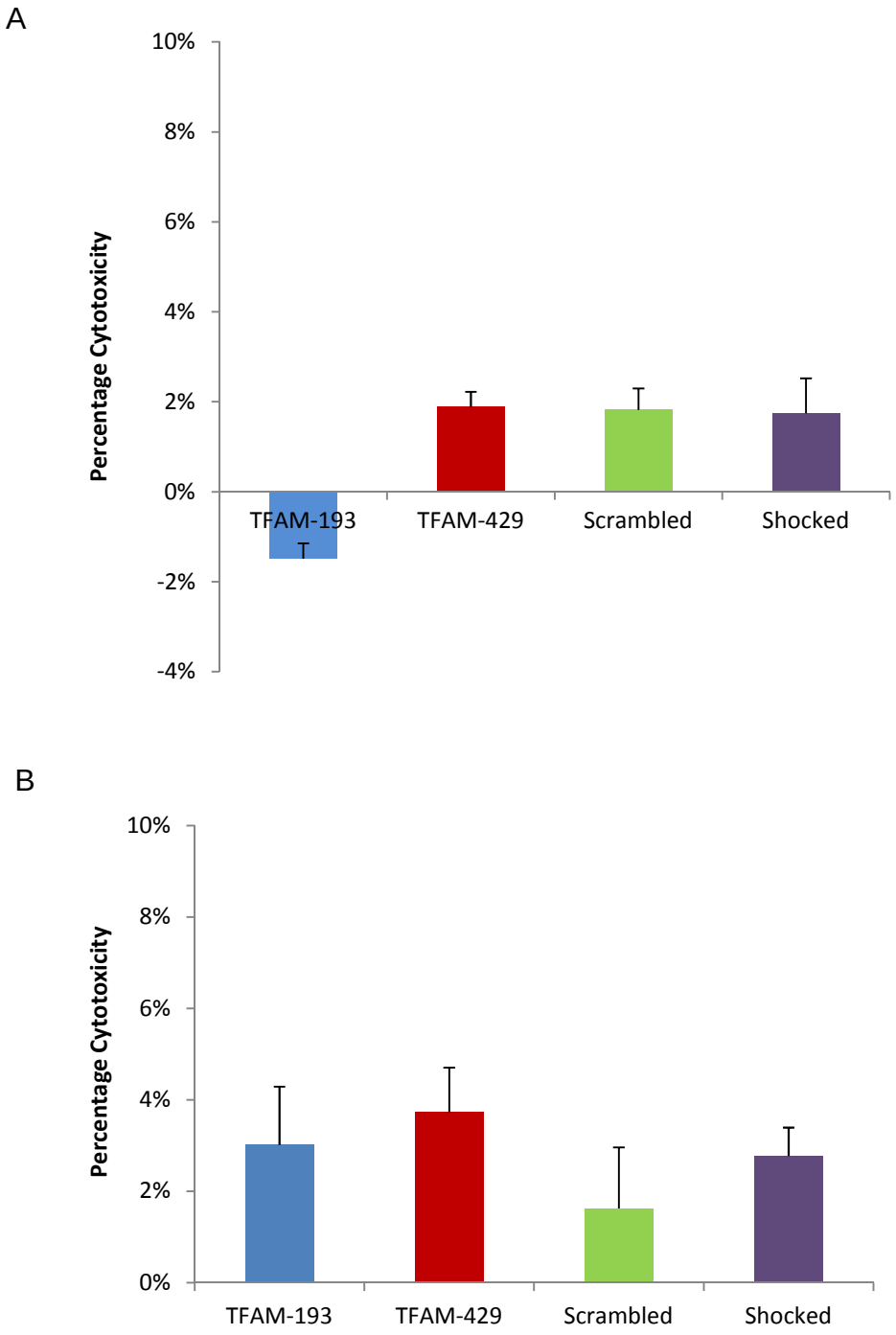

Figure 29 Cell viability following transfection: cell morphology and cytotoxicity

MIN6 cells were transfected and allowed to settle overnight. The following day, 24 hrs post transfection, cells were washed and transfection medium was changed to remove dead cells that had not survived electroporation. Cell cytotoxicity was then measured as a percentage of the positive control by an LDH assay after removing the culture medium 72 hrs (A) and 96 hrs (B) post transfection. Cells were imaged using a Nikon Eclipse TE2000-S microscope and Photmetrics CoolSNAP HQ2 Turbo 1394 camera at x20 magnification 24 hrs, 48 hrs and 72 hrs after initial transfection (C).

C

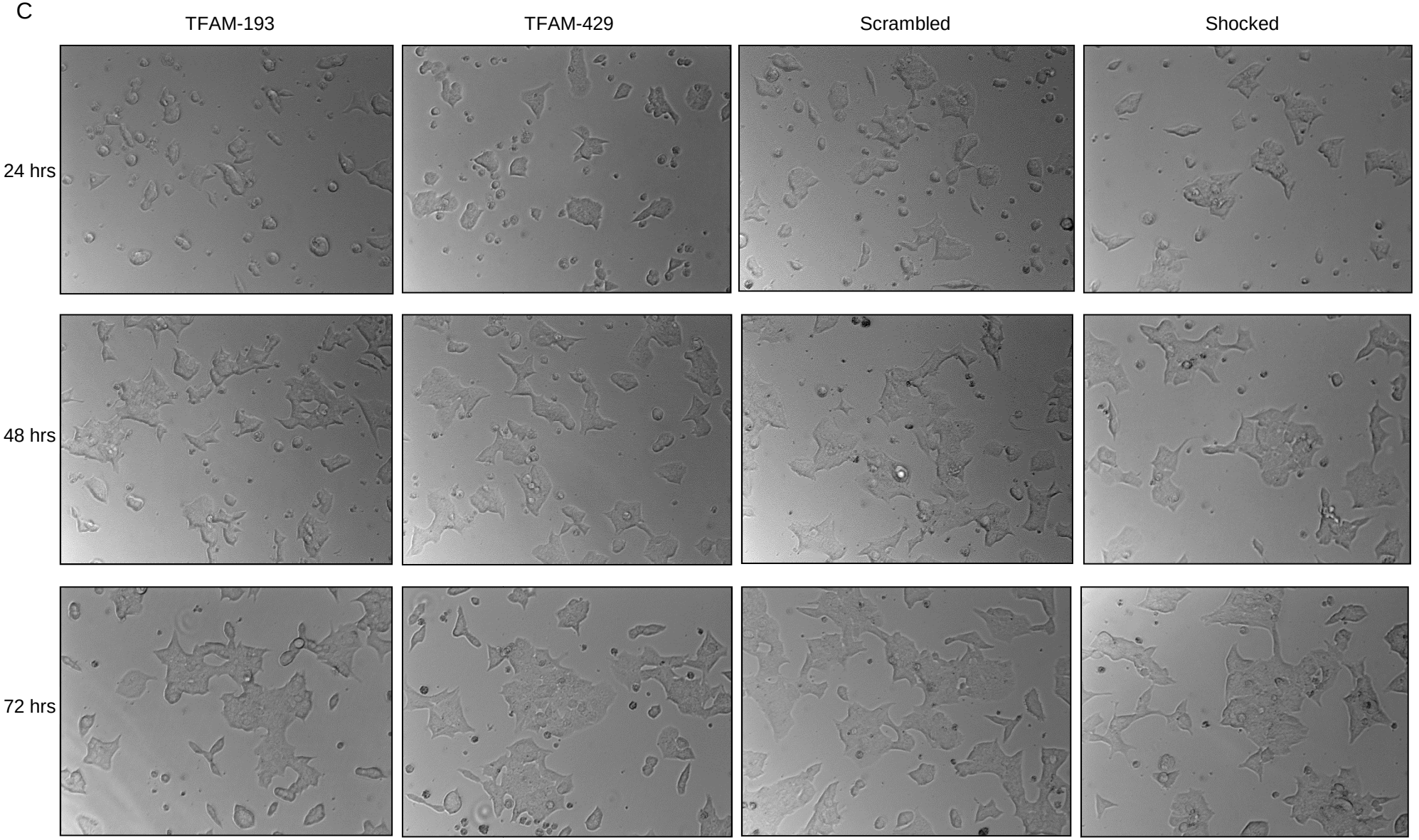

4.5 Discussion

Previous *in vitro* studies investigating TFAM knock down have produced primary cell cultures from tissues extracted from TFAM knock out animal models, including tissue specific disruption of the *TFAM* gene in mouse pancreatic β-cells (Silva, et al., 2000), mouse forebrain neurones (Sorensen, et al., 2001) and mouse cardiac and skeletal muscle (Wang, et al., 1999). There have also been *in vitro* studies implementing siRNA gene silencing to produce TFAM knock down. For one group, this involved transfecting human 143B TK^- cells with a plasmid by the calcium-phosphate precipitation method, then culturing the isolated transfected cells for 3 months (Jeng, et al., 2008). Another group used electroporation and siRNA technology to silence TFAM mRNA in 3T3-L1 adipocytes (Shi, et al., 2008). After failing to reliably knockdown TFAM expression using lipid-based transfection techniques, we enlisted the help of Invitrogen, through collaboration with our industrial partner, Unilever Plc, to develop a transfection protocol that would reliably knock down TFAM mRNA expression specifically in MIN6 cells. Our aim was that this genetic manipulation of mitochondrial biogenesis would complement the didanosine mtDNA depletion model developed in Chapter 3, which relied on chemical manipulation.

Invitrogen began this work by optimising an electroporation protocol that silenced TFAM mRNA by a substantial 70%, 24 hrs post transfection. Our plan was to investigate whether TFAM gene silencing had a consequential effect on mtDNA levels. Therefore, we needed to ensure enough time had elapsed for the reduced TFAM mRNA to be translated, resulting in a reduction in TFAM protein, and whether this would have a significant effect on mtDNA levels. For this reason, we decided to harvest cells 48 hrs and 72 hrs post transfection.

We were able to repeat the protocol set out by Invitrogen, and achieved a significant >80% knock down in TFAM mRNA 48 hrs and 72 hrs post transfection ($p<0.0001$). We accomplished a slightly greater TFAM knock down compared to Invitrogen, which may be explained by the fact we harvested the cells 24 / 48 hrs later than Invitrogen, thus allowing time for a greater knock down. The next step was to look at what effect this was having on mtDNA levels. Our initial findings suggested that mtDNA was depleted by 40% 72 hrs

post transfection in TFAM knock down cells, but mtDNA depletion was not seen 48 hrs post transfection. To corroborate these results, we first repeated the transfection experiment multiple times, and found that 72 hrs post transfection, mtDNA was indeed significantly depleted by 40% using both the TFAM-193 and TFAM-429 siRNA probes ($p<0.0001$). Although, it seemed that the TFAM-429 probe produced slightly greater mtDNA depletion compared to the TFAM-193 probe, but not significantly so. We then validated our findings further by measuring our mtDNA encoded ND5 target gene relative to a second nDNA encoded reference gene, CDKN2A. Again, we found that mtDNA levels were depleted by 40% in TFAM siRNA transfected cells, 72 hrs post transfection.

The 40% depletion in mtDNA following TFAM knock down we have reported is echoed in many other studies. The pioneering research performed by Larsson *et al.* showed that in heterozygous TFAM knockout mice, mtDNA levels were decreased by 35-40% compared to wild type mice. The group also concluded that homozygous TFAM knockout mice possessed a lethal phenotype causing them to died during gestation (Larsson, et al., 1998). By silencing TFAM gene expression specifically in neurones, Sorensen *et al.* produced mitochondrial late-onset neurodegeneration (MILON) mice, and found that the mice had a 40% reduction in mtDNA from 2 months of age, when compared to wild type mice. An *in vitro* study by Shi *et al.* implemented siRNA technology to silence TFAM gene expression whilst investigating adipocyte differentiation. The group managed to decrease TFAM mRNA expression by 80% also, and found that this resulted in a 30% mtDNA depletion compared to the Scrambled controls 72 hrs post transfection, which mirrors our findings precisely (Shi, et al., 2008). However, Wrendenberg *et al.* reported a slightly greater mtDNA depletion of 70% following tissue specific TFAM gene silencing in mouse skeletal muscle.

As with the didanosine mtDNA depletion model, our target was to achieve 50% mtDNA depletion. We saw no effect on mtDNA levels 48 hrs post transfection which may be explained by a slow turnover rate of the TFAM protein, which has been estimated as having a half-life of >12 hrs (Maniura-Weber, et al., 2004). Because we saw no effect on mtDNA levels at 48 hrs, but a 40% decrease 72 hrs post transfection, we wanted to extend the incubation period after initial transfection to see if this would allow greater mtDNA depletion. After 96 hrs post transfection, mtDNA was depleted by 50% using the TFAM-429 probe, and

this level of mtDNA depletion was sustained at 144 hrs post transfection. However, this was at the cost of an increase in cytotoxicity in the MIN6 cells. Again, the TFAM-429 seems to produce better mtDNA depletion as the TFAM-193 probe can only produce a maximum of 40% mtDNA depletion 72 hrs and 96 hrs post transfection, but only a 30% mtDNA depletion 144 hrs post transfection. The slight increase in mtDNA 144 hrs post transfection could be the mtDNA repopulating after the transient effects of the TFAM-193 siRNA start to wear off. This is supported by the fact that TFAM mRNA levels begin to increase from >80% TFAM gene silencing 72 hrs post transfection, to 60-70% TFAM gene silencing 96 hrs post transfection and only 40-60% TFAM gene silencing 144 hrs post transfection.

So in summary, it seems that by extending the incubation period after initial transfection, we get a slightly better 50% mtDNA depletion with the TFAM-429 probe only 96 hrs post transfection, but at the expense of increased cytotoxicity. By 96 hrs post transfection, we see the transient effects of the siRNA begin to fade as TFAM mRNA expression increases. This suggests that the only way to deplete mtDNA levels further would be to re-transfect the cells. But the level of mtDNA depletion we have reported is corroborated by other groups (Larsson, et al., 1998; Shi, et al., 2008; Sorensen, et al., 2001). Therefore we can confirm that by silencing TFAM mRNA expression by >80% in MIN6 cells using electroporation transfection, we can reliably deplete mtDNA levels by 40% 72 hrs post transfection. Now we have managed to optimise two models of mtDNA depletion in MIN6 cells, using both chemical and genetic intervention of mitochondrial biogenesis, we can now utilise both depletion models to investigate the effects of mtDNA depletion on β-cell and mitochondrial function.

Chapter 5

The effect of mtDNA depletion on mitochondrial function

5 The effect of mtDNA depletion on mitochondrial function

5.1 Introduction

Now that we had successfully optimised two independent models to deplete mtDNA levels by approximately 40-50%, we were keen to see what effect this had on mitochondrial function. Studies to date have created severe mtDNA depletion in pancreatic β-cells by chemical inhibition of mtDNA replication (Hayakawa, et al., 1998; Kennedy, et al., 1998; Soejima, et al., 1996; Tsuruzoe, et al., 1998), or tissue specific knock down of the mitochondrial transcription factor TFAM (Silva, et al., 2000). These groups have successfully shown that severe mtDNA depletion drastically affects mitochondrial function by causing: respiratory chain dysfunction (Kennedy, et al., 1998; Silva, et al., 2000; Soejima, et al., 1996; Tsuruzoe, et al., 1998), reduced mtDNA transcription (Hayakawa, et al., 1998; Soejima, et al., 1996; Tsuruzoe, et al., 1998) and translation (Soejima, et al., 1996), impaired Ca^{2+} signalling (Hayakawa, et al., 1998; Silva, et al., 2000; Soejima, et al., 1996; Tsuruzoe, et al., 1998), reduced mitochondrial membrane hyperpolarisation (Kennedy, et al., 1998; Silva, et al., 2000), reduced oxygen consumption (Soejima, et al., 1996) and reduced ATP content (Kennedy, et al., 1998; Tsuruzoe, et al., 1998).

These studies have managed to show the effects of severe mtDNA depletion on mitochondrial function, but little is known regarding the effects of partial mtDNA depletion on mitochondrial function. Using the two models of mtDNA depletion optimised in Chapters 3 and 4, we wanted to investigate the effect of partial mtDNA depletion, to levels seen in ageing human islets (Cree, et al., 2008), on mitochondrial function.

5.2 Aims

The aim of this chapter was to explore the effect of partial mtDNA depletion on mitochondrial function in MIN6 cells. We compared both mtDNA depletion models on aspects of mitochondrial function including:

- COX1 mRNA expression using real-time PCR
- COX1 protein levels using western blotting
- ATP content using a luciferase ATP assay
- Mitochondrial membrane potential using JC-1 staining

5.3 Methods

5.3.1 JC-1 staining

The JC-1 dye is commonly used to measure mitochondrial membrane potential as it has a unique property: when in the cell cytosol, it exists in a monomeric form and emits a green fluorescence; when the dye enters the mitochondrial matrix however, it forms J-aggregates and emits a red fluorescence. The cationic dye selectively enters the mitochondrial matrix by utilising the mitochondrial membrane potential, which is much lower than that of the plasma membrane. Once inside the mitochondrial matrix, the low mitochondrial membrane potential causes the monomeric JC-1 to aggregate, thus forming J-aggregates. This causes a spectral shift, resulting in the dye emitting red fluorescence (see Figure 30). The proportion of red and green fluorescence was measured using a live cell fluorescence microscope, and mitochondrial membrane potential was calculated as a ratio of red / green fluorescence. JC-1 cytosolic monomers were imaged using a 470 nm ± 40 nm excitation filter, 520 nm ± 40 nm emission filter whereas JC-1 mitochondrial J-aggregates were imaged using a 575 nm ± 25 nm excitation filter, 632 nm ± 40 nm emission filter.

Briefly, MIN6 cells were incubated with JC-1 staining medium for 10 mins at 37ºC to allow the dye to permeate the cells. Cells were then washed in pre-warmed PBS before normal MIN6 growth medium was added prior to imaging the cells immediately. All images were then quantified using ImageJ and the mitochondrial membrane potential calculated as the ratio of red / green fluorescence (see Section 2.10.2 for further details).

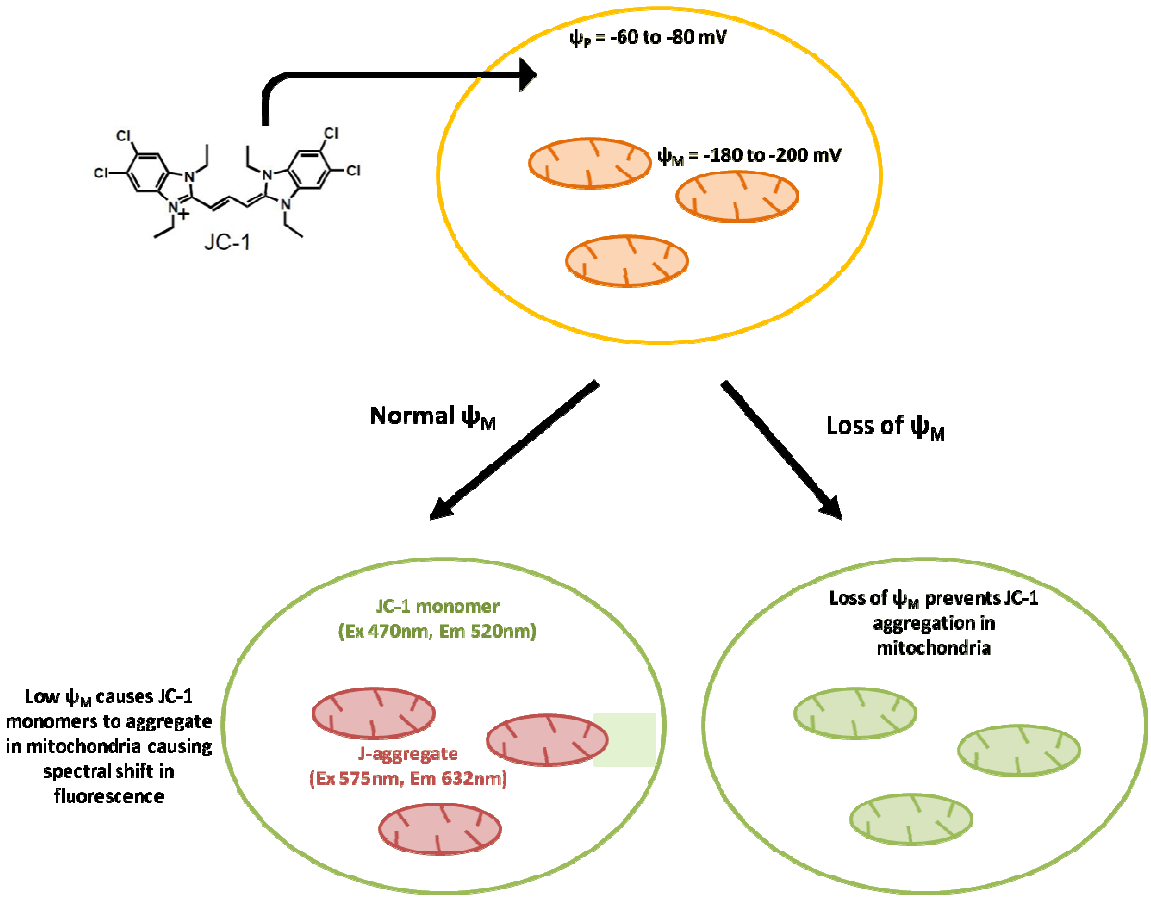

Figure 30 Measurement of mitochondrial membrane potential using JC-1

JC-1 enters the cytosol down the plasma membrane potential (ψ_P) gradient where it exists in monomeric form in the cytosol, emitting green fluorescence at 520 nm ± 40 nm when excited at a wavelength of 470 nm ± 40 nm. Monomeric JC-1 selectively enters the mitochondrial matrix, which is of a lower electrical potential to the cytosol, where it aggregates to form J-aggregates. This causes a spectral shift resulting in the J-aggregate JC-1 emitting a red fluorescence at 632 nm ± 40 nm when excited at a wavelength of 575 nm ± 25 nm. Loss of mitochondrial membrane potential (ψ_M) prevents JC-1 monomers aggregating in the mitochondrial matrix, resulting in loss of red fluorescence. Mitochondrial membrane potential is measured as a ratio of red / green fluorescence.

5.4 Results

5.4.1 mtDNA depletion causes reduced mitochondrial gene transcription

One of the first measures of mitochondrial function we decided to investigate was mitochondrial gene transcription. We considered the didanosine model of mtDNA depletion first. MIN6 cells were treated with 50 μM ddI or PBS for a period of 5 days, before harvesting cells and extracting RNA. RNA was quantified and reverse transcribe before assessing mitochondrial gene expression using TaqMan hydrolysis probes and real-time PCR. We chose to investigate the COX1 mtDNA subunit of cytochrome c oxidase, Complex IV, as our target gene. The three mtDNA encoded subunits of Complex IV (COX1, COX2 and COX3) initially form a holoenzyme which is pivotal for the assembly of the rest of the complex (Larsson, 2010) and so, COX1 is an important mtDNA encoded subunit. Our reference gene was nDNA encoded β2-microglobulin (B2M), a component of the Class 1 major histocompatibility complex (MHC) on the cell surface of most nucleated cells (Gussow, et al., 1987).

In Figure 31, we see that didanosine-induced mtDNA depletion significantly reduces mitochondrial gene expression by 45.3% compared to vehicle control PBS cells ($p<0.0001$).

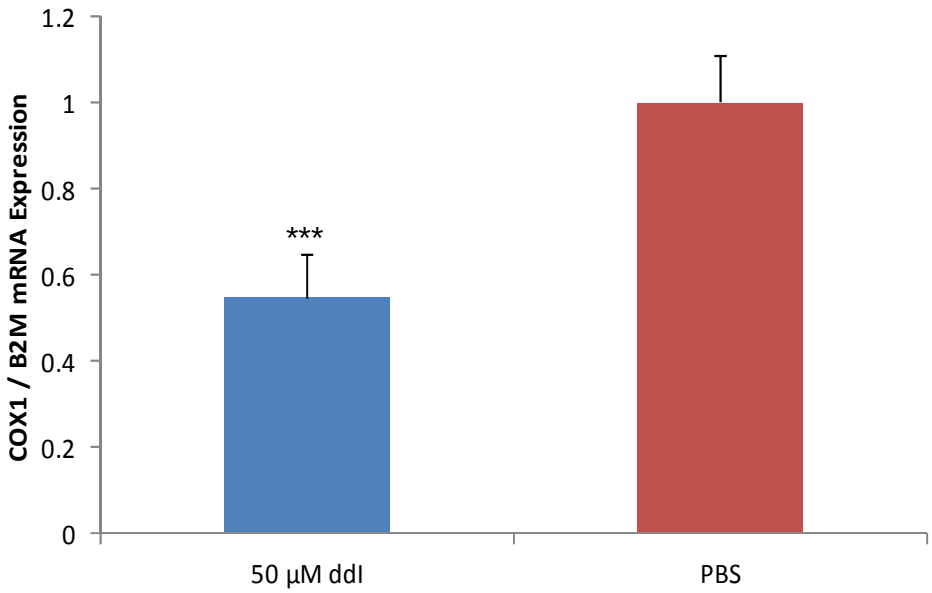

Figure 31 COX1 mRNA expression following didanosine-induced mtDNA depletion

MIN6 cells were treated with 50 µM ddI for a period of 5 days before cells were harvested and RNA extracted. RNA was quantified and reverse transcribed, and real-time PCR performed using TaqMan hydrolysis probes. mtDNA encoded COX1 mRNA expression was calculated relative to the nDNA encoded B2M reference gene. Data are normalised to PBS vehicle control cells. Experiment repeated 3 times in triplicate. Error bars representative of SEM. *** $p<0.0001$

Similarly, we repeated the same experiment but using the TFAM mtDNA depletion model. MIN6 cells were transfected using the TFAM-193 and TFAM-429 siRNA probes to silence TFAM mRNA expression. Cells were then incubated at 37 ºC for 72 hrs before harvesting. RNA was extracted, quantified and reverse transcribed prior to real-time PCR. COX1 mRNA expression was examined relative to the reference gene B2M. In support of the didanosine mtDNA depletion model, we also see reduced COX1 mRNA expression using the TFAM silencing model of mtDNA depletion (Figure 32). There is a 23.9% and 33.4% decrease in COX1 mRNA expression using the TFAM-193 and TFAM-429 siRNA probes respectively, compared to the Scrambled control cells ($p<0.001$ and $p<0.0001$, respectively). The TFAM-429 probe produced a greater decrease in COX1 gene expression. This is consistent with the mtDNA depletion data for the TFAM mtDNA depletion model, whereby the TFAM-429 probe produced greater mtDNA depletion also, compared to the TFAM-193 probe. It is also known for this set of experiments, TFAM mRNA expression was silenced by 80.7% ± 0.092 and 79.1% ± 0.04 (mean ± SEM) in TFAM-193 and TFAM-429 cells respectively, compared to the Scrambled control cells in these 3 experimental repeats (data not shown).

In summary, both methods of mtDNA depletion result in decreased mtDNA gene expression. But it is worth noting that COX1 gene expression is more fully suppressed following didanosine-induced mtDNA depletion, compared to TFAM silencing-induced mtDNA depletion.

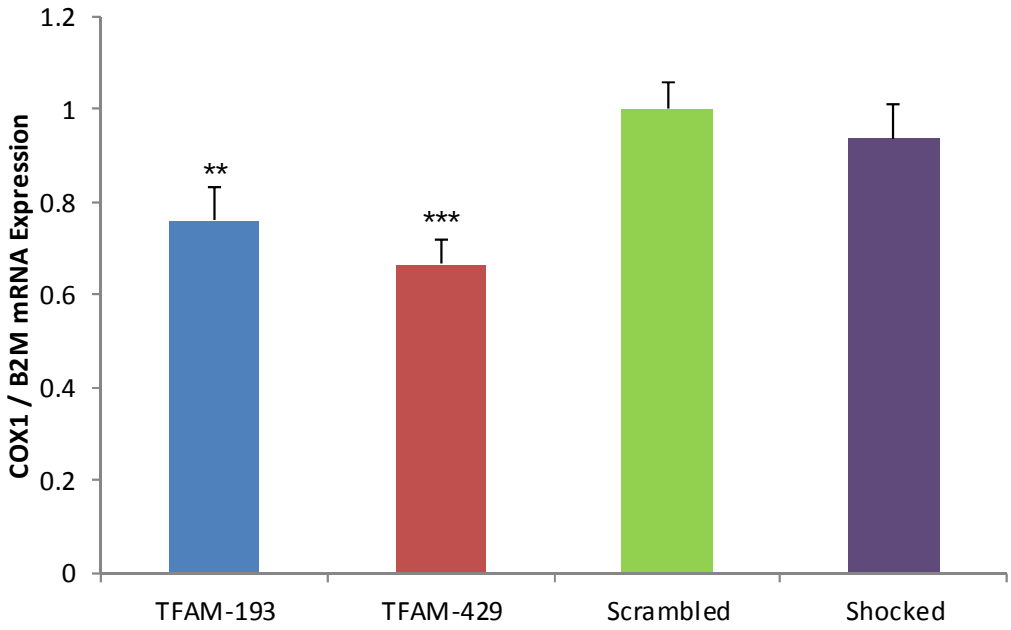

Figure 32 COX1 mRNA expression following TFAM silencing-induced mtDNA depletion

MIN6 cells were transfected with TFAM-193, TFAM-429 or Scrambled siRNA probes, or with no siRNA (Shocked). Cells were incubated at 37 ºC for 72 hrs before harvesting. RNA was extracted, quantified and reverse transcribed, and real-time PCR performed using TaqMan hydrolysis probes. COX1 mRNA expression was measured relative to the B2M reference gene. Data are normalised to Scrambled control cells. Experiment repeated 3 times in triplicate. Error bars representative of SEM. ** $p<0.001$, *** $p<0.0001$

5.4.2 mtDNA depletion causes a decrease in mitochondrial encoded protein levels

To confirm whether the reduction in COX1 gene expression had a knock on effect on COX1 protein levels, we performed a series of western blots to determine COX1 protein levels following mtDNA depletion. We decided to analyse COX1 protein levels in mtDNA depleted MIN6 cells using the didanosine-induced mtDNA depletion first. This was for the reason that the didanosine model produced the greatest mtDNA depletion, as well as the greatest decrease in COX1 gene expression, when compared to the TFAM mtDNA depletion model. After MIN6 mtDNA had been depleted following 5 day 50 μM ddI treatment, cells were harvested in protein extraction buffer and protein quantified using the Bradford assay. Twenty five μg protein was separated by SDS-PAGE, and the separated proteins transferred onto a nitrocellulose membrane, which was then used to probe for COX1, SDH70 and β-Actin proteins. SDH70 is the 70 kDa subunit of succinate dehydrogenase, Complex II, the only mitochondrial complex whose subunits are entirely nDNA encoded and so, should not be affected by mtDNA depletion. Protein loading was assessed using β-Actin.

We performed two separate experiments in quadruplicate, and then analysed the samples from each experiment using two independent western blots. This was because each blot was cut in half to allow separate probing of COX1 and β-Actin, as the proteins were very similar in size (40 kDa and 42 kDa respectively), and there were only a limited number of wells per gel. One of the blots was then washed and re-probed with the SDH70 antibody. The SDH70 protein was expected to be 70 kDa in size and so, would show up on a different area of the blot, thus allowing easy distinction from COX1 / β-Actin proteins (all antibodies used were monoclonal, but were raised in mouse and so, the same secondary antibody was used).

The results of both experimental repeats are shown in Figure 33. In both western blots of both repeats, we can visually discern a difference in COX1 band density with the ddI bands tending to be slightly less intense than the PBS bands (Figure 33Ai and 33Bi). Comparing the COX1 bands to those of SDH70 and β-Actin, visually, there does not seem to be an obvious difference in band density between ddI treated and PBS control cells when probed with SDH70 or β-Actin. These visual observations are supported by the optical density (OD) readings obtained from densitometric analysis.

When the OD readings are used to calculate the ratio of COX1 protein to the β-Actin loading control, we see that COX1 protein is reduced in ddI treated cells by approximately 30% in repeat 1 (Figure 33Aii) and 40% in repeat 2 (Figure 33Bii) when normalised to PBS control cells. The β-Actin loading control bands are uniform in all blots, indicating that this difference in COX1 protein in ddI treated cells is not a result of unequal protein loading. When we calculate the ratio of SDH70 / β-Actin however, we see that there is no real difference in the protein ratios in ddI treated and PBS control cells (Figure 33Aiii and 33Biii), showing that there is a loss in mtDNA encoded protein subunits only in mtDNA depleted cells.

When the data from both experimental repeats are combined, we see that overall, there is a 34.3% decrease in COX1 protein in ddI treated cells compared to PBS control cells ($p=0.015$) (Figure 34A). However, we see no change in SDH70 protein levels with ddI treatment compared with PBS control cells, which was to be expected as SDH70 is nDNA encoded and so, would not be affected my mtDNA depletion (Figure 34B).

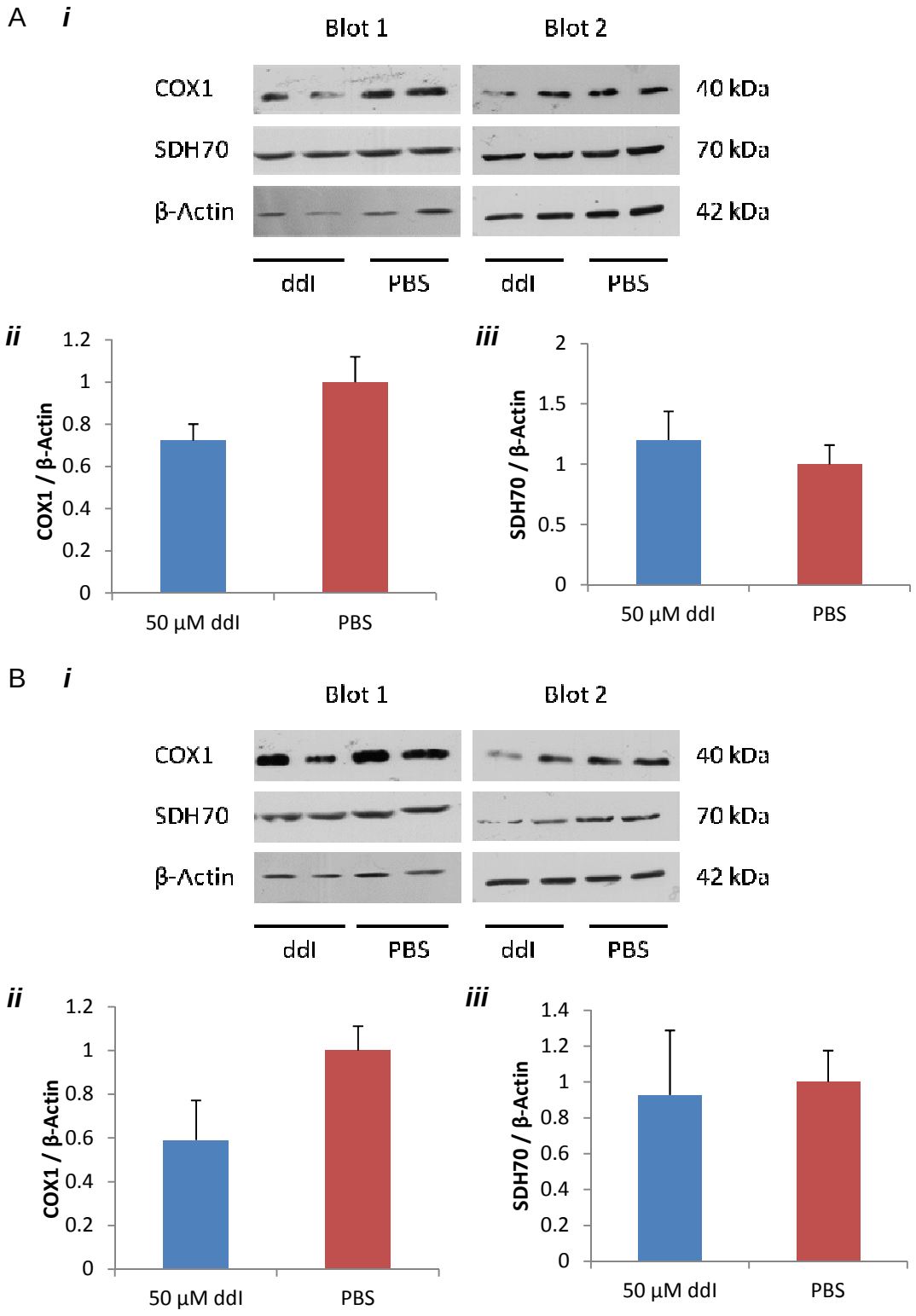

Figure 33 Effect of didanosine-induced mtDNA depletion on mtDNA encoded proteins

MIN6 cells were treated with 50 µM ddI for 5 days to deplete mtDNA. Protein was extracted and analysed by western blotting, probing for COX1, SDH70 (nDNA encoded subunit of Complex II) and β-Actin (loading control) proteins. Protein bands were quantified by densitometry, and OD readings used to calculate the ratio of COX1 and SDH70 proteins relative to β-Actin. Experiment repeated twice in quadruplicate, with each repeat assayed in two independent western blots. The blots for repeat 1 (A) and repeat 2 (B) are shown, error bars represent SD. Data normalised to PBS control cells.

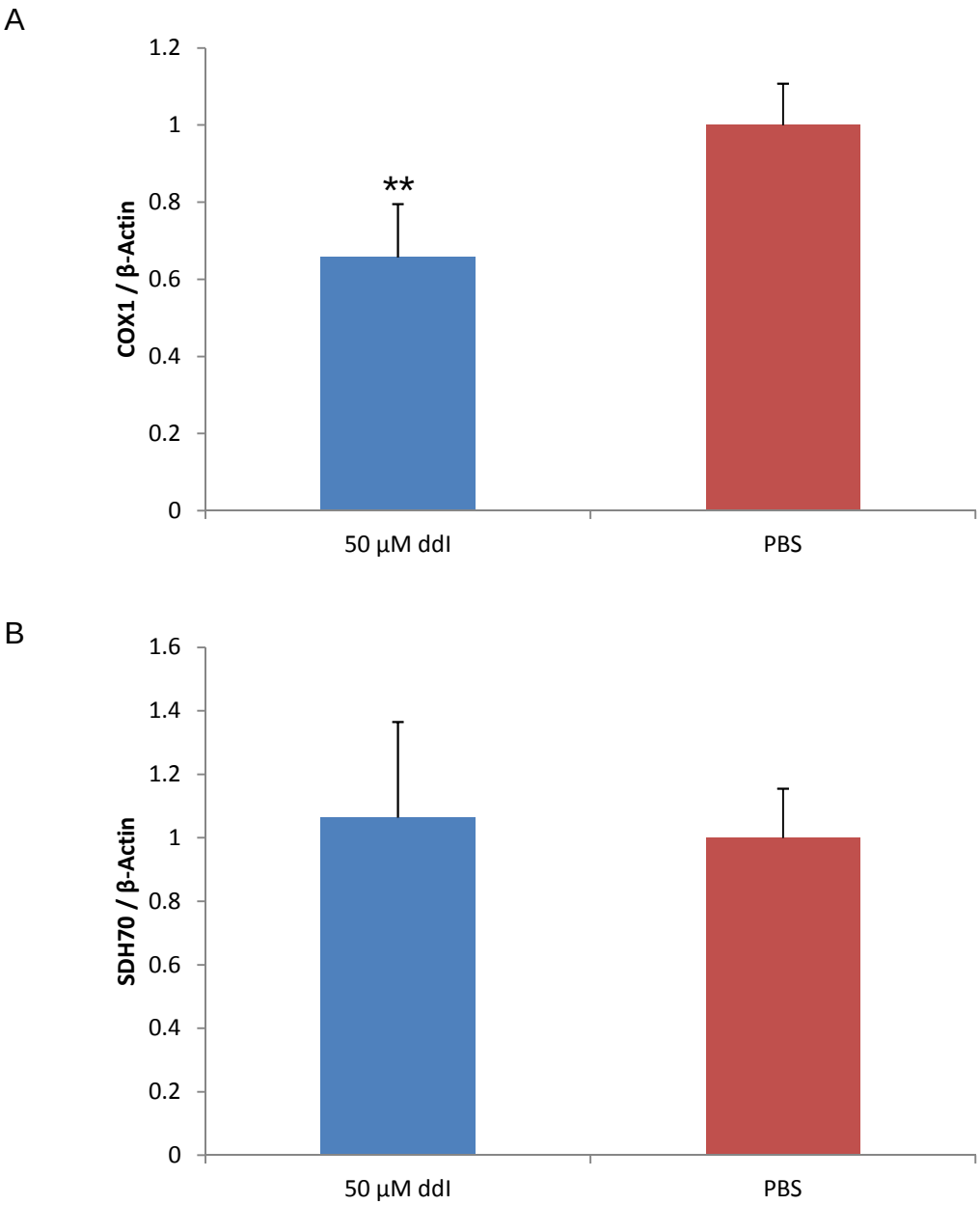

Figure 34 Effect of didanosine-induced mtDNA depletion on mtDNA encoded proteins (both repeats combined)

The data from both experimental repeats presented Figure 33 were combined. COX1 (A) and SDH70 (B) proteins were both normalised to β-Actin loading control. Data shown from 2 experiments performed in quadruplicate, error bars representative of SEM. ** p=0.015. Data normalised to PBS control cells.

After encouraging results of a decline in COX1 protein levels in mtDNA depleted cells using the didanosine mtDNA depletion model, we decided to investigate whether the same would be seen using the TFAM silencing method of mtDNA depletion. The transfections were performed in 24 well tissue culture plates and as we required 25 μg protein to load per lane during SDS-PAGE, we needed to pool the protein lysates together from 3 separate wells to make one sample. It was decided at this point that as the TFAM-429 siRNA probe had consistently performed better than the TFAM-193 siRNA probe, we would continue using the TFAM-429 probe only. In addition, we were confident that the Scrambled siRNA probe was not having adverse affects on the cells in comparison to the Shocked cells. Therefore, in future experiments, it was decided that we would silence TFAM mRNA using the TFAM-429 siRNA probe only, and that cells transfected with the Scrambled siRNA would act as our control cells.

MIN6 cells were transfected with TFAM-429 or Scrambled siRNA probes and incubated at 37 ºC. Seventy two hrs post transfection, cells were harvested in protein extraction buffer and quantified using the Bradford assay. As with samples obtained following didanosine-induced mtDNA depletion, 25 μg protein was separated by SDS-PAGE. Separated proteins were transferred onto a nitrocellulose membrane and mouse monoclonal antibodies were used to probe for COX1, SDH70 and β-Actin proteins. Bound antibodies were detected using enhanced chemiluminescence (ECL) and photographic film. Protein bands were quantified using densitometry.

The experiment was repeated three times in duplicate. Each of the three repeats is shown in Figure 35. In repeats 1 and 2, we can see that some TFAM-429 bands probed with the COX1 antibody are slightly less intense compared to those of the Scrambled cells (Figure 35Ai and 35Bi), but in repeat 3, visually there does not seem to be much difference between TFAM-429 cells or Scrambled control cells probed with the COX1 antibody (Figure 35Ci). The β-Actin loading looks to be comparable in all three repeats, and SDH70 bands appear uniform in all samples in all repeats (Figure 35Ai, 35Bi and 35Ci).

These observations are supported by the densitometry OD readings. The ratio of COX1 / β-Actin protein is reduced in repeats 1 and 2 by around 30-40% in TFAM-429 cells compared to Scrambled control cells (Figure 35Aii and 35Bii). However, the reduction in the COX1 / β-Actin protein ratio is less pronounced in repeat 3 (Figure 35Cii). As seen with the didanosine mtDNA depletion model, there is no difference in SDH70 / β-Actin protein levels in TFAM-429 and Scrambled transfected cells (Figure 35Aiii, 35Biii and 35Ciii).

When the results from all three repeats are combined, we see that overall, there is a 21.7% decrease in COX1 protein levels in TFAM-429 transfected cells compared to Scrambled transfection control cells (Figure 35Di). Although this decrease in COX1 protein is not significant, there is a definite trend. Corroborating the results seen with the didanosine model, there is no change in SDH70 protein levels following TFAM silencing-induced mtDNA depletion (Figure 35Dii).

In conclusion, there is a trend of decreased COX1 protein levels following TFAM gene silencing which would need further repeats to deem its significance. This is in support of the decreased COX1 mRNA expression found following TFAM gene silencing-induced mtDNA depletion. However, this decrease in COX1 protein is not as prominent as that obtained using the didanosine model of mtDNA depletion.

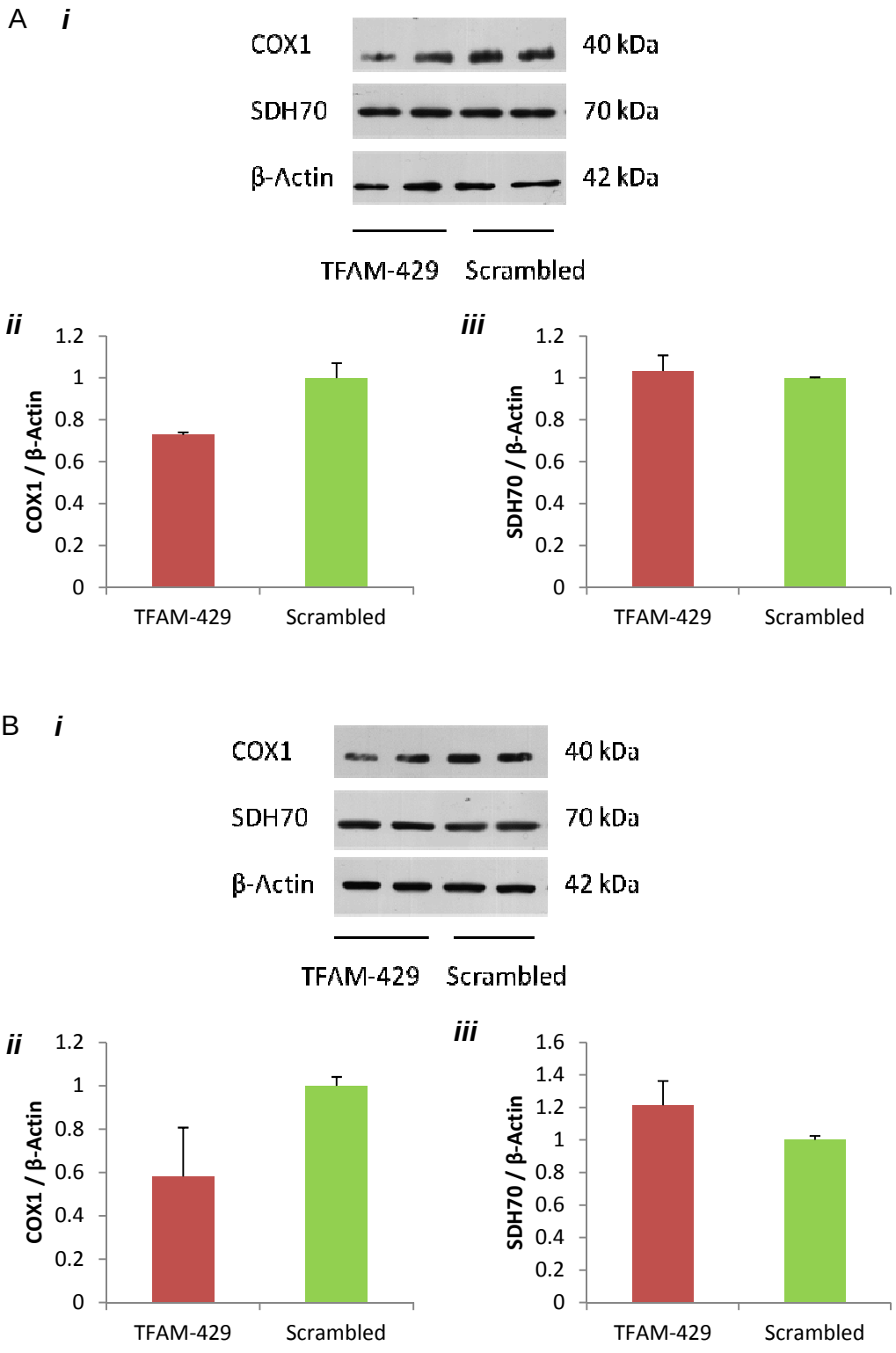

Figure 35 Effect of TFAM silencing-induced mtDNA depletion on mtDNA encoded proteins

MIN6 cells were transfected with TFAM-429 or Scrambled siRNA probes and harvested 72 hrs post transfection. Protein was extracted and analysed by western blotting, probing for COX1, SDH70, and β-Actin proteins. Protein bands were quantified by densitometry, and OD readings used to calculate the ratio of COX1 and SDH70 proteins relative to β-Actin. Three experiments were performed in duplicate. The blots for repeat 1 (A), repeat 2 (B) and repeat 3 (C) are shown, error bars represent SD. All repeats were then combined (D), error bars represent SEM. Data normalised to Scrambled control cells.

C *i*

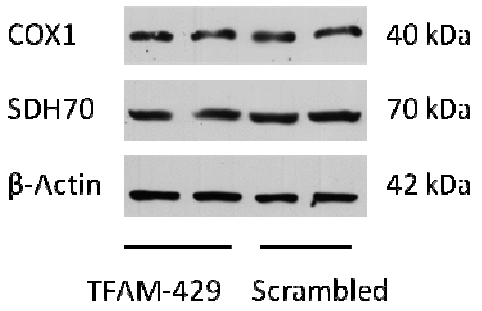

ii

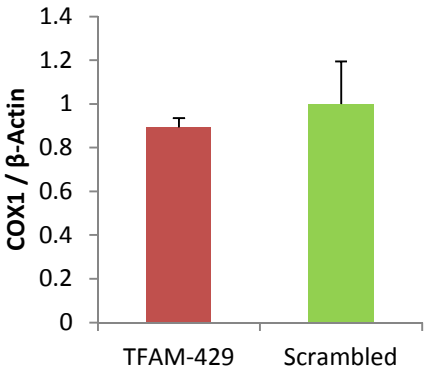

iii

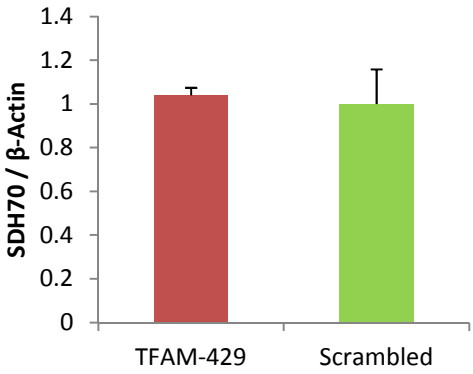

D *i*

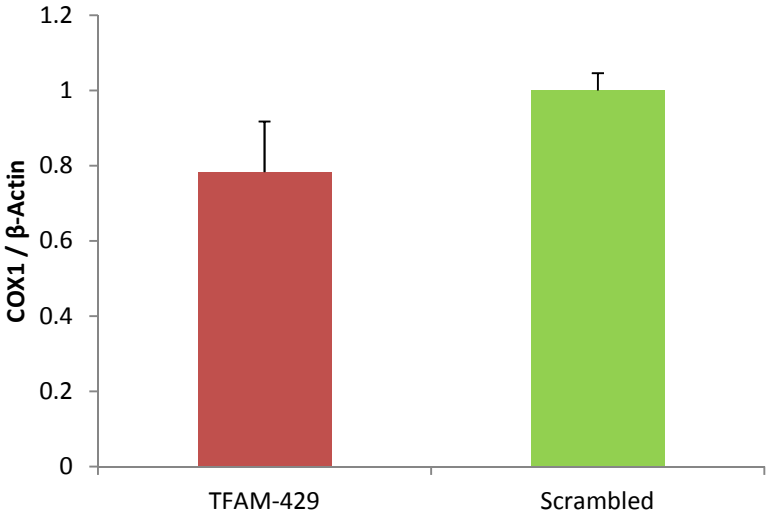

ii

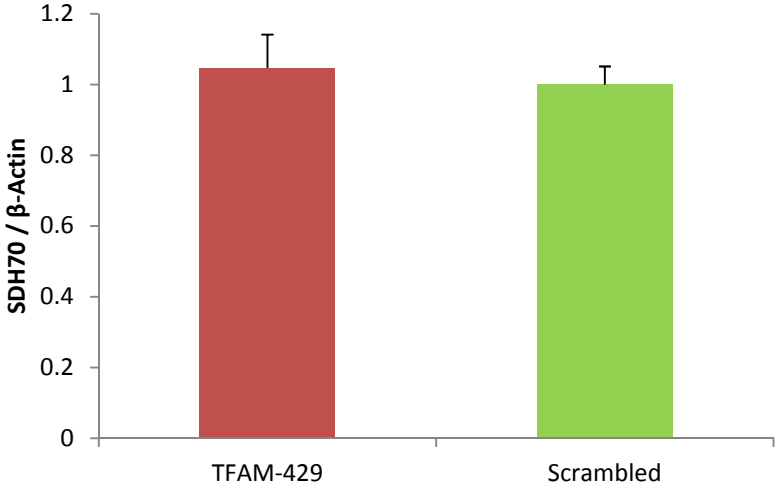

5.4.3 mtDNA depletion has no effect on ATP content

The next measure of mitochondrial function we decided to investigate was ATP content. So far we have seen that partial mtDNA depletion causes a reduction in COX1 mRNA and protein levels. We were keen to examine whether this decrease in COX1 mRNA and protein resulted in respiratory chain dysfunction and as a consequence, did this affect ATP production. Similarly to investigations on COX1 protein, we decided to test the didanosine mtDNA depletion model first as this model produced the greatest mtDNA depletion.

Cells were treated with 50 μM ddI for 5 days to deplete mtDNA. Cells were then stimulated with 3 mM (basal) or 25 mM (high) glucose for 1 hr, before being harvested in perchloric acid to prevent degradation of ATP. ATP lysates were centrifuged to pellet cell debris. The supernatant was retained and used to quantify ATP content. The cell debris pellet was resuspended in NaOH and used to quantify protein using the Lowry assay (protein levels were adjusted to account for loss of protein following perchloric acid harvesting, see Appendix Figure 2). ATP content was then determined using an ATP luciferase assay, with resultant luminescence measured using a luminometer. ATP content of unknown samples was then calculated against a standard curve of known ATP concentrations and was normalised to protein.

In Figure 36, we can see that there is no real difference in ATP content of ddI treated cells compared to PBS control cells. This is apparent whether the cells are stimulated with 3 mM basal glucose or 25 mM high glucose. What is interesting though is that there is no increase in ATP content in either control or ddI treated cells following 25 mM glucose stimulation. We would have expected an increase in ATP content in control cells following 25 mM glucose stimulation as ATP is needed to drive glucose-stimulated insulin secretion.

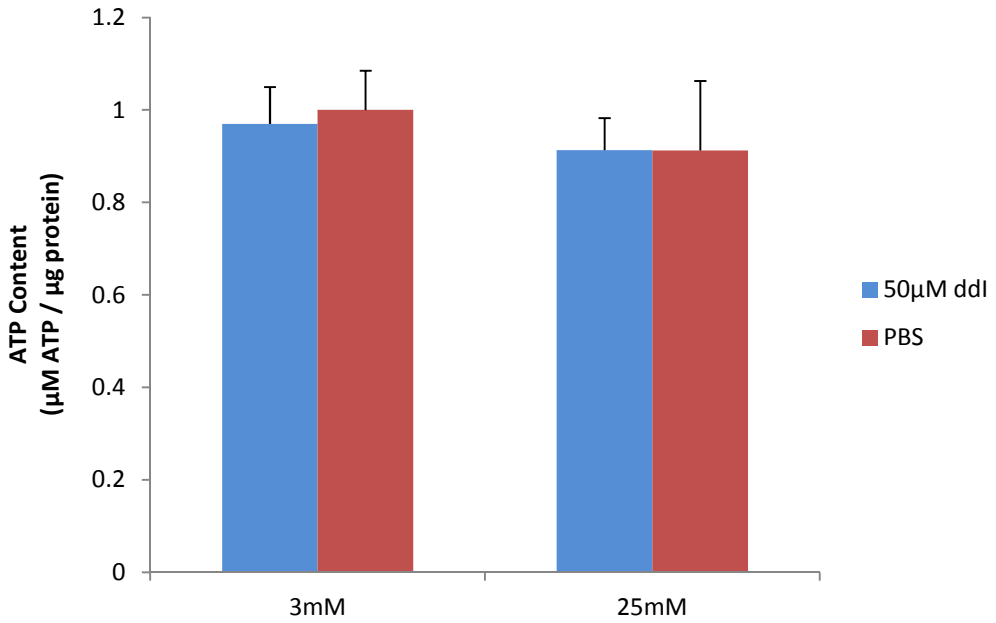

Figure 36 ATP content following didanosine-induced mtDNA depletion and glucose stimulation

mtDNA levels were depleted in MIN6 cells following 5 day incubation with 50 µM ddI. Cells were then stimulated with either 3 mM (basal) or 25 mM (high) glucose for 1 hr after which, cells were harvested in perchloric acid. ATP content was determined by an ATP luciferase assay against a standard curve of known ATP concentrations, which were then normalised to protein content. Data shown are from 4 separate experiments performed in triplicate, error bars representative of SEM. Data normalised to 3 mM basal glucose stimulated PBS cells.

We continued our investigations on the effect of mtDNA depletion on ATP content using the TFAM silencing mtDNA depletion model (Figure 37). Cells were transfected with the TFAM-429 or Scrambled control siRNA. Seventy two hrs post transfection, cells were stimulated with either 3 mM or 25 mM glucose prior to harvesting in perchloric acid. As with harvesting protein from transfected cells in Section 5.4.2, cell lysates from three wells of a 24 well tissue culture plate were pooled together to make one sample. The cell lysate was centrifuged to separate the supernatant, which was used to determine ATP content, from the cell debris, which was used to determine protein concentration.

We can see that as with didanosine-induced mtDNA depletion, there does not seem to be a difference in the ATP content of TFAM-429 and Scrambled transfected cells when faced with 25 mM glucose stimulation. When cells were stimulated with 3 mM basal glucose however, TFAM-429 cells appear to contain slightly more ATP compared to Scrambled control cells. We see that in both TFAM-429 and Scrambled control cells, ATP content increases following 25 mM glucose stimulation compared to basal 3 mM glucose stimulation. This is in contrast to the didanosine mtDNA depletion model, where we do not see a change in ATP content with increasing glucose concentration.

Summarising the effect of partial mtDNA depletion on whole cell ATP content, it seems that with both mtDNA depletion models, there is no difference in the ATP content of mtDNA depleted cells compared to control cells. In the TFAM mtDNA depletion model, we see an increase in ATP content following 25 mM glucose stimulation compared to basal 3 mM glucose stimulation, which is apparent in both TFAM-429 and Scrambled control cells. However, this increase in ATP content with glucose stimulation is not seen using the didanosine-induced mtDNA depletion model, in either PBS control or ddI treated cells.

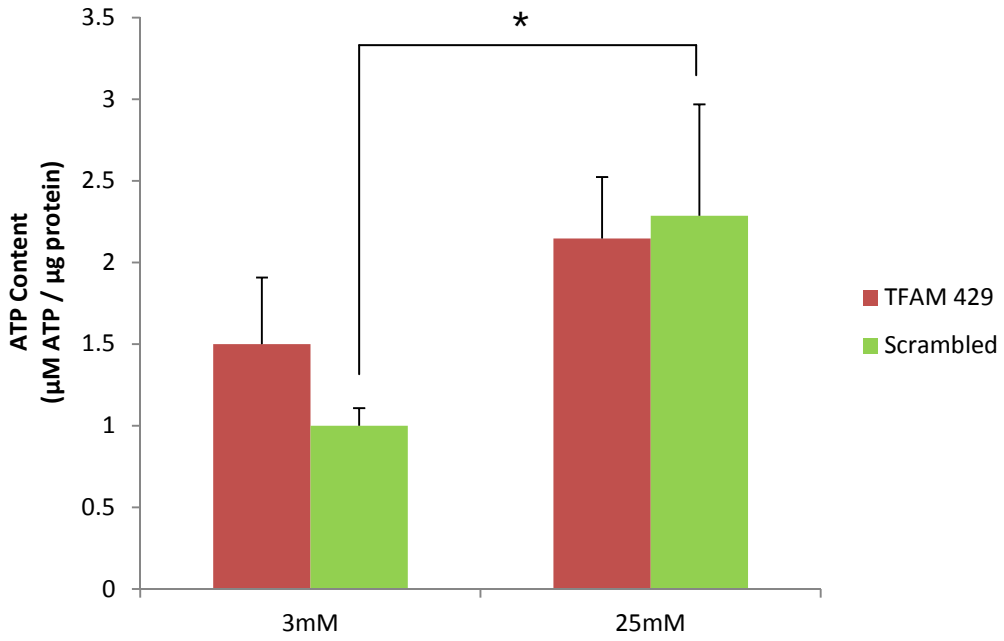

Figure 37 ATP content following TFAM silencing-induced mtDNA depletion and glucose stimulation

MIN6 cells were transfected with TFAM-429 or Scrambled siRNA probes. Seventy two hrs post transfection, cells were stimulated with either 3 mM or 25 mM glucose for 1 hr after which, cells were harvested in perchloric acid. ATP content was determined by an ATP luciferase assay against a standard curve of known ATP concentrations, which were then normalised to protein content. Data shown are from 4 separate experiments performed in duplicate, error bars representative of SEM. Data normalised to 3 mM basal glucose stimulated Scrambled cells. * $p<0.05$

5.4.4 mtDNA depletion does not affect mitochondrial membrane potential

To round up our investigations on the effects of partial mtDNA depletion on mitochondrial function, we wanted to explore whether mtDNA depletion directly affected mitochondrial membrane potential. We measured mitochondrial membrane potential by staining cells with the cationic JC-1 fluorescent dye, which fluoresces green in the cell cytosol and red in the cell mitochondria. To ensure we could measure changes in mitochondrial membrane potential, we first treated cells with hydrogen peroxide (H_2O_2), which abolishes mitochondrial membrane potential (Figure 38). H_2O_2 was added to normal live MIN6 cells, immediately after which, cells were imaged using a live cell microscope at time 0 mins. The same field of cells was then periodically imaged at 5 min intervals, until 20 mins after initial H_2O_2 addition. The red fluorescence emitted by the JC-J-aggregates in the cell mitochondria is clearly visible at time 0 mins after initial H_2O_2 addition. Also, the location of red fluorescence can be distinguished from that of the cytosolic green fluorescence emitted from the JC-1 monomers (Figure 38). After 5 mins post H_2O_2 treatment, we see a drastic reduction in the amount of red fluorescence emitted, indicating a loss of mitochondrial membrane potential. Red fluorescence progressively decreases throughout prolonged H_2O_2 exposure, until it is virtually non-existent after only 15 mins H_2O_2 treatment. Comparing this to the green fluorescence of the JC-1 monomers in the cytosol, there is no obvious change in green fluorescence throughout H_2O_2 exposure. Photo bleaching is evident in the green fluorescence images, especially during the later time points, which is to be expected with prolonged UV exposure on the same field of cells.

Fluorescent images were quantified using the ImageJ computer software programme. Red and green fluorescence was quantified at each time point and can be seen in Figure 39A. The image quantification supports the visual observations made: that green fluorescence does not change, but red fluorescence progressively decreases with increased H_2O_2 exposure. The mean sum of fluorescence obtained from ImageJ quantification was then used to find the ratio of red / green fluorescence and can be seen in Figure 39B. We can see that red / green fluorescence, which is representative of mitochondrial membrane potential, progressively decreases with prolonged H_2O_2 treatment and was completely abolished after only 20 mins H_2O_2 exposure.

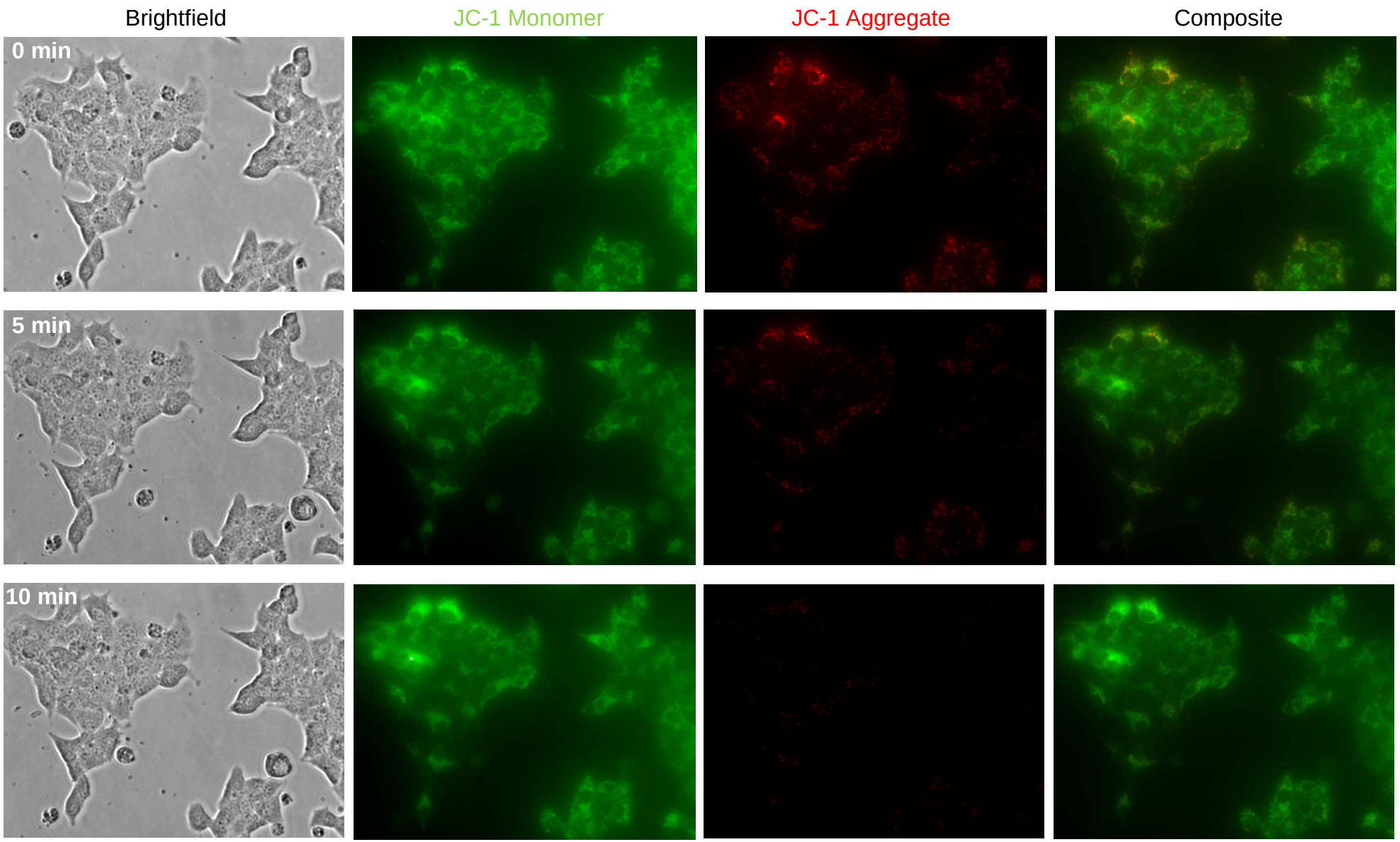
Brightfield
JC-1 Monomer
JC-1 Aggregate
Composite
0 min
5 min
10 min

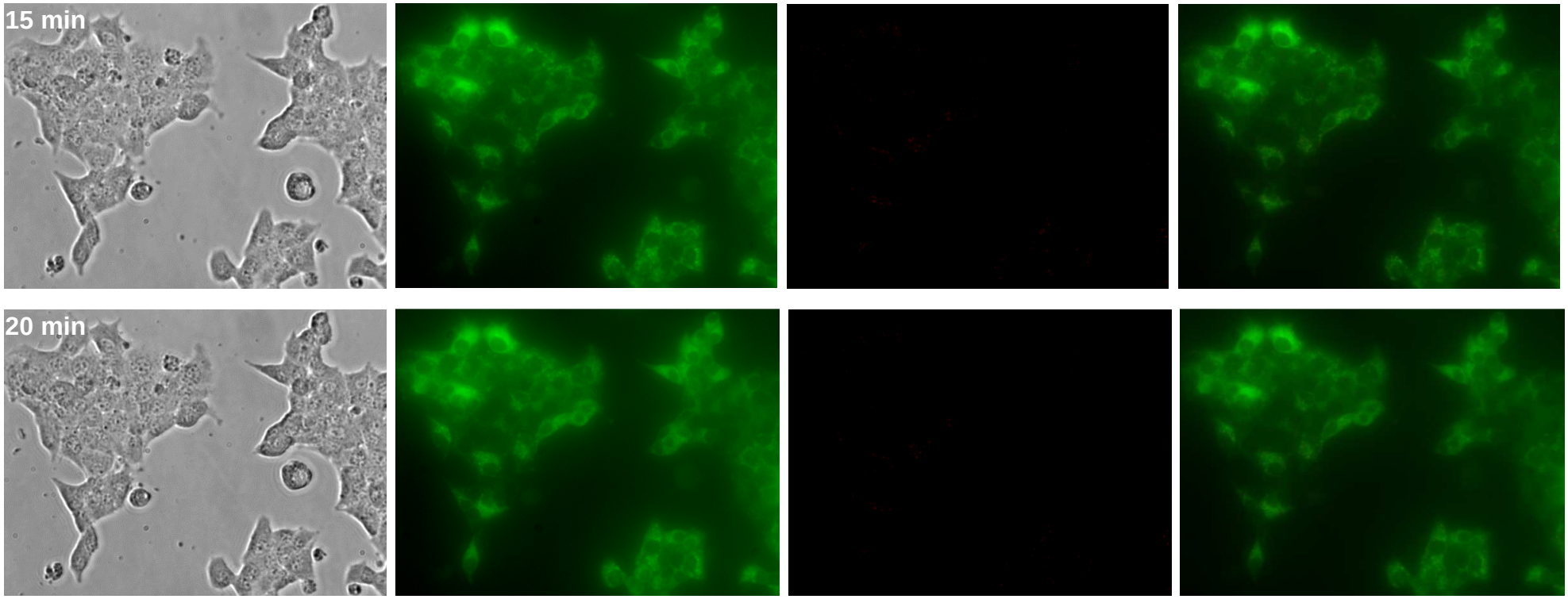

Figure 38 JC-1 staining in MIN6 cells following H_2O_2 treatment

JC-1 staining was used to measure mitochondrial membrane potential in MIN6 cells. The JC-1 dye exists in its monomeric form in the cell cytosol and emits a green fluorescence. JC-1 selectively enters the mitochondria where it aggregates and emits a red fluorescence. To show that we could measure loss of mitochondrial membrane potential, we treated live cells with hydrogen peroxide (H_2O_2) which abolishes the mitochondrial membrane potential. Live cells were imaged immediately after H_2O_2 was added (0 mins) using a live cell microscope. Images were then taken periodically at 5 min intervals until 20 mins post H_2O_2 treatment.

A

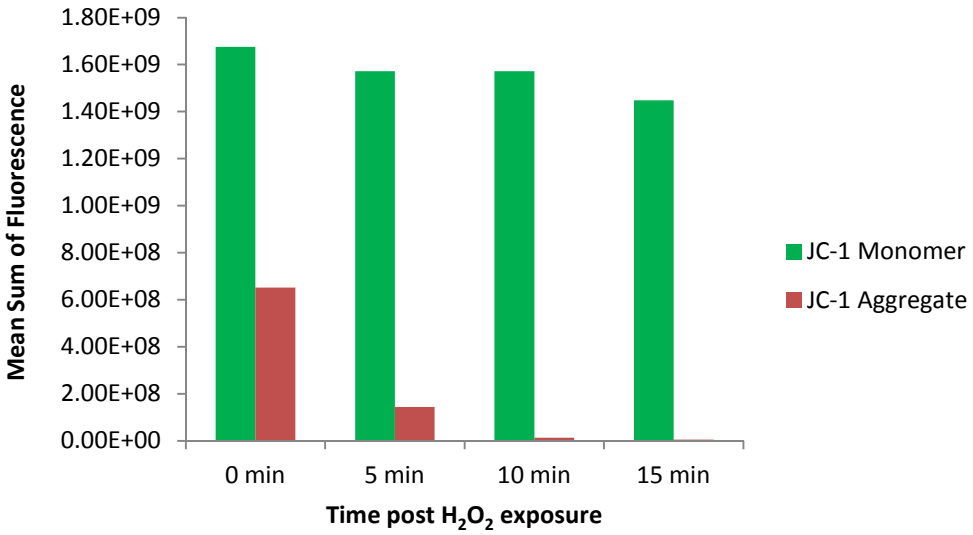

B

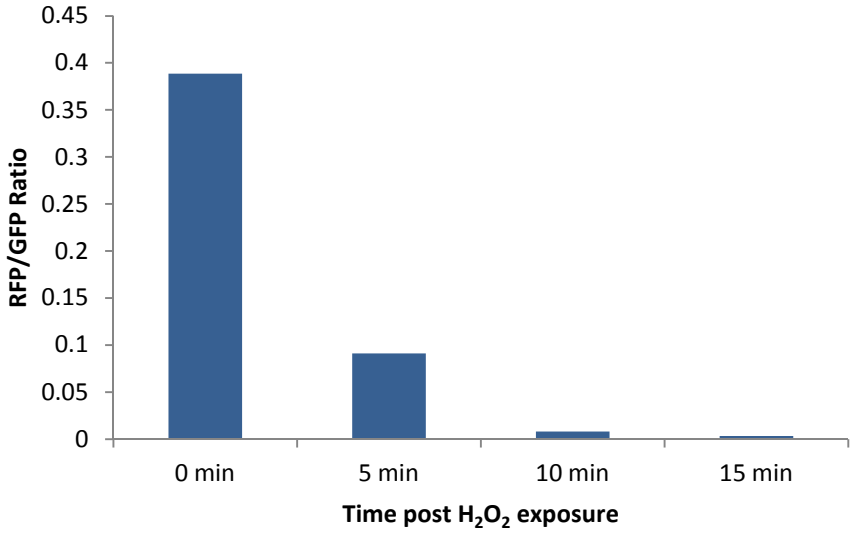

Figure 39 ImageJ quantification of mitochondrial membrane potential following H_2O_2 exposure

The images taken in Figure 38 were quantified using the ImageJ computer software programme. The programme was used to calculate the mean sum of fluorescence for both green and red fluorescent images at each time point after H_2O_2 addition (A). The mean sum of fluorescence values were then used to calculate the ratio of red / green fluorescence, which is representative of the mitochondrial membrane potential (B).

Now that we could detect loss of mitochondrial membrane potential using JC-1 staining, we proceeded to treat MIN6 cells with 50 μM ddI for 5 days to investigate what effect partial mtDNA depletion had on mitochondrial membrane potential. As with previous measures of mitochondrial function, we decided to try out the didanosine-induced mtDNA depletion method initially as this produced the greatest degree of mtDNA depletion. After the 5 day ddI treatment period, cells were stained with JC-1 staining medium containing JC-1 and the nuclear stain Hoechst 33342. Figure 40A shows representative images of one field from one well of ddI treated cells, and one field from one well of PBS treated cells. The experiment was repeated twice in duplicate wells, with 6 random fields taken of each well. Visually, there is no clear drastic difference in the green cytosolic JC-1 fluorescence or the red mitochondrial JC-1 fluorescence in ddI treated and PBS control cells (Figure 40A). This observation was confirmed following ImageJ quantification, with no difference seen in the ratio of red / green fluorescence in ddI treated and PBS control cells (Figure 40B). The partial mtDNA depletion following didanosine treatment does not appear to have an effect on mitochondrial membrane potential.

Because the degree of mtDNA depletion was greater using the didanosine model of mtDNA depletion, and because we failed to see an effect on mitochondrial membrane potential using this model, it was decided that measuring mitochondrial membrane potential in TFAM transcriptionally silenced cells was not necessary.

A

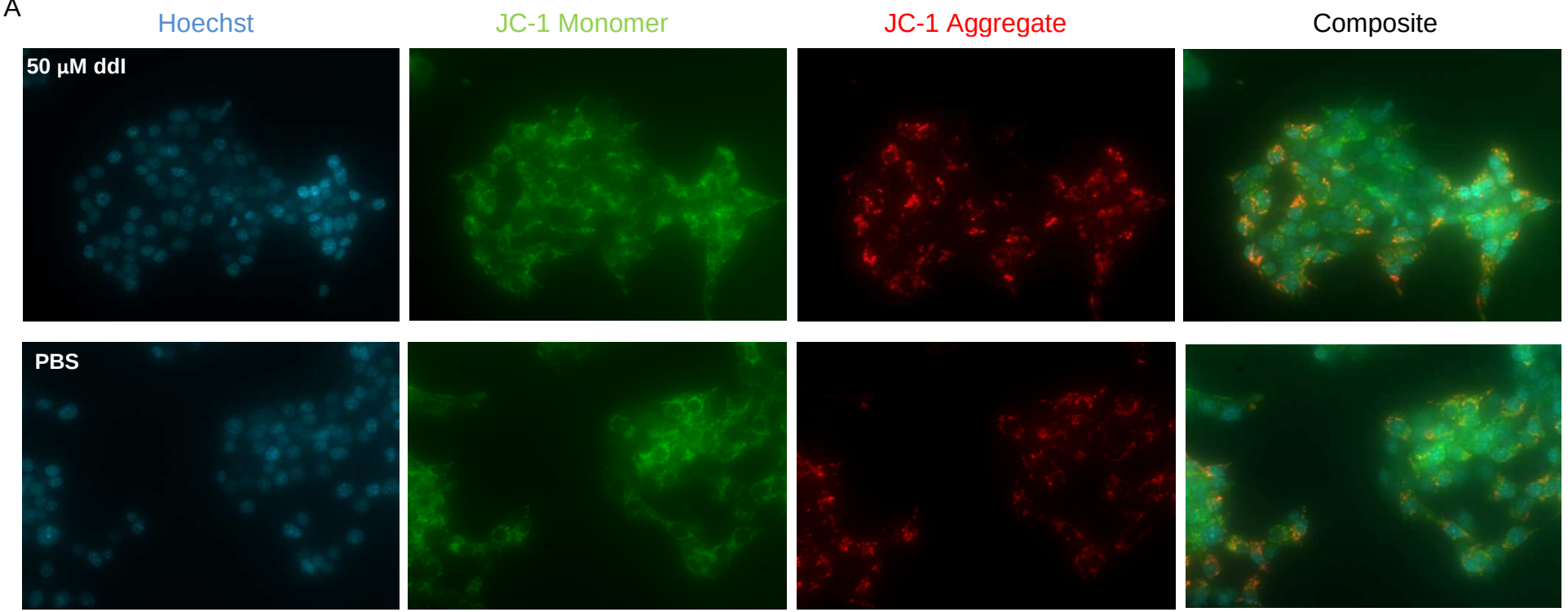

B

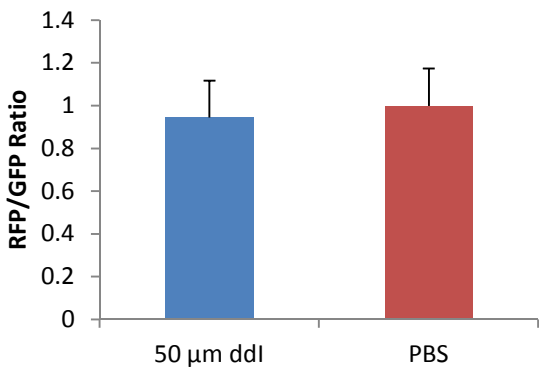

Figure 40 The effect of partial didanosine-induced mtDNA depletion on mitochondrial membrane potential

MIN6 cells were treated with 50 µM ddI for 5 days to deplete mtDNA levels. Cells were then stained with JC-1 and the nuclear stain Hoechst 33342. Experiment was repeated twice in duplicate, with 6 random fields taken for each well. Images in (A) are representative of one field of one ddI treated well, and one field of one PBS control well. Images were then quantified using ImageJ, error bars representative of SEM (B).

5.5 Discussion

Different aspects of mitochondrial function have been examined following mtDNA depletion in previous studies, but we decided to explore what effect mtDNA depletion had specifically on mitochondrial gene expression and protein translation, as well as ATP content and mitochondrial membrane potential.

Upon investigating mtDNA gene transcription, we decided to focus on the COX1 gene; one of the mtDNA encoded subunits of cytochrome c oxidase, Complex IV, of the respiratory chain. Cytochrome c oxidase consists of 13 protein subunits in total, 10 of which are nDNA encoded and 3 are mtDNA encoded (Dell'agnello, et al., 2007; Fontanesi, et al., 2006). The 3 mtDNA encoded subunits, COX1, COX2 and COX3, are essentially required to form the catalytic holoenzyme of the cytochrome c oxidase and so, their loss would be detrimental not only for catalytic function of the complex, but for the complex assembly also (Fontanesi, et al., 2006; Larsson, 2010). We are able to conclude that partial mtDNA depletion, whether by didanosine treatment or TFAM gene silencing, results in decreased COX1 mRNA expression. The level of COX1 suppression was greater following didanosine-induced mtDNA depletion compared to TFAM silencing-induced mtDNA depletion, but we believe this was due to the didanosine model of mtDNA depletion causing slightly greater mtDNA depletion compared to the TFAM model. That being said, we did achieve significant reduction in COX1 gene expression using the TFAM mtDNA depletion model also.

Out results are in agreement with many other reports detailing the loss of mtDNA gene expression following mtDNA depletion (Gauthier, et al., 2009; Hayakawa, et al., 1998; Soejima, et al., 1996; Tsuruzoe, et al., 1998). Some reports have looked at the mtDNA encoded components of cytochrome c oxidase in MIN6 cells just as we have however, these studies completely eradicated mtDNA levels following prolonged EtBr treatment and so, understandably, mtDNA gene expression was severely suppressed, if not nonexistent (Soejima, et al., 1996; Tsuruzoe, et al., 1998). One group has managed to create partial mtDNA depletion following transcriptional silencing of the β-cell master transcription factor PDX1 (Gauthier, et al., 2009). By infecting rat islets with a PDX-1 specific adenovirus, the group managed to silence PDX-

1 transcription by 90% relative to control islets, which resulted in a 50% reduction in TFAM mRNA levels. Concomitantly, this caused a 40% decrease in mtDNA levels and a 40% reduction in ND1 mRNA expression, a mtDNA encoded subunit of NADH dehydrogenase (Complex I) (Gauthier, et al., 2009). In accordance with Gauthier *et al.*'s findings, we also managed to achieve 40-50% depletion in mtDNA levels using both of our depletion models, which resulted in an overall 45% decrease and 24-33% decrease in COX1 gene expression following didanosine-induced and TFAM silencing-induced mtDNA depletion respectively.

Following the loss of mtDNA gene expression, we were keen to see if this culminated in the loss of mtDNA encoded protein. Again, we focused on the COX1 protein but we also looked at the nDNA encoded SDH70 subunit of succinate dehydrogenase (Complex II). Succinate dehydrogenase is the only complex of the respiratory chain that is entirely nDNA encoded with no mtDNA components and so, should be immune to the effects of mtDNA depletion. After performing a series of western blots, we found that reduced COX1 gene expression as a result of mtDNA depletion affects COX1 protein levels also. We saw a 34% loss in COX1 protein levels in didanosine-induced mtDNA depleted cells relative to control PBS cells. When using the TFAM model of mtDNA depletion however, we saw a slightly less 22% decrease in COX1 protein levels.

This difference in the level of COX1 protein decrease between the two models may be explained by the different degree of mtDNA depletion obtained from each model: the didanosine model produced a 50% reduction in mtDNA whereas the TFAM model only produced 40% mtDNA depletion. Another explanation for the slightly less decrease in COX1 protein levels following TFAM gene silencing could be the turnover rate of the COX1 protein. Many mitochondrial encoded proteins are predicted to have half-lives of up to several days (Aschenbrenner, et al., 1970; Ip, et al., 1974). In addition, the cytochrome c oxidase complex is predicted to have a turnover rate of 5.7 days in rat liver (Ip, et al., 1974). Therefore, it is possible that the 72 hrs post transfection was not long enough to see full COX1 protein turnover in the TFAM mtDNA depletion model, in comparison to the 5 day treatment period with didanosine. An interesting observation to be made from the TFAM depletion model western

blots is that two of the experimental repeats showed clear loss of COX1 protein in mtDNA depleted cells, whereas in one repeat, the loss in COX1 protein was open to debate. It is widely recognised that there is a mtDNA threshold level, below which is when we begin to see phenotypic or biochemical defects in the cell (Bai, et al., 2000; Moraes, et al., 1992; Sciacco, et al., 1994). It may be that in the TFAM mtDNA depletion model where we induce a 40% reduction in the level of mtDNA, that we are just on the cusp of the mtDNA threshold? Could this explain how some repeats show a reduction in COX1 protein and some repeats do not?

The final conclusion to be made from the protein studies is that mtDNA depletion did not seem to have an effect on nDNA encoded subunits of the mitochondrial respiratory chain. The protein levels of nDNA encoded SDH70 in mtDNA depleted cells were comparable to SDH70 protein levels in control cells, which was seen using both mtDNA depletion models. This shows unequivocally that in both mtDNA depletion models, the artificial mtDNA depletion we manage to induce only affects mtDNA encoded components of the respiratory chain. Gathier *et al.* were able to show that partial mtDNA depletion following PDX1 silencing resulted in decreased ND1 gene expression (mtDNA encoded), but failed to have an effect on SDH gene expression (nDNA encoded) (Gauthier, et al., 2009). Although the group only looked at mRNA expression and not protein levels, their findings support ours in that mtDNA depletion only effects mtDNA encoded genes and polypeptides. Another group showed a reduction in mitochondrial protein translation in p^0 MIN6 cells with no mtDNA, but as expected, the level of protein was barely detectable and so not comparable with our own results (Soejima, et al., 1996). Other groups have shown a progressive decrease in mtDNA encoded proteins in ageing muscle (Lanza, et al., 2008; Short, et al., 2005; Taanman, et al., 1997).

Encouraged by our findings that partial mtDNA depletion has an effect on mtDNA gene transcription and protein levels, we continued our investigations on mitochondrial function by analysing ATP content following glucose stimulation. Closure of ATP-gated K^+ channels in the plasma membrane of pancreatic β-cells is a pivotal step in glucose-stimulated insulin secretion (Ashcroft, et al., 1994). The rise in the cytosolic ATP/ADP ratio following glucose metabolism is key in investigating K^+ channel closure, which relies on

ATP generated from the electron transport chain (see Figure 3 and Section 1.1.6). Therefore, by first depleting mtDNA levels and then stimulating the mtDNA depleted cells with basal (3 mM) or high (25 mM) glucose, we wanted to see what effects this had on ATP content.

Didanosine-induced or TFAM silencing-induced mtDNA depletion does not seem to have an effect on ATP content in mtDNA depleted cells compared to control cells. This was apparent whether the cells were stimulated with basal or high glucose concentrations. Even though the partial mtDNA depletion we have induced in these models affects mtDNA transcription and translation, it does not have an effect on ATP content. Other studies investigating the effects of mtDNA depletion on ATP content have conducted their experiments in a similar manner to us, in that rodent pancreatic β-cells have been stimulated with varying glucose concentrations before harvesting in acidic solutions which require neutralising prior to performing a luminescence assay (Kennedy, et al., 1991; Tsuruzoe, et al., 1998). However, these studies were performed on p^0 pancreatic β-cells containing no mtDNA and so understandably, the ATP production in these p^0 cells was severely hindered (Tsuruzoe, et al., 1998), or not present at all (Kennedy, et al., 1991). In addition, the age-related decline in mtDNA copy number in human muscle was found to correlate with an age-related decline in ATP content (Lanza, et al., 2008). The fact that other groups have reported a decrease in ATP content following mtDNA depletion may be attributable to the degree of mtDNA depletion reported in these papers. It seems that the level we have depleted mtDNA in both of our depletion models is not enough to hinder ATP production.

It is also worth noting that even though the electron transport chain is the major source of ATP production, other pathways can be utilised for ATP production such as glycolysis. For instance, it is know that cancer cells experience mitochondrial respiratory chain dysfunction and increased glycolysis (Kaipparettu, et al., 2010). As MIN6 cells are derived from a mouse insulinoma, is it possible that MIN6 cells rely on glycolysis for their main source of ATP which is why we are not seeing an effect of partial mtDNA depletion on ATP content? But when mtDNA is completely removed, as seen in the Kennedy *et al.* and Tsuruzoe *et al.* studies on p^0 cells (Kennedy, et al., 1991; Tsuruzoe, et

al., 1998), the ATP produced via glycolysis is not enough to sustain glucose-stimulated insulin secretion.

Interestingly, when using the TFAM silencing-induced mtDNA depletion model, cells responded with an increased ATP content to glucose stimulation. When cells were stimulated with 25 mM glucose, ATP content increased in both TFAM-429 and Scrambled control cells. This was to be expected as an increase in ATP is needed to drive glucose-stimulated insulin secretion, and has been reported in control pancreatic β-cells with intact mtDNA levels in similar studies (Kennedy, et al., 1991; Tsuruzoe, et al., 1998). We are unsure as to why the cells used in the didanosine model did not respond in the same way to glucose stimulation. The reason cannot be off target effects of the drug as no change in ATP content with increasing glucose stimulation was seen in control PBS cells also. One would question whether the cells actually responded to the glucose stimulation in the first place. To be sure of this, analysis of the insulin secretion samples from the same cells would be required, to be sure that an increase in insulin secretion was seen following 25 mM glucose stimulation.

Our final measure of mitochondrial function was that of mitochondrial membrane potential using the JC-1 cationic fluorescent dye. We successfully abolished mitochondrial membrane potential after only 20 mins H_2O_2 treatment, which we managed to quantify using ImageJ, and so we were confident that we were able to quantify changes in mitochondrial membrane potential. However, we found that there was no difference in the mitochondrial membrane potential of didanosine-induced mtDNA depleted cells compared to control PBS cells. Other groups have used fluorescent probes such as rhodamine 123 to measure mitochondrial membrane potential, but as we have seen with many other measures of mitochondrial function, these groups reported reduced hyperpolarisation in pancreatic β-cells with severe mtDNA depletion (Kennedy, et al., 1998; Silva, et al., 2000), and not partial mtDNA depletion.

5.6 Conclusions

We can therefore conclude that partial mtDNA depletion by 50% or 40%, using drug inhibition of mtDNA replication or gene silencing of key mitochondrial transcription factors respectively, does have an effect on some aspects of

mitochondrial function. Key findings include a significant 33-45% reduction in the mtDNA encoded COX1 gene, which culminated in a 22-34% decrease in COX1 protein. COX1 is one of the three mtDNA encoded subunits that assemble to form the holoenzyme of cytochrome c oxidase, Complex IV, and so loss of this protein would impair the mitochondrial respiratory chain. However, we did not see a decrease in the nDNA encoded subunit SDH70, a component of succinate dehydrogenase, Complex II. This implies that the decrease in COX1 gene expression and the resultant loss of COX1 protein is the consequence of mtDNA depletion.

We measured other indices of mitochondrial function including ATP content and mitochondrial membrane potential however, we did not find the partial mtDNA depletion inflicted on MIN6 cells following didanosine treatment or transcriptional silencing of the TFAM transcription factor, was enough to cause an effect. More severe mtDNA depletion which is greater than 40-50% may be needed in order to see an effect on cellular ATP content or mitochondrial membrane potential.

The key question now is whether the decrease in mitochondrial function seen with partial mtDNA depletion has an effect of glucose-stimulated insulin secretion.

5.7 Limitations

Potential criticisms may be made of the methods employed when harvesting protein and ATP samples using the TFAM mtDNA depletion model. Transfections were performed in 24 well plates and samples were combined from three separate wells in order to make one sample, thus ensuring enough lysate for subsequent analyses. However, this may have introduced a large and unhelpful degree of variation unnecessarily. Performing transfections in 6 well plates, as we did when treating cells with didanosine would have been more ideal but due to time constraints, we were unable to re-optimise the protocol given to us by Invitrogen to cater for transfecting cells in larger 6 well plates.

Another limitation may lie in the method of quantifying ATP content. We chose to extract the ATP from cells using an acidic solution, similar to other studies

(Kennedy, et al., 1991; Tsuruzoe, et al., 1998), but decided to retain the cell debris after centrifugation in order to quantify whole cell protein concentration, which would be used to normalise ATP content to protein. It could be argued that this may be introducing unnecessary variation also. Even though cells were seeded at the same density, whether prior to didanosine treatment or during transfection, cells were then incubated for 72 hrs or for 5 days, depending on the method of mtDNA depletion. We could have then assumed that all cells grew at the same rate in all wells, but we wanted to be sure that any potential differences in ATP content were undoubtedly due to mtDNA depletion and not differences in cell number. By harvesting cells using perchloric acid, we prevented degradation of ATP, but experienced a reduction in whole cell protein in the process. We know this because during each experiment, we had wells of cells in which we only extracted protein and so, we used these wells to adjust for the loss of protein following perchloric acid extraction (see Figure 2 in Appendix). Therefore, it could be argued that we are introducing more variation. But even though previous studies have normalised ATP content to protein, they have used representative wells in which they have extracted protein and have assumed that all wells are equal (Kennedy, et al., 1991). Included in Figure 3 of the Appendix are the data from the ATP experiments, without protein normalisation.

Finally, it could be debated whether the reduction in mtDNA gene expression and subsequent loss of mtDNA encoded protein we have reported is enough to define mitochondrial dysfunction. What about oxygen consumption or cytochrome c oxidase (COX) complex activity? Measurement of oxygen consumption requires a vast number of cells and with the TFAM model of mtDNA depletion especially, we would have struggled to meet the demand. We did attempt COX/SDH staining, which we thought would be a great measure of COX complex activity, however, we found the MIN6 cells showed severe toxic effects to the staining procedure resulting in cell death.

Chapter 6

The effect of mtDNA depletion on Insulin secretion

6 The effect of mtDNA depletion on insulin secretion

6.1 Introduction

Our results so far have detailed the optimisation of two independent models of partial mtDNA depletion in MIN6 cells. We then found that both methods of mtDNA depletion were comparable, and mitochondrial dysfunction ensued with a significant decrease in mtDNA transcription resulting in loss of mtDNA encoded proteins. However, we found that ATP content and mitochondrial membrane potential were not affected by partial mtDNA depletion. As glucose metabolism and insulin secretion are closely associated in pancreatic β-cells (Wollheim, 2000), our next question was does the partial loss of mtDNA copy number affect glucose-stimulated insulin secretion?

Many reports have documented impairment in insulin secretion following mtDNA depletion in rodent pancreatic β-cells (Hayakawa, et al., 1998; Kennedy, et al., 1998; Soejima, et al., 1996; Tsuruzoe, et al., 1998) and rodent animal models (Gauthier, et al., 2009; Silva, et al., 2000). Some groups have managed to restore the loss in insulin secretion following mtDNA depletion by treating cells with membrane depolarising agents (Hayakawa, et al., 1998; Kennedy, et al., 1998; Tsuruzoe, et al., 1998) or by repopulation of cybrid clones with foreign mtDNA (Soejima, et al., 1996). The restoration of insulin secretion in these studies pinpoints the impairment of insulin secretion being mitochondrial in origin.

6.2 Aims

The aim of this chapter was to explore what effect mtDNA depletion in MIN6 cells had on glucose-stimulated insulin secretion. Using the two mtDNA depletion models optimised in Chapters 3 and 4, we:

- Investigated glucose-stimulated insulin secretion in mtDNA depleted cells, using 3 mM and 25 mM glucose, compared to control cells.
- Examined the insulin content of mtDNA depleted cells post glucose-stimulated insulin secretion, compared to control cells.
- Measured insulin gene expression following mtDNA depletion.

- Explored the effect of the insulin secretagogue glibenclamide on insulin secretion in mtDNA depleted cells.

6.3 Results

6.3.1 MIN6 cells respond to increasing glucose stimulation by secreting increased insulin

We initially picked MIN6 cells when embarking on this project because they were reported to respond to changes in glucose concentration (Ishihara, et al., 1994; Miyazaki, et al., 1990). To test this, we first stimulated MIN6 cells with increasing concentrations of glucose ranging from 0 – 25 mM for a period of 1 hr. The cell supernatant was removed and used to determine insulin secretion using a rat insulin ELISA. A rat insulin ELISA was used as there is high sequence homology between rat and mouse insulin and at the time, there was no mouse insulin ELISA available. Insulin secretion was determined using a standard curve of known insulin concentrations.

There is an obvious positive correlation between glucose concentration and insulin secretion, which is dose-dependent (Figure 41). The glucose concentrations used are obviously not in the physiological range seen in humans. However, in mice, the normoglycaemic range is considered to be 7 – 10 mM glucose, with hyperglycaemia diagnosed when glucose exceeds 20 mM (Keren, et al., 2000; Kunjathoor, et al., 1996; Park, et al., 1998). As MIN6 cells are a mouse pancreatic β-cell line, it was decided that we would stimulate cells with 3 mM glucose to represent low, basal glucose stimulation, and with 25 mM glucose to represent high glucose stimulation.

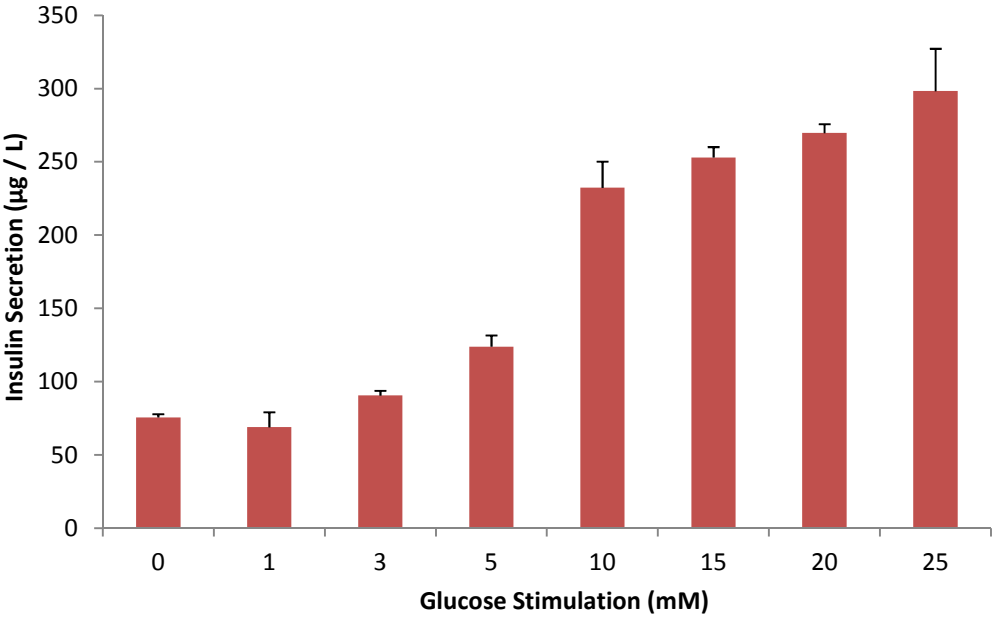

Figure 41 Glucose-stimulated insulin secretion in MIN6 cells

MIN6 cells were stimulated with increasing concentrations of glucose for 1 hr. Cell supernatant was removed and insulin secretion was determined using a rat insulin ELISA against a standard curve of known insulin concentrations. Experiment repeated once in triplicate, error bars representative of SD.

6.3.2 Didanosine-induced mtDNA depletion causes an increase in insulin secretion following 25 mM glucose stimulation

Now that we were confident that the MIN6 cells could respond to varying concentrations of glucose, we wanted to deplete mtDNA levels first using the didanosine model of mtDNA depletion, to see what effect this had on insulin secretion. Cells were treated for 5 days with 50 μM ddI to deplete mtDNA, after which, cells were stimulated for 1 hr with either 3 mM or 25 mM glucose. The cell supernatant was removed and insulin secretion determined using a rat insulin ELISA against a standard curve of known insulin concentrations. Protein was extracted from the MIN6 cells, quantified via a Bradford assay, and used to normalise insulin secretion to whole cell protein content.

In Figure 42A, we see that both didanosine treated and PBS control cells respond to increased glucose stimulation by secreting more insulin, which supports the data presented in Figure 41. There is a significant 6.5-fold and 4.5-fold increase in insulin secretion at 25 mM glucose stimulation compared to 3 mM glucose stimulation, in both didanosine treated and PBS control cells respectively ($p<0.001$). Furthermore, there does not seem to be a difference in insulin secretion of didanosine treated and PBS control cells when faced with 3 mM glucose challenge. However, we do see a difference in insulin response in didanosine treated and PBS control cells following a high glucose challenge. Surprisingly, we see that didanosine treated cells secrete significantly more insulin compared to PBS control cells, when stimulated with 25 mM glucose ($p=0.0026$).

This result was unexpected as we predicted the loss of mtDNA would result in decreased insulin secretion. We repeated the experiment a total of 6 times to ensure we were recording a true result. Our only explanation as to why didanosine-induced mtDNA depletion caused an increase in insulin secretion following 25 mM glucose stimulation was that didanosine was possibly having off target effects on the MIN6 cells.

Because protein was extracted from cells to normalise insulin secretion, additional wells were seeded in each experiment so we could extract DNA and measure mtDNA depletion. We can confirm that mtDNA levels were reduced by 50% in ddI treated cells compared to PBS control cells (Figure 42B).

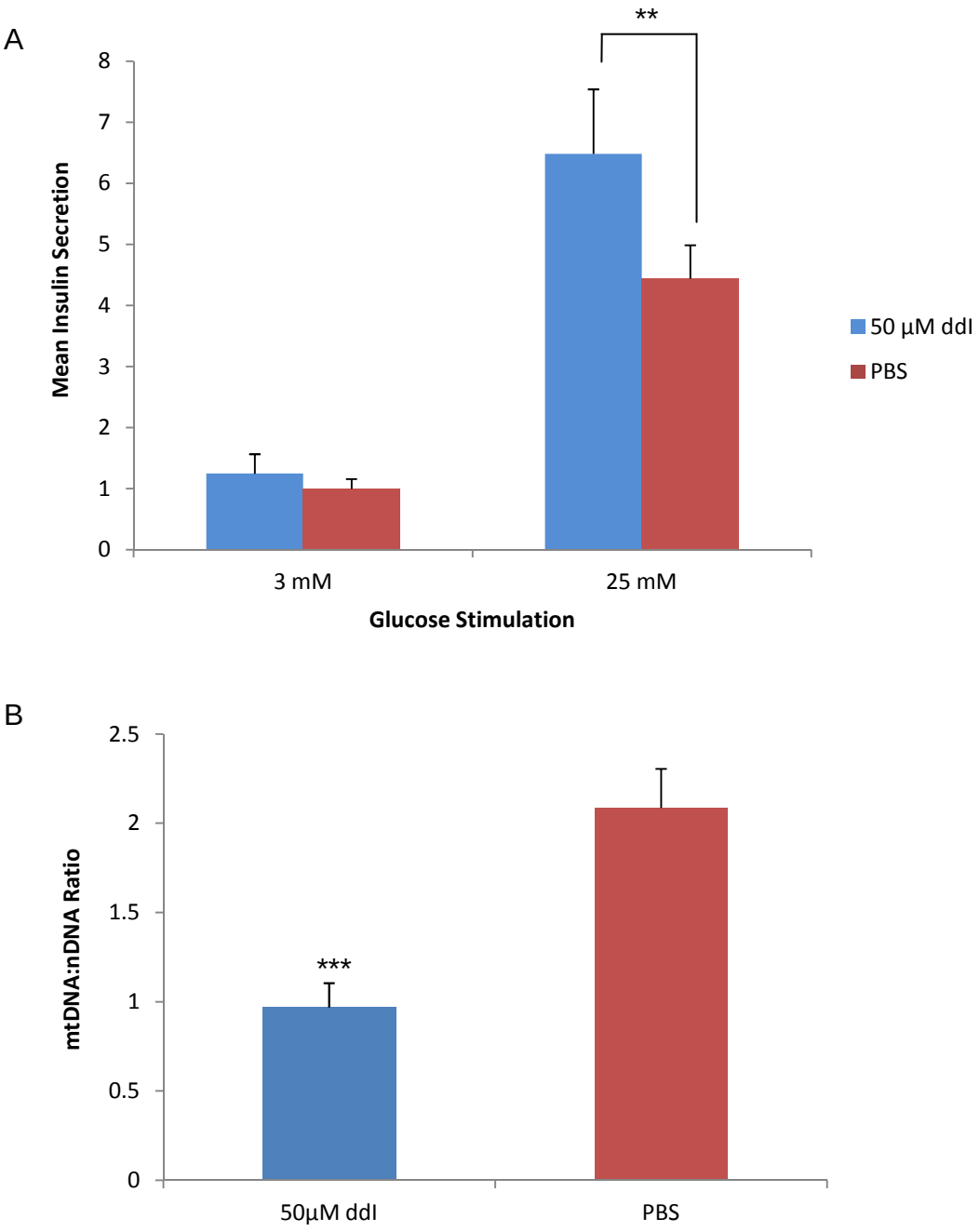

Figure 42 The effect of didanosine-induced mtDNA depletion on glucose-stimulated insulin secretion

(A) MIN6 cells were treated for 5 days with 50 µM ddI to deplete mtDNA. Cells were then stimulated with basal (3 mM) or high (25 mM) glucose concentrations for a period of 1 hr. Cell supernatant was removed and insulin secretion determined by insulin ELISA against a standard curve of known insulin concentrations. Protein was extracted from the MIN6 cells and used to normalise insulin secretion. Data normalised to 3 mM glucose stimulated PBS control cells. (B) mtDNA levels were checked by seeding additional wells whereby DNA was extracted and used in the mtDNA copy number assay. Data shown are from 6 separate experiments (A) or 3 separate experiments (B), each performed in triplicate. Error bars are representative of SEM. ** $p = 0.0026$, *** $p<0.001$

6.3.3 TFAM silencing-induced mtDNA depletion causes a decrease in insulin secretion following 25 mM glucose stimulation

To corroborate our theory that didanosine may cause off target effects on insulin secretion, we investigated the effect of TFAM silencing-induced mtDNA depletion on insulin secretion to see if we obtained similar results. MIN6 cells were transfected with TFAM-429 or Scrambled siRNA probes and incubated for 72 hrs to deplete mtDNA levels. Cells were then stimulated with either 3 mM or 25 mM glucose for a period of 1 hr. Insulin secretion was determined using an insulin ELISA and insulin secretion was normalised to whole cell protein content.

As with the didanosine mtDNA depletion model, both TFAM-429 and Scrambled transfected cells responded to 25 mM glucose stimulation by secreting significantly more insulin, compared to 3 mM glucose stimulation ($p<0.001$) (Figure 43A). However, we are starting to see divergence in the two methods of mtDNA depletion in their effects on insulin secretion. Insulin secretion was seen to be significantly less in TFAM-429 cells compared to Scrambled control cells, when cells were faced with 3 mM ($p=0.004$) and 25 mM ($p=0.03$) glucose stimulation. This is in total contrast to the results seen with the didanosine mtDNA depletion model, which further supports our hypothesis that didanosine is perhaps exhibiting off target effects on insulin secretion in the MIN6 cells.

As with the didanosine mtDNA depletion model, additional wells were transfected so we could extract DNA and measure mtDNA depletion using the mtDNA copy number assay. We can confirm that mtDNA levels were depleted by 40% in TFAM-429 transfected cells compared to Scrambled control cells (Figure 43B).

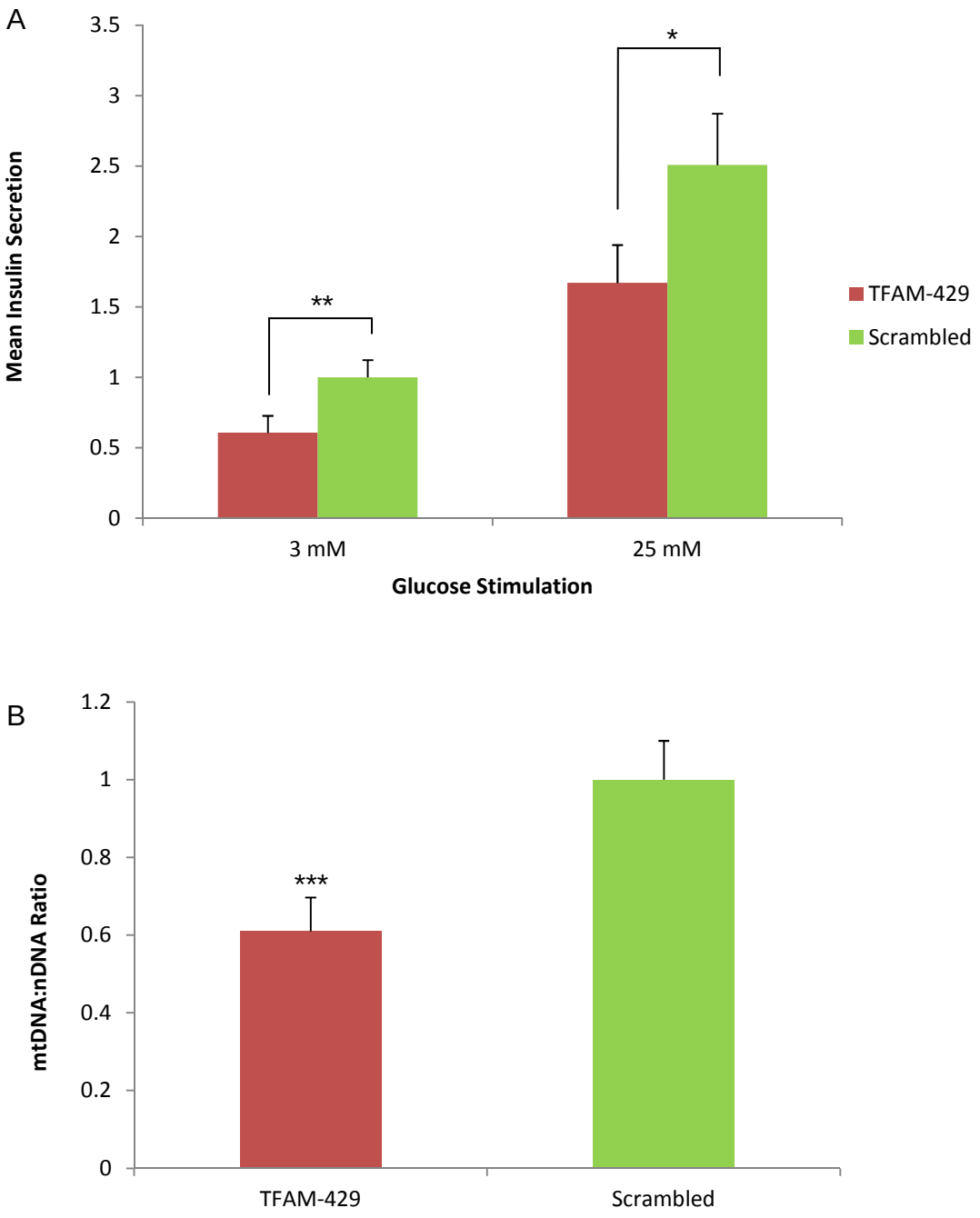

Figure 43 The effect of TFAM silencing-induced mtDNA depletion on glucose-stimulated insulin secretion

(A) MIN6 cells were transfected with TFAM-429 or Scrambled siRNA to deplete mtDNA. Seventy two hrs post transfection, cells were stimulated with basal (3 mM) or high (25 mM) glucose concentrations for a period of 1 hr. Cell supernatant was removed and insulin secretion determined by insulin ELISA against a standard curve of known insulin concentrations. Protein was extracted from the MIN6 cells and used to normalise insulin secretion. Data normalised to 3 mM glucose stimulated Scrambled control cells. (B) mtDNA levels were checked by seeding additional wells whereby DNA was extracted and used in the mtDNA copy number assay. Data shown are from 5 separate experiments (A) or 3 separate experiments (B), each performed in triplicate. Error bars are representative of SEM. * p=0.03, ** p = 0.004, *** p<0.001

6.3.4 The effect of mtDNA depletion on insulin content

To understand the reason behind the differences in insulin secretion in our two models of mtDNA depletion after 25 mM glucose stimulation, we decided to investigate the insulin content of cells post glucose-stimulated insulin secretion. Starting with the didanosine mtDNA depletion model first, we depleted mtDNA levels following 50 μM didanosine treatment for 5 days. Just as we had done previously, cells were then stimulated with 3 mM or 25 mM glucose for 1 hr. Cell supernatant was removed and cells were then harvested in ice cold PBS. Insulin was liberated from cells after repeated freezing of cells in liquid nitrogen, and rapidly thawing them in a water bath. As with insulin secretion, insulin content was determined following insulin ELISA. Protein content was determined using the same PBS lysate, and insulin content was normalised to whole cell protein content.

In Figure 44, we start to understand why ddI treated cells secrete more insulin, because it seems they contain more insulin compared to PBS control cells. When control PBS cells are stimulated with high 25 mM glucose, we see insulin content increase by 50% compared to 3 mM glucose stimulation. This is to be expected as the increased insulin content with increased glucose stimulation would be required to increase insulin secretion. In ddI treated cells however, we still see an increase in insulin content with increased glucose stimulation, but it is much greater than that seen in PBS control cells. Didanosine treated cells contain approximately 30% more insulin compared to PBS control cells following 3 mM glucose stimulation, and approximately 45% more insulin compared to PBS control cells following 25 mM glucose stimulation (data showed no statistical significance).

We conducted the same experiment using the TFAM mtDNA depletion model (Figure 45). We found that in Scrambled control cells, there was a 53% increase in insulin content in cells stimulated with 25 mM glucose compared to cells stimulated with 3 mM glucose. This mimics what we found in PBS control cells when using the didanosine mtDNA depletion model. However, there was no change in the insulin content of TFAM-429 cells with increased glucose stimulation compared to basal glucose. Not only that, but it seems that TFAM-

429 cells contained less insulin compared to Scrambled control cells, which was more pronounced following 25 mM glucose stimulation.

In summary, our results suggest that there is an approximate 50% increase in insulin content in the respective control cells (PBS and Scrambled) following 25 mM glucose stimulation, compared to 3 mM glucose stimulation. After 25 mM glucose stimulation, didanosine-induced mtDNA depleted cells tended to have a greater insulin content compared to PBS control cells, whereas TFAM silenced mtDNA depleted cells have less insulin content compared to Scrambled control cells. These differences in insulin content following 25 mM glucose stimulation are in line with the differences seen in insulin secretion when comparing the two mtDNA depletion models.

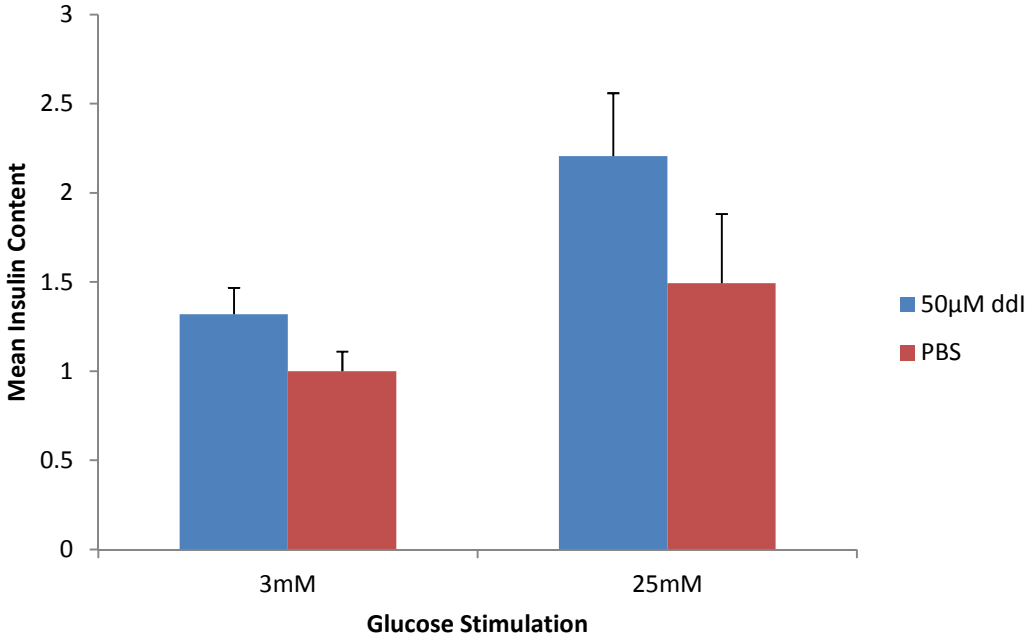

Figure 44 The effect of didanosine-induced mtDNA depletion on insulin content following glucose-stimulated insulin secretion

mtDNA levels were reduced following incubation with 50 µM ddI for 5 days. Cells were stimulated with either 3 mM or 25 mM glucose before removing cell supernatant and harvesting cells in PBS. Insulin was liberated from cells by repeated freeze/thaw using liquid nitrogen. Insulin content was determined by insulin ELISA and was normalised to whole cell protein content. Experiment was repeated 3 times in triplicate, error bars represent SEM. Data normalised to 3 mM glucose stimulated PBS control cells.

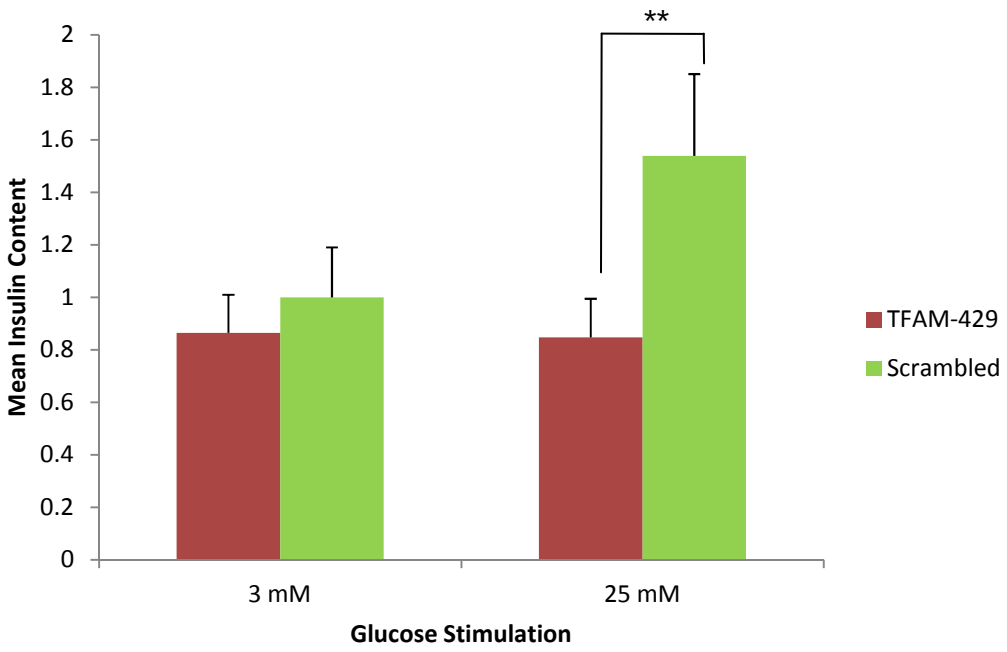

Figure 45 The effect of TFAM silencing-induced mtDNA depletion on insulin content following glucose-stimulated insulin secretion

MIN6 cells were transfected with either TFAM-429 or Scrambled siRNA probes to deplete mtDNA levels. Cells were stimulated with either 3 mM or 25 mM glucose before removing cell supernatant and harvesting cells in PBS. Insulin was liberated from cells by repeated freeze/thaw using liquid nitrogen. Insulin content was determined by insulin ELISA and was normalised to whole cell protein content. Experiment was repeated 3 times in triplicate, error bars represent SEM. Data normalised to 3 mM glucose stimulated Scrambled cells. ** p=0.01

6.3.5 The effect of mtDNA depletion on insulin gene expression

In an attempted to uncover why after 25 mM glucose stimulation didanosine-induced mtDNA depleted cells secreted more insulin and contained more insulin, whereas TFAM silenced mtDNA depleted cells secreted less insulin and contained less insulin when compared to control cells, we wanted to investigate *Ins1* insulin gene expression.

MIN6 cells were depleted of their mtDNA following 5 day 50 μM ddI treatment or TFAM transcriptional silencing. RNA was then extracted from cells, quantified and reverse transcribed. Real-time PCR was used to assess *Ins1* gene expression relative to reference gene *B2M* using TaqMan hydrolysis probes.

In didanosine-induced mtDNA depleted cells, *Ins1* gene expression is reduced by 20% compared to PBS control cells ($p<0.001$) (Figure 46A). Could this decrease in *Ins1* gene expression be an attempt to reduce the amount of insulin protein in didanosine treated MIN6 cells? Conversely, in TFAM silencing-induced mtDNA depleted cells, there is no change in *Ins1* gene expression (Figure 46B), suggesting that the decrease in insulin secretion and insulin content in these cells is not due to reduced gene expression.

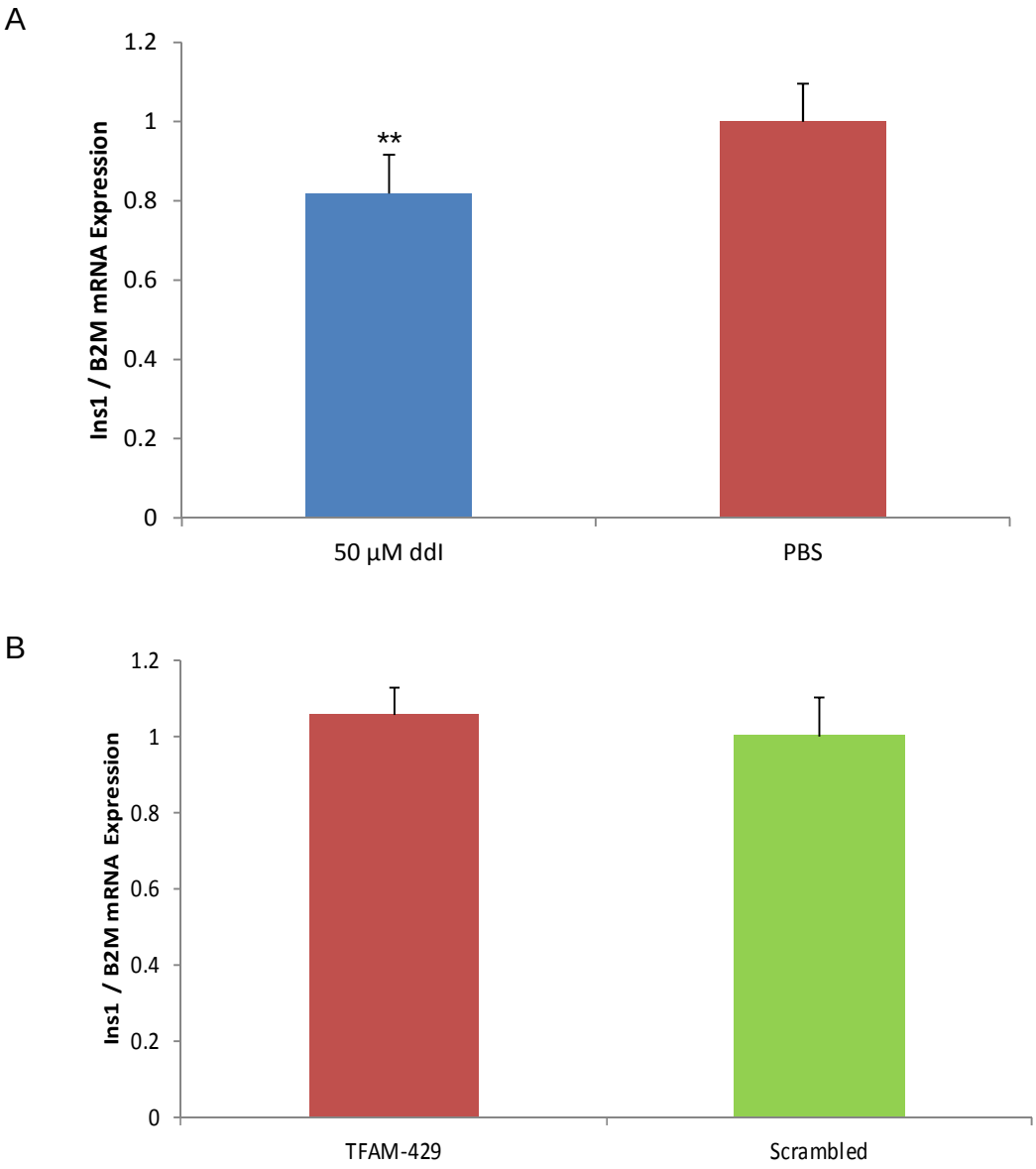

Figure 46 The effect of mtDNA depletion on *Ins1* insulin gene expression

MIN6 cells were depleted of mtDNA following didanosine treatment (A) or TFAM transcriptional silencing (B). RNA was then extracted from cells, quantified and reverse transcribed. Real-time PCR was used to determine target gene *Ins1* expression relative reference gene *B2M*. Data shown are from three individual experiments performed in sextuplet (A) or triplicate (B). Error bars represent SEM. ** $p<0.001$

6.3.6 The effect of glibenclamide on MIN6 cells

We are still unable to explain why didanosine treatment causes an increase in insulin secretion and insulin content in didanosine treated cells. However, using the TFAM model where we had successfully impaired insulin secretion following mtDNA depletion, we were interested to see what effect the insulin secretagogue glibenclamide had on MIN6 cells. Glibenclamide is a second generation sulphonylurea drug used in the treatment of T2DM. It targets the sulphonylurea receptor 1 (SUR1) protein on the β-cell K^+ channel, promoting channel closure and subsequent plasma membrane depolarisation. Therefore, the sulphonylurea drug can be seen to bypass certain processes of the glucose-stimulated insulin secretion pathway.

The data presented in sections 6.3.6 and 6.3.7 was completed under my supervision and guidance by Meutia Kumaheri, for her Masters by Research which was submitted July 2012.

To examine the response of normal MIN6 cells to glibenclamide, cells were exposed to glibenclamide between the range of 0.01 μM and 10 μM for 1 hr, along with either basal 3 mM glucose stimulation or high 25 mM glucose stimulation. Glibenclamide was reconstituted in DMSO and so, DMSO was used as the drug vehicle control. To ensure that DMSO was not having off target effects on the cells, we also used a media control in which no glibenclamide or DMSO was added, only 3 mM or 25 mM glucose.

Glibenclamide can be seen to augment insulin secretion following 3 mM glucose stimulation compared to both the media and drug vehicle controls, especially with 0.1 μM and 1 μM glibenclamide ($p<0.05$) (Figure 47). After 25 mM glucose stimulation, we see significant increases in insulin secretion in all glibenclamide treated and control cells relative to the media control cells stimulated with 3 mM glucose. It is interesting that we do not see an additive response of high 25 mM glucose with glibenclamide, but that 25 mM glucose stimulation in media and drug vehicle control cells stimulates the maximal insulin secretory response. It can also be noted that the DMSO drug solvent used does not seem to be exhibiting off target effects, with the response of these cells mimicking that of media control cells.

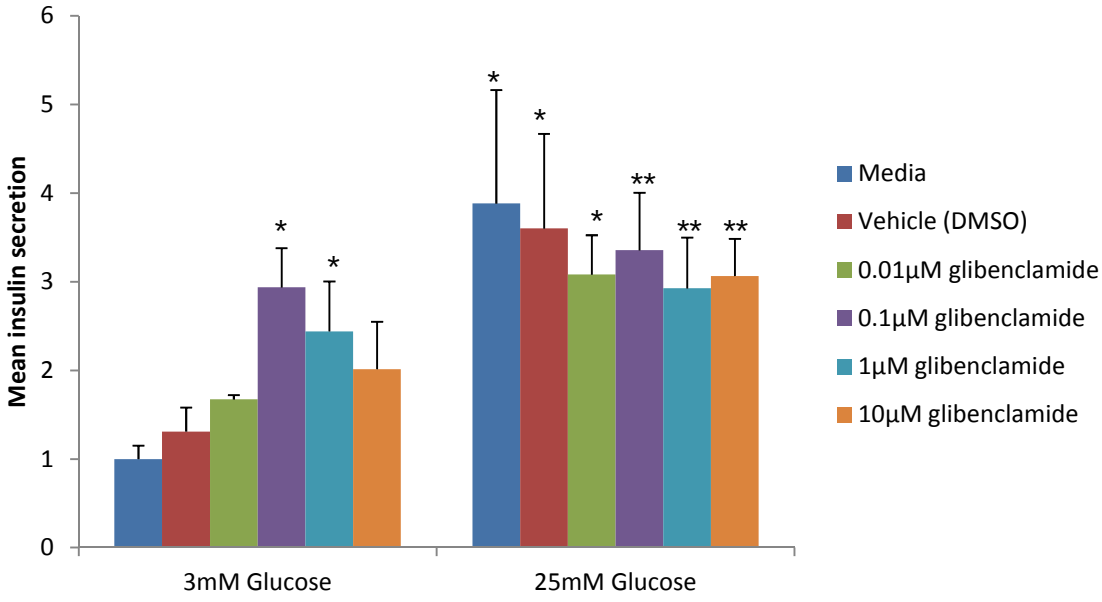

Figure 47 The effect of varying concentrations of glibenclamide on insulin secretion after basal 3 mM and high 25 mM glucose stimulation

Normal MIN6 cells were stimulated with basal 3 mM glucose or high 25 mM glucose for 1 hr with 0.01 µM, 0.1 µM, 1 µM or 10 µM glibenclamide. DMSO was the drug vehicle control, and media cells did not contain any glibenclamide or DMSO. Cell supernatant was retained and insulin secretion determined by insulin ELISA, which was normalised to whole cell protein content. Data presented are from 3 separate experiments each performed in duplicate, and are normalised to basal 3 mM glucose media control cells. Error bars representative of SEM. * $p<0.05$, ** $p<0.01$ vs DMSO vehicle control cells at 3 mM glucose.

The data presented Figure 47 was reconfigured to represent the effect of basal 3 mM and high 25 mM glucose stimulation on glibenclamide treatment (Figure 48). High 25 mM glucose stimulation provokes a significant increase in insulin secretion in media and vehicle control cells, as well as the lowest 0.01 μM glibenclamide concentration used, relative to 3 mM glucose stimulation in these cells ($p<0.05$). However, there is not great difference in the insulin secretion of 0.1 μM, 1 μM and 10 μM glibenclamide treated cells following 3 mM or 25 mM glucose stimulation. In fact, it seems insulin secretion slightly decreases with the highest glibenclamide concentrations used, perhaps indicating toxic effects at these concentrations.

Therefore in summary, it seems that after 25 mM glucose stimulation, there is no additive effect of increasing glibenclamide concentration on insulin secretion. For future studies, we would be looking to use 0.1 μM glibenclamide as this concentration invokes a significant and optimal increase in insulin secretion at 3 mM glucose stimulation.

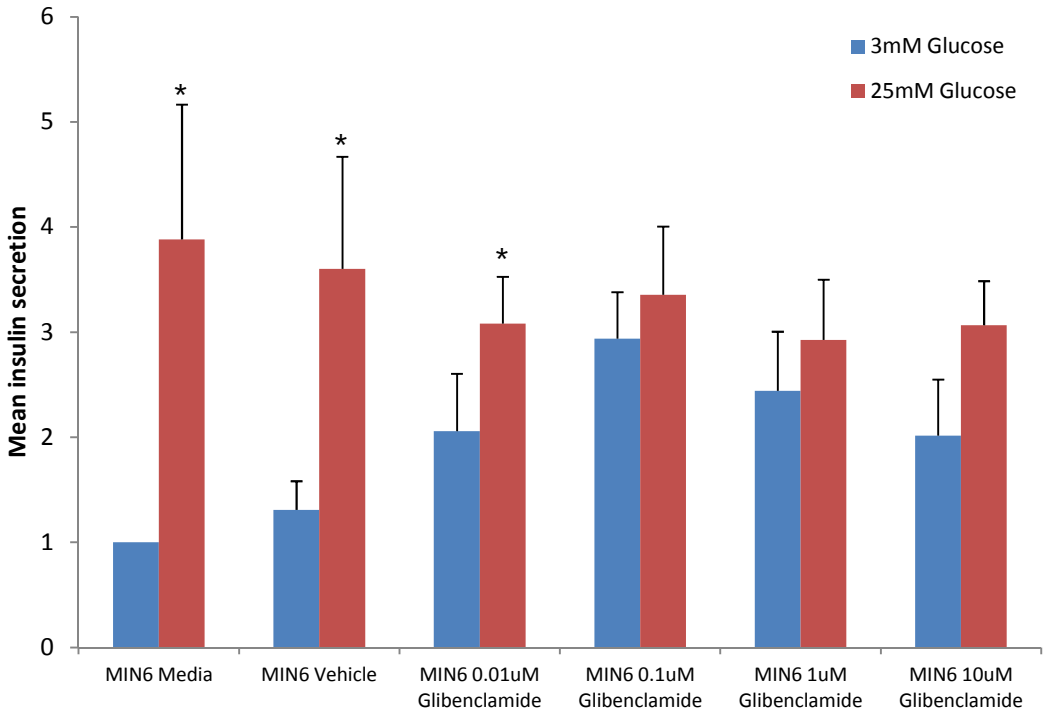

Figure 48 The effect of basal 3 mM and high 25 mM glucose stimulation on glibenclamide treatment

The data presented in Figure 47 was reconfigured to represent the fold-change in insulin secretion after 3 mM and 25 mM glucose stimulation on glibenclamide treatment. DMSO was the drug vehicle control, and media cells did not contain any glibenclamide or DMSO. Data presented are from 3 separate experiments each performed in duplicate, and are normalised to basal 3 mM glucose media control cells. Error bars representative of SEM. * $p<0.05$ vs insulin secretion at 3 mM glucose for each condition.

6.3.7 Glibenclamide rescues the impaired insulin secretion seen with TFAM silencing-induced mtDNA depletion

Having defined how normal MIN6 cells respond to glibenclamide treatment, we wanted to see how this response differed with mtDNA depletion. Cells were transfected with either TFAM-429 or Scrambled control probes and incubated for 72 hrs post transfection. They were then stimulated with basal 3 mM glucose or high 25 mM glucose for 1 hr, with or without 0.1 μM glibenclamide. Insulin secretion was determined by rat insulin ELISA and normalised to whole cell protein content. The results are presented in Figure 49.

The data corroborate what we have seen previously, that insulin secretion is impaired in TFAM-429 cells after 25 mM glucose stimulation compared to Scrambled control cells ($p<0.05$). After basal 3 mM glucose stimulation, insulin secretion is comparable in TFAM-429 cells and Scrambled control cells, but can be seen to significantly increase by 2.81-fold and 2.73-fold respectively with 0.1 μM glibenclamide treatment ($p<0.01$). After high 25 mM glucose stimulation however, we see the glibenclamide restores insulin secretion to normal in the TFAM-429 cells compared to control cells.

Therefore, we have managed to restore the insulin secretion deficit in mtDNA depleted MIN6 cells seen after 25 mM glucose stimulation by treating cells with 0.1 μM glibenclamide. This leads us to suggest the impairment in insulin secretion we have seen occurs prior to K^+ channel closure.

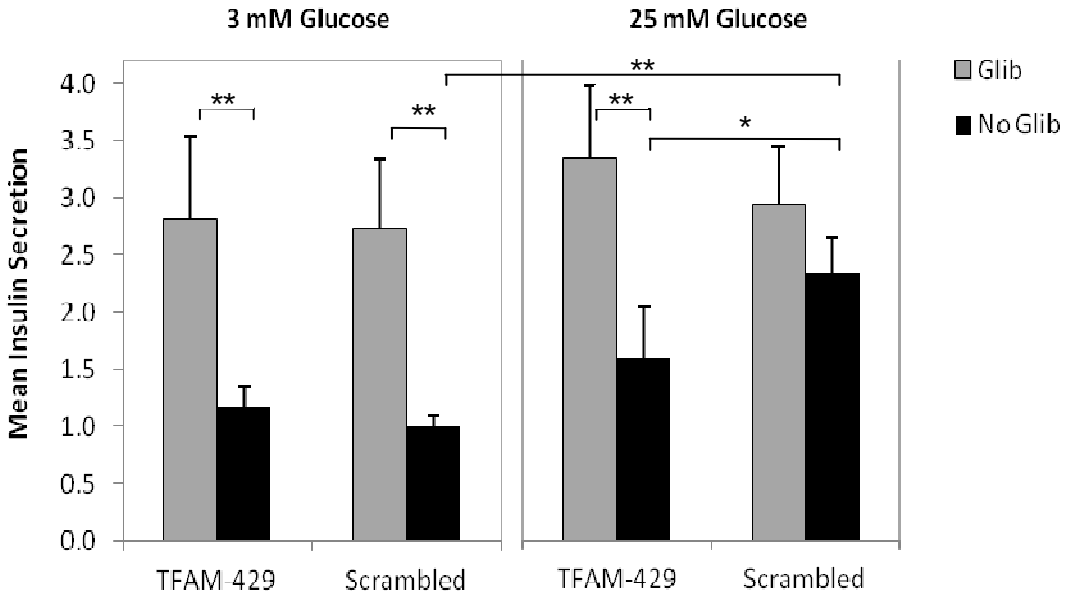

Figure 49 The effect of glibenclamide on insulin secretion in TFAM silencing-induced mtDNA depleted cells

Mitochondrial DNA levels were partially depleted following TFAM transcriptional silencing and incubation for 72 hrs post transfection. Cells were then stimulated with basal 3 mM or high 25 mM glucose for a period of 1 hr, supplemented with or without 0.1 μM glibenclamide. Insulin secretion was determined by insulin ELISA and normalised to whole cell protein content. Data shown are from 4 separated experiments performed in triplicate, and are normalised to Scrambled negative control cells stimulated with 3 mM glucose without glibenclamide. Error bars representative of SEM. * $p<0.05$, ** $p<0.01$

6.4 Discussion

Glucose-stimulated insulin secretion is one of the main functions of the pancreatic β-cell. First phase and second phase insulin secretion were found to be significantly reduced in patients diagnosed with prediabetes and T2DM (Hosker, et al., 1989; Porte, 2001; Wollheim, 2000). Impaired insulin secretion is also a key characteristic of patients suffering from mitochondrial diabetes (Lynn, et al., 2003; Maassen, et al., 2004). Decreased insulin secretion has been linked to increasing age (Basu, et al., 2003; Chang and Halter, 2003; Gao, et al., 2011; Suzuki, et al., 1997) and mtDNA depletion (Gauthier, et al., 2009; Hayakawa, et al., 1998; Kennedy, et al., 1998; Silva, et al., 2000; Soejima, et al., 1996; Tsuruzoe, et al., 1998). Insulin secretion is closely associated with glucose metabolism (Wollheim, 2000), which involves the mitochondrial respiratory chain.

Following didanosine-induced mtDNA depletion, we were quite surprised to find that there was an increase in insulin secretion at 25 mM glucose stimulation. During stimulus-secretion coupling in the pancreatic β-cell, the rise in cytosolic ATP/ADP ratio following glucose metabolism is a pivotal step in order to promote closure of plasma membrane-bound K^+ channels, resulting in subsequent membrane depolarisation and Ca^{2+} influx. Therefore, the loss of mtDNA would be predicted to affect the mtDNA encoded components of the respiratory chain, as we reported in the previous chapter, culminating in decreased ATP production and subsequent insulin secretion. And indeed, when we deplete mtDNA levels using TFAM transcriptional silencing, we found that insulin secretion was reduced in these cells by 39% compared to control cells ($p=0.03$) following high 25 mM glucose stimulation. We therefore began to suspect that didanosine drug treatment was perhaps exerting off target effects on MIN6 cells in regards to insulin secretion.

Didanosine (ddI) is one of the 7 certified nucleoside analogue reverse transcriptase inhibitor (NRTI) drugs currently used in the treatment of HIV (Höschele, 2006). As a nucleoside analogue of the nucleotide adenosine, ddI competes with endogenous adenosine for incorporation into the replicating mtDNA strand (Lewis, et al., 2003; Mitsuya, et al., 1990). However, ddI lacks the 3'-OH group required to form phosphodiester linkages and so, strand

termination ensues following ddI incorporation (Mitsuya, et al., 1990). Long term NRTI-drug use has been reported to have severe side effects on mitochondrial toxicity thought to be via oxidative damage to mtDNA (de la Asuncion, et al., 1999; Szabados, et al., 1999; Yamaguchi, et al., 2002). It is also known that a number of HIV patients receiving NRTI drug therapy later develop T2DM (Brown and Glesby, 2012; Brown, et al., 2005; Hadigan, et al., 2001; Lo, et al., 2005; Tien, et al., 2008) with prolonged NRTI treatment being linked to insulin resistance (Blanco, et al., 2011; Tien, et al., 2008), hyperinsulinaemia (Hadigan, et al., 2001; Mallon, et al., 2005) and hyperlactataemia (Lo, et al., 2005). Hadigan *et al.* reported that HIV patients receiving NRTI therapy presented hyperinsulinaemia at both fasting and post-glucose challenge, which was supported by these patients displaying increased insulin resistance and increased β-cell dysfunction also (Hadigan, et al., 2001). These results are in support of our own findings in that didanosine treated cells were found to secrete more insulin after high 25 mM glucose stimulation. Mallon *et al.* also reported hyperinsulinaemia in HIV patients receiving NRTI therapy however the patients studied also presented lipodystrophy, a common phenotype of HIV patients (Brown and Glesby, 2012) and so, the reported hyperinsulinaemia cannot be solely attributed to NRTI use alone (Mallon, et al., 2005). Because it is known that some patients do also develop T2DM, it may be that the acute effect of ddI is to increase insulin secretion, but that longer term there may be associated β-cell failure.

Nonetheless, these studies substantiate our theory that didanosine is perhaps exhibiting off target effects on insulin secretion. We attempted to investigate why didanosine treated cells secrete increased insulin in response to high glucose and we found that these cells actually contained 32% more insulin compared to control cells. This can partly explain how these cells secrete more insulin. However, there is a 20% reduction in insulin *Ins1* gene expression, which does not explain the increase in insulin content. Our only explanation is that the MIN6 cells attempt to oppose the off target effects of didanosine by possibly downregulating insulin gene expression in a negative feedback mechanism.

Unlike humans who possess only one copy of the insulin gene, rodents have 2 non-allelic copies of the insulin gene: insulin 1 (Ins1) and insulin 2 (Ins2)

(Steiner, et al., 1985). Ins2 has most sequence homology to the human insulin gene, whereas Ins1 is thought to have arisen through a retrotransposition event (Steiner, et al., 1985). Both *Ins1* and *Ins2* genes are expressed in MIN6 cells (Roderigo-Milne, et al., 2002). It is known that intracellular changes in glucose concentrations act to regulate insulin gene expression via the regulatory β-cell specific transcription factors PDX1 (pancreatic and duodenal homeobox-1), NeuroD1 (neurogenic differentiation 1) and MafA (V-maf musculoaponeurotic fibrosarcoma oncogene homologue A) (Andrali, et al., 2008). But there is also evidence to suggest autocrine regulation of insulin gene expression in human pancreatic β-cells, as they are reported to express components of the insulin signalling pathway such as insulin receptor substrate-1 and -2 (IRS-1 and -2), phosphoinositide 3-kinase (PI3K) and phosphoinositide-dependent protein kinase-1 (PDK1) (Muller, et al., 2006). We found that *Ins1* gene expression was reduced in didanosine treated cells and so it is possible to hypothesise that MIN6 cells downregulate their *Ins1* gene expression via autocrine signalling, in an attempt to reduced insulin protein content.

In total contrast, when mtDNA levels were depleted following TFAM transcriptional silencing, we found that insulin secretion was decreased in mtDNA depleted cells compared to control cells, which was more pronounced after 25 mM glucose stimulation. Similar results have been reported in MIN6 cells (Soejima, et al., 1996; Tsuruzoe, et al., 1998), and clonal rat INS-1 pancreatic β-cells (Kennedy, et al., 1998), following chemical inhibition of mtDNA replication; however, these studies generated p^0 cells in which mtDNA was drastically reduced by >90%. It comes as no surprise that the p^0 cells failed to respond to increased glucose stimulation, with insulin secretion at 25 mM glucose comparable to that at low basal glucose (Kennedy, et al., 1998; Soejima, et al., 1996; Tsuruzoe, et al., 1998). The finding that mtDNA depletion hinders glucose-stimulated insulin secretion has also been replicated in transgenic mouse (Silva, et al., 2000) and rat (Gauthier, et al., 2009) animal models.

However, the severe mtDNA depletion reproduced in animal models (Silva, et al., 2000) and rodent cell lines (Hayakawa, et al., 1998; Kennedy, et al., 1998; Soejima, et al., 1996; Tsuruzoe, et al., 1998) does not accurately reflect mtDNA depletion in a clinical setting. In human pancreatic islets, it was noted that there

was a 50% decrease in the mean mtDNA copy number in non-diabetic islet donors aged between 17 and 75 years (Cree, et al., 2008). Concurrently, Ihm *et al.* correlated the decline in glucose-stimulated insulin secretion and decreased ATP content to islet donor age (Ihm, et al., 2006). Gauthier *et al.* observed partial mtDNA depletion to similar levels produced by ourselves following transcriptional silencing of the β-cell regulatory transcription factor PDX1 (Gauthier, et al., 2009). By silencing *Pdx1* gene expression by >90%, the group found this depleted mtDNA levels by 40% via TFAM suppression, which resulted in impaired insulin secretion at high glucose stimulation only (Gauthier, et al., 2009). Pancreatic β-cell insulin content was not reported. The group were then able to show that the mtDNA depletion and impaired insulin secretion following *Pdx-1* silencing hinged on TFAM suppression by adenoviral transduction of rat islets to increase *TFAM* expression. Both mtDNA copy number and insulin secretion were restored to levels comparable to control cells (Gauthier, et al., 2009). However, PDX1 is a critical regulator of β-cell function and mass, and it is clear that altered PDX1 expression affects multiple gene pathways in addition to *TFAM* expression (Babu, et al., 2007). In this sense, the model is not a specific model of mtDNA depletion unlike the targeted *TFAM* knockdown developed in this project.

We were able to restore impaired insulin secretion in *TFAM* silenced mtDNA depleted cells to levels comparable with control cells following treatment with the insulin secretagogue glibenclamide. Glibenclamide is an oral hypoglycaemic agent used as an effective treatment in T2DM by targeting the sulphonylurea receptor 1 (SUR1) subunit of the ATP-gated K^+ channel situated in the β-cell plasma membrane. Upon targeting the SUR1 protein, glibenclamide promotes K^+ channel closure and plasma membrane depolarisation (Proks, et al., 2002). Glucose-stimulated insulin secretion was also partially restored in mtDNA depleted mouse clonal β-cells following treatment with glibenclamide (Hayakawa, et al., 1998; Tsuruzoe, et al., 1998) or in rat clonal INS-1 cells using the depolarising agent KCl (Kennedy, et al., 1998). Whereas Soejima *et al.* restored the defective insulin secretion seen with mtDNA depletion by repopulating cybrid MIN6 clones with foreign mtDNA (Soejima, et al., 1996). These studies, along with our own results, signify that the impairment in insulin secretion following mtDNA depletion is prior to K^+

channel closure, with the work by Soejima *et al.* pinpointing the defect to be mtDNA in origin (Soejima, et al., 1996).

This is strengthened by our finding that there was no difference in *Ins1* insulin gene expression in TFAM silenced mtDNA depleted cells compared to control cells, allowing us to conclude that the deficit in insulin secretion is not due to reduced insulin gene transcription. A similar finding was reported by Soejima *et al.* and Hayakawa *et al.* who found that *Ins1* gene expression did not change in severely mtDNA depleted mouse clonal β-cells compared to control cells (Hayakawa, et al., 1998; Soejima, et al., 1996), even after low and high glucose stimulation (Soejima, et al., 1996). We did find however that there was decreased insulin content in TFAM silenced mtDNA depleted cells compared to control cells. Conversely, other groups have reported no significant change (Silva, et al., 2000) or an increase (Hayakawa, et al., 1998; Silva, et al., 2000; Tsuruzoe, et al., 1998) in insulin content in rodent pancreatic β-cells or islets. This disparity may be explained by the slightly imprecise methods of detecting insulin content, where one cannot be entirely sure whether we are detecting mature insulin or immature proinsulin (see Limitations section 6.6).

6.5 Conclusions

In conclusion, we start to see a divergence in the two mtDNA depletion models we have optimised in terms of insulin secretion. We were surprised to find that didanosine-induced mtDNA depletion resulted in an increase in insulin secretion when cells were posed with high 25 mM glucose stimulation. Didanosine is currently used in NRTI drug therapy in HIV patients. It has been reported that HIV patients exhibit hyperinsulinaemia and increased insulin resistance, which may explain why a large number of HIV patients later develop T2DM. The off target effects didanosine displays on insulin secretion we have demonstrated in this chapter have not been reported in the literature. However, more research is certainly deemed necessary in order to determine why didanosine treatment causes pancreatic β-cells to secrete and produce more insulin.

In contrast, mtDNA depletion following TFAM transcriptional silencing caused significant impairment in insulin secretion following 25 mM glucose stimulation. Like many other studies, we managed to restore impaired insulin secretion in

TFAM silenced mtDNA depleted cells following treatment with the insulin secretagogue glibenclamide. We therefore conclude that the defect in insulin secretion in TFAM silenced mtDNA depleted cells must occur prior to K^+ channel closure. We also found that there was no change in *Ins1* gene expression following mtDNA depletion, suggesting that the defect in insulin secretion is not due to changes in insulin gene expression. This leads us to believe that the culprit of impaired insulin secretion is possibly respiratory chain dysfunction, as a result of the decreased COX1 mRNA and protein levels we reported in the previous chapter.

6.6 Limitations

Possible limitations in this chapter can be seen in the detection of insulin content of the MIN6 cells. We used a commercial ELISA kit designed for rat; yet there is high sequence homology (75%) to the mouse insulin protein, which is why it was chosen. However, there is also cross-reactivity to mouse proinsulin 1 and proinsulin 2 (33% and 51% respectively). The translation product from *Ins* gene mRNA is preproinsulin; which contains an N-terminal signal peptide that subsequently becomes cleaved during insulin granule maturation to form proinsulin (Steiner, et al., 1985). Because there is cross-reactivity between the mouse proinsulin proteins and insulin, we are unable to confirm what form of insulin we have detected. Therefore, it is difficult to conclude why we see decreased insulin content in TFAM transcriptionally silenced cells compared to control cells: is it due to translation of the insulin gene or insulin protein processing? There are also ELISA commercial kits available for detecting proinsulin with <1% cross-reactivity to insulin, so perhaps these could be utilised for future studies?

There is no doubt however that we have detected mature insulin after glucose-stimulated insulin secretion, because the supernatant was harvested and used to determine insulin secretion. But criticism could be made on the static incubation used. Other groups have used static incubation also (Hayakawa, et al., 1998; Kennedy, et al., 1998; Soejima, et al., 1996; Tsuruzoe, et al., 1998) whereas others have used perifusion (Silva, et al., 2000) whereby cells are bathed in a continuous supply of fresh medium. Perhaps this would have been

a more correct method as it would also more accurately reflect what occurs *in vivo*?

An overall limitation in this study is that measurements of mtDNA depletion, β-cell function and mitochondrial function were performed in separate cells. This was a limitation that we struggled to avoid as it was difficult to extract DNA, RNA and protein simultaneously. We attempted it with a commercial extraction kit, as well as with Trizol reagent, but we found that the quality of DNA was very poor, and the solutes require to resuspend the protein interfered with the Bradford dye during protein quantification.

Finally, we only detected *Ins1* gene expression, like many other studies (Hayakawa, et al., 1998; Soejima, et al., 1996). However, there have been reports of differential expression of the *Ins1* and *Ins2* genes in different tissues (Deltour, et al., 2004), including pancreatic β-cells (Roderigo-Milne, et al., 2002) so perhaps we should have measured *Ins2* gene expression also?

Chapter 7

General Discussion

7 General Discussion

7.1 General Discussion

The prevalence of T2DM has been found to increase with advancing age (Cowie, et al., 2006; Cowie, et al., 2009; Harris, et al., 1987). This is thought to be due to the age-related progressive decline in pancreatic β-cell function (Rudenski, et al., 1988), which results in an age-related decrease in insulin secretion (Chang and Halter, 2003) and an associated deterioration in glucose tolerance (Basu, et al., 2003). Insulin secretion relies heavily on the ATP generated by mitochondrial oxidative phosphorylation (Wollheim, 2000). This is supported in cellular models in which mtDNA has been severely depleted, resulting in impaired insulin secretion (Kennedy, et al., 1998; Silva, et al., 2000; Soejima, et al., 1996; Tsuruzoe, et al., 1998). It is also known that certain mtDNA abnormalities are diabetogenic, particularly the A3243G mutation, which has been associated with impaired insulin secretion (Lynn, et al., 2003; Maassen, et al., 2004). An age-related decline in mtDNA copy number has been reported in numerous human tissues (Cree, et al., 2008; Kaaman, et al., 2007; Laderman, et al., 1996; Short, et al., 2005). In pancreatic islets, Cree *et al.* showed that mtDNA copy number was significantly reduced in non-diabetic islet donors aged ≥50 years compared to donors aged ≤50 years; and that the mean mtDNA copy number decreased by 50% in individuals aged between 17 and 75 years (Cree, et al., 2008). Therefore, we were keen to investigate whether partial mtDNA depletion to levels of around 50% in pancreatic β-cells is merely a biomarker of ageing, or whether it directly affects β-cell function and insulin secretion.

We began by optimising two independent models of mtDNA depletion in the murine pancreatic β-cell line, MIN6. The first mtDNA depletion model relied on chemical inhibition of mtDNA replication using the adenosine nucleoside analogue didanosine. Didanosine is currently an effective means of treating HIV patients as it targets the HIV reverse transcriptase enzyme thus preventing HIV viral DNA replication. But it has also been found to have high affinity for the mitochondrial polymerase γ, POLG (Kakunda, 2000; Lewis, et al., 2003). Didanosine competes with endogenous adenosine for incorporation into the

growing mtDNA strand and as didanosine lacks the 3'-OH group required for the phosphodiester linkage, subsequent stalling of POLG and strand termination ensues (Lewis, et al., 2003; Mitsuya, et al., 1990). Lake-Bakaar *et al.* were able to show that 8 day treatment of human pancreatic endocrine cells, Capan-1 cells, with 20 μM ddI results in 70% reduction of mtDNA levels. Indeed, we similarly found that by treating MIN6 cells with 50 μM ddI for 5 days resulted in 50% mtDNA depletion (Lake-Bakaar, et al., 2001).

Our second model of mtDNA depletion silenced *TFAM* gene transcription using siRNA technology. TFAM is an important nuclear encoded mitochondrial DNA transcription factor found to play a key role in mtDNA transcription (Campbell, et al., 2012; Ohgaki, et al., 2007), as well as mtDNA copy number (Ekstrand, et al., 2004) and maintenance (Larsson, 2010). Indeed, tissue specific (Silva, et al., 2000; Sorensen, et al., 2001; Wang, et al., 1999) and global knockdown (Larsson, et al., 1998) of the *TFAM* gene in mouse animal models has proven an effective means of depleting mtDNA levels. It has also been shown that severe (>90%) loss of the β-cell specific regulatory transcription factor PDX1 was also found to significantly deplete mtDNA levels by around 30%, which was unexpectedly shown to occur through TFAM suppression (Gauthier, et al., 2009). Similarly, after transcriptionally silencing the *TFAM* gene >80%, we achieved a 40% reduction in mtDNA levels. Therefore, in summary, both mtDNA depletion models produced a comparable degree of mtDNA depletion to levels seen in aged human islets (Cree, et al., 2008).

Using the two models of mtDNA depletion, we moved on to investigate what effect partial mtDNA depletion was having on mitochondrial function. COX1, cytochrome c oxidase subunit 1, is one of the three mtDNA encoded subunits of cytochrome c oxidase (Complex IV), and is essential during the assembly of the cytochrome c oxidase complex (Fontanesi, et al., 2006; Larsson, 2010). By inducing partial mtDNA depletion in MIN6 cells, we managed to produce a 45% and 33% reduction in COX1 mRNA expression using the didanosine and TFAM mtDNA depletion models respectively. Upon analysis of COX1 protein, we were able to show that that decreased *COX1* gene expression translated to decreased COX1 protein. We observed that COX1 protein was reduced by 34% and 22% in the didanosine and TFAM mtDNA depletion models respectively. Our finding that mtDNA depletion results in decreased mtDNA

transcription and protein translation has also been shown in previous studies in rodent clonal β-cells (Hayakawa, et al., 1998; Soejima, et al., 1996; Tsuruzoe, et al., 1998) and rodent pancreatic islets (Gauthier, et al., 2009).

We also measured ATP content as a measure of mitochondrial function. However, we found that neither didanosine-induced nor TFAM silencing-induced mtDNA depletion had an effect on the ATP content in mtDNA depleted cells compared to control cells. We found this was the case whether the cells were stimulated with low 3 mM or high 25 mM glucose. Therefore, it seems the partial mtDNA depletion we have created in both models is enough to effect mtDNA gene transcription and translation, but it does not affect ATP content. Our results are in contrast to other groups who have reported a substantial decrease in ATP production following high 25 mM glucose stimulation in mtDNA depleted cells (Kennedy, et al., 1998; Tsuruzoe, et al., 1998). But unlike ourselves, these groups have produced severe mtDNA depletion of >90%. Therefore, the fact that other groups have reported a loss in ATP production following mtDNA depletion may be attributable to the degree of mtDNA depletion produced in these studies.

It is also worth mentioning that although the electron transport chain is the main generator of ATP, other cellular pathways such as glycolysis can be utilised for ATP production too. In fact, it is known that cancer cells experience mitochondrial respiratory chain dysfunction and increased glycolysis (Kaipparettu, et al., 2010). MIN6 cells are derived from a mouse insulinoma and so, could it be possible that MIN6 cells rely on glycolysis instead of the respiratory chain for their source of ATP? Could this be the reason why the partial mtDNA depletion we produced did not affect ATP production, because glycolysis is not affected by mtDNA depletion? But in the Kennedy *et al.* and Tsuruzoe *et al.* studies where they depleted mtDNA >90%, the energy generated by glycolysis was not enough to sustain glucose-stimulated insulin secretion alone, which is why they saw a decrease in ATP production? Our result could also be limited by the nature of the technique we used, was it specific enough to detect small changes in ATP content?

We also investigated the effect of mtDNA depletion on mitochondrial membrane potential using the JC-1 cationic fluorescent dye. However, like the ATP

content data, we did not see an effect of didanosine-induced mtDNA depletion on mitochondrial membrane potential. As with the ATP content data, we found disparity between our results and the literature. Using another mitochondrial fluorescent probe, rhodamine 123, it has been shown that there is reduced hyperpolarisation in pancreatic β-cells with mtDNA depletion (Kennedy, et al., 1998; Silva, et al., 2000). However, these reports examined cells with severe mtDNA depletion (>90%) and not partial mtDNA depletion as we have done, which may explain this discrepancy.

So in summary, it appears that the partial mtDNA we created using both mtDNA depletion models caused a decrease in COX1 mRNA and subsequent reduction in COX1 protein levels. However, we failed to see an effect of partial mtDNA depletion on ATP content or mitochondrial membrane potential. Our next question was: does the partial mtDNA depletion generated in both models impair glucose-stimulated insulin secretion? It is at this point that we begin to notice a divergence in the two mtDNA depletion models. We were surprised to find that didanosine treated cells secreted more insulin in response to high 25 mM glucose stimulation compared to control cells. We hypothesise that this is possibly due to didanosine treatment exhibiting off target effects on insulin secretion.

Didanosine drug therapy in HIV patients has been closely related to the onset of acute pancreatitis (Butler, et al., 1993; Martin, et al., 1994). It is also interesting to note that a proportion of HIV patients receiving NRTI therapy later go on to develop T2DM (Brown and Glesby, 2012; Brown, et al., 2005; Hadigan, et al., 2001; Lo, et al., 2005; Tien, et al., 2008). This may be explained by prolonged NRTI use being associated with insulin resistance (Blanco, et al., 2011; Tien, et al., 2008) and hyperinsulinaemia (Hadigan, et al., 2001; Mallon, et al., 2005). What is currently lacking in the literature are possible mechanisms as to why these patients are insulin resistant and hyperinsulinaemic. The fact that we have reported increased insulin secretion and increased insulin content in didanosine-induced mtDNA depleted cells may go some way to possibly explaining this, but more research is certainly needed to uncover reasons why.

When mtDNA was depleted following TFAM transcriptional silencing however, we found that insulin secretion was significantly impaired in mtDNA depleted

cells compared to control cells following high 25 mM glucose stimulation. It has also been shown that glucose-stimulated insulin secretion is impaired following mtDNA depletion in rodent clonal β-cells (Kennedy, et al., 1998; Soejima, et al., 1996; Tsuruzoe, et al., 1998) and rodent animal models (Gauthier, et al., 2009; Silva, et al., 2000). Similar to our results obtained using the TFAM mtDNA depletion model, it was found that insulin secretion was significantly deceased following high glucose stimulation in mtDNA depleted cells (Gauthier, et al., 2009; Kennedy, et al., 1998; Silva, et al., 2000; Soejima, et al., 1996; Tsuruzoe, et al., 1998).

However, we also found that insulin secretion was also significantly impaired following basal 3 mM glucose stimulation. Therefore, when you compare the fold increase in insulin secretion after high glucose stimulation, it is similar in both TFAM-429 cells and Scrambled control cells. But there seems to be slight discrepancy in that we did not detect this same decrease in insulin secretion at basal glucose in the TFAM-429 silenced cells following glibenclamide treatment. This may be because of the fewer number of repeats in these experiments, or indeed because the experimental conditions were slightly different in that data were normalised to DMSO vehicle control cells. In light of this, our key finding is that absolute insulin secretion is decreased following TFAM-induced mtDNA depletion in both the glibenclamide and non-glibenclamide studies, and this is the main and consistent finding of the work.

So what might be causing the reduced insulin secretion seen in TFAM silenced mtDNA depleted cells? We observed a decrease in COX1 mRNA and protein in these cells and so, an obvious candidate would be reduced ATP from the respiratory chain in mtDNA depleted cells. However, we also reported no change in ATP content in TFAM mtDNA depleted cells, so something else must be causing the impaired insulin secretion. We found no change in the *Ins1* insulin gene expression in TFAM silenced mtDNA depleted cells, so the defect is not due to a reduction in insulin gene transcription. There was however, decreased insulin content in TFAM silenced mtDNA depleted cells, but we are unable to confirm whether this decrease in insulin content is a result of reduced protein translation from the *Ins1* gene, or a default in the insulin processing pathway during granule maturation. Silva *et al.* produced tissue specific TFAM knockdown in mice and found that along with severe mtDNA depletion in

pancreatic β-cells, the phenotype of the TFAM knockout mice changed with time. Interestingly, the group found that there was an age-dependent decrease in β-cell mass (Silva, et al., 2000). Therefore, could the decrease in glucose-stimulated insulin secretion we have observed in TFAM silenced mtDNA depleted cells be due to other mechanisms such as apoptosis? We did not measure cell number in the TFAM mtDNA depletion model, but found no difference in DNA, RNA or protein levels in TFAM-429 transfected cells compared to Scrambled control cells. One thing we can conclude however, is that the deficit in insulin secretion must be prior to the closure of K^+ channels because we managed to rescue insulin secretion in TFAM mtDNA depleted cells following treatment with the insulin secretagogue glibenclamide.

Glibenclamide is an effective oral hypoglycaemic agent used in the treatment of T2DM (Groop, 1992). By targeting the sulphonylurea receptor SUR1 protein of the K^+ channel situated on the β-cell plasma membrane, glibenclamide causes K^+ channel closure and subsequent membrane depolarisation (Proks, et al., 2002). Glibenclamide has been predicted to circulate in blood plasma at concentrations below 0.4 μM and so, the concentrations we used are within the pharmacological range (Anello, et al., 1999; Jaber, et al., 1994). Our finding that the impaired glucose-stimulated insulin secretion seen with partial mtDNA depletion is restored following glibenclamide treatment is supported by other studies that have also used glibenclamide (Hayakawa, et al., 1998; Tsuruzoe, et al., 1998) or other membrane depolarising agents such as KCl (Kennedy, et al., 1998). Taken together, these studies, along with our own results using the TFAM mtDNA depletion model, signify that the reduced insulin secretion seen following mtDNA depletion occurs prior to K^+ channel closure and is perhaps mtDNA in origin.

7.2 Conclusions

Our original aim was to investigate the effects of partial mtDNA depletion on pancreatic β-cell function and mitochondrial function. We found that mtDNA depletion in MIN6 cells to levels seen in human islets with ageing has a direct effect on insulin secretion when depleting mtDNA via *TFAM* gene silencing. This effect on insulin secretion may be due to a defective electron transport chain following a decrease in the mtDNA encoded components. There was no

change in ATP levels or mitochondrial membrane potential. We found impaired insulin secretion was rescued following treatment with the insulin secretagogue glibenclamide, suggesting that the deficit in insulin secretion occurs prior to K^+ channel closure. However, we also reported that didanosine-induced mtDNA depletion resulted in an increase in insulin secretion, which we postulate to be due to possible off target effects of the drug. Strategies to slow or even prevent islet mtDNA depletion in man could help to preserve insulin secretion and delay the development of Type 2 diabetes.

7.3 Future Work

We have managed to produce two independent models of mtDNA depletion that partially deplete mtDNA by 40-50%. However, both of these models produce acute and transient mtDNA depletion therefore, future studies into the effect of chronic partial mtDNA depletion might more accurately reflect mtDNA depletion in a clinical setting. It has been shown that chronic mtDNA depletion in mouse models resulted in reduced pancreatic β-cell mass (Silva, et al., 2000).

Also, investigations into TFAM protein levels following TFAM gene silencing would indicate whether or not we have managed to affect the TFAM protein. This is something that was attempted during this project however; the commercial antibodies used were non-specific, producing multiple protein bands. We evaluated certain aspects of mitochondrial function following mtDNA depletion during this project, but other key measures that could be investigated include calcium signalling and β-cell apoptosis.

Finally, exploration of therapeutics to increase mtDNA copy number would be beneficial. Certain studies have shown an increase in mtDNA copy number following increased *TFAM* gene expression (Ekstrand, et al., 2004; Gauthier, et al., 2009). Investigation into therapeutics that could stimulate mitochondrial biogenesis via TFAM would help alleviate the decrease in mtDNA copy number seen with advancing age.

Appendix

Appendix

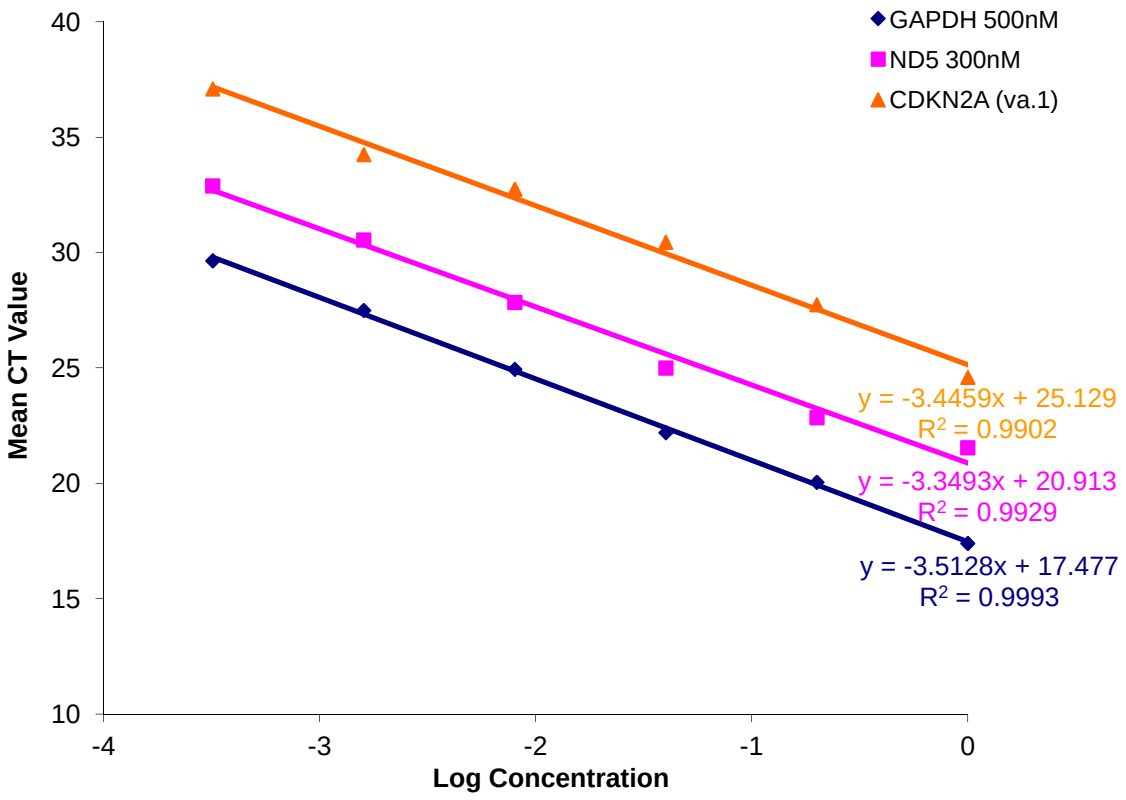

Figure 1 Standard curves for ND5 (300nM), GAPDH (500 nM) and CDKN2A va.1 (QuantiTect Assay Mm_Cdkn2a_va.1_SG)

Complementary DNA was serially diluted 1:5 and amplified by real-time PCR using SYBR-Green and primers specific for GAPDH (500 nM), ND5 (300 nM) or CDKN2A (QuantiTect Assay Mm_Cdkn2a_va.1_SG). The CDKN2A QuantiTect assay (Qiagen, Crawley, UK; Cat No QT01164891) was already optimised and 2 µl was added per 20 µl reaction. Reaction efficiencies were 92.61% (GAPDH), 98.87% (ND5) and 95.07% (CDKN2A).

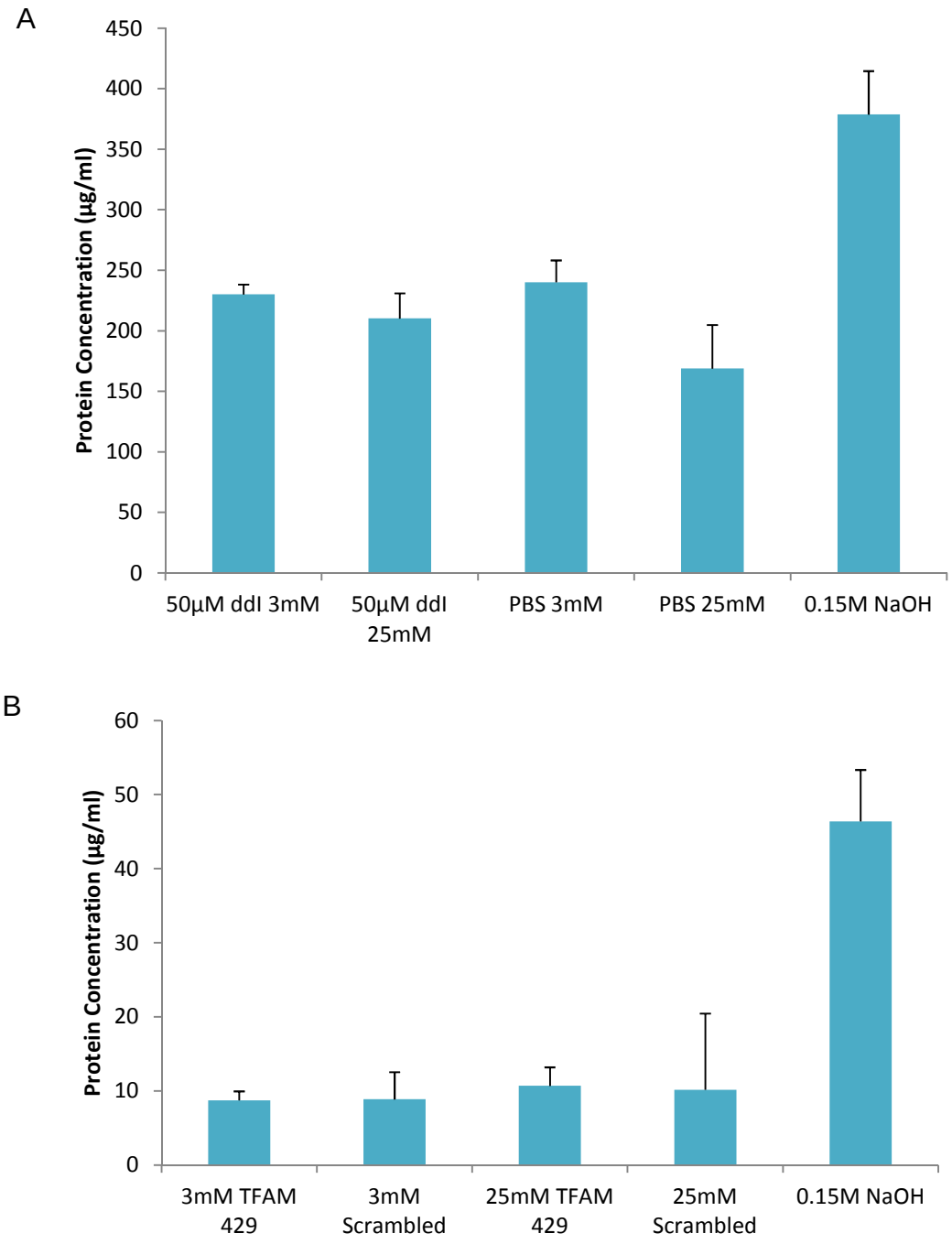

Figure 2 Correction for protein loss following perchloric acid ATP extraction

During analysis of ATP content (Section 5.4.3), cells were harvested in perchloric acid to prevent degradation of ATP. Cell lysates were then centrifuged, the supernatant removed for ATP analysis and the cell debris pellet resuspended in 0.15 M NaOH. Protein quantification was obtained using a Lowry assay. It was evident that harvesting cells in perchloric acid resulted in loss of whole cell protein content and so, this loss of protein was corrected for using control wells in which cells were harvested in NaOH only. We found an approximate 50% loss of protein when processing didanosine model samples (A), but this loss of protein was slightly greater in TFAM model samples (B), possibly because of fewer cells in these wells.

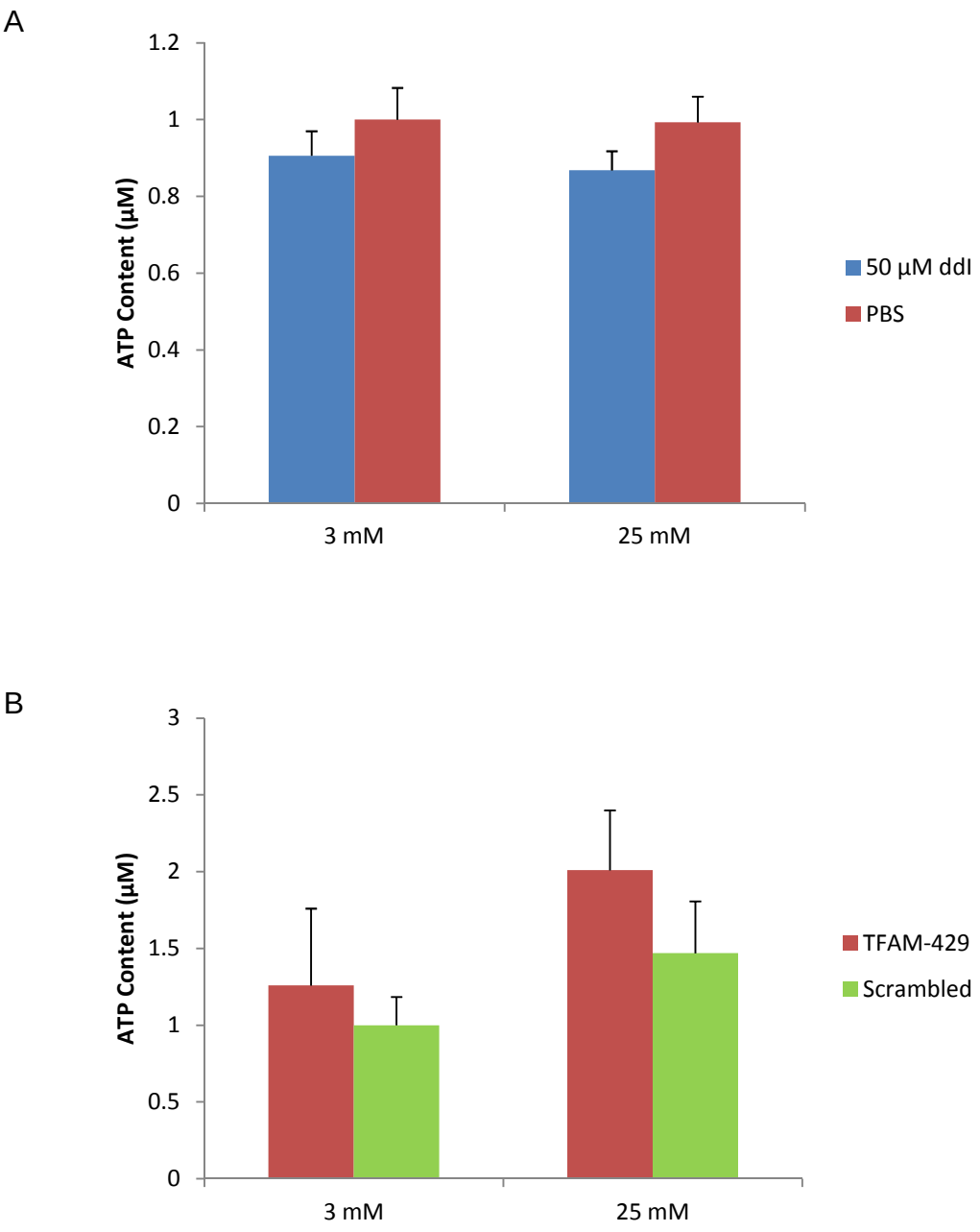

Figure 3 ATP content of MIN6 cells following partial mtDNA depletion: raw data

This is the data from Section 5.4.3 prior to protein normalisation. MIN6 cells were partially depleted of mtDNA following didanosine treatment (A) or TFAM transcriptional silencing (B) and ATP content measured as previously describe in Section 5.4.3.

References

References

Alam, T. I., Kanki, T., Muta, T., Ukaji, K., Abe, Y., Nakayama, H.*, et al.* (2003) Human mitochondrial DNA is packaged with TFAM. *Nucl. Acids Res.,* **31**, 1640-1645.

Altshuler, D., Hirschhorn, J. N., Klannemark, M., Lindgren, C. M., Vohl, M. C., Nemesh, J.*, et al.* (2000) The common PPARgamma Pro12Ala polymorphism is associated with decreased risk of type 2 diabetes. *Nat. Gen.,* **26**, 76-80.

Andrali, S. S., Sampley, M. L., Vanderford, N. L. & Ozcan, S. (2008) Glucose regulation of insulin gene expression in pancreatic beta-cells. *Biochem. J.,* **415**, 1-10.

Anello, M., Gilon, P. & Henquin, J. C. (1999) Alterations of insulin secretion from mouse islets treated with sulphonylureas: perturbations of Ca2+ regulation prevail over changes in insulin content. *Br. J. Pharmacol.,* **127**, 1883-1891.

Annis, A. M., Caulder, M., Cook, M. L. & Duquette, D. (2005) Family History, Diabetes, and Other Demographic and Risk Factors Among Participants of the National Health and Nutrition Examination Survey 1999–2002. In. Centers for Disease Control and Prevention (CDC), Online version available http://www.cdc.gov/pcd/issues/2005/apr/04_0131.htm.

Aschenbrenner, B.*, et al.* (1970) Haem a, cytochrome c and total protein turnover in mitochondria from rat heart and liver, *Biochem. J.*, **119**, 157-160.

Ashcroft, F. M., Proks, P., Smith, P. A., Ämmälä, C., Bokvist, K. & Rorsman, P. (1994) Stimulus–secretion coupling in pancreatic β cells. *J. Biol. Chem.,* **55**, 54-65.

Atkinson, M. A. & Maclaren, N. K. (1994) The pathogenesis of insulin-dependant Diabetes Mellitus. *New Eng. J. Med.,* **331**, 1428-1436.

Attardi, G. & Schatz, G. (1988) Biogenesis of mitochondria. *Annu. Rev. Cell. Biol.,* **4**, 289-333.

Babu, D. A., Deering, T. G. & Mirmira, R. G. (2007) A feat of metabolic proportions: Pdx1 orchestrates islet development and function in the maintenance of glucose homeostasis. *Mol. Gen. Metab.,* **92**, 43-55.

Bai, Y., Shakeley, R. M. & Attardi, G. (2000) Tight Control of Respiration by NADH Dehydrogenase ND5 Subunit Gene Expression in Mouse Mitochondria. *Molec. Cell. Biol.,* **20**, 805-815.

Balaban, R. S., Nemoto, S. & Finkel, T. (2005) Mitochondria, Oxidants, and Aging. *Cell,* **120**, 483-495.

Barcellona, M. L., Cardiel, G. & Gratton, E. (1990) Time-resolved fluorescence of DAPI in solution and bound to polydeoxynucleotides. *Biochemical and Biophysical Research Communications,* **170**, 270-280.

Barazzoni, R., Short, K. R. & Nair, K. S. (2000) Effects of aging on mitochondrial DNA copy number and cytochrome c oxidase gene expression in rat skeletal muscle, liver, and heart. *J. Biol. Chem.,* **275**, 3343-3347.

Barrientos, A., Casademont, J., Cardellach, F., Estivill, X., Urbano-Marquez, A. & Nunes, V. (1997) Reduced steady-state levels of mitochondrial RNA and increased mitochondrial DNA amount in human brain with aging. *Mol. Brain Res.,* **52**, 284-289.

Basu, R., Breda, E., Oberg, A. L., Powell, C. C., Dalla Man, C., Basu, A.*, et al.* (2003) Mechanisms of the Age-Associated Deterioration in Glucose Tolerance. Contribution of Alterations in Insulin Secretion, Action, and Clearance. *Diabetes,* **52**, 1738-1748.

Benda, C. (1898) *Arch. Anat. Physiol*, 393-398.

Bender, A., Krishnan, K. J., Morris, C. M., Taylor, G. A., Reeve, A. K., Perry, R. H.*, et al.* (2006) High levels of mitochondrial DNA deletions in substantia nigra neurons in aging and Parkinson disease. *Nat. Gen.,* **38**, 515-517.

Berthelier, C., Kergoat, M. & Portha, B. (1997) Lack of deterioration of insulin action with aging in the GK rat: a contrasted adaptation as compared with nondiabetic rats. *Metabolism,* **46**, 890-896.

Blanco, F., Barreiro, P., Ryan, P., Vispo, E., Martin-Carbonero, L., Tuma, P.*, et al.* (2011) Risk factors for advanced liver fibrosis in HIV-infected individuals: role of antiretroviral drugs and insulin resistance. *J. Viral Hepat.,* **18**, 11-16.

Bogenhagen, D. F. & Clayton, D. A. (1977) Mouse L cell mitochondrial DNA molecules are selected randomly for replication throughout the cell cycle. *Cell,* **11**, 719-727.

Bonnefond, A., Froguel, P. & Vaxillaire, M. (2010) The emerging genetics of type 2 diabetes. *Trends Mol. Med.,* **16**, 407-416.

Bowmaker, M., Yang, M. J., Yasukawa, T., Reyes, A., Jacobs, H. T., Huberman, J. A.*, et al.* (2003) Mammalian mitochondrial DNA replicates bidirectionally from an initiation zone. *J. Biol. Chem.,* **278**, 50961–50969.

Bradford, M. M. (1976) A Rapid and Sensitive Method for the Quantitation of Microgram Quantities of Protein Utilizing the Principle of Protein-Dye Binding. *Anal. Biochem.,* **72**, 248-254.

Brown, T. T. & Glesby, M. J. (2012) Management of the metabolic effects of HIV and HIV drugs. *Nat. Rev. Endocrinol.,* **8**, 11-21.

Brown, T. T., Li, X., Cole, S. R., Kingsley, L. A., Palella, F. J., Riddler, S. A.*, et al.* (2005) Cumulative exposure to nucleoside analogue reverse transcriptase inhibitors is associated with insulin resistance markers in the Multicenter AIDS Cohort Study. *AIDS,* **19**, 1375-1383.

Butler, K. M., Venzon, D., Henry, N., Husson, R. N., Mueller, B. U., Balis, F. M.*, et al.* (1993) Pancreatitis in human immunodeficiency virus-infected children receiving dideoxyinosine. *Pediatrics,* **91**, 747-751.

Campbell, C. T., Kolesar, J. E. & Kaufman, B. A. (2012) Mitochondrial transcription factor A regulates mitochondrial transcription initiation, DNA packaging, and genome copy number. *Biochim. Biophys. Acta,* **1819**, 921-929.

Carrodeguas, J. A., Theis, K., Bogenhagen, D. F. & Kisker, C. (2001) Crystal Structure and Deletion Analysis Show that the Accessory Subunit of Mammalian DNA Polymerase γ, PolγB, Functions as a Homodimer. *Mol. Cell,* **7**, 43-54.

Cauchi, S., El Achhab, Y., Choquet, H., Dina, C., Krempler, F., Weitgasser, R.*, et al.* (2007) TCF7L2 is reproducibly associated with type 2 diabetes in various ethnic groups: a global meta-analysis. *J. Mol. Med. (Berl.),* **85**, 777-782.

Centre for Disease Control and Prevention. (2011) 2011 National Diabetes Fact Sheet. In, Available online at http://www.cdc.gov/diabetes/pubs/estimates11.htm.

Chandel, N. & Schumacker, P. T. (1999) Cells depleted of mitochondrial DNA (p^0) yield insight into physiological mechanisms. *FEBS Letters,* **454**, 173-176.

Chang, A. M. & Halter, J. B. (2003) Aging and insulin secretion. *Am. J. Physiol. Endocrinol. Metab.,* **284**, E7-E12.

Christianson, T. W. & Clayton, D. A. (1986) In vitro transcription of human mitochondrial DNA: accurate termination requires a region of DNA sequence that can function bidirectionally. *PNAS,* **83**, 6277-6281.

Clay Montier, L. L., Deng, J. J. & Bai, Y. (2009) Number matters: control of mammalian mitochondrial DNA copy number. *J. Gen. Genomics,* **36**, 125-131.

Clayton, D. A. (1982) Replication of animal mitochondrial DNA. *Cell,* **28**, 693-705.

Clayton, D. A., Doda, J. N. & Friedberg, E. C. (1974) The absence of a pyrimidine dimer repair mechanism in mammalian mitochondria. *PNAS,* **71**, 2777-2781.

Cotney, J., Wang, Z. & Shadel, G. S. (2007) Relative abundance of the human mitochondrial transcription system and distinct roles for h-mtTFB1 and h-mtTFB2 in mitochondrial biogenesis and gene expression. *Nucleic Acids Res.,* **35**, 4042-4054.

Cottrell, D. A., Blakely, E. L., Johnson, M. A., Ince, P. G., Borthwick, G. M. & Turnbull, D. M. (2001) Cytochrome c oxidase deficient cells accumulate in the hippocampus and choroid plexus with age. *Neurobiol Aging,* **22**, 265-272.

Cottrell, D. A., Blakely, E. L., Johnson, M. A., Ince, P. G. & Turnbull, D. M. (2001) Mitochondrial enzyme-deficient hippocampal neurons and choroidal cells in AD. *Neurology,* **57**, 260-264.

Cowie, C. C., Rust, K. F., Byrd-Holt, D. D., Eberhardt, M. S., Flegal, K. M., Engelgau, M. M.*, et al.* (2006) Prevalence of diabetes and impaired fasting glucose in adults in the U.S. population: National Health And Nutrition Examination Survey 1999-2002. *Diabetes Care,* **29**, 1263-1268.

Cowie, C. C., Rust, K. F., Ford, E. S., Eberhardt, M. S., Byrd-Holt, D. D., Li, C.*, et al.* (2009) Full accounting of diabetes and pre-diabetes in the U.S. population in 1988-1994 and 2005-2006. *Diabetes Care,* **32**, 287-294.

Cree, L. M., Patel, S. K., Pyle, A., Lynn, S., Turnbull, D. M., Chinnery, P. F.*, et al.* (2008) Age-related decline in mitochondrial DNA copy number in isolated human pancreatic islets. *Diabetologia,* **51**, 1440–1443.

Dairaghi, D. J., Shadel, G. S. & Clayton, D. A. (1995) Addition of a 29 residue carboxyl-terminal tail converts a simple HMG box-containing protein into a transcriptional activator. *J. Mol. Biol.,* **249**, 11-28.

de la Asuncion, J. G., del Olmo, M. L., Sastre, J., Pallardo, F. V. & Vina, J. (1999) Zidovudine (AZT) causes an oxidation of mitochondrial DNA in mouse liver. *Hepatology,* **29**, 985-987.

Dell'agnello, C.*, et al.* (2007) Increased longevity and refractoriness to Ca(2+)-dependent neurodegeneration in Surf1 knockout mice, *Hum. Mol. Genet.*, **16**, 431-444.

Deltour, L., Vandamme, J., Jouvenot, Y., Duvillie, B., Kelemen, K., Schaerly, P.*, et al.* (2004) Differential expression and imprinting status of Ins1 and Ins2 genes in extraembryonic tissues of laboratory mice. *Gene Expr. Patterns,* **5**, 297-300.

Diabetes UK. (2006) Hyperglycaemia, Hypogylcaemia. In, Online version available http://www.diabetes.org.uk/Guide-to-diabetes/Living_with_diabetes/Caring-for-children-with-diabetes/Children-with-diabetes-at-school/Hyperglycaemia/ and

http://www.diabetes.org.uk/Guide-to-diabetes/Living_with_diabetes/Caring-for-children-with-diabetes/Children-with-diabetes-at-school/Hypoglycaemia-hypo/.

Diabetes UK. (2009) Causes and risk factors. In, Online version available http://www.diabetes.org.uk/Guide-to-diabetes/Introduction-to-diabetes/Causes_and_Risk_Factors/.

Ekstrand, M. I., Falkenberg, M., Rantanen, A., Park, C. B., Gaspari, M., Hultenby, K.*, et al.* (2004) Mitochondrial transcription factor A regulates mtDNA copy number in mammals. *Hum. Molec. Gen.,* **13**, 935–944.

Evans, M. J. & Scarpulla, R. C. (1989) Interaction of nuclear factors with multiple sites in the somatic cytochrome c promoter. Characterization of upstream NRF-1, ATF, and intron Sp1 recognition sequences. *J. Biol. Chem.,* **264**, 14361-14369.

Falkenberg, M., Gaspari, M., Rantanen, A., Trifunovic, A., Larsson, N. G. & Gustafsson, C. M. (2002) Mitochondrial transcription factors B1 and B2 activate transcription of human mtDNA. *Nat. Gen.,* **31**, 289-294.

Fayet, G., Jansson, M., Sternberg, D., Moslemi, A. R., Blondy, P., Lombes, A.*, et al.* (2002) Ageing muscle: clonal expansions of mitochondrial DNA point mutations and deletions cause focal impairment of mitochondrial function. *Neuromuscul. Disord.,* **12**, 484-493.

FDA. (2009) HIV/AIDS Historical Time Line 1981-1990. In, http://www.fda.gov/ForConsumers/ByAudience/ForPatientAdvocates/HIVandAIDSActivities/ucm151074.htm.

Florez, J. C., Jablonski, K. A., Sun, M. W., Bayley, N., Kahn, S. E., Shamoon, H.*, et al.* (2007) Effects of the type 2 diabetes-associated PPARG P12A polymorphism on progression to diabetes and response to troglitazone. *J. Clin. Endocrinol. Metab.,* **92**, 1502-1509.

Fontanesi, F.*, et al.* (2006) Assembly of mitochondrial cytochrome c-oxidase, a complicated and highly regulated cellular process, *Am. J. Physiol. Cell Physiol.*, **291**, C1129-C1147.

Frayling, T. M., Timpson, N. J., Weedon, M. N., Zeggini, E., Freathy, R. M., Lindgren, C. M.*, et al.* (2007) A common variant in the FTO gene is associated with body mass index and predisposes to childhood and adult obesity. *Science,* **316**, 889-894.

Gao, W., Bihorel, S., DuBois, D. C., Almon, R. R. & Jusko, W. J. (2011) Mechanism-based disease progression modeling of type 2 diabetes in Goto-Kakizaki rats. *J. Pharmacokinet. Pharmacodyn.,* **38**, 143-162.

Gauthier, B. R., Wiederkehr, A., Baquie, M., Dai, C., Powers, A. C., Kerr-Conte, J.*, et al.* (2009) PDX1 deficiency causes mitochondrial dysfunction and defective insulin secretion through TFAM suppression. *Cell Metab.,* **10**, 110-118.

Ghivizzani, S. C., Madsen, C. S., Nelen, M. R., Ammini, C. V. & Hauswirth, W. W. (1994) In organello footprint analysis of human mitochondrial DNA: human mitochondrial transcription factor A interactions at the origin of replication. *Mol. Cell. Biol.,* **14**, 7717-7730.

Gleyzer, N., Vercauteren, K. & Scarpulla, R. C. (2005) Control of Mitochondrial Transcription Specificity Factors (TFB1M and TFB2M) by Nuclear Respiratory Factors (NRF-1 and NRF-2) and PGC-1 Family Coactivators. *Molec. Cell. Biol.,* **25**, 1354-1366.

Goodman, M. N., Dluz, S. M., McElaney, M. A., Belur, E. & Ruderman, N. B. (1983) Glucose uptake and insulin sensitivity in rat muscle: changes during 3-96 weeks of age. *Am. J. Physiol.,* **244**, E93-E100.

Goto, Y., Kakizaki, M. & Masaki, N. (1976) Production of spontaneous diabetic rats by repetition of selective breeding. *Tohoku. J. Exp. Med.,* **119**, 85-90.

Goto, Y., Nonaka, I. & Horai, S. (1990) A mutation in the tRNA(Leu)(UUR) gene associated with the MELAS subgroup of mitochondrial encephalomyopathies. *Nature,* **348**, 651-653.

Grant, S. F., Thorleifsson, G., Reynisdottir, I., Benediktsson, R., Manolescu, A., Sainz, J.*, et al.* (2006) Variant of transcription factor 7-like 2 (TCF7L2) gene confers risk of type 2 diabetes. *Nat. Gen.,* **38**, 320-323.

Gray, M. W. (1988) Organelle origins and ribosomal RNA. *Biochem. Cell Biol.,* **66**, 325-348.

Gray, M. W. (1989) Origin and evolution of mitochondrial DNA. *Annu. Rev. Cell Biol.,* **5**, 25-50.

Groop, L. C. (1992) Sulfonylureas in NIDDM. *Diabetes Care,* **15**, 737-754.

Gupte, S., Labinskyy, N., Gupte, R., Csiszar, A., Ungvari, Z. & Edwards, J. G. (2010) Role of NAD(P)H oxidase in superoxide generation and endothelial dysfunction in Goto-Kakizaki (GK) rats as a model of nonobese NIDDM. *PLoS One,* **5**, e11800.

Gussow, D*., et al.* (1987) The human beta 2-microglobulin gene. Primary structure and definition of the transcriptional unit, *J. Immunol.*, **139**, 3132-3138.

Hadigan, C., Meigs, J. B., Corcoran, C., Rietschel, P., Piecuch, S., Basgoz, N*., et al.* (2001) Metabolic abnormalities and cardiovascular disease risk factors in adults with human immunodeficiency virus infection and lipodystrophy. *Clin. Infect. Dis.,* **32**, 130-139.

Handschin, C. & Spiegelman, B. M. (2006) Peroxisome Proliferator-Activated Receptor γ Coactivator 1 Coactivators, Energy Homeostasis, and Metabolism. *Endocr. Rev.,* **27**, 728-735.

Hani, E. H., Boutin, P., Durand, E., Inoue, H., Permutt, M. A., Velho, G*., et al.* (1998) Missense mutations in the pancreatic islet beta cell inwardly rectifying K+ channel gene (KIR6.2/BIR): a meta-analysis suggests a role in the polygenic basis of Type II diabetes mellitus in Caucasians. *Diabetologia,* **41**, 1511-1515.

Harman, D. (1956) Aging: a theory based on free radical and radiation chemistry. *J. Gerontol.,* **11**.

Harris, M. I., Hadden, W. C., Knowler, W. C. & Bennett, P. H. (1987) Prevalence of diabetes and impaired glucose tolerance and plasma glucose levels in U.S. population aged 20-74 yr. *Diabetes,* **36**, 523-534.

Hartmann, N., Reichwald, K., Wittig, I., Drose, S., Schmeisser, S., Luck, C*., et al.* (2011) Mitochondrial DNA copy number and function decrease with age in the short-lived fish Nothobranchius furzeri. *Aging Cell,* **10**, 824-831.

Hayakawa, M., Torii, K., Sugiyama, S., Tanaka, M. & Ozawa, T. (1991) Age-associated accumulation of 8-hydroxydeoxyguanosine in mitochondrial DNA of human diaphragm. *Biochem. Biophys. Res. Commun.,* **179**, 1023-1029.

Hayakawa, T., Noda, M., Yasuda, K., Yorifuji, H., Taniguchi, S., Miwa, I*., et al.* (1998) Ethidium Bromide-induced Inhibition of Mitochondrial Gene Transcription Suppresses Glucose-stimulated Insulin Release in the Mouse Pancreatic β-Cell Line βHC9. *J. Biol. Chem.,* **273**, 20300-20307.

He, L., Chinnery, P. F., Durham, S. E., Blakely, E. L., Wardell, T. M., Borthwick, G. M*., et al.* (2002) Detection and quantification of mitochondrial DNA deletions in individual cells by real-time PCR. *Nucleic Acids Res.,* **30**, e68.

Hitman, G. A. (1999) *Type 2 Diabetes Prediction and Prevention, Chapter 2*. John Wiley & Sons, Chichester.

Holloszy, J. O. & Coyle, E. F. (1984) Adaptations of skeletal muscle to endurance exercise and their metabolic consequences. *J. Appl. Physiol.,* **56**, 831-838.

Holt, I. J., Harding, A. E. & Morgan-Hughes, J. A. (1988) Deletions of muscle mitochondrial DNA in patients with mitochondrial myopathies. *Nature,* **331**, 717-719.

Holt, I. J., Lorimer, H. E. & Jacobs, H. T. (2000) Coupled leading- and lagging-strand synthesis of mammalian mitochondrial DNA. *Cell,* **100**, 515-524.

Hosker, J. P., Rudenski, A. S., Burnett, M. A., Matthews, D. R. & Turner, R. C. (1989) Similar reduction of first- and second-phase B-cell responses at three different glucose levels in type II diabetes and the effect of gliclazide therapy. *Metabolism,* **38**, 767-772.

Höschele, D. (2006) Cell culture models for the investigation of NRTI-induced mitochondrial toxicity. Relevance for the prediction of clinical toxicity. *Toxicology in Vitro,* **20**, 535-546.

IDF. (2011) *Diabetes Atlas Fifth Edition*, Online version available at www.idf.org/diabetesatlas.

Ihm, S. H., Matsumoto, I., Sawada, T., Nakano, M., Zhang, H. J., Ansite, J. D., *et al.* (2006) Effect of donor age on function of isolated human islets. *Diabetes,* **55**, 1361-1368.

Imamura, M. & Maeda, S. (2011) Genetics of type 2 diabetes: the GWAS era and future perspectives [Review]. *Endocr. J.,* **58**, 723-739.

Ip, M.M., Chee, P.Y. and Swick, R.W. (1974) Turnover of hepatic mitochondrial ornithine aminotransferase and cytochrome oxidase using (14C)carbonate as tracer, *Biochim. Biophys. Acta*, **354**, 29-38.

Ishihara, H., Asano, T., Tsukuda, K., Katagiri, H., Inukai, K., Anai, M., *et al.* (1994) Overexpression of Hexokinase 1 but not GLUT1 Glucose Transporter Alters Concentration Dependence of Glucose-stimulated Insulin Secretion in Pancreatic β-Cell Line MIN6. *J. Biol. Chem.,* **269**, 3081-3087.

Jaber, L. A., Antal, E. J., Slaughter, R. L. & Welshman, I. R. (1994) Comparison of pharmacokinetics and pharmacodynamics of short- and long-term glyburide therapy in NIDDM. *Diabetes Care,* **17**, 1300-1306.

Jeng, J.Y., *et al.* (2008) Maintenance of mitochondrial DNA copy number and expression are essential for preservation of mitochondrial function and cell growth, *J. Cell. Biochem.*, **103**, 347-357.

Kaaman, M., Sparks, L. M., van Harmelen, V., Smith, S. R., Sjolin, E., Dahlman, I., *et al.* (2007) Strong association between mitochondrial DNA copy number and lipogenesis in human white adipose tissue. *Diabetologia,* **50**, 2526-2533.

Kaipparettu, B.A., Ma, Y. and Wong, L.J. (2010) Functional effects of cancer mitochondria on energy metabolism and tumorigenesis: utility of transmitochondrial cybrids, *Ann. N. Y. Acad. Sci.*, **1201**, 137-146.

Kakunda, T. N. (2000) Pharmacology of Nucleoside and Nucleotide Reverse Transcriptase Inhibitor-Induced Mitochondrial Toxicity. *Clinical Therapeutics,* **22**, 685-708.

Kaufman, B. A., Durisic, N., Mativetsky, J. M., Costantino, S., Hancock, M. A., Grutter, P.*, et al.* (2007) The mitochondrial transcription factor TFAM coordinates the assembly of multiple DNA molecules into nucleoid-like structures. *Mol. Biol. Cell,* **18**, 3225-3236.

Kennedy, E. D., Maechler, P. & Wollheim, C. B. (1998) Effects of Depletion of Mitochondrial DNA in Metabolism Secretion Coupling in INS-1 Cells. *Diabetes,* **47**, 374-380.

Kennedy, J. M., Lobacz, S. R. & Kelley, S. W. (1991) Mitochondrial DNA replication and transcription are dissociated during embryonic cardiac hypertrophy. *Am. J. Physiol.,* **261**, C1091-C1098.

Keren, P., George, J., Shaish, A., Levkovitz, H., Janakovic, Z., Afek, A.*, et al.* (2000) Effect of hyperglycemia and hyperlipidemia on atherosclerosis in LDL receptor-deficient mice: establishment of a combined model and association with heat shock protein 65 immunity. *Diabetes,* **49**, 1064-1109.

King, M. P. & Attardi, G. (1989) Human Cells Lacking mtDNA: Repopulation with Exogenous Mitochondria by Complementation. *Science,* **246**, 500-503.

Klip, A., Tsakiridis, T., Marette, A. & Ortiz, P. A. (1994) Regulation of expression of glucose transporters by glucose: a review of studies in vivo and in cell cultures. *FASEB,* **8**, 43-53.

Koeck, T., Olsson, A. H., Nitert, M. D., Sharoyko, V. V., Ladenvall, C., Kotova, O.*, et al.* (2011) A common variant in TFB1M is associated with reduced insulin secretion and increased future risk of type 2 diabetes. *Cell. Metab.,* **13**, 80-91.

Kruse, B., Narasimhan, N. & Attardi, G. (1989) Termination of transcription in human mitochondria: identification and purification of a DNA binding protein factor that promotes termination. *Cell,* **58**, 391-397.

Kubista, M., Åkerman, B. & Nordén, B. (1987) Characterization of Interaction between DNA and 4',6-Diamidino-2-phenylindole by Optical Spectroscopy. *Biochemistry,* **26**, 4545-4553.

Kujoth, G. C., Bradshaw, P. C., Haroon, S. & Prolla, T. A. (2007) The role of mitochondrial DNA mutations in mammalian aging. *PLoS Genet.,* **3**, e24.

Kujoth, G. C., Hiona, A., Pugh, T. D., Someya, S., Panzer, K., Wohlgemuth, S. E.*, et al.* (2005) Mitochondrial DNA mutations, oxidative stress, and apoptosis in mammalian aging. *Science,* **309**, 481-484.

Kunjathoor, V. V., Wilson, D. L. & LeBoeuf, R. C. (1996) Increased atherosclerosis in streptozotocin-induced diabetic mice. *J. Clin. Invest.,* **97**, 1767-1773.

Laderman, K. A., Penny, J. R., Mazzucchelli, F., Bresolin, N., Scarlato, G. & Attardi, G. (1996) Aging-dependant functional alterations of mitochondrial DNA

(mtDNA) from human fibroblasts transferred in mtDNA-less cells. *J. Biol. Chem.,* **271**, 15891-15897.

Lakatta, E. G. (1993) Cardiovascular regulatory mechanisms in advanced age. *Physiol. Rev.,* **73**, 413-467.

Lake-Bakaar, G., Mazzoccoli, V., Dickman, K. & Lyubsky, S. (2001) Differential Effects of Nucleoside Analogs on Oxidative Phosphorylation in Human Pancreatic Cells. *Digestive Disease and Sciences,* **46**, 1853–1863.

Lanza, I. R., Short, D. K., Short, K. R., Raghavakaimal, S., Basu, R., Joyner, M. J.*, et al.* (2008) Endurance exercise as a countermeasure for aging. *Diabetes,* **57**, 2933-2942.

Larsson, N. G. (2010) Somatic mitochondrial DNA mutations in mammalian aging. *Annu. Rev. Biochem.,* **79**, 683-706.

Larsson, N. G., Wang, J., Wilhelmsson, H., Oldfors, A., Rustin, P., Lewandoski, M.*, et al.* (1998) Mitochondrial transcription factor A is necessary for mtDNA maintenance and embryogenesis in mice. *Nat. Gen.,* **18**, 231–236.

Leahy, J. L. (2005) Pathogenesis of Type 2 Diabetes Mellitus. *Arch. Med. Res.,* **36**, 197-209.

Lee, H. R. & Johnson, K. A. (2006) Fidelity of the human mitochondrial DNA polymerase. *J. Biol. Chem.,* **281**, 36236-36240.

Lewis, W., Day, B. J. & Copeland, W. C. (2003) Mitochondrial toxicity of NRTI antiviral drugs: An integrated cellular perspective. *Nat. Rev.,* **2**, 812-822.

Li, H., Wang, J., Wilhelmsson, H., Hansson, H., Thore, P., Duffy, J.*, et al.* (2000) Genetic modification of survival in tissue-specific knockout mice with mitochondrial cardiomyopathy. *PNAS,* **97**, 3467–3472.

Lister, J. & Nash, J. (1951) Constitution and insulin sensitivity in diabetes mellitus. *Br. Med. J.*, 376-379.

Litonin, D., Sologub, M., Shi, Y., Savkina, M., Anikin, M., Falkenberg, M.*, et al.* (2010) Human mitochondrial transcription revisited: only TFAM and TFB2M are required for transcription of the mitochondrial genes in vitro. *J. Biol. Chem.,* **285**, 18129-18133.

Lo, J. C., Kazemi, M. R., Hsue, P. Y., Martin, J. N., Deeks, S. G., Schambelan, M.*, et al.* (2005) The relationship between nucleoside analogue treatment duration, insulin resistance, and fasting arterialized lactate level in patients with HIV infection. *Clin. Infect. Dis.,* **41**, 1335-1340.

Lodish, H., Berk, A., Matsudaira, P., Kaiser, C. A., Krieger, M., Scott, M. P.*, et al.* (2004) *Molecular Cell Biology*. W.H. Freeman & Company, New York.

Longley, M. J., Nguyen, D., Kunkel, T. A. & Copeland, W. C. (2001) The fidelity of human DNA polymerase gamma with and without exonucleolytic proofreading and the p55 accessory subunit. *J. Biol. Chem.,* **276**, 38555-38562.

Lowry, O. H., ROSEBROUGH, N. J., LEWIS FARR, A. & RANDALL, R. J. (1951) PROTEIN MEASUREMENT WITH THE FOLIN PHENOL REAGENT. *J. Biol. Chem.,* **193**, 265-275.

Lynn, S., Borthwick, G. M., Charnley, R. M., Walker, M. & Turnbull, D. M. (2003) Heteroplasmic ratio of the A3243G mitochondrial DNA mutation in single pancreatic beta cells. *Diabetologia,* **46**, 296-299.

Maassen, J. A., 't Hart, L. M., van Essen, E., Heine, R. J., Nijpels, G., Jahangir Tafrechi, R. S.*, et al.* (2004) Mitochondrial Diabetes, Molecular Mechanisms and Clinical Presentation. *Diabetes,* **53**, S103-S109.

Maassen, J. A., van Essen, E., van den Ouweland, J. M. & Lemkes, H. H. (2001) Molecular and clinical aspects of mitochondrial diabetes mellitus. *Exp. Clin. Endocrinol. Diabetes,* **109**, 127-134.

Madsen, C. S., Ghivizzani, S. C. & Hauswirth, W. W. (1993) In vivo and in vitro evidence for slipped mispairing in mammalian mitochondria. *Proc Natl Acad Sci U S A,* **90**, 7671-7675.

Maechler, P. & Wollheim, C. (2001) Mitochondrial function in normal and diabetic β-cells. *Nature,* **414**, 807-812.

Magda, D., Lecane, P., Prescott, J., Thieman, P., Ma, X., Dranchak, P. K.*, et al.* (2008) mtDNA depletion confers specific gene expression profiles in human cells grown in culture in xenograft. *BMC Genomics,* **9**, 521-540.

Mallon, P. W., Wand, H., Law, M., Miller, J., Cooper, D. A. & Carr, A. (2005) Buffalo hump seen in HIV-associated lipodystrophy is associated with hyperinsulinemia but not dyslipidemia. *J. Acquir. Immune Defic. Syndr.,* **38**, 156-162.

Maniura-Weber, K., Goffart, S., Garstka, H. L., Montoya, J. & Wiesner, R. J. (2004) Transient overexpression of mitochondrial transcription factor A (TFAM) is sufficient to stimulate mitochondrial DNA transcription, but not sufficient to increase mtDNA copy number in cultured cells. *Nucleic Acids Res.,* **32**, 6015-6027.

Margulis, L. (1981) *Symbiosis in Cell Evolution.* Freeman, San Francisco.

Martin, J. L., Brown, C. E., Matthews-Davis, N. & Reardon, J. E. (1994) Effects of antiviral nucleoside analogs on human DNA polymerases and mitochondrial DNA synthesis. *Antimicrob. Agents Chemother.,* **38**, 2743-2749.

Matschinsky, F. M. & Ellerman, J. E. (1968) Metabolism of Glucose in the Islets of Langerhans. *J. Biol. Chem.,* **243**, 2730-2736.

Matschinsky, F. M., Magnuson, M. A., Zelent, D., Jetton, T. L., Doliba, N., Han, Y.*, et al.* (2006) The Network of Glucokinase-Expressing Cells in Glucose Homeostasis and the Potential of Glucokinase Activators for Diabetes Therapy. *Diabetes,* **55**, 1-12.

McCord, J. M. & Fridovich, I. (1969) Superoxide dismutase. An enzymic function for erythrocuprein (hemocuprein). *J. Biol. Chem.,* **244**, 6049-6055.

McCord, J. M. & Fridovich, I. (1988) Superoxide Dimutase: The First Twenty Years (1968-1988). *Free Rad. Biol. & Med.,* **5**, 363-369.

Meerson, F. Z. & Pomoinitsky, V. D. (1972) The role of high-energy phosphate compounds in the development of cardiac hypertrophy. *J. Mol. Cell Cardiol.,* **4**, 571-597.

Menshikova, E. V., Ritov, V. B., Fairfull, L., Ferrell, R. E., Kelley, D. E. & Goodpaster, B. H. (2006) Effects of exercise on mitochondrial content and function in aging human skeletal muscle. *J. Gerontol. A. Biol. Sci. Med. Sci.,* **61**, 534-540.

Metodiev, M. D., Lesko, N., Park, C. B., Camara, Y., Shi, Y., Wibom, R*., et al.* (2009) Methylation of 12S rRNA is necessary for in vivo stability of the small subunit of the mammalian mitochondrial ribosome. *Cell Metab.,* **9**, 386-397.

Michikawa, Y., Mazzucchelli, F., Bresolin, N., Scarlato, G. & Attardi, G. (1999) Aging-dependent large accumulation of point mutations in the human mtDNA control region for replication. *Science,* **286**, 774-779.

Miller, F. J., Rosenfeldt, F. L., Zhang, C., Linnane, A. W. & Nagley, P. (2003) Precise determination of mitochondrial DNA copy number in human skeletal and cardiac muscle by a PCR-based assay: lack of change of copy number with age. *Nucleic Acids Res.,* **31**, e61.

Mitsuya, H., Yarchoan, R. & Broder, S. (1990) Molecular targets for AIDS therapy. *Science,* **249**, 1533-1544.

Miyazaki, J. I., Araki, K., Yamoto, E., Ikegami, H., Asano, T., Shibasaki, Y*., et al.* (1990) Establishment of a Pancreatic β Cell Line That Retains Glucose-Inducible Insulin Secretion: Special Reference to Expression of Glucose Transporter Isoforms. *Endocrin.,* **127**, 126-132.

Mootha, V. K., Lindgren, C. M., Eriksson, K. F., Subramanian, A., Sihag, S., Lehar, J*., et al.* (2003) PGC-1α-responsive genes involved in oxidative phosphorylation are coordinately downregulated in human diabetes. *Nat. Gen.,* **34**, 267-273.

Moraes, C. T., Ricci, E., Bonilla, E., DiMauro, S. & Schon, E. A. (1992) The Mitochondrial tRNALeu(UUR) Mutation in Mitochondrial Encephalomyopathy, Lactic Acidosis, and Strokelike Episodes (MELAS): Genetic, Biochemical, and Morphological Correlations in Skeletal Muscle. *Am. J. Hum. Gen.,* **50**, 934-949.

Moslemi, A. R., Melberg, A., Holme, E. & Oldfors, A. (1996) Clonal expansion of mitochondrial DNA with multiple deletions in autosomal dominant progressive external ophthalmoplegia. *Ann. Neurol.,* **40**, 707-713.

Movassat, J., Bailbe, D., Lubrano-Berthelier, C., Picarel-Blanchot, F., Bertin, E., Mourot, J*., et al.* (2008) Follow-up of GK rats during prediabetes highlights increased insulin action and fat deposition despite low insulin secretion. *Am. J. Physiol. Endocrinol. Metab.,* **294**, E168-E175.

Muller, D., Huang, G. C., Amiel, S., Jones, P. M. & Persaud, S. J. (2006) Identification of insulin signaling elements in human beta-cells: autocrine regulation of insulin gene expression. *Diabetes,* **55**, 2835-2842.

Muller-Hocker, J. (1989) Cytochrome-c-oxidase deficient cardiomyocytes in the human heart--an age-related phenomenon. A histochemical ultracytochemical study. *Am. J. Pathol.,* **134**, 1167-1173.

Muller-Hocker, J. (1990) Cytochrome c oxidase deficient fibres in the limb muscle and diaphragm of man without muscular disease: an age-related alteration. *J. Neurol. Sci.,* **100**, 14-21.

Neel, J. V. (1962) Diabetes Mellitus: A "Thrifty" Genotype Rendered Detrimental by "Progress"? *Am. J. Hum. Gen.,* **14**, 353–362.

NICE. (2008) TYPE 2 DIABETES: National clinical guideline for management in primary and secondary care (update). 46 pp.

Nie, J., DuBois, D. C., Jusko, W. J. & Almon, R. R. (2011) Mechanistic population modeling of diabetes disease progression in Goto-Kakizaki rat muscle. *Biopharm. Drug Dispos.,* **32**, 50-63.

O'Rourke, C. M., Davis, J. A., Saltiel, A. R. & Cornicelli, J. A. (1997) Metabolic effects of troglitazone in the Goto-Kakizaki rat, a non-obese and normolipidemic rodent model of non-insulin-dependent diabetes mellitus. *Metabolism,* **46**, 192-198.

Ohgaki, K., Kanki, T., Fukuoh, A., Kurisaki, H., Aoki, Y., Ikeuchi, M.*, et al.* (2007) The C-terminal tail of mitochondrial transcription factor a markedly strengthens its general binding to DNA. *J. Biochem.,* **141**, 201-211.

Oliver-Krasinski, J. M. & Stoffers, D. A. (2008) On the origin of the beta cell. *Genes. Dev.,* **22**, 1998-2021.

Parisi, M. A. & Clayton, D. A. (1991) Similarity of Human Mitochondrial Transcription Factor 1 to High Mobility Group Proteins. *Science,* **252**, 965-969.

Park, L., Raman, K. G., Lee, K. J., Lu, Y., Ferran, L. J., Jr., Chow, W. S.*, et al.* (1998) Suppression of accelerated diabetic atherosclerosis by the soluble receptor for advanced glycation endproducts. *Nat. Med.,* **4**, 1025-1031.

Park, S. Y. & Lee, W. (2007) The depletion of cellular mitochondrial DNA causes insulin resistance through the alteration of insulin receptor substrate-1 in rat myocytes. *Diabetes Res. Clin. Pract.,* **77**, S165-S171.

Pascoe, L., Tura, A., Patel, S. K., Ibrahim, I. M., Ferrannini, E., Zeggini, E.*, et al.* (2007) Common variants of the novel type 2 diabetes genes CDKAL1 and HHEX/IDE are associated with decreased pancreatic beta-cell function. *Diabetes,* **56**, 3101-3104.

Petersen, K. F., Befroy, D., Dufour, S., Dziura, J., Ariyan, C., Rothman, D. L.*, et al.* (2003) Mitochondrial Dysfunction in the Elderly: Possible Role in Insulin Resistance. *Science,* **300**.

Poitout, V. & Robertson, R. P. (2002) Minireview: Secondary β-Cell Failure in Type 2 Diabetes - A Convergence of Glucotoxicity and Lipotoxicity. *Endocrin.,* **143**, 339-342.

Porte, D. (2001) Clinical importance of insulin secretion and its interaction with insulin resistance in the treatment of type 2 diabetes mellitus and its complications. *Diabetes Metab. Res. Rev.,* **17**, 181-188.

Praet, S. F. E. & Van Loon, L. J. C. (2009) Exercise therapy in Type 2 diabetes. *Acta Diabetologia,* **46**, 263-278.

Prentki, M., Joly, E., El-Assaad, W. & Roduit, R. (2002) Malonyl-CoA Signaling, Lipid Partitioning, and Glucolipotoxicity Role in β-Cell Adaptation and Failure in the Etiology of Diabetes. *Diabetes,* **51**, S405-S413.

Proks, P., Reimann, F., Green, N., Gribble, F. & Ashcroft, F. (2002) Sulfonylurea stimulation of insulin secretion. *Diabetes,* **51 Suppl 3**, S368-S376.

Puigserver, P. & Spiegelman, B. M. (2003) Peroxisome Proliferation-Activated Receptor-γ Coactivator 1α (PGC-1α): Transcriptional Coactivator and Metabolic Regulator. *Endocr. Rev.,* **24**, 78-90.

Rajamanickam, C., Merten, S., Kwiatkowska-Patzer, B., Chuang, C. H., Zak, R. & Rabinowitz, M. (1979) Changes in mitochondrial DNA in cardiac hypertrophy in the rat. *Circ. Res.,* **45**, 505-515.

Rasbach, K. A., Green, P. T. & Schnellmann, R. G. (2008) The Mitochondrial Biogenesis Regulator PGC-1alpha is Degraded by the Proteasome and Calpain Pathways in Renal Cells. *FASEB,* **22**, 605.610.

Ravassard, P., Hazhouz, Y., Pechberty, S., Bricout-Neveu, E., Armanet, M., Czernichow, P.*, et al.* (2011) A genetically engineered human pancreatic β cell line exhibiting glucose-inducible insulin secretion. *J. Biol. Chem.,* **121**, 3589-3597.

Resnick, H. E., Harris, M. I., Brock, D. B. & Harris, T. B. (2000) American Diabetes Association diabetes diagnostic criteria, advancing age, and cardiovascular disease risk profiles. *Diabetes Care,* **23**, 176–180.

Richter, C. (1988) Do mitochondrial DNA fragments promote cancer and aging? *FEBS Lett.,* **241**, 1-5.

Richter, C., Park, J. W. & Ames, B. N. (1988) Normal oxidative damage to mitochondrial and nuclear DNA is extensive. *PNAS,* **85**, 6465-6467.

Roderigo-Milne, H., Hauge-Evans, A. C., Persaud, S. J. & Jones, P. M. (2002) Differential expression of insulin genes 1 and 2 in MIN6 cells and pseudoislets. *Biochem. Biophys. Res. Commun.,* **296**, 589-595.

Rossignol, R., Faustin, B., Rocher, C., Malgat, M., Mazat, J. P. & Letellier, T. (2003) Miotchondrial threshold effects. *Biochem. J.,* **370**, 751-762.

Rudenski, A. S., Hadden, D. R., Atkinson, A. B., Kennedy, L., Matthews, D. R., Merrett, J. D.*, et al.* (1988) Natural history of pancreatic islet B-cell function in type 2 diabetes mellitus studied over six years by homeostasis model assessment. *Diabet. Med.,* **5**, 36-41.

Rung, J., Cauchi, S., Albrechtsen, A., Shen, L., Rocheleau, G., Cavalcanti-Proenca, C.*, et al.* (2009) Genetic variant near IRS1 is associated with type 2 diabetes, insulin resistance and hyperinsulinemia. *Nat. Gen,,* **41**, 1110-1115.

Saxena, R.*, et al.* (2007) Genome-wide association analysis identifies loci for type 2 diabetes and triglyceride levels, *Science*, **316**, 1331-1336.

Schmittgen, T. D. & Livak, K. J. (2008) Analyzing real-time PCR data by the comparative C(T) method. *Nat. Protoc.,* **3**, 1101-1108.

Sciacco, M., Bonilla, E., Schon, E. A., DiMauro, S. & Moraes, C. T. (1994) Distribution of wild-type and common deletion forms of mtDNA in normal and respiration-deficient muscle fibers from patients with mitochondrial myopathy. *Hum. Molec. Gen.,* **3**, 13-19.

Servitja, J. M. & Ferrer, J. (2004) Transcriptional networks controlling pancreatic development and beta cell function. *Diabetologia,* **47**, 597-613.

Shadel, G. S. & Clayton, D. A. (1993) Mitochondrial transcription initiation: variation and conservation. *J. Biol. Chem.,* **268**, 16083-16086.

Shi, X.*, et al.* (2008) Paradoxical effect of mitochondrial respiratory chain impairment on insulin signaling and glucose transport in adipose cells, *J. Biol. Chem.*, **283**, 30658-30667.

Shigenaga, M. K., Hagen, T. M. & Ames, B. N. (1994) Oxidative damage and mitochondrial decay in aging. *PNAS,* **91**, 10771-10778.

Shmookler Reis, R. J. & Goldstein, S. (1983) Mitochondrial DNA in mortal and immortal human cells. Genome number, integrity, and methylation. *J. Biol. Chem.,* **258**, 9078-9085.

Short, K. R., Bigelow, M. L., Kahl, J., Singh, R., Coenen-Schimke, J. C., Raghavakaimal, S.*, et al.* (2005) Declinie in skeletal muscle mitochondrial function with aging in humans. *PNAS,* **102**, 5618-5623.

Shoubridge, E. A. (2001) Nuclear genetic defects of oxidative phosphorylation. *Hum. Mol. Gen.,* **10**, 2277-2284.

Silva, J. P., Köhler, M., Graff, C., Oldfors, A., Magnuson, M. A., Berggren, P. O.*, et al.* (2000) Impaired insulin secretion and β-cell loss in tissue-specific knockout mice with mitochondrial diabetes. *Nat. Gen.,* **26**, 336-340.

Singh, K. K. (2006) Mitochondria Damage Checkpoint, Aging, and Cancer. *Ann. N. Y. Acad. Sci.,* **1067**, 182-190.

Sladek, R., Rocheleau, G., Rung, J., Dina, C., Shen, L., Serre, D.*, et al.* (2007) A genome-wide association study identifies novel risk loci for type 2 diabetes. *Nature,* **445**, 881-885.

Soejima, A., Inoue, K., Takai, D., Kaneko, M., Ishihara, H., Okai, Y.*, et al.* (1996) Mitochondrial DNA Is Required for Regulation of Glucose-stimulated Insulin Secretion in a Mouse Pancreatic Beta Cell Line, MIN6. *J. Biol. Chem.,* **271**, 26194-16199.

Sorensen, L., Ekstrand, M., Silva, J. P., Lindqvist, E., Xu, B., Rustin, P.*, et al.* (2001) Late-Onset Corticohippocampal Neurodepletion Attributable to Catastrophic Failure of Oxidative Phosphorylation in MILON Mice. *J. Neurosci.,* **21**, 8082–8090.

Spelbrink, J. N., Li, F. Y., Tiranti, V., Nikali, K., Yuan, Q. P., Tariq, M., *et al.* (2001) Human mitochondrial DNA deletions associated with mutations in the gene encoding Twinkle, a phage T7 gene 4-like protein localized in mitochondria. *Nat. Gen.,* **28**, 223-231.

Steiner, D. F., Chan, S. J., Welsh, J. M. & Kwok, S. C. (1985) Structure and evolution of the insulin gene. *Annu. Rev. Genet.,* **19**, 463-484.

Steinthorsdottir, V., Thorleifsson, G., Reynisdottir, I., Benediktsson, R., Jonsdottir, T., Walters, G. B., *et al.* (2007) A variant in CDKAL1 influences insulin response and risk of type 2 diabetes. *Nat. Gen.,* **39**, 770-775.

Stryer, L. (1995) *Biochemistry (4th Edition)*. W.H. Freeman & Co., New York.

Suzuki, N., Aizawa, T., Asanuma, N., Sato, Y., Komatsu, M., Hidaka, H., *et al.* (1997) An early insulin intervention accelerates pancreatic beta-cell dysfunction in young Goto-Kakizaki rats, a model of naturally occurring noninsulin-dependent diabetes. *Endocrinology,* **138**, 1106-1110.

Szabados, E., Fischer, G. M., Toth, K., Csete, B., Nemeti, B., Trombitas, K., *et al.* (1999) Role of reactive oxygen species and poly-ADP-ribose polymerase in the development of AZT-induced cardiomyopathy in rat. *Free Radic. Biol. Med.,* **26**, 309-317.

Taanman, J.W., *et al.* (1997) Molecular mechanisms in mitochondrial DNA depletion syndrome, *Hum. Mol. Genet.*, **6**, 935-942.

Takamatsu, C., Umeda, S., Ohsato, T., Ohno, T., Abe, Y., Fukuoh, A., *et al.* (2002) Regulation of mitochondrial D-loops by transcription factor A and single-stranded binding protein. *EMBO Rep.,* **3**, 451-456.

Taylor, R. (2011) Reversing type 2 diabetes. *Practical Diabetes,* **28**, 377-378a.

Taylor, R. W., Barron, M. J., Borthwick, G. M., Gospel, A., Chinnery, P. F., Samuels, D. C., *et al.* (2003) Mitochondrial DNA mutations in human colonic crypt stem cells. *J. Clin. Invest.,* **112**, 1351-1360.

Taylor, R. W. & Turnbull, D. M. (2005) Mitochondrial DNA mutations in human disease. *Nat. Rev.,* **6**, 389-402.

Tien, P. C., Schneider, M. F., Cole, S. R., Levine, A. M., Cohen, M., DeHovitz, J., *et al.* (2008) Antiretroviral therapy exposure and insulin resistance in the Women's Interagency HIV study. *J. Acquir. Immune Defic. Syndr.,* **49**, 369-376.

Tontonoz, P., Hu, E. & Spiegelman, B. M. (1994) Stimulation of adipogenesis in fibroblasts by PPARγ2, a lipid activated transcription factor. *Cell,* **79**, 1147-1156.

Trenell, M., Hollingsworth, K. G., Lim, E. L. & Taylor, R. (2008) Increased Daily Walking Improves Lipid Oxidation Without Changes in Mitochondrial Function in Type 2 Diabetes. *Diabetes Care,* **31**, 1644-1649.

Trifunovic, A., Wredenberg, A., Falkenberg, M., Spelbrink, J. N., Rovio, A. T., Bruder, C. E., *et al.* (2004) Premature ageing in mice expressing defective mitochondrial DNA polymerase. *Nature,* **429**, 417-423.

Tsuruzoe, K., Araki, E., Furukawa, N., Shirotani, T., Matsumoto, K., Kaneko, K.*, et al.* (1998) Creation and characterization of a mitochondrial DNA-depleted pancreatic beta-cell line: impaired insulin secretion induced by glucose, leucine, and sulfonylureas. *Diabetes,* **47**, 621-631.

van den Ouweland, J. M. W., Lemkes, H. H. P. J., Ruitenbeek, W., Sandkuijl, L. A., de Vijlder, M. F., Struyvenberg, P. A. A.*, et al.* (1992) Mutation in mitochondrial $tRNA^{Leu\ (UUR)}$ gene in a large pedigree with maternally transmitted type II diabetes mellitus and deafness. *Nat. Gen.,* **1**, 368–371.

Virbasius, J. V. & Scarpulla, R. C. (1994) Activation of the human mitochondrial transcription factor A gene by nuclear respiratory factors: A potential regulatory link between nuclear and mitochondrial gene expression in organelle biogenesis. *PNAS,* **91**, 1309-1313.

Wang, J., Wilhelmsson, H., Graff, C., Li, H., Oldfors, A., Rustin, P.*, et al.* (1999) Dilated cardiomyopathy and atrioventricular conduction blocks induced by heart-specific inactivation of mitochondrial DNA gene expression. *Nat. Gen.,* **21**, 133-137.

Wang, Y. & Bogenhagen, D. F. (2006) Human mitochondrial DNA nucleoids are linked to protein folding machinery and metabolic enzymes at the mitochondrial inner membrane. *J. Biol. Chem.,* **281**, 25791-25802.

Welle, S., Bhatt, K., Shah, B., Needler, N., Delehanty, J. M. & Thornton, C. A. (2003) Reduced amount of mitochondrial DNA in aged human muscle. *J. Appl. Physiol.,* **94**, 1479-1484.

WHO. (1999) Definition, Diagnosis and Classification of Diabetes Mellitus and its Complications, Part 1: Diagnosis and Classification of Diabetes Mellitus. Geneva, 4-5 pp.

WHO. (2006) Definition and diagnosis of diabetes mellitus and intermediate hyperglycemia. Geneva, 1-3 pp.

WHO. (2008a) 10 Facts About Diabetes. In, Online version available http://www.who.int/diabetes/en/.

WHO. (2008b) Diabetes Programme - WHO European Region. In, Online version available http://www.who.int/diabetes/facts/world_figures/en/index4.html.

Willis, T. (1674-1675) Pharmaceutice rationalis, sive diatriba de medicamentorum operationibus in humano corpore. In, Oxford, London.

Wollheim, C. B. (2000) Beta-cell mitochondria in the regulation of insulin secretion: a new culprit in Type II diabetes. *Diabetologia,* **43**, 265-277.

Wredenberg, A., Wibom, R., Wilhelmsson, H., Graff, C., Wiener, H. H., Burden, S. J.*, et al.* (2002) Increased mitochondrial mass in mitochondrial myopathy mice. *PNAS,* **99**, 15066–15071.

Yamaguchi, T., Katoh, I. & Kurata, S. (2002) Azidothymidine causes functional and structural destruction of mitochondria, glutathione deficiency and HIV-1 promoter sensitization. *Eur. J. Biochem.,* **269**, 2782-2788.

Yang, M. Y., Bowmaker, M., Reyes, A., Vergani, L., Angeli, P., Gringeri, E.*, et al.* (2002) Biased incorporation of ribonucleotides on the mitochondrial L-strand accounts for apparent strand-asymmetric DNA replication. *Cell,* **111**, 495-505.

Zeggini, E., Scott, L. J., Saxena, R., Voight, B. F., Marchini, J. L., Hu, T.*, et al.* (2008) Meta-analysis of genome-wide association data and large-scale replication identifies additional susceptibility loci for type 2 diabetes. *Nat. Gen.,* **40**, 638-645.

Zhang, C., Liu, V. W., Addessi, C. L., Sheffield, D. A., Linnane, A. W. & Nagley, P. (1998) Differential occurrence of mutations in mitochondrial DNA of human skeletal muscle during aging. *Hum. Mutat.,* **11**, 360-371.

Zheng, W., Khrapko, K., Coller, H. A., Thilly, W. G. & Copeland, W. C. (2006) Origins of human mitochondrial point mutations as DNA polymerase gamma-mediated errors. *Mutat. Res.,* **599**, 11-20.

Zhu, X., Peng, X., Guan, M. X. & Yan, Q. (2009) Pathogenic mutations of nuclear genes associated with mitochondrial disorders. *Acta Biochim Biophys Sin (Shanghai),* **41**, 179-187.